Exploiting Precision Medicine in Rhabdomyosarcoma

Dissertation*

zur

Erlangung der naturwissenschaftlichen Doktorwürde
(Dr. sc. nat.)

vorgelegt der

Mathematisch-naturwissenschaftlichen Fakultät

der

Universität Zürich

von

Gabriele Manzella

aus

Italien

Promotionskommission

Prof. Dr.**Beat Schäfer**
Prof. Dr.**Lukas Sommer**
Prof. Dr.**Konrad Basler**

Zürich, 2018

To my parents and my grandparents

The experimental work presented in this thesis was performed at the Department of Oncology and Children's Research Center, University Children's Hospital Zurich. The supervision of this thesis was conducted by Prof. Dr. Beat W. Schäfer (Department of Oncology, University Children's Hospital Zurich), Prof. Dr. Lukas Sommer (Institute of Anatomy, University of Zurich) and Prof. Dr. Konrad Basler (Institute of Molecular Life Sciences, University of Zurich).

Zurich, 2017
Gabriele Manzella

Table of Contents

1. Summary

Historically, cancers have been histologically classified based on the embryonic origin of the normal tissue they most closely resemble, thus providing diagnostic and prognostic information as well as guidance for therapy. Nowadays, with the advent of more sophisticated next-generation sequencing (NGS) technologies we are able to catalogue genetic aberrations for each cancer type, which facilitate the identification of potential therapeutic targets and/or predictive biomarkers. However, the relative homogenous genomic landscape of pediatric cancers constitutes a major shortcoming for genome-based strategies to nominate actionable targets. One example is rhabdomyosarcoma (RMS), the most common soft-tissue sarcoma in children, which presents two main subtypes, embryonal (ERMS) and alveolar (ARMS) RMS. Despite the great progress that has been made for treatment of RMS with conventional therapies, up to 30 percent of patients still have dismal outcome and no targeted therapy has entered into clinical practice so far. The recently described genetic landscape revealed the presence of only rare mutations, apart from the most recognized driver alteration which is the occurrence of either PAX3-FOXO1 or to a lesser extent PAX7-FOXO1 in ~80% of diagnosed ARMS. Although comprehensive genomic profiling would readily capture such lesions, these do not match therapeutic possibilities. Hence, procedures to functionally test the druggability of identified aberrations or inform on alternative treatment options for individual patients would complement the work of pathologists or bioinformaticians and ultimately guide the treating physicians. One possibility takes advantage of direct drug-profiling of patient tumor cells. Such high-throughput drug screens have been widely performed in the past for cancer cell lines but only few identified compounds have met clinical utility. The failure of existing pre-clinical models raised concerns about their ability to recapitulate characteristics of native tumors indicating an urgent need to improve traditional culture protocols. Hence, to fill this gap we aimed here to establish an *in vitro* drug-profiling platform for RMS. To this end, we first generated a large panel of patient-derived xenografts (PDXs) and then screened 18 different culture conditions to find the suitable parameters for *in vitro* culture of isolated cancer cells. In this context, we describe for the first time the detrimental effect of serum on primary RMS cell cultures (RPCs) and provide new culture methods that closely preserve the clonal composition and phenotypic characteristics of the parental tumor. Yet, we show proof-of-concept pharmacological profiles of RPCs by using a library of FDA-approved drugs or compounds in clinical development to pinpoint drug sensitivities in individual patients. In this regard, we describe the effect of AKT inhibitors, which exhibited a strong patient-specific activity, further corroborating the utility of personalized pre-clinical systems. Interestingly, we were able to detect samples refractory to the standard-of-care therapies for RMS, reflecting the clinical course of the initial patients thus providing a retrospective validation of our model. By using a combinatorial large drug-screen approach, we

identified ABT-263 as top scoring drug capable of sensitizing resistant RPCs to conventional chemotherapeutics (doxorubicin, etoposide and vincristine). From a mechanistic standpoint we show that ABT-263/standard chemotherapy exploit the BCL-XL/MCL-1 axis and partially rely on the induction of the pro-apoptotic BH3-only protein NOXA. Finally, we also outline a clear correlation between over-activation of Hh signaling and tumor recurrence in our set of PDX and RPCs and demonstrate the feasibility of pharmacologically targeting a cancer stem cell (CSC) signal to counteract chemo-resistance.

Taken together, the studies presented in this thesis underscore the functional relevance of novel pre-clinical models to prioritize actionable drug targets or combinatorial options for RMS patients for which conventional therapies are failing.

2. Zusammenfassung

Lange Zeit war histologische Analyse die Methode der Wahl zur Tumor Klassifizierung. Die über Jahrzehnte immer weiter verfeinerte Subklassifizierung in Kombination mit Korrelation mit Therapieerfolg vereinfacht auch heutzutage die Wahl der Therapie und erlaubt damit verbundene prognostische Voraussagen.

Mit dem Aufkommen von Hochdurchsatz-Sequenzierverfahren können nun die ursächlichen genetischen Veränderungen in den verschiedenen Tumortypen ermittelt werden. Diese Methode ermöglicht die direkte Identifizierung von therapeutischen Zielen und/oder prognostischen Markern in individuellen Tumoren. Dies ist insbesondere bei Tumoren mit vielen Mutationen von grossem Nutzen. Bei kindlichen Tumoren ist die Zahl an genetischen Veränderungen pro Tumor allerdings sehr klein. Dies wiederum schränkt die Menge an möglichen therapeutischen Zielen, welche mittels Sequenzierung identifiziert werden können, stark ein. Ein Beispiel für einen solchen Tumor ist das Rhabdomyosarkom (RMS). Das RMS ist das häufigste Weichteilsarkom bei Kindern, wobei man zwei Haupt-Subtypen unterscheidet, das alveoläre (aRMS) und das embryonale (eRMS) RMS. Trotz grossen Fortschritten bei der Behandlung mit konventionellen Therapien sterben heutzutage immer noch rund 30 Prozent aller Patienten an diesem Tumor und neuartige, gezielte Medikamente sind leider noch nicht erhältlich.

Das kürzlich beschriebene Mutationsspektrum im RMS zeigt, dass rund 80 Prozent der Fälle hauptsächlich die schon länger als ursächliche Mutationen bekannten, spezifischen Fusionsproteine PAX3-FOXO1 und PAX7-FOXO1 aufweisen. Die Zahl weiterer Mutationen ist hingegen ist sehr klein und ausserdem als Therapieziel meist ungeeignet. Daher wäre ein Testsystem, mit welchem man den Effekt von neuen Medikamenten direkt auf RMS Patientenzellen messen kann, von grossem Nutzen für die Klinik. Zwar wurden in der Vergangenheit einige Versuche in diese Richtung unternommen, dies hat aber leider nur in seltenen Fällen zur Entdeckung von klinisch wirksamen Medikamenten geführt. Ein wichtiger Grund dafür ist, dass für diese Versuche meist eine geringe Zahl an etablierten Zelllinien verwendet wurde, welche die Charakteristika der Patiententumore in ungenügender Weise abbilden. Eine Verbesserung der Modelsysteme würde somit eine wichtige Lücke schliessen. Das Ziel der hier vorliegenden Arbeit war daher, eine optimierte *in vitro* und *in vivo* Plattform für Medikamententests am RMS zu etablieren. Dazu haben wir erst eine grosse Anzahl von RMS Tumoren als Xenografts in Mäusen etabliert. Anschliessend haben wir 18 verschiedene Kulturbedingungen getestet, um die optimalen Bedingungen für die *in vitro* Kultur von daraus isolierten RMS Zellen zu finden. Wir konnten dabei zeigen, dass insbesondere Kälberserum, eine wichtige Komponente klassischer Zellkulturmedien, eine toxische Wirkung auf die Primärzellen hat. Unter bestimmten Serum-freien Bedingungen hingegen proliferieren die RMS Zellen nicht nur, sondern es bleiben auch wichtige Eigenschaften wie die klonale Zusammensetzung und der

charakteristische Phänotyp des Ursprungstumors erhalten. Wir haben derartig kultivierte Zellen daher in einem zweiten Schritt als Model für Screenings mit einer Bibliothek an klinisch erhältlichen Medikamenten verwendet. Dies führte zur Entdeckung, dass RMS Zellen von gewissen Patienten sensitiv gegenüber AKT Inhibitoren sind. Mit Zellen aus Tumoren, welche resistent gegenüber der Standardchemotherapie sind, wurde ein analoges Screening in Kombination mit Chemotherapie durchgeführt. Dabei entdeckten wir, dass die Substanz ABT-263 RMS Tumore für die Standardtherapie (Doxorubicin, Etoposid und Vincristin) resensitisiert. Eine genauere mechanistische Analyse zeigte, dass dieser Effekt durch eine Kombination der Blockierung von BCL-XL durch ABT-263 und Runterregulierung von Mcl1 durch die Chemotherapie zustande kommt. BCL-XL und MCL-1 sind zwei anti-apoptotische Proteine, welche in resistenten Tumoren häufig hochreguliert sind.

Zum Schluss konnten wir mittels unserer Xenograft Sammlung auch eine klare Korrelation von aktiviertem Hedgehog-Signaling und Tumor-Rückfall zeigen. Pharmakologische Blockierung dieses mit Stammzellen assoziierten Signalwegs hatte ebenfalls eine resensitisierende Wirkung gegenüber der Standardtherapie.

Zusammengefasst bestätigt unsere Studie, dass optimierte Tumormodelle einen wichtigen Beitrag zu einer effizienteren und zielführenderen Identifikation von Therapieansätzen für das RMS leisten können.

3. List of Abbreviations

ABC	ATP-binding cassette
aCGH	array comparative genomic hybridization
ADAM	A disintegrin and metalloproteinase
AKT (PKB)	Protein kinase B
ALDH1	Aldehyde Dehydrogenase 1
ALL	acute lymphoblastic leukemia
AML	acute myelogenous leukemia
APAF	apoptosis protease-activating factor 1
APC	Adenomatous polyposis coli
ARMS	Alveolar RMS
ATM	Ataxia-telangiectasia mutated
ATR	Ataxia-telangiectasia and RAD3-related protein
AXIN2	Axis inhibition protein 2
BAD	BCL-2-associated death promoter
BAK	BCL-2 antagonist/killer
BAX	BCL-2 associated X protein
BCC	basal cell carcinomas
BCL-2	B-cell lymphoma 2
BCL-B	BCL-2-like protein B
BCL-XL	B-cell lymphoma-extra large
BCNS	Basal Cell Nevus Syndrome
BCOR	Back central optic radius
BFL/A1	BCL-2-related protein A1
BID	BH3-interacting domain death agonist
BIM	(BCL2L11) BCL-2-like protein 11
BMF	BCL-2-modifying factor
BOC	brother of CDO
CAM	chorioallantoic membrane
CDK4	Cyclin-dependent kinase 4
CDKN	Cyclin-dependent kinase inhibitor
CDO	cell adhesion molecule down-regulated by oncogenes
CDX	cell-derived xenografts
CKI	casein kinase family
CLL	chronic lymphocytic leukemia
CML	Chronic myeloid leukemia
CMT1000	Center for Molecular Therapeutic 1000
CNS	central nervous system
CNV	copy number variants
COG	children’s oncology group
CRC	colorectal cancer
CRISPR/cas9	Clustered Regularly Interspaced Short Palindromic Repeats/ associated protein-9 nuclease
CSC	cancer-stem cell
CSL	CBF1/Suppressor of Hairless/LAG1
DAPI	4’,6-Diamidino-2-Phanylindole
DHH	Desert Hedgehog
DISP	Dispatched
DLL	Delta-like ligand
DMEM	Dulbecco’s Minimum Essential Medium

DMSO	Dimethylsulphoxide
DPD	dihydropyrimidine dehydrogenase
DTP	Developmental Therapeutic Program
ECM	extracellular matrix
EpSSG	European paediatric Soft tissue sarcoma study group
ER	estrogen receptor
ERK	Extracellular signal Regulated Kinase
ERMS	Embryonal RMS
ESC	Embryonic stem cells
FBS	Fetal Bovine Serum
FBXW7	F-box/WD repeat-containing protein 7
FDA	Food and Drug Administration
FGFR	Fibroblast growth factor receptor
FISH	fluorescence in situ hybridization
FOXO	Forkhead box O
Fz	Frizzled
GAS1	Growth arrest-specific gene 1
GEM	genetic-engineered mice
GEMM	Genetically engineered mouse models
GF	growth factor
GLI	Glioma-associated oncogene
GPCR	G-protein-coupled receptor
GSK3-β	glycogen synthase kinase 3 β
HBC	human breast cancer
HDAC1	histone deacetylase 1
HES	Hairy and enhancer of split-1
HEY	Hairy/enhancer-of-split related with YRPW motif protein1
Hh	Hedgehog
HHIP	Hedgehog-interacting protein
IGF	Insulin growth factor
IHC	immunoistochemistry
IHH	Indian Hedgehog
IRSG	Intergroup Rhabdomyosarcoma Study Group
JAG	Jagged
JFCR39	Japanese Foundation for Cancer Research
LEF1	Lymphoid enhancer-binding factor 1
LRP	lipoprotein receptor-related protein
MCL-1	Induced myeloid leukemia cell differentiation
MDM	Mouse double minute
MDR1	multidrug resistance protein 1
MEK	Mitogen-activated protein kinase
mESC	mouse embryonic stem cell
MM	multiple myeloma
MOMP	mitochondrial outer membrane permeabilization
MRF	myogenic-regulatory factors
MTOR	mammalian target of rapamycin
MYC	Myelocytomatosis oncogene
MYF	Myogenic factor
NCI	National Cancer Institute
NF1	Neurofibromin 1
NICD	Notch intracellular domain
NOS	not otherwise specified

NSCLC	non-small cell lung cancer
PCP	planar cell polarity
PDGFRA	Platelet-derived growth factor receptor A
PDX	patient-derived xenografts
PFN	PAX-fusion negative
PFP	PAX-fusion positive
PI3K	Phosphoinositide-3-kinase
PKA	Protein kinase A
PLK1	Polo-like Kinase 1
PPTP	Pediatric Preclinical Testing Program
PUMA	P-53 upregulated modulator of apoptosis
qRT-PCR	quantitative Real-Time Polymerase Chain Reaction
RAS	Renin-Angiotensin System
RBPJ	Recombination signal binding protein for immunoglobulin Kappa J region
RMS	Rhabdomyosarcoma
RPCs	RMS primary cultures
RT	radiotherapy
SC	stem cell
SFRP3	secreted frizzled-related protein 3
sgRNA	small guide RNA
SHH	Sonic hedgehog
SMN	second malignant neoplasm
SMO	Smoothened
SSR	site-specific-recombinase
SUFU	suppressed of fused
Tam	4-hydroxytamoxifen
TCF/LEF	T-cell factor/lymphois-enhancer factor
TIC	tumor-initiating cell
TMZ	temozolomide
TRE	tet-regulatory elements
tTA	tetracycline transactivator protein
WNT	Wingless related integration site

4. Introduction[1]

4.1. Cancer: a general overview

Cancer is a group of diseases characterized by an abnormal growth of "malignant" cells, able to invade their surrounding stroma and eventually spread throughout the body. It represents the second leading cause of death with about 22,000 deceases a day worldwide and is predicted to rise by 40% in 2030 [1, 2].

There are more than 100 types of cancers, which can be classified into four main groups based on their histological origin: carcinoma (from epithelial cells), sarcoma (from mesenchymal cells), hematological tumors (from blood cells) and neuroectodermal malignancies (from cells of the nervous system). A report from 2012 estimated that in adults, cancers of the lung, the prostate, the breast and the colon are the most common and account for the majority of cancer-related deaths worldwide (Figure 1A, right) [1]. A different scenario is observed for childhood cancers (0-14 years), which have a different incidence and tumor spectrum. For instance, they represent less than 2% of the global cancer burden albeit remain a leading cause of death in children in developed countries. Children develop mostly hematologic tumors followed by brain tumors and sarcoma (Figure 1A, left) [3, 4]. The causative mechanisms of cancer can be intrinsic or extrinsic. Among intrinsic mechanisms we find genetic alterations that can be hereditary or caused by random accidents of nature [5, 6]. Extrinsic factors include mainly exposure to chemicals (i.e. asbestos, benzene etc.), physical agents (ionizing and non-ionizing radiation) or biological components (virus or bacteria) as well as age and life style (exercise, tobacco or alcohol consumption etc.). Each of these factors, directly or indirectly, can promote the transition of a single cell (monoclonal model) or multiple cells (polyclonal model) from a "normal" to a "malignant" state. At the molecular level, this is a multistep process in which cells gradually acquire the ability to switch on pro-proliferative, anti-apoptotic and self-sufficient growth signals through both genetic and epigenetic changes that ultimately lead to the formation of a tumor mass with the potential to metastasize (Figure 1B) [7, 8]. It is now clear that such structure is composed of genotypically and phenotypically distinct tumor cells, which also collaborate with stromal counterparts to build up a well-defined cancer ecosystem protected from immuno detection and provided of oxygen and nutrient supply (Figure 1B) [9, 10]. The evidence of these malignant traits can explain why treatment remains still a challenging task for the majority of cancer types. In principle, the ideal therapy aims at the cessation of the tumorigenic state by inducing cell death, senescence or differentiation while sparing normal cells. To do so, an important prerequisite is the availability of pre-clinical models being discussed in the next chapter.

[1] The paragraphs 4.6.2.3, 4.6.2.3.1, chapter 4.7 and paragraph 7.4 have been adapted from the published review: Manzella, G. and Schäfer, B.W., Interfering with Hedgehog Pathway: *New Avenues for Targeted Therapy in Rhabdomyosarcoma. Current drug targets*, 2016. **17**(11): p.1228-1234.

A

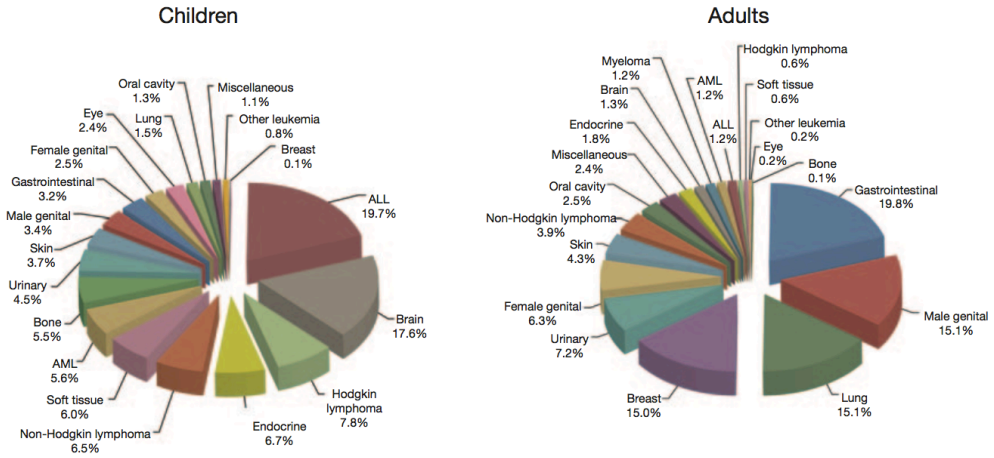

B

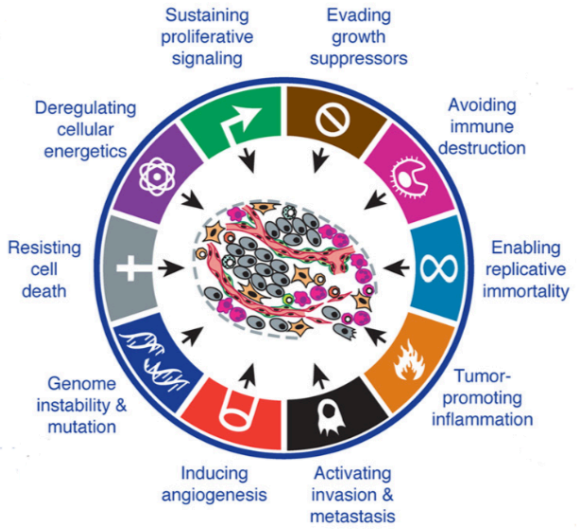

Figure 1. Frequency of cancer in children and adults and Hallmarks of cancer. (A) Frequency of cancer diagnosed in children (left) and adults (right) according to 2012 Surveillance, Epidemiology and End Results (SEER) data. Adapted from [3]. **(B)** The 10 malignant traits characterizing cancer. Adapted from [10].

4.2. Pre-clinical models of cancer

The final goal of cancer research is to find medical agents of clinical benefit. They include nonspecific cytotoxic chemotherapeutics, which interfere with rapidly dividing cells irrespective of normal or cancerous phenotype and targeted therapy, which is oriented towards a cancer specific vulnerability. If chemotherapy remains the standard of care for the majority of cancers, molecular-oriented compounds are also on their way to the clinic. Successful examples of these are retinoic

acid for treatment of leukemia bearing *PML-RARα* translocation, herceptin for HER2+ breast cancers and gleevec for BCR-ABL+ chronic myeloid leukemia (CML) patients [11]. To achieve this, both basic and translational research rely on the use of pre-clinical models that can serve as tools to study the biology of cancer and design new treatment strategies [12]. Both *in vitro* and *in vivo* models are widely used in pre-clinical settings and each of them has strengths and weaknesses.

4.2.1. *In vitro* models

4.2.1.1. Cancer cell lines: historical perspective

In 1952 Gey and colleagues established the first human cancer cell line, which was derived from an adenocarcinama of the cervix and named Hela (Figure 2) [13, 14]. They reported a "continuous culture for almost 1 year in a mixture of chicken plasma, bovine embryo extract and human placenta cord serum" [15]. This was also the period when Dulbecco described the first procedures of propagation of monolayer cultures through the use of trypsin, which is routinely used in standard culture protocols nowadays [16]. Only few years later, traditional cell culture media were defined in order to limit the variability of biological fluids or tissue extracts, and together with the development of methods of cryopreservation, boosted the generation of cancer cell lines from a wide range of tumor types [16-18]. However, in the late 1970s, the validity of cancer cell lines as pre-clinical model was questioned by the study of Nelson and Flandermeyer who documented an inter- and intraspecies contamination of most of the cell cultures available at that time (279 cell lines) [19]. Thus, most of the pre-clinical platforms were based on mouse allograft models of which the Developmental Therapeutic Program (DTP) from the National Cancer Institute (NCI) is a well-known example since 1955. Over almost 30 years of drug testing, only few compounds entered the clinic comprising mostly cytotoxic drugs (i.e. vincristine and procarbazine), and later on was clearly demonstrated the poor predictive value of such models [20-22]. Based on these disappointing data, cancer cell lines caught again the attention as new tools to anticipate drug response in cancer patients. The pioneering initiative in this direction was the National Cancer Institute 60 (NCI60) program launched in the late 1980s, intended to offer a new anticancer screen platform able to interrogate a panel of 60 cancer cell lines (representative of 9 tumor types) for the response to 10.000 compounds a year [23]. This big scientific effort, represented not only the base for future high-throughput technologies, but led to the discovery of new candidate anticancer agents. One example, is the proteasome inhibitor bortezomib, which was approved by US Food and Drug Administration (FDA) for the treatment of myeloma only 8 years since its discovery [23]. Additionally, the Japanese Foundation for Cancer Research (JFCR39) platform in 1999 and the Molecular Therapeutic 1000 (CMT1000) screen in 2006 were established with the goal in mind of increasing the repertoire of cancer cell lines for drug profile

and facilitate data extrapolation based on new data mining techniques able to predict mechanisms of action of new compounds (Figure 2) [18, 23]. Importantly, with the advent of new genomic- and transcriptomic-based technologies, it was possible to integrate mutational information or gene expression signatures with drug sensitivities, which opened the possibility of stratifying patients according to molecular attributes rather than to histiopathologic proprieties [18]. This underscores also the enormous heterogeneity across cancer patients and raises the question to which extent cancer cell lines or patient-derived cells can capture the inter- and intra-tumor diversity.

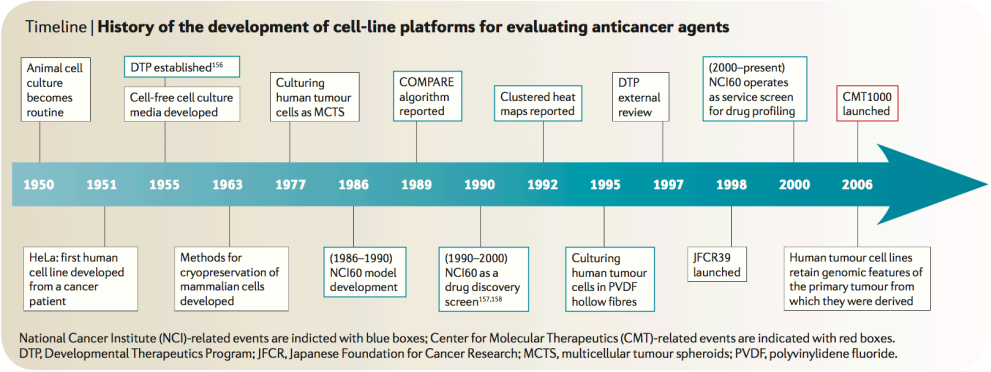

Figure 2. Timeline of the key discoveries for the establishment of *in vitro* pre-clinical models. Adapted from [18].

4.2.1.2. Cancer cell lines and patient-derived cells: the pros and cons

As mentioned above, 2D culture of cancer cells is a gold standard model for cancer research that helped to increase our current understanding of the molecular circuitry of cancer as well as to identify molecular targets for translation research purposes. An easy explanation for their widespread use can be ascribed to three main characteristics: 1) easy to manipulate and propagate, 2) suitable for large high-throughput approaches and 3) circumvent ethical issues and challenges associated with labor-intensive and time consuming animal models [24]. However, monolayer cell cultures cannot suit the perfect cancer model and inherent caveats should be taken into considerations according to the research question to address. For instance, an important criticism accompanying this model is that it lacks of heterotypic interactions with stromal cells, a functional relevant feature of the primary tumor (Figure 3). As consequence, only cell-autonomous effects can be assessed, thus precluding the possibility of identifying cancer vulnerabilities dependent on the microenvironment (i.e. vasculature, immune system etc.) or leading to misinterpretation regarding the importance of relevant signaling pathways [25, 26]. Also, repeatedly *in vitro* passaged cancer cell lines are often associated with “plastic” artifacts

due to genomic instability and are selected for high proliferative cells leading to a loss of tumor heterogeneity (Figure 3) [12, 27, 28]. However, these limitations might be mitigated with the use of short-term culture of patient-derived cells, which can also accomplish the important function of maintaining the representation of rare cancers for *in vitro* biological studies [25]. Furthermore, patient-derived cells might replace the multitude of misidentified cancer cell lines still in circulation among the scientific community and also extend the knowledge of patient-to-patient variability for personalized medicine interventions [19, 25]. Nevertheless, their derivation is often limited by the size of the tumor biopsies or technical difficulties. Hence, new culture methods have been recently described for certain cancers together with new biologically relevant *in vitro* model systems [18, 26, 29, 30].

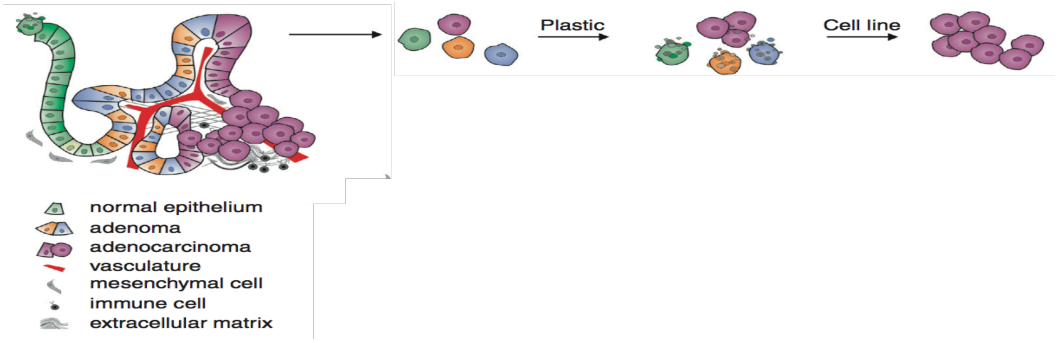

Figure 3. Derivation of cell lines from the primary tumor. Schematic representation of the two main drawbacks associated with traditional approach of culturing cancer cell lines namely loss of tumor microenviroment and clonal selection. Modified from [31].

4.2.1.3. 3D models: a lesson from developmental biology for the formation of tumor organoids

Tumor organoids can be simply described as cancer cells embedded in a three-dimensional (3D) matrix, which can self-organize in an organ-like structure reminiscent of the original tumor architecture. The idea of expanding normal tissues *ex vivo* is an old concept that started in the early 1900's with the hanging drop method for culturing tissue fragments, which was further refined in the 1950's with the studies of chicken embryogenesis [32, 33]. Twenty years later, the extracellular matrix (ECM) was recognized as a critical component of tissues that can affect cell morphogenesis and differentiation (i.e. hepatocytes and mammary epithelial cells), a feature that could not be mimicked on simple plastic [34]. Notably, with the discovery of matrigel in 1977 (matrix extracted from chondrosarcomas) and the establishment of the first mouse embryonic stem cell (mESC) line in 1981, researchers had all the tools to recapitulate mechanisms of

organogenesis in complex 3D *in vitro* systems [34, 35]. However, only with the seminal studies of Hans Clevers and Yoshiki Sasai in the late 2000's that organoids became popular among the scientific community [24]. Indeed, mini organ-like structures could be finally established by combining defined culture conditions mimicking the specific tissue microenviroment together with the use of stem cells or progenitor cells and matrix support (Figure 4). These structures fulfill two important characteristics of morphogenesis namely cell segregation and fate specification of progenitor cells [35]. Consequently, they have important implications in disease modeling such as infectious and degenerative diseases as well as cancer.

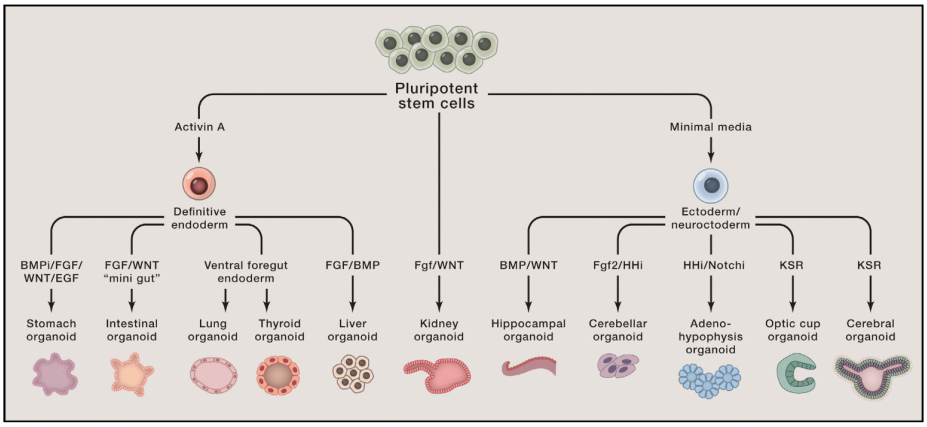

Figure 4. Schematic overview of the current organoids generated from PSCs. Adapted from **[36].**

4.2.1.4. Tumor organoids as preclinical model

Tumor organoids represent the evolution of 2D cancer cell lines and cover the "dimensionality" of *in vivo* tumor models (Figure 5). Currently, they have been established from a variety of cancer entities including colorectal, prostate, pancreas and glioblastoma tumors [37-40]. Due to their spatial organization, tumor organoids are suitable to capture the heterogenic cellular distribution and to study how this is influenced by the tumor microenviroment including exposure to nutrients, oxygen and growth factors although this occurs by simple diffusion. For instance, in glioblastoma-derived organoids it was possible to recapitulate the perivascular and hypoxic niche characterizing the primary tumor specimens. In particular, a defined hierarchical organization of the tumor cells was observed, with proliferative $SOX2^{+}$ cancer-stem cells (CSCs) populating the periphery of the organoids close to the differentiated and radiosensitive $SOX2^{-}$ cells whereas quiescent and radioresistant CSCs were confined to the hypoxic regions. Therefore, this enables the investigation of dynamic changes within phenotypically and functionally diverse cancer cell subpopulations, which might affect therapy response [40]. Similarly, organoids derived from early and late stage colorectal cancer patients offered an *in vitro* platform to investigate niche factor

requirements during cancer evolution along with occurring genetic alterations [41]. This latter could be modeled in engineered organoids via Cripr/CAS9 and helped to clarify that driver mutations followed by genomic instability are needed for the invasive behavior of colorectal cancers [42]. Such study also highlights the feasibility of genetic manipulation in tumor organoids. Despite recent findings pointing towards implementation of tumor organoids for precision medicine strategies, still it may take some time before this methodology enters co-clinical programs. In fact, high-throughput drug screens in tumor organoids require considerable expertise and the heterogeneity in size, shape and drug penetration can complicate the reproducibility of drug-response analysis [43]. Similar to cancer cell lines, tumor organoids lack the cellular microenviroment albeit "heterotypic organoids" might be explored in the near future. Yet, the 3D architecture is not amenable to blood tumors, accounting for a large fraction of all human cancers and for which *in vitro* studies are still hampered by the absence of efficient culture methods. Overall, tumor organoids can be viewed as a "young" but attractive and promising predictive technology that falls in between traditional cancer cell lines and *in vivo* mouse models of cancer.

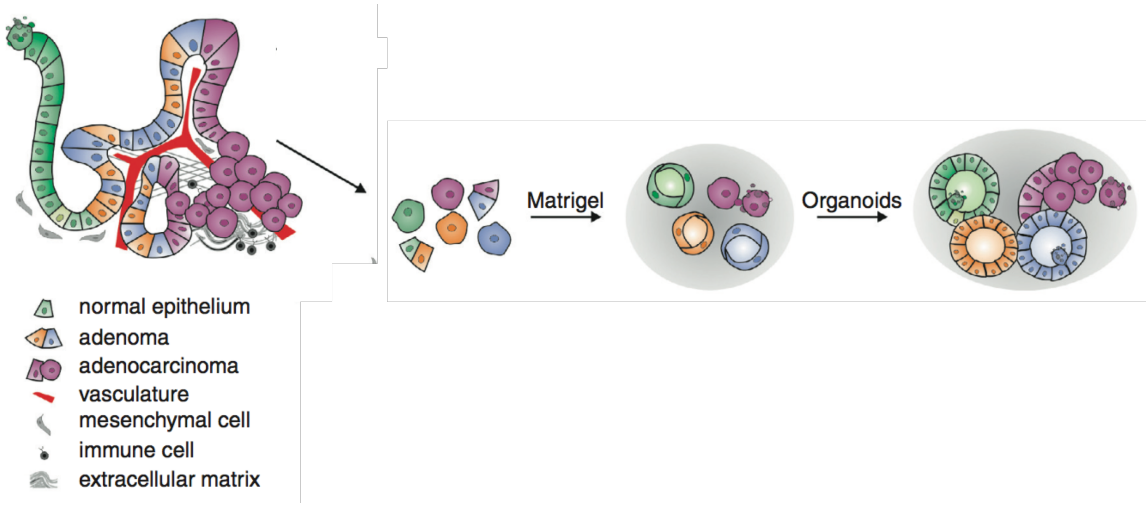

Figure 5. Generation of tumor organoids. Organoids can be generated upon embedding tumor-derived cell suspensions in matrigel and under defined culture conditions. Clonal heterogeneity and tissue architecture can be preserved but similar to cancer cell lines, only homotypic interactions are present. Modified from [31].

4.2.2. *In vivo* models: Mouse models

Mice constitute a versatile tool for modeling human diseases due to their close genomic (including disease-related genes) and anatomic similarity to humans, relatively easy to handle, little in size and the fact that they multiply quickly. However, important differences exist including transcription regulation, chromatin organization, immune system, drug metabolism and lifetime [44, 45]. Hence, which would be the most appropriate predictive model of human cancer? Ideally,

tumors resembling the human counterpart should arise from genetic lesions and/or environmental factors responsible for human cancers through a multistep process occurring in a native microenvironment [46]. Although many of these features could be recapitulated in genetic-engineered mice (GEM) and carcinogen-induced cancer models, still the molecular and cellular diversity encountered in cancer patients might be better preserved in patient-derived xenografts (PDXs). Some of these models will be discussed in the next paragraph.

4.2.2.1. PDX models

PDX models are generated by implantation of freshly resected tumor biopsies as tumor pieces or cell suspensions in immunodeficient mice (often NOD/SCID and NOD/SCID/IL2λ-receptor null (NSG)) either subcutaneously or orthotopically (Figure 6). Since tumor tissues are expanded and maintained in a more physiological environment *in vivo*, PDXs are considered to provide a better approximation of human tumor biology than cell-derived xenografts (CDXs), which are generated from transplantation of cancer cell lines adapted to thrive on plastic. Accordingly, several studies demonstrated a general preservation of tumor patient characteristics in these non-autochthonous models in terms of genetic and transcriptomic landscape as well as histopathologic features although continuous mouse-to-mouse passages are associated with a progressive replacement of human with murine stroma [47]. Such validations can be performed by copy number variants (CNVs) analysis and DNA sequencing to study the clonal composition, immunoistochemistry (IHC) to detect lineage-specific markers and RNA sequencing approaches to confirm concordance of gene expression profiles between tumor donor and PDX [47]. Despite the fact that expanding patient-derived tumor tissues directly into mice is not a new concept, only recently there has been a renewed interest in PDX models from both the industry and academia. Probably this is due to an increasing availability of systematic clinical data annotation and sample collections, accessibility to novel and more affordable genome sequencing technologies for tumor characterization along with the recognized failure of traditional pre-clinical platforms. In fact, PDX models have major advantages for drug development studies. They offer the unique opportunity of simulating clinical trials in a population of PDX carrying mice reflecting the inter-patient and intra-tumor heterogeneity encountered in the clinic. This is demonstrated by the close treatment response concordance (~ 90%) between PDX and original tumors achieved in human breast cancer (HBC) or non-small cell lung cancer (NSCLC) [48-50]. Such phenotype is not limited to conventional therapies but can be also extended to targeted agents as observed for the anticipated resistance to MEK, PI3K/mTOR and EGFR inhibitors in KRAS-mutant colorectal PDX models [47]. Hence, PDX-based pre-clinical trials might inform on patient stratifications and guide decision-making process for treatment. In line with this, a parallel drug testing in PDX models and humans has been proposed for a real-time assessment of treatment response, which can provide

alternative treatment modalities for the patient and integrate functional information about potential resistance mechanisms (reviewed in [51]). Although ongoing trials demonstrate the feasibility of these approaches, the establishment of PDXs is often hampered by the low take-rate and the long time of engraftment [51]. In fact this can be affected by different variables such as mouse strain, site of inoculation, tumor type (i.e. NSCLCs have a high take rate) or subtype (i.e. metastatic or recurrent tumors are often over-represented) [47]. To limit the cost, enlarge the spectrum of compounds to test and obtain predictive information in a beneficial time frame for the patient, the "one mouse, one patient paradigm" has been proposed [52, 53]. The experimental model posits that treatment in individual mice carrying independent patient-derived tumors can reflect the response of a larger population, thus encompasses the need of using large cohorts of mice. However, the lack of human stroma and intact immune system are the major drawbacks of these models, which can be partially overcome with the new "humanized" mouse models although they are still in their infancy and currently remain challenging and expensive [54].

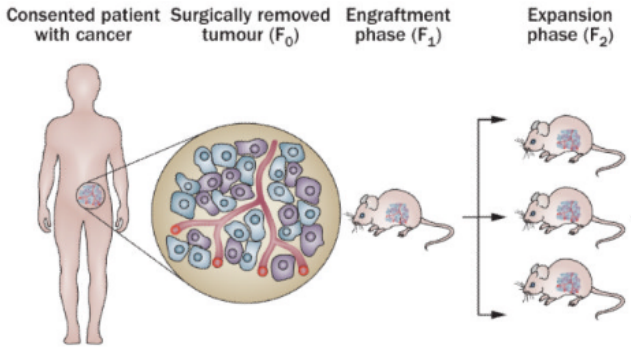

Figure 6. Establishment of PDX models. Tumor biopsies from cancer patients are directly implanted into the mouse host. After a variable latency phase, tumors eventually grow and can be further expanded in a new cohort to perform biological studies. This system prevents plastic adaptation, preserves molecular and cellular characteristics of the original specimen but *in vivo* passages are associated with a gradually loss of the human stroma. Modified from [55].

4.2.2.2. GEMM

Genetically engineered mouse models (GEMM) provide an *autochthonous* system to model *de novo* cancer formation and progression upon genetic manipulation of the host genome. They can be simply classified in transgenic and endogenous GEMM (Figure 7). In transgenic GEMM, the transgene (i.e. exogenous cDNA encoding for an oncogene or a dominant negative tumor suppressor gene) is expressed at non-physiological levels under either constitutive or lineage specific promoters into the germline (Embryonic stem cells (ESCs)) or somatic cells (tissue-directed expression via adenoviral constructs) (Figure 7A) [56]. Also, spatiotemporal regulation of the transgene can be achieved via two common methods, the tetracycline (tet)-inducible system

or tamoxifen-regulatable proteins (Figure 7A) [57, 58]. Briefly, in the former case, tet-regulatory elements (TRE) are placed upstream of a minimal promoter driving the expression of the cDNA of interest whereas the tetracycline transactivator protein (tTA) or its mutated form (rtTA) is controlled by tissue-specific promoters. In presence of doxocycline, a tetracycline derivative, tTA binding is displaced from TRE and the expression of the target gene is inhibited (TET-OFF) whereas rtTA binding is induced thus promoting transcription of the gene product (TET-ON) (Figure 7A, upper and middle panel).

The tamoxifen system is mostly used to generate inducible transcription factors or recombinases. Here, a tissue-specific promoter drives the expression of the target fused to the estrogen receptor (ER), which hijacks the regulated protein into the cytosol in its inactivated form. Hence, the presence of the ER ligand, 4-hydroxytamoxifen (Tam) promotes the nuclear translocation of the active chimeric product (Figure 7A, lower panel).

In endogenous GEMM, traditional or novel genomic targeting tools (i.e. spontaneous homologous recombination, engineered nucleases and CRISPR/CAS9 system) enable genome-editing modifications (i.e. knock-out or knock-in) at the endogenous loci of ESCs [56]. Thus, deletion of tumor suppressor genes or insertion of cancer-specific mutations can be applied under their native regulatory machineries. Also in this case, conditional models are available, which rely on site-specific-recombinase (SSR) systems such as the CRE-loxP technology (Figure 7B) [59]. This method is based on the tissue-specific or inducible expression of the recombinase CRE and insertion of pair of inverted DNA elements, or loxP sites (elements recognized by CRE) in the gene of interest. LoxP sites can flank a particular exon of the target sequence and depending on their orientation, CRE can induce deletion or inversion thus disrupting the gene function. Otherwise, a stop codon flanked by loxP can be placed to suppress gene function, which can be reversed by the CRE-mediated excision of the STOP codon. Conditional knock-out not only allows a spatio-temporal control but can bypass embryonic lethality following genetic manipulations in the germline. Generally, GEMM are particularly suitable models to study homeotypic tumor-stroma interactions and dissect the role of the tumor microenviroment or immune system in cancer [54]. For example, by using GEMM was possible to functionally explore the contribution of mutations found in human stromal compartments and their implication in tumorigenesis as revealed for Tp53 deficiency or loss of TGF-β responsiveness in mouse fibroblasts that accelerates prostate cancer [60, 61]. Also, it was documented an augmented aggressiveness of skin cancer following metalloproteinase supply of bone marrow-derived cells or that mice depleted of Tp53 and Perforin expression are predisposed to lymphoma, a phenotype that is partially dependent on cytotoxic CD8(+) T lymphocytes [62, 63]. Importantly, GEMM helped not only in understanding the tumor promoting features of several oncogenes but also to distinguish their role a different phases of cancer progression. The most notable example is the TGF-β paradox in cancer, a cytokine that can elicit tumor-promoting or suppressive functions

depending on the stage of the tumor [64]. Probably, one of the most exciting applications of GEMM remains the possibility of investigating the cell-of-origin in cancer, which may have relevant implications for the design of therapies or detection of early-disease biomarkers [65]. More importantly, key studies demonstrate the rationale of using GEMM as pre-clinical platform to validate the response of targeted therapies or combination strategies in murine tumors harboring mutations similar to those found in human cancers [66-68]. Accordingly, it has been proposed the use of GEMM for testing therapies in defined genetic contexts that guides clinicians in the identification of the best treatment for a particular group of patients [69]. However, similar to PDX models, also GEMM are expensive and laborious as well as require specialized expertise to deal with extensive complex breeding. Additional shortcomings include the poor genetic variability of the tumors and the non-synchronous tumorigenesis [11]. Taken together, GEMM share to a certain extent, common characteristics with other *in vivo* models but they faithfully recapitulate not only cell-intrinsic but also cell-extrinsic proprieties of cancer.

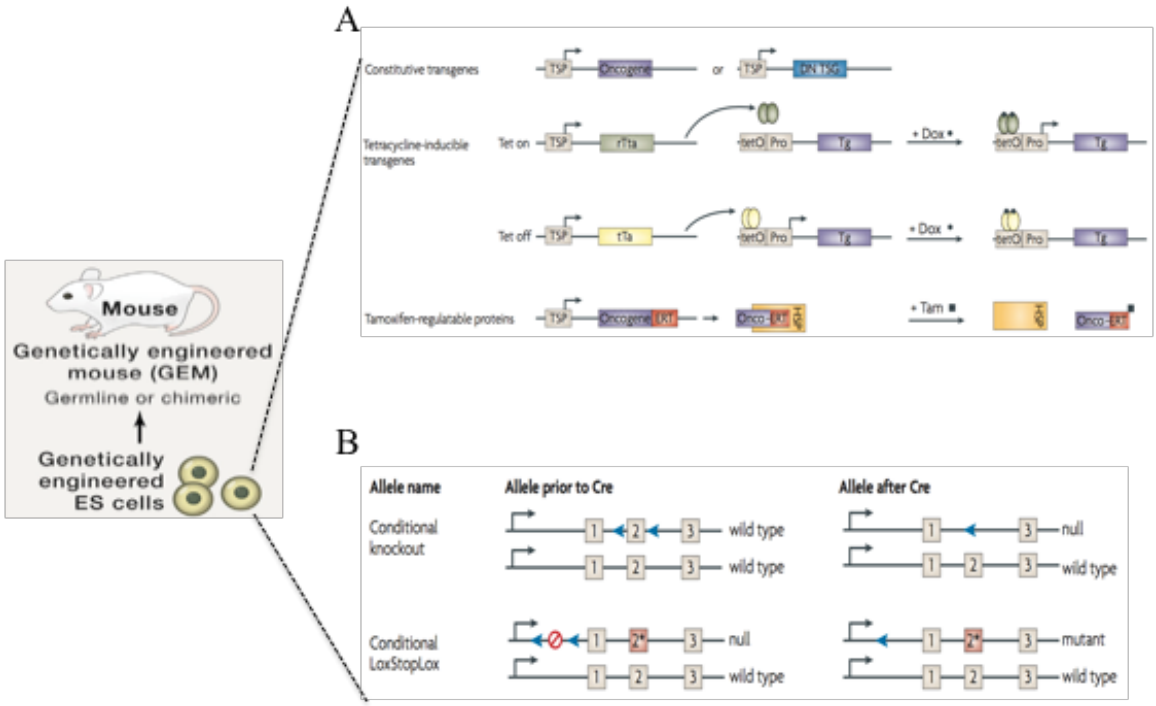

Figure 7. Transgenic and endogenous GEMM. (A) Transgenic GEMM. (A, upper panel) Constitutive and inducible expression of an oncogene or a dominant negative tumor-suppressor gene (DN TSG) under an exogenous tissue-specific promoter (TSP). **(A, middle panel)** Tetracycline-Inducible expression of the transgene (Tg) via TET-ON (doxocycline triggers the expression of Tg) or TET-OFF system (doxocycline blocks transcription of Tg). **(A, lower panel)** Inducible expression of the oncogene via the tamoxifen system. The protein of interest is fused to the estrogen receptor (ERT) and is sequestered into the cytosol by the heat shock protein (HSP) whereas the presence of tamoxifen (TAM) activates the chimeric product. **(B) Conditional endogenous GEMM. (B, upper panel)** The recombinase CRE can be expressed to induce gene knock-out via recognition of the LoxP sites (blue arrowheads) flanking an exon of interest placed in the same orientation**.** Also, a stop codon flanked by LoxP sites can be inserted into a gene of interest previously mutated (asterix denotes mutations) to inhibit its expression. Only in presence

of CRE, the mutated allele can be re-expressed via excision of the stop codon **(B, lower panel)**. Modifed from [11, 56].

4.3. Chemoresistance in cancer: intrinsic and acquired resistance

In the early 1900s, Paul Ehrlich coined the word “Chemotherapy” to describe the use of chemicals as therapy for disease. Thereafter, most of the drugs originally used for cancer treatment included nitrogen mustard, folate antagonists (i.e. methotrexate), antibiotics (i.e. actinomycin D), thiopurines (i.e. 5-fluorouracil (5-FU)), plant alkaloids (i.e. procarbazine), and corticoids [22]. They were developed with the idea of killing cancer cells without a real rationale for their tumor specificity and represent what we commonly call “standard chemotherapy”. Despite the general skepticism on their application in patients in 1960s due to their side effects, the subsequent adjustment of treatment protocols, the availability of alternative pre-clinical models, the implementation of new drug combinations and multimodal schedules led to a remarkable improvement in progression-free survival of cancer patients. The best examples remain leukemia, Hodgkin’s disease and metastatic testicular cancers [70-72]. Interestingly, also in the era of the “targeted therapy”, cytotoxic drugs are still considered the standard of care treatment for a wide range of cancer entities. Nonetheless, nowadays, complete eradication of cancer is at least partially hindered by the onset of relapse disease following resistance to both conventional and molecularly targeted therapy.

Drug resistance can emerge as *de novo* self-defense mechanism to counteract anti-cancer therapy (acquired resistance) or be a native characteristic of the tumor that preexists prior to treatment (intrinsic resistance). Although in the first scenario, genetic determinants cannot be excluded, it is more likely that the exposure to the drug can induce an adaptation process from a drug sensitive to a drug-tolerant phenotype trough epigenetic changes and/or fluctuations in gene expression. Hence, cells surviving to the selective pressure of the drug, can be further selected and promote the emergence of a resistant population [73-75]. This dynamically survival strategy might explain why some relapsed cancers can be re-sensitized to the initial treatment upon a period of “drug holyday” [76, 77]. In the second case, intrinsically resistant subpopulations are present in the bulk of the tumor before treatment start and eventually outgrow under drug therapy. Re-population of the lesion can be driven by few hundreds to thousands cells and occur over a long time frame as demonstrated for chemorefractory metastatic colorectal cancer (CRC) receiving an EGFR inhibitor (ponatinib) [78]. Therefore, assuming a tumor mass composed of 10^9 cells, one would expect to find one resistant cell (neutral prior to treatment) in a million cells [79]. The proportion of resistant cells harboring a mutation that also increases the fitness of the cell independently on the treatment is anticipated to be intuitively higher. Paradoxically, even deleterious resistant mutations (conferring low fitness) are predicted to still populate late-stage cancers [80]. Beside the genetic heterogeneity, also non-genetic alterations can play a pivotal

role in intrinsic cancer resistance including aberrant activity of signaling pathways, drug target modulation (changes in expression levels), cell cycle arrest, metabolic reprogramming and epigenetic changes [81-83]. Each of these functional proprieties can be incorporated by the CSCs, which are recognized as relevant mediators of drug resistance since are often spared by chemotherapy [84]. CSCs and the underlying molecular mechanisms of drug resistance will be described in the next paragraph.

4.3.1. Cancer stem cells and chemoresistance

CSCs are defined as tumor-initiating cells (TICs) characterized by self-renewal ability, multi-lineage differentiation potential, long-term tumorigenicity and are especially refractory to conventional anti-mitotic agents (Figure 8A) [85-87]. Due to their similarity to stem cells (SCc), CSCs are believed to arise from genetic or epigenetic alterations of their normal counterpart. This is also in line with the view that they can give rise to a tumor progeny composed of cells at distinct stages of differentiation reflecting the lineage hierarchy of the tissue of origin [87]. For example, CSCs in pediatric brain tumors resemble neural stem cells sharing the propensity to generate neural-lineage cells (i.e. neurons and glia) when transplanted *in vivo* [88]. However, it has been postulated that CSCs might also originate from a more mature cell type via a de-differentiation process that promotes stemness [89-91]. The CSC model is particularly fascinating as it looks at cancer as an abnormal organ that conserves mechanisms operating during normal development and organ function. Indeed, SCs are essential for morphogenesis at the embryonic stage and for tissue homeostasis later on, thereby contributing to a tight balance of tissue-specific SC pools and differentiated cells during tissue turnover and repair [92]. Similarly, CSCs are expected to restore the tumor hierarchy upon exogenous insults such as chemotherapy or radiotherapy thus promoting cancer relapse. In support of this hypothesis, an elegant lineage tracing study in GEMM of glioblastoma demonstrated that nestin^{+} CSCs (GFP labeled) were left behind by temozolomide (TMZ) treatment, an alkylating agent used for the management of brain cancer patients [93]. Interestingly, tumor could be re-established by the residual GFP^{+} cells upon drug withdraw and ablation of this subset of cells impaired tumor development. Accordingly, two independent studies showed that leukemia initiating cells present in untreated tumors were enriched upon chemotherapy and could drive relapse disease [94, 95].

Several molecular mechanisms of drug resistance have been attributed to CSCs including over-expression of drug efflux pumps or detoxifying enzymes, quiescence, capacity to survive DNA damage mediated by overexpression of DNA repair systems and evasion of apoptosis (Figure 8A) [81, 84, 92].

Cells can take up drug molecules via either active transport or passive diffusion but the mechanism whereby chemotherapy gets into cells is poorly understood. Nevertheless, de-

regulation of drug uptake constitutes an obvious “escape” system for cancer cells to get rid of cytotoxic drugs. The most studied transporters in the context of drug resistance are the ATP-binding cassette (ABC) efflux pumps, which actively transport drugs out of cells. Among them, ABCB1 (or multidrug resistance protein 1, MDR1), ABCG2 (or breast cancer resistance protein) and ABCC1 (or multidrug resistance associated protein 1) have been shown to be up-regulated in many cancers and to correlate with poor overall survival [82, 96-98]. A second barrier mounted by cancer cells to counteract the effect of chemotherapeutics is drug inactivation. In this regard, dihydropyrimidine dehydrogenase (DPD) and Aldehyde Dehydrogenase 1 (ALDH1), are well known detoxifying enzymes conferring resistance to 5-FU and alkylating agents, respectively [82, 99]. As consequence, the activity of both ABC transporters and ALDH1 are also used as surrogate markers to identify and purify CSCs in cancer. A further peculiarity of CSCs is their ability to hide from anti-mitotic drugs by slowing down the cell cycle reaching a quiescent state, a way to repair DNA, avoid additional deleterious mutations and escape apoptosis [92]. Furthermore, cell cycle restriction can be induced by environmental clues, including physical interaction with the niche (i.e. bone morrow for leukemic blasts) or by niche-derived factors (i.e. endothelial derived thrombospondin 1 for dormant breast cancer cells) [100-103]. Probably, this plasticity might explain the long time needed before tumor recurrence occurs and represents the main hurdle to conventional anti-cancer agents targeting active cycling cells either in the S (DNA damaging agents) or M phase (anti-mitotic compounds). Hence, the killing rate of a drug does not necessary correlate with a therapeutic benefit since resistant clones might be refractory to the treatment. On the other hand, compounds with a low killing rate but targeting resistant clones, are anticipated to be paradoxically more efficient in tumor control or eradication (Figure 8B) [79].

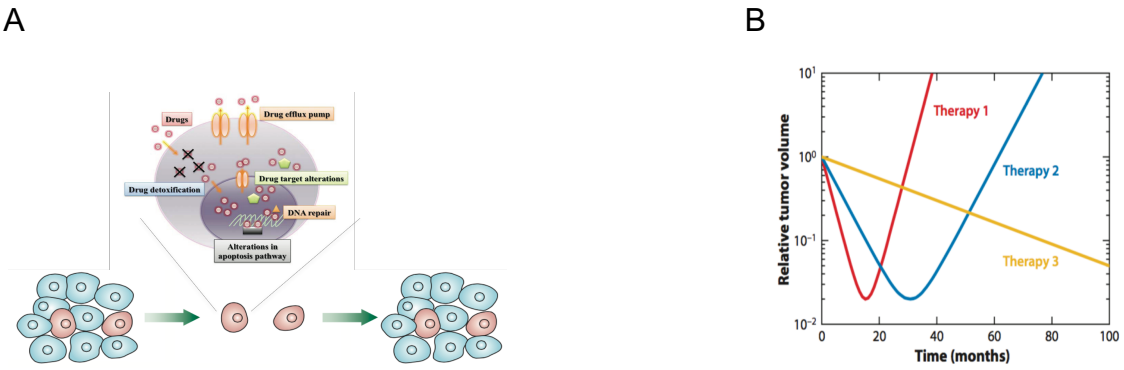

Figure 8. Intrinsic model of chemoresistance following the CSC model and therapeutic challenges. (A) CSCs (red) are intrinsically resistant to conventional treatment through several molecular mechanisms including altered drug efflux, drug target, DNA repair, apoptosis and increased detoxification ability. Therefore CSCs are selected following treatment and can re-populate the tumor lesion. Modified from [104, 105] **(B)** Mathematical model depicting three scenarios: Therapy 1 and 2 with the highest killing rate are initially more effective (first year) but

eventually fail longer control of cancer. However, therapy 3 with the lowest killing activity but specific for resistant clones leads to tumor eradication. Adapted from [79].

4.3.2. Evading apoptosis and chemoresistance

Although conventional chemotherapy remains the mainstay of cancer treatment, its mode of action has been poorly understood so far. The original rationale relied on the assumption that anticancer agents should interfere with the high division rate of cancer cells, which would be more vulnerable than normal cells. This basic idea is probably the key of success for traditional cytotoxic agents and would justify their therapeutic window observed in cancer patients. However, it does not explain why some high proliferative tumors are resistant and some low cycling cancers are more sensitive to chemotherapy [106]. Albeit many of the factors mentioned earlier can play a role, one possibility is that cancers might be differentially susceptible " to die". One of the most studied form of cell death is apoptosis or programmed cell death characterized by cell shrinkage, chromatin condensation and DNA fragmentation, membrane blebbing followed by the formation of apoptotic bodies ready to be phagocytosed by macrophages [107]. Disabling apoptosis is one of the pre-requisites needed for a cell to become cancerous but does not mean that tumor cells are insensitive to apoptotic stimuli [9, 10, 108]. Paradoxically, the oncogenic stress present in malignant cells can lower their apoptotic threshold, a phenomenon known as "priming" for death (Figure 9) [106, 109]. Indeed, two landmark studies demonstrated that cancers not only are more primed to die than normal tissues but that priming is also an indicator of chemosensitivity or risk of recurrence (Figure 9) [106, 110]. A corollary is that when tumors encounter apoptotic signals such as those provoked by chemotherapeutics, is likely that a selection process of cells evading apoptosis takes place and contributes to chemoresistance [108].

Death signaling from chemotherapy, ultimately lead to either activation of pro-apoptotic signaling or inhibition of pro-survival factors. One example is the BCL-2 family, which mainly mediates the intrinsic apoptosis or mitochondrial pathway. This family includes "effectors" (BAX and BAK), activators (BIM, BID and PUMA), sensitizers (NOXA, BAD and BMF) and inhibitors (BCL-2, BCL-XL, MCL-1, BFL/A1 and BCL-B) of apoptosis [111]. Hence, in presence of a stress signal (i.e. chemotherapy), pro-apoptotic "effectors" can be activated and their oligomerization promotes mitochondrial outer membrane permeabilization (MOMP) followed by cytocrome C release into the cytosol. Here, it promotes the formation of the apoptosome, a complex composed of the initiator caspase 9 and the apoptosis protease-activating factor 1 (APAF), leading to proteolytic activation of the executioner caspases (caspase 3 and 7) and cell death [82].

Both BCl-2 and BCL-XL over-expression and combined BAX/BAK loss can confer resistance to chemotherapy, although genetic inactivation of BAX/BAK is rarely found in cancer [108, 112-115]. Furthermore, BAX, PUMA and NOXA are also transcriptional targets of TP-53, which is mutated in ~50% of cancer entities and often activated upon DNA damage to induce either apoptosis or

cell cycle arrest [116-119]. Therefore, it is not surprising that a non-functional TP-53 is accompanied with resistance to standard genotoxic chemotherapy regimens and worse prognosis.

The beauty of anti-apoptotic compounds targeting directly the mitochondrial machinery is that they can bypass the need of an intact TP-53. For instance, a small molecule inhibitor of BCL-2 (ABT-199) was recently approved by FDA for the treatment of chronic lymphocytic leukemia (CLL) patients harboring 17p chromosomal deletion (containing *TP-53*) [120]. Yet, promising results from phase II clinical trials in refractory acute myelogenous leukemia (AML) patients have been recently shown for ABT-199 as single agent [121]. The specificity of ABT-199 for BCL-2, overcomes the on-target thrombocytopenia associated with the inhibition of BCL-XL by ABT-263, a pan BH3 mimetic targeting BCL-2, BCL-XL and BLC-W [122]. However, pre-clinical data still support the use of low doses ABT-263 in combinatorial treatments (mainly with standard chemotherapy), which might be exploited also for non BCL-2 driven-malignancies (Figure 9C) [123-126]. The feasibility of targeting the apoptotic machinery by using for example BH3 mimetics that simulate the function of pro-apoptotic BCL-2 members, opened new avenues for cancer treatment and is demonstrated by the impressive responses observed in some cancer entities, mostly lymphomas. This renewed interest of pharmaceutical companies led also to the development of specific inhibitors of other BCL-2 members, such as BCL-XL and MCL-1, which already entered clinical trials for hematological malignancies. Since MCL-1 is well known to compensate for BCL-2 or BCL-XL inhibition, the combination of a specific inhibitor of MCL-1 and BCL-2 (or BCL-XL) might offer a valid approach to limit the onset of resistance to BH3 mimetics [127].

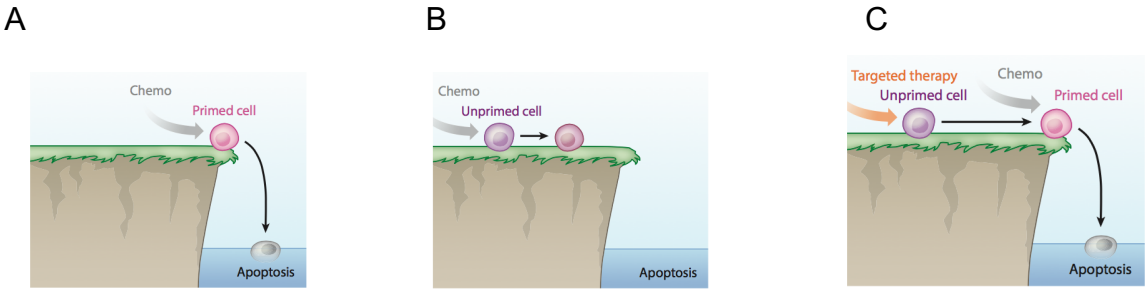

Figure 9. Priming for apoptosis and response to chemotherapy. (A) Cancer cells that are more close to the edge of apoptosis ("primed") are also more sensitive to further apoptotic stimuli (i.e the ones induced by chemotherapy) that induce irreversible commitment to cell death. **(B)** **"**Unprimed" cells are more resistant to the anti-cancer activity of cytotoxic drugs since they are more distant from the cliff's edge **(C)** "Unprimed" cells can be pushed closer to the cliff's edge by a sensitizer agent that "prime" cancer cells for apoptosis (i.e. BH3-mimetics) and only following a second stress signal, cell death can occur. Adapted from [108].

4.4. Pediatric cancers: epidemiology, etiology and treatment

Although childhood cancers are relatively uncommon, they represent the first cause of disease-related death in children (0 to 14 years of age) with an incidence of ~0.015% every year [128]. The most common cancers in children younger than 15 years old are acute lymphoblastic leukemia (ALL) (25.4%), central nervous system (CNS) tumors (20.6%) and sarcomas (10.9%) [129]. However, the distribution of cancers for 15-19-year olds is drastically different accounting mainly Hodgkin disease (16.2%), germ-cell/gonadal tumors (12.5%) and a lower incidence of CNS cancers (9.8%) (Figure 10A) [129]. This discrepancy might reflect the need for the oncogenic event to occur at defined developmental stages when a specific cell population might be present or be more abundant. For example, the peak of incidence for bone tumors correlates with the phase of skeletal growth spurt in adolescence when de-regulation of bone-lineage transcription factors might take place [130]. Therefore, given the short latency of tumors occurring early in life, is likely that intrinsic “errors” in development rather then environmental risk factors, might cause tumorigenesis. This might also explain the rare occurrence of pediatric carcinomas and the low mutational burden of childhood cancers, which mostly harbor chromosomal rearrangements (Figure 10B) [7, 131]. Also, the distinct biology of childhood tumors might underlie the different therapeutic response and outcome between children and adults presenting the same disease.

Pediatric cancer patients are generally treated with a multimodal protocol including surgery, radiotherapy and chemotherapy. Such approach led to a dramatic improvement of the overall survival from 28% in 1960 to a near 80% to date (Figure 10C) [132]. Despite this great success, survival rates for high-risk group pediatric sarcomas, retinoblastoma and ALL remains dismal under current treatment strategies [133]. Importantly, long-term side effects following aggressive chemotherapy and radiotherapy regimens remain a critical clinical concern. In fact, one third of the survivors experience a severe or life threatening effect such as organ dysfunctions or development of second malignant neoplasms (SMNs) [134]. Hence, less toxic and more effective therapies are urgently needed. One valid option is offered by the targeted therapy but only few FDA approved agents entered the clinic and are mostly limited to hematological pediatric tumors [133]. Additionally, drug development for childhood cancers is hampered by the poor interest of pharma companies and the small population of children who can participate into clinical trials. Therefore, to prioritize therapies approved for adult cancers that might be tested in children, the NCI founded the Pediatric Preclinical Testing Program (PPTP), a consortium for screening agents in clinical development in PDX models of childhood cancer [132]. However only few drugs are tested annually and the tolerated drug doses in children might be completely different from adults due to dissimilarities in drug absorption kinetics, expression of metabolic enzymes and the limited functionality of immature excretory organs [132].

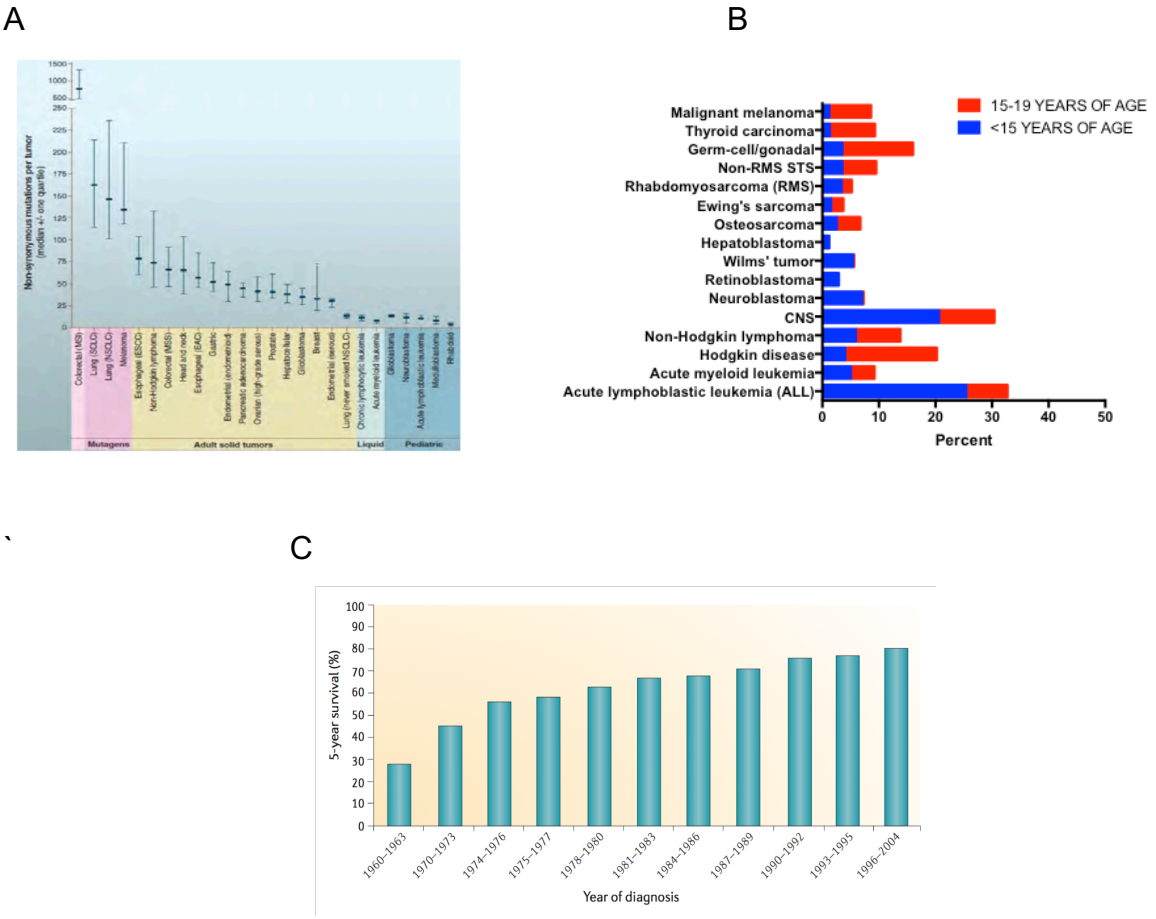

Figure 10. Tumor incidence by age in children, number of somatic mutations in a wide range of cancer entities and survival rate for pediatric cancers. (A) Tumor incidence in children younger than 15 years old (blue bar) or between 15 and 19 years old (red bar). Adapted from [129]. **(B)** Horizontal bars indicate the 25 and 75% quartiles. MSI, microsatellite instability; SCLC, small cell lung cancers; NSCLC, non–small cell lung cancers; ESCC, esophageal squamous cell carcinomas; MSS, microsatellite stable; EAC, esophageal adenocarcinomas. Adapted from [7]. **(C)** 5-year survival rate for childhood cancer patients between 1960 and 2004. Adapted from [132].

4.5. Rhabdomyosarcoma

4.5.1. Epidemyology and histological classification

Rhabdomyosarcoma (RMS) is a striate-muscle lineage malignancy that accounts for about 48% of all soft tissue sarcomas diagnosed in children or adolescents younger then 14 years old [128]. This corresponds to ~4.3 cases per million children (0-19 years old) with the peak of incidence at 5 years of age or younger and is slightly more common in males than females (>1.15) [128]. According to the histological classification, the two most common subtypes of RMS are the embryonal (ERMS) (~75% of RMS) and the alveolar (~16% of RMS) RMS followed by pleomorphic RMS, undifferentiated RMS and “not otherwise specified” RMS (NOS). However,

NOS and pleomorphic RMS are relatively more common in adults and are associated with a poorer outcome than RMS in children [135] ERMS and ARMS are distinguishable both at the histological and localization level (Figure 11). For example, ERMS shows a clear pattern of skeletal muscle differentiation, from a more immature mesenchymal to more differentiated, elongated muscle tumor cells and with a stromal-rich appearance whereas ARMS is composed of small, round, poor differentiated and densely packed cells organized around spaces reminiscent of pulmonary alveoli (Figure 11B) [136]. ERMS can arise anywhere in the body, but it occurs mainly in the head&neck (29% of the cases) and genitals (18%) whereas ARMS is more frequent in the extremities (39%) followed by head&neck (22%) [128].

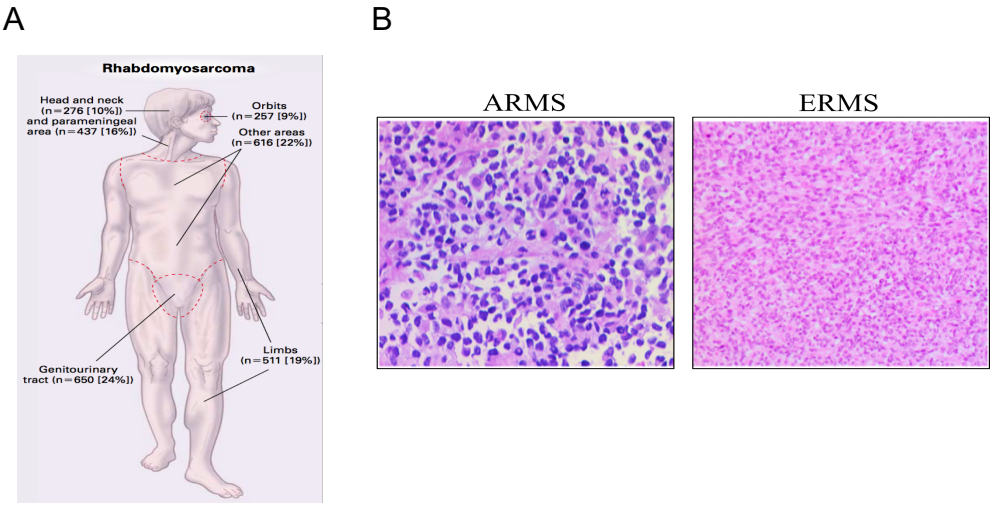

Figure 11. RMS localization and histology. (A) Primary sites of RMS. Adapted from **[137]. (B)** Hematoxylin & Eosin staining of ARMS (left) and ERMS (right).

4.5.2. Diagnosis and prognosis

The diagnosis of RMS is based on the identification of skeletal-muscle differentiation features or rhabdomyoblast-like cells (from greek: rhabdo = cross striated + myo= muscle) which is routinely performed via immunoistochemical staining for muscle specific proteins. These include, DESMIN, MYOGLOBULIN, Z-BAND PROTEIN, MYO D, MYOSIN, MUSCLE-SPECIFIC ACTIN and MYOGENIN [138, 139]. DESMIN positivity is widely found in RMS whereas MYOGENIN seems to be more expressed in ARMS compared to ERMS [140, 141]. Further confirmation of RMS can be achieved via electron microscopy to visualize Z band-material and ACTIN-MYOSIN bundles. The histological appearance of the tumor provides both classification criteria and prognostic information with ERMS having an intermediate prognosis whereas ARMS and undifferentiated RMS have the worse outcome [142, 143]. However, further variables of prognostic significance include age (children younger than 1 or older than 9 years have unfavorable prognosis), localization of the primary tumor site (i.e. limbs are considered unfavorable sites), number of

metastatic sites at diagnosis and bone morrow involvement. If all of these factors are combined, a better patient stratification of responders or non-responders to standard therapy can be achieved [144]. Additionally, molecular tools are also implemented in the clinic when the diagnosis is uncertain. For instance, RT-PCR or fluorescence *in situ* hybridization (FISH) are supportive technologies to identify ARMS harboring chromosomal translocations resulting in PAX3-FOXO1 or PAX7-FOXO1 fusion proteins [145, 146]. The potency of molecular-based stratification is highlighted by the fact that 20% of histologically classified ARMS lack expression of these chimeric factors and are molecularly and clinically indistinguishable from ERMS [147, 148].

After diagnosis of the histological type of RMS, doctors evaluate the extent of the tumor mass and if it has spread, by assigning a cancer stage, which help for the stratification of patients in risk groups (low-, intermediate- and high-risk groups) and guides for treatment options. Two major staging system are applied for the management of RMS patients namely TNM staging and clinical grouping staging (CG) system, developed by the Intergroup Rhabdomyosarcoma Study Group (IRSG) [149, 150]. The TNM system is applied before treatment start and classifies RMS in four stages based on tumor site and size, involvement of lymph nodes and presence of distant metastasis. The CG system defines four clinical groups according to the extent of their initial surgery and cancer spread. This is particularly important since it was shown that patients with completely excised tumors have a better prognosis than patients with residual tumor [151].

4.5.3. Treatment

Nowadays, RMS patients are treated with a multimodal approach, which includes surgery radiotherapy (RT) and combination of chemotherapy regimens. This is the result of numerous clinical trials performed mainly by the soft tissue sarcoma committee of children's oncology group (COG) in the United States and the European paediatric Soft tissue sarcoma study group (EpSSG) over the last 40 years [152].

Surgery is performed if the functionality of the organs can be preserved and if there are not severe cosmetic consequences. For instance, wide local excision is highly recommended for RMS occurring in the prostate, the bladder and extremities whereas is often not necessary for vulvar, vaginal and orbital tumors which are highly sensitive to chemotherapy and is often limited to incisional biopsies for not superficial head and neck RMS.

RT is applied to remove residual tumor mass where surgery is not complete or not feasible such as head, neck and pelvis. Additionally, RT seems to provide a better outcome also for completely resected ARMS tumors [153]. However, 70% of patients with orbital tumors have impaired vision, many have developmental abnormalities, fibrosis and SMNs [154, 155]. For this reason EpSSG limits the use of RT in young children (i.e. RT is not recommended for tumors that regress

completely after chemotherapy) whereas COG investigators suggest a local aggressive treatment already at the diagnosis [152].

Systemic chemotherapy is an indispensible tool to reduce tumor burden or attempt to eradicate metastatic lesions. Over decades, several combinations of de-bulking chemotherapeutics with or without RT, modifications of dose schedules and implementations of risk-based patient stratifications contributed to nearly triple the survival rate of pediatric RMS since the early 1960s [156]. The mainstay standard chemotherapy regimen is the VAC protocol pioneered by Wilbur et al. in 1974, which combines vincristine, actinomycin D and cyclophosphamide [157]. In some cases of low-risk groups, cyclophosphamide is omitted whereas for intermediate and high-risk groups topoisomerase inhibitors are often included (i.e. doxorubicin, etoposide, irinotecan, topotecan etc.) [152].

Despite advances in therapy, there has been only a modest improvement over the last three decades and still metastatic spread, resistance to cytotoxic chemotherapeutic agents followed by long-term sequelae represent the main challenge for the achievement of a complete cure. Indeed, 30% of RMS patients continue to experience relapse disease and only 17% of these survive after 5 years with a median surivival time from the first recurrence of only 0.8 years [158]. The treatment plan for this group of patients is not well defined and in most of the cases the only option is an intensification of chemotherapy (often the same as previously administered) but the success rate remains very dismal [159, 160]. Once relapse occurs, several factors can guide treatment strategies including time to relapse since treatment was completed, if local, regional or distant recurrence and the regimen of chemotherapy and/or radiotherapy administered previously in the patient. Usually recurrence is common after maximum 3 years but if tumors progress under therapy, the prognosis is very poor (~12% probability to survive 4-years post-relapse) and becomes incurable if it is disseminated [161]. In these cases, palliative radiotherapy can help to reduce pain or prevent spinal cord compression. Hence, there is an increasing need to find alternative and more innovative therapeutic modalities, which might help high-risk group RMS patients and limit the incidence of metastasis and relapse. Although targeted therapy has not entered clinical practice for the management of RMS so far, the increasing knowledge about the molecular mechanisms underlying the disease will certainly provide the basis for new RMS-directed therapies in the near future.

4.6. Biology of Rhabdomyosarcoma

4.6.1. Genetic landscape and etiology

ARMS and ERMS have been classically identified as the two main RMS subtypes based on their distinct histology. However, it is now clear that such classification, although holds prognostic significance, is too simplistic. In fact, when we have a deep look into the genetic features of RMS

we can distinguish two clear clusters, PAX-fusion positive (PFP) and PAX-fusion negative (PFN) tumors, which have distinct gene expression signatures, methylation patterns and genetic landscape [162-165]. Briefly, about 80% of ARMS are PFP, of which the majority are characterized by the t(2;13)(q35;q14) and a small fraction by the t(1;13)(p36;q14) chromosomal rearrangements resulting in the PAX3-FOXO1 and PAX7-FOXO1 fusion proteins, respectively [166]. Alternate PAX-fusion products have also been identified such as PAX3-FOXO4 (single case), PAX3-NCOA1, PAX3-NCOA2 and PAX3-INO80D (single case) [167]. In this subgroup, the DNA binding domain of the PAX product is fused to the transcriptional trans-activation domain of the fusion partner, generating aberrant transcription factors that at least in the case of PAX3-FOXO1 (the most characterized) is essential for the etiology and maintenance of this subtype of RMS [167-170]. Generally, PFP have a very low mutation burden compared to PFN tumors, with an average of 0.1 protein-coding mutation/Mb and no recurrent point mutations. In some cases the chimeric protein is the only somatic aberration present, highlighting once again its pivotal tumorigenic function (Figure 12) [164]. Additionally, loci containing *CDK4* (12q13-q14, 12% of the cases) and *MYCN* (2p24, 20% of the cases) genes are the most frequently amplified in PFP samples and the former is associated with worse-failure free and overall survival [171]. In contrast, PFN tumors have a more complex genetic landscape with recurrent mutations in the RAS pathway including NRAS, HRAS and KRAS themselves where the mutations are mutually exclusive across PFN patients but are never found in PFP samples. Further alterations in the RAS family members include the catalytic subunit of PI3K (PIK3CA) up-stream of RAS and one of the direct effectors NF1 (Figure 12) [164, 172]. The iper-activation of the RAS signaling might represent one of the earliest causative de-regulation occurring during PFN tumorigenesis as demonstrated by zebrafish models of RAS-induced RMS [173]. Interestingly, RAS status might be used as new bio-marker to better stratify PFN patients, since it was shown that 75% of the high-risk and 45% of the intermediate risk group patients contained mutations in the RAS pathway but none of them is found in low-risk groups [172]. Although this indicates a certain dependency of PFN tumors on the RAS machinery, most of the inhibitors tested against the RAS/PI3K pathway had no significant activity in short term cultures derived from PFN xenografts. In contrast, agents targeting oxidative stress were the most effective suggesting a new vulnerability for PFN cases [172]. Another striking genetic signature specific for PFN tumors is the recurrent alteration of the P53 axis (~26% of PFN) including mutations in *TP-53* itself, amplifications of its negative regulators *MDM4* or *MDM2* and loss of *CDKN2A* (*p16/p14 ARF*), a physiological inhibitor of MDM2 [164, 172]. Additional alterations include the cell cycle regulator FBXW7 (missense mutations), receptor tyrosin kinases (FGFR4, PDGFRA and ERBB2), the transcriptional repressor BCOR and loss of heterozygosity (LOH) at 11p15.5 locus containing *H19*, *IGF2* and *CDKN1C*, which probably contributes to IGF2 over-expression and dependency on IGF axis.

Despite the genetic diversity, PFP and PFN have a common myogenic make-up, composed of myoblast-like cells that seem to be trapped in a proliferative state. However, the degree of skeletal muscle differentiation differs between the two subtypes and might reflect the distinct cell of origin. According to this, different mouse models demonstrated that PFN tumors develop from a wide range of muscle cells including undifferentiated satellite cells, progenitor cells and maturing myoblasts [174, 175]. Notably, they can also arise from pre-adypocite precursors as well, probably explaining the existence of RMS in anatomic sites lacking skeletal muscle [176]. On the other hand, the only mouse model of PFP that mimics the human counterpart was generated by a conditional knock-in of *Pax3-Foxo1* in the terminal skeletal muscle differentiated Myf-6-expressing cells with or without *InK4a/ARF* or *Tp53* deletion [177]. This might support a reprogramming activity of PAX3-FOXO1 toward a more immature phenotype during skeletal muscle development and is consistent with the fact that forced expression of PAX3 or PAX7 impair differentiation of myoblasts and satellite cells, respectively [167, 178]. Yet, intricate epigenetic networks have also been proposed as potential mechanisms of the deregulated myogenic program driven by PAX fusions [179]. Since RMS might be the result of defects in embryonic processes regulating skeletal muscle lineage, is not surprising to find recurrent aberrations of developmental signaling pathways being discussed in the next chapter.

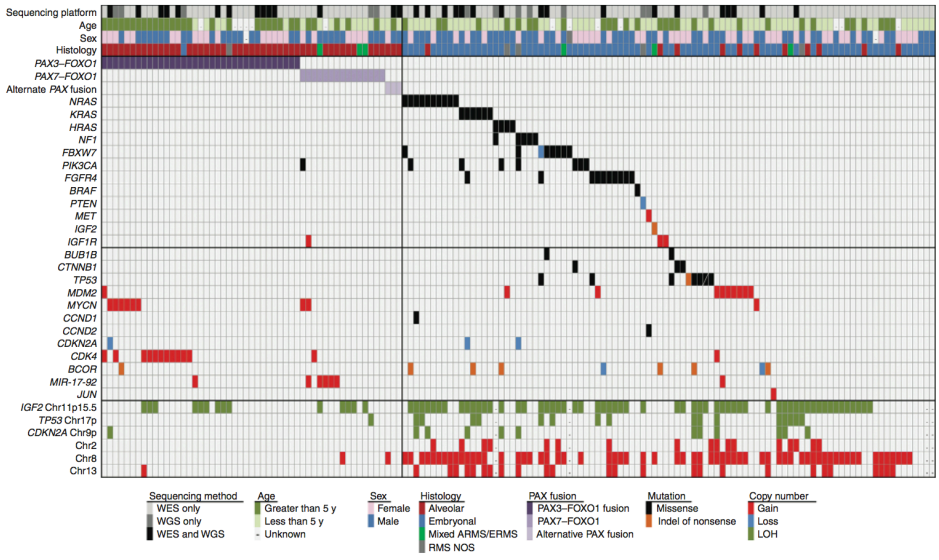

Figure 12. The genomic landscape of RMS. Adapted from **[164].**

4.6.2. Aberrant developmental signaling pathways in RMS

The Notch, Wnt and Hedgehog (Hh) signaling pathways have critical functions during skeletal muscle development or regeneration by regulating self-renewal, differentiation, proliferation and

survival of muscle stem cell pools or their progeny [180]. In RMS, both Notch and Hh have been shown to have tumor-promoting effects whereas canonical Wnt signaling has been recently recognized as a *bona fide* tumor-suppressor pathway.

4.6.2.1. Notch pathway

The Notch signaling activation requires the communication between neighboring cells since both Notch receptors and ligands are transmembrane proteins. In mammals, there are six canonical Notch ligands (Delta-like 1, 2, 3 and 4 (DLL1-4), JAGGED 1 and JAGGED 2) and four receptors (NOTCH1, 2, 3 and 4). Once the ligand binds the cognate receptor, a two-step preoteolytic cleavage mediated by metallo-proteinases (ADAM) first and then by the γ-secretase enzyme, allows the release of the intracellular fragment (intracellular Notch, NICD) into the cytosol before its nuclear translocation where it forms a complex with CSL (CBF1/Suppressor of Hairless/LAG1)/RBPJ to regulate transcription. Among Notch target genes, the most common are HES, HEY, MYC, CyclinD3 (CCND3) and CDKN1A (Figure 13) [181].

Different types of anti-Notch signaling agents are in clinical development including monoclonal antibodies (i.e. mAB targeting DLL4), decoy Notch receptors, inhibitors of Notch transcription complex and γ-secretase (Figure 13). These latter have shown some promising results in pre-clinical and clinical trials but are often associated with toxicities in the gastrointestinal tract due to alterations of crypt progenitors [181].

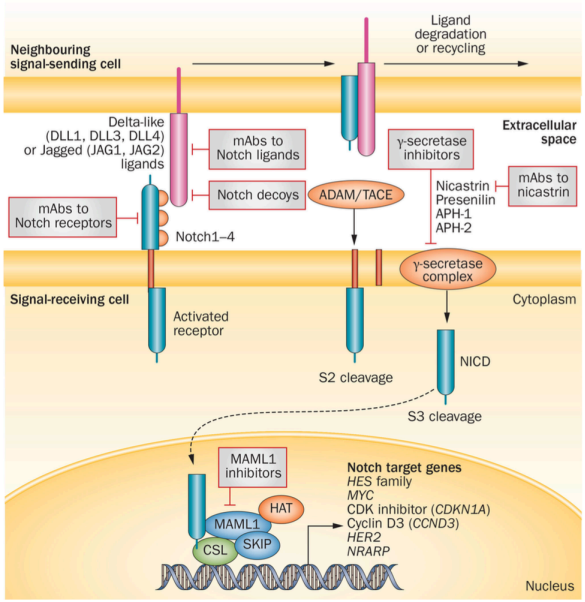

Figure 13. Notch signaling pathway. Canonical Notch signaling and relavant antagonists in clinical development. Adapted from [181].

Notch target genes such as HEY1 and HES1 as well as Notch receptors (NOTCH 2 and to a lesser extent NOTCH 3) have been found to be highly up-regulated in RMS primary tumors or cell lines, indicating iper-activation of the pathway [182, 183]. Accordingly, silencing of HEY1 or HES1 decreases cell proliferation whereas inhibition of NOTCH 3 also increases terminal skeletal muscle differentiation. Although NOTCH 1 seems not over-expressed in RMS, its interference by both genetic and pharmacological means reduces tumor growth *in vivo* [182, 183]. This is corroborated by a recent study showing that constitutive activation of NOTCH1 promotes self-renewal and tumorigenicity in a zebrafish model of PFN RMS by partially blocking the ME2C-mediated skeletal muscle differentiation [184]. Finally, single cases of NOTCH 1, 2 and 3 mutations have been documented for RMS and are associated specifically with PFN tumors [172].

4.6.2.2. Wnt pathway

Currently, three different Wnt pathways have been recognized: the canonical, the non-canonical planar cell polarity (PCP) and the non-canonical Wnt/Ca^{2+} signaling. Among these, the most studied is the canonical Wnt signaling pathway, which is involved in many aspects of embryonic development including cell fate specification during myogenesis by controlling myogenic-regulatory factors (MRFs) [185].

WNT ligands comprise a large family of secreted proteins, which upon binding to the FRIZZLED (Fz)/ lipoprotein receptor-related protein (LRP) complex, favor the stabilization and subsequent nuclear translocation of β-CATENIN, the main effector of Wnt signaling. In the nucleus, β-CATENIN forms a complex with the T-cell factor/lymphois-enhancer factor (TCF/LEF) to activate the transcription of the down-stream target genes (i.e. AXIN2, MYC and cyclinD1). In absence of the ligands, the pathway is in an off state leading to a rapid destruction of β-CATENIN upon phosphorilation by the serine/threonine kinases CK1 and GSK3α/β. Hence, β-CATENIN is trapped in the destruction complex formed by AXIN, Adenomatous polyposis coli (APC) and β-TrCP, which target β-CATENIN for the final step of proteasomal degradation (Figure 14) [186].

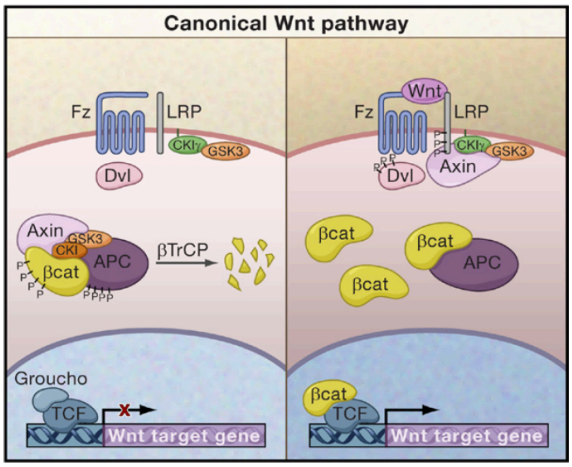

Figure 14. Canonical Wnt signaling. Adapted from [186].

Although canonical Wnt signaling activation has oncogenic activities in many types of cancers (mostly colon cancer), this seems not the case for RMS [187]. Indeed, different lines of evidence suggest that either inhibition of upstream antagonists such as secreted frizzled-related protein 3 (SFRP3) or interference with activators of the destruction complex (i.e. GSK3β) induce myogenic differentiation and impair proliferation in RMS [188, 189]. Similarly, investigations of the downstream transcription factor LEF1 (activator of Wnt signaling) led to the conclusion that it constrains the aggressiveness of RMS [190]. Therefore, these studies suggest that the pro-differentiation ability of canonical Wnt pathway during muscle regeneration is also conserved in RMS [191]. However, if this is a general mechanism or applies only to a subgroup of RMS tumors, remains to be addressed since activating mutations of *β-CATENIN* have been reported for a subset of RMS patients [172].

4.6.2.3. Hedgehog pathway

As most of the molecular circuits, the mammalian Hh signaling can be 'dissected' into its main components including ligands (Desert Hedgehog (DHH), Indian Hedgehog (IHH) and Sonic hedgehog (SHH)), an inhibitory transmembrane receptor (Patched (PTCH)), a ligand-activated co-receptor (Smoothened (SMO)) and the down-stream effectors (Glioma-associated oncogene (GLI) transcription factors GLI1, GLI2 and GLI3)) mediating the cellular response (Figure 15). Even though the exact role of the three Hh ligands in vertebrate is not fully understood, they have overlapping roles or elicit different responses mainly depending on their spatial and temporal localization. For example, SHH is essential for limb development as well as neural tube formation [192, 193], IHH promotes chondrocytes proliferation and bone specification [194, 195], while DHH is mainly expressed in testis, where it is involved in male sexual differentiation [196]. The common feature of Hh ligands is their lipophilicity due to a dual lipidation by the binding of a

cholesterol molecule to the C-terminus and a palmitoyl group to the N-terminus. In particular, the cholesterol moiety is required for the autocleavage of the inactive precursor in an active N-terminal form before being released by Dispatched (DISP), a transmembrane transporter acting on the signal-sending cell [197, 198]. The binding of Hh ligands to the 12-transmembrane-span protein PTCH promotes ligand-receptor internalization and subsequent lysosomal degradation [199]. Hence, SMO, a member of the G-protein-coupled receptor (GPCR) family translocates to the mammalian primary cilium and releases the downstream GLI zing-finger transcription factors from suppressed of fused (SUFU) inhibition. In vertebrates, GLI1, GLI2 and GLI3, mediate the expression of Hh target genes, most of which are still unknown [200, 201]. GLI2 and GLI3 are the main Hh-regulated activator and repressor, respectively. They both contain an N-terminal repressive and C-terminal activating domain. The Hh Off-state allows the C-terminally truncated GLI3 to block the transcription of the Hh responsive genes. In contrast, Hh ligand-mediated activation of the pathway leads to the processing of GLI full-length proteins in C-terminal transcriptional activators and degradation of the N-terminal repressor forms. Moreover, the balance of active/repressive proteins is tightly controlled by post-translational modifications and may be altered in cancer [202]. On the other hand, GLI1 is a constitutive activator lacking the N-terminal repressor domain and its expression is directly regulated by GLI2 in response to Hh ligands as well as by non-canonical Hh signaling [200, 203].

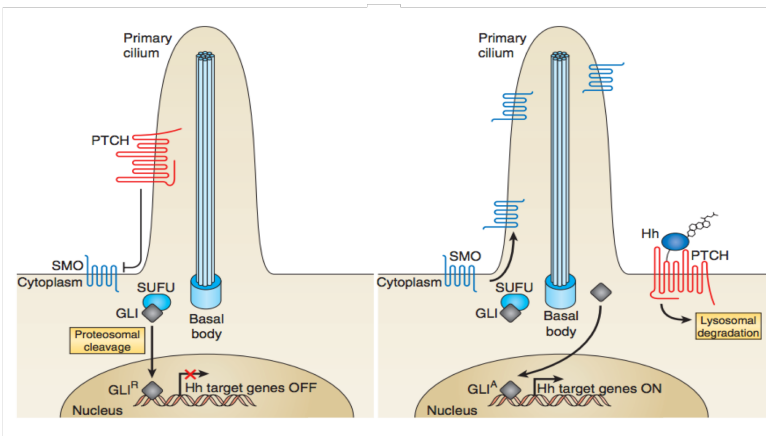

Figure 15. Hedgehog pathway. (left) Hh off state and (right) Hh activation. Adapted from [204]

4.6.2.3.1. The 'self control' of Hedgehog pathway

Several mechanisms modulate the response to Hh signals at different cellular levels. First, cell adhesion molecule down-regulated by oncogenes (CDO) and brother of CDO (BOC), are two transmembrane proteins, which act as 'helpers' of PTCH to bind the ligands and trigger Hh pathway activation [205]. A recent report has identified BOC as a mediator of Hh-induced DNA damage leading to medulloblastoma progression, indicating the relevance of these proteins in

controlling Hh signaling [206]. Growth arrest-specific gene 1 (GAS1) and Hedgehog-interacting protein (HHIP) are two vertebrate-specific cell surface proteins, which positively and negatively regulate Hh distribution, respectively [202, 207, 208]. Second, different kinases, phosphatases and ubiquitin ligases can post-translationally modify Hh pathway members to control signaling activity. For instance, in absence of Hh ligands, GLI transcription factors are sequentially phosphorylated by protein kinase A (PKA), glycogen synthase kinase 3 β (GSK3-β) and different members of casein kinase family (CKI). This allows the ubiquitination and subsequent proteasome-mediated degradation of the C-terminal transactivation domains. This process is reverted by SMO activation, which limits GLI phosphorylation and leads to stabilization of the full-length or C-terminal activator forms [209]. Moreover, GLI1 and GLI2 can undergo acetylation as a repressive signal for their transcriptional output whereas the histone deacetylase 1 (HDAC1)-dependent deacetylation does the opposite [210]. Finally, a further control of the pathway is offered by GLI-mediated transcription of three Hh components PTCH1, HHIP and GLI1, activating both positive and negative feedback loops. In this respect, their expression is considered as the most reliable readout of Hh pathway activation.

4.7. Role of Hedgehog pathway in RMS

The first link between Hh and cancer comes from studies of Gorlin Syndrome (also called Basal Cell Nevus Syndrome, BCNS), a heritable condition characterized by several developmental abnormalities and association with higher risk to develop tumors than the normal population, mostly multiple basal cell carcinomas (BCC), medulloblastoma, and RMS (although at very low incidence) [211, 212]. Since its discovery in 1960, different researches attempted to identify the locus associated with this autosomal dominant disease. Finally, more than thirty years later, *PTCH* has been reported as the candidate gene responsible for BCNS and therefore as a tumor suppressor gene [213-216]. Subsequently, the generation of mice heterozygous for *Ptch* confirmed the involvement of Hh pathway over-activation in RMS tumorigenesis [217]. According with this, up-regulation of Hh target genes such as GLI1 and PTCH1 has been demonstrated by retrospective analysis of RMS patient samples or in human RMS cell lines [218-222]. Additionally, activation of Hh pathway seems to be specific for PFN tumors and significantly identifies patients with poor prognosis [219, 220, 223, 224]. Despite this recognized role of Hh in RMS, the contribution of the ligand-based signaling versus non-canonical pathway activation in sporadic RMS is still unclear. Discordant studies searching for inactivating mutations in *PTCH* or *SUFU* genes and amplifications in *SMO* or *GLI* loci have been published. For instance, a cytogenetic approach of 12 separate RMS patients identified 4 cases with losses in the chromosomal region containing the *PTCH1* gene [225]. Similarly, a linkage analysis led to comparable conclusions in one third of PFN samples analyzed [218]. Controversially, Calzada et al., did not detect mutations in the coding sequence of *PTCH1* in 14 RMS sequenced [226]. This is corroborated by another

study showing absence of *PTCH1* loss-of-function mutations or *SMO* amplifications in 26 PFN tumors examined [220]. Also, a recent whole-genome sequencing (WGS) analysis on 16 RMS tumors ruled out the presence of mutations in members of Hh pathway [172]. Also, SHH immunoreactivity is not common in RMS and the higher Hh activity in PFN compared to PFP does not correlate with SHH mRNA levels, which are unchanged between the two subtypes [218-220]. However, we have previously found a positive correlation of IHH and DHH mRNA levels with the expression of Hh target genes in RMS supporting the hypothesis of a ligand-mediated activation of Hh pathway [224].Therefore, underestimation of the role of the other two Hh ligands might have led to misleading conclusions and further studies need to more carefully elucidate their role in RMS. In summary, hyperactivity of Hh pathway is a common feature in the PFN RMS and only a subset of RMS exhibits mutations in components of the Hh pathway, which would potentially argue for non-canonical pathway activation. However, the role of other tumor-associated pathways, which can interplay with diverse components of Hh signaling and thereby contribute to its activation, is still poorly investigated.

4.7.1. Mouse models of Hedgehog-driven RMS

Investigation of the 'cell of origin' is one of the most intriguing research topics in RMS. To this end, gene-targeting tools developed over the last years have been used to generate animal models of RMS, highlighting the central role of Hh in the tumorigenesis of this pediatric soft tissue sarcoma. In 1998 Hahn et al., established the first mouse model of RMS directly involving Hh pathway. The authors showed that *Ptch1* haplodeficient mice develop RMS tumors with molecular features of the PFN subtype although with low frequency [217, 227]. Accordingly, all RMS from *Ptch*$^{+/-}$ mice over-expressed Gli1 and Insulin-like growth factor 2 (Igf2). Furthermore, the epistatic function of *Igf2* to *Ptch1* was later confirmed in mice double mutants for *Ptch1* and *Igf2* (*Ptch*$^{+/-}$ and *Igf2*$^{+/-}$) [228]. In contrast to *Ptch1*$^{+/-}$ mouse models, ubiquitous activation of a mutated form of a *Smo* allele (*Rosa26-SmoM2*) leads to the generation of RMS with higher penetrance [229]. In addition, mice heterozygous for *Sufu* (*Sufu*$^{+/-}$) in *P53*$^{-/-}$ or *Ptch1*$^{+/-}$ background harbor RMS tumors to the same extend as *Ptch1*$^{+/-}$ mice [230, 231]. By contrast, mice *Sufu*$^{+/-}$ develop only microscopic skin lesions. This suggests that *P53* knockout affects the tumorigenesis of *Sufu* $^{+/-}$ mice and that there is no genetic interaction between *Ptch1* and *Sufu* loci in RMS tumorigenesis. Recently, Rajurkar et al., provided additional insights into the link between aberrant Hh pathway activation and the cellular context responsible for RMS tumorigenesis [232]. They reported that specific expression of SmoM2 in postnatal (P10) Shh-producing cells as well as in Gli1-expressing cells did not lead to RMS formation within 4 months. This was also true for forced expression of SmoM2, Gli2 (Gli2ΔN) alone or in combination with Gli1 in postnatal satellite cells (Pax7 positive). Therefore, the authors ruled out the possibility of Hh-induced postnatal RMS formation in Hh-expressing compartments and myogenic cells, which is consistent with another

study suggesting the adipocyte lineage as the PFN-initiating population [233]. Surprisingly, restriction of Smo-M2 expression to adipocytes resulted in 80% incidence of PFN RMS which is far higher than *Ptch1*$^{+/-}$ and *Sufu*$^{+/-}$;*P53*$^{-/-}$ mice. More important, RMS was the only type of tumor detected, providing a tool to investigate therapeutic strategies specifically for this tumor. Such a model might explain why RMS originates from regions of the body lacking skeletal muscle (i.e. genitourinary and biliary tract) [233]. Controversially, Rubin at al. demonstrated that concomitant inactivation of *Ptch1* and *P53* (*Ptch1*$^{+/-}$,*P53*$^{-/-}$) in a wide range of cells of the myogenic lineage (satellite cells, early and more differentiated myoblasts) contribute to RMS, which is not the case of *P53* loss alone [234]. In general, discrepancies in the tumor incidence for *Ptch1*$^{+/-}$ and *Smo-M2* mice might reflect differences in signaling activity or suggest that they do not completely lie on the same axis to promote RMS tumorigenesis. Alternatively, the stage at which the pathway is switched on in these mouse models might account for distinct susceptibility to this tumor. For example, the large population of uncommitted precursors present at the early embryonic phase might be an important source of RMS onset in *Ptch1*$^{+/-}$ mice during development [227]. All together, these findings underscore the crucial function of Hh pathway in RMS tumorigenesis even though the cellular context and the time at which the uncontrolled activation of the pathway becomes oncogenic is still not clear. Finally, different mouse models have been proposed as preclinical platforms for RMS-specific therapies (Figure 16). However, if these models recapitulate the human situation need further clarification.

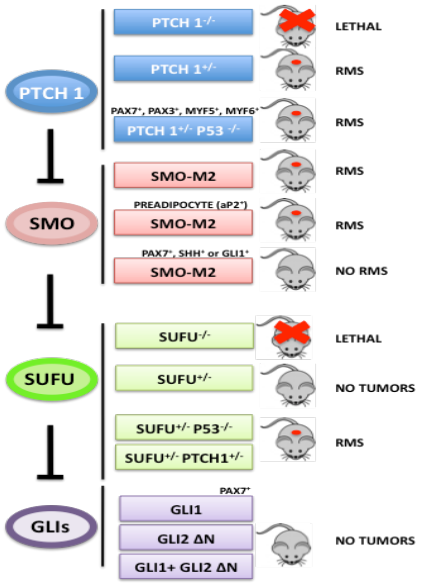

Figure 16. Mouse models of Hh-driven RMS. Genetic manipulation of different components of Hh pathway such as Ptch1, Sufu and Smo leads to RMS tumorigenesis. *Sufu* inactivation favors RMS formation only in combination with *P53* knock-out whereas *Ptch1*$^{+/-}$ can do the same without *P53* ablation. Also combination of *Ptch1*$^{+/-}$ and *P53*$^{-/-}$ specifically in the myogenic compartment gener- ates RMS. Similarly, constitutive and ubiquitous activation of Smo- M2 or

specific expression in preadipocytes causes RMS but not if expressed in Hh expressing or responsive cells as well as in satellite cells. Finally, Gli1/2 activity in $Pax7^+$ cells is not sufficient for RMS initiation. Adapted from [235].

5. Subject of Investigation

RMS accounts for the majority of pediatric soft-tissue sarcomas and current treatment regimens are based on traditional multimodal protocols including surgery, radiotherapy and chemotherapy. Despite the recognized clinical benefit of these conventional therapies, no further progress has been made in the past decades and the response of high-risk groups remains dismal. Moreover, the lack of a molecularly oriented therapy for the management of RMS patients outlines the need to revisit pre-clinical models for translating research findings into clinical practice. Hence, in the present thesis, we set out to develop a reliable pre-clinical system to anticipate drug responses in RMS patients and study chemo-sensitizing mechanisms to conventional treatments. To pursuit this latter, we either employed unbiased high-throughput drug screens or tested the potential of anti-CSC approaches.
Overall, we defined the following aims:

1. To establish a novel pre-clinical platform to model inter-patient heterogeneity and test personalized treatment strategies for RMS patients (Manuscript 1).

2. To identify combinatorial therapeutic options for RMS patients refractory to standard-of-care therapies (Manuscript 2).

3. To study the role of Hh signaling, a CSC-associated pathway, in the context of chemoresistance (Manuscript 3).

6. Results

6.1. Manuscript 1

A Personalized Pre-clinical Platform To Guide Treatment Decisions for Rhabdomyosarcoma Patients

[1]Manzella G., [1]Römmele M., [1]Zhang L., [1]Tchinda J., [2]Bode P.K., [1]Niggli F., [1,2] Schäfer B.W. and [1,3] Wachtel M.

[1] Department of Oncology, University Children's hospital of Zurich, Switzerland

[2] Institute of surgical pathology, University hospital of Zurich, Switzerland

[3] Equally contributing senior authors

Manuscript in preparation

Personal contribution: Wachtel M. and I performed all experiments, except:

-*in vivo* experiments: performed by Römmele M. (Supp. Figure 1B)

-aCGH analysis: performed by Zhang L. (Figure 3B and suppl. Figure 2)

-immunoistochemistry (IHC): performed by Bode P.K. (Figure 3A)

I was further responsible for data interpretation, writing and formatting of this manuscript.

Introduction

Cancer is a complex and heterogeneous disease, which represents a leading cause of death worldwide and the subject of global attention over the past century. In this regard, innovative genomic and proteomic technologies developed during the last decades contributed to major advances in the understanding of the underlying biology and treatment of this malignancy leading to a significant decrease of cancer-related deaths to date [1, 2]. Especially genetic analysis nowadays is a clinical routine for many cancers and allows identification of patient specific driver oncogenes that serve as relevant therapeutic targets. Unfortunately, genome-based drug selection is not feasible for tumors which are driven by mutated but "undruggable" targets and have an otherwise low mutational burden, a characteristic of many pediatric sarcoma and leukemia.

One tumor type belonging to this class is Rhabdomyosarcoma (RMS), which is the most common soft-tissue sarcoma in children and subsumes different histological subtypes all having cells with characteristics of skeletal-muscle differentiation. The two main subtypes, alveolar (ARMS) and embryonal (ERMS) RMS, are characterized by distinct genetic alterations. Most ARMS are associated with specific chromosomal translocations leading to the formation of either PAX3-FOXO1 or PAX7-FOXO1 fusion protein, which are critical oncogenic factors driving the disease as well as providing a diagnostic and/or prognostic value, but as transcription factors are challenging drug targets [3-5]. A part of the ERMS is characterized by mutational activation of the Ras pathway. Consistent with the low mutation rate of cancers in children, only 17.8 and 6.4 somatic mutations per tumor were found in ARMS and ERMS, respectively. On average, only 5 of these are expressed, and a small fraction holds the potential for druggability [4]. Despite the great progress that has been made for treatment of RMS, up to 30 percent of patients still have dismal outcome under current therapeutic strategies and no targeted therapy has entered into clinical practice so far [6]. The lack of a molecular-oriented therapy for the management of RMS highlights the need for improvement of cancer research to find relevant new therapeutics.

Hence, to address these limitations alternative drug selection processes might be used. One possibility is represented by the unbiased use of drug libraries for screening for cancer –specific vulnerabilities, an approach which necessitates an appropriate cancer model system. Along this view, cancer cell lines have been used as gold standard model for cancer research since the first derivation of a human cell line from a cancer patient in the early '50s, which also served as important tool to define culture media and procedures of cell propagation *in vitro* [7]. The low success rate of translation of preclinical data acquired with cell lines to the clinics however has called the suitability of cell lines as preclinical models into question. Indeed, long-term passaged cell lines are often associated with down-regulation of important signaling pathways, gain of additional genomic aberrations and loss of intra-tumor heterogeneity that fail to recapitulate the

initial tumor where they were derived from [8-11]. Hence, to overcome some of these caveats, patient-derived xenografts (PDXs) have been routinely used to assess therapy efficacy, pharmacodynamic/pharmacokinetic parameters and study tumor-stroma interactions [12, 13]. Although PDX models offer an important platform for expansion of patient-derived biopsies and closely resemble the original tumor specimen at the morphological and molecular level, they might be not affordable in terms of cost and space for many laboratories and are unsuitable for large high throughput drug testing [14, 15]. For instance, in the Pediatric Preclinical Testing Program (PPTP), a multi-institutional consortium for evaluating drug candidates in a large cohort of PDXs representative of childhood cancers, only 12 drugs annually are tested [16]. This makes PDX as a good model for drug validation rather than for drug discovery [17]. For the latter primary cultures of cancer cells represent more suitable model. Importantly however, protocols for primary cancer cell cultures have been established in only a small number of entities yet [10, 11, 18].

Here, we set out to develop a functional predictive preclinical "toolkit" which combines the use of PDX models and primary cultures for RMS. In this respect, we present a systematic characterization of optimized culture conditions for PDX-derived RMS cells and provide a side-by-side comparison with standard culture protocols. Importantly, we detected that traditional culture conditions with presence of serum has a toxic effect on primary RMS cells and leads to the outgrowth of resistant clones. Additionally, we show the feasibility of using our *in vitro* drug platform-based screen to pinpoint patient-specific pharmacological vulnerabilities with a high-fidelity prediction of the *in vivo* response, which will help to prioritize actionable drug targets in the pre-clinical settings.

Results

In vitro culture condition screen with PDX-derived rhabdomyosarcoma cells

In order to set up a culture system that closely preserves the phenotypic and molecular characteristics of the parental tumor, we followed the scheme depicted in (Figure 1A). First, we aimed to determine the optimal culture conditions supporting the growth of the RMS tumor cells (RTCs) *in vitro*. For that, at least two independent tumors from 8 different RMS PDX models (3 ARMS and 5 ERMS established previously [15, 19] and in this study (Suppl. Table 1)) were allowed to grow s.c. in mice up to 1 cm^3, followed by tumor isolation, dissociation into single cell suspension and culture in a 96-well plate format. We compared 18 different culture conditions by combining each of three different media (DMEM and F10 both supplemented with 10% heat inactivated fetal bovine serum (FBS) and Neurobasal (NB) supplemented with serum replacement B-27) with three different vessel substrates (no coating, Matrigel and gelatin coatings), each in presence or absence of EGF plus bFGF (GF). When cells reached confluency in one of the conditions (normally within 1-3 weeks), cell viability was determined by WST-1

assay. In parallel, cell morphology was analyzed microscopically. This first approach revealed that F-10 based media was generally not effective in supporting RTC growth and therefore was not further studied (Figure 1B). In contrast, NB based medium supported growth of cells from most PDX, especially in combination with Matrigel. In some cases, NB medium supplemented with GF and combined with Matrigel coating even scored as the top condition, such as for SJRHB013759_X1C (ARMS) and RMS_ZH04_XC (ERMS) with cell viability values ranging between ~126% to 307% of the DMEM-GF condition, which was used as reference (Figure 1 B and Suppl. Table 2). DMEM based conditions, independent from coating or presence and absence of growth factors, supported survival of cells across all samples but SJRHB013759_X1C (Figure 1B and Suppl. Table 2). In several cases, the DMEM conditions led to the highest cell viability values measured. Importantly however, morphological analysis revealed that cells in DMEM medium often had an increased size and were rich in stress-fibers, suggesting that these cells, despite being viable during this short-term culture, might have stopped proliferation at some point (Suppl. Figure 1A). In case of two aRMS samples (SJRHB013757_G1C and SJRHB010463_X16C) elongated and multinucleated cells with a myotube-like morphology were detected in DMEM cultures (Figure 1C and Suppl. Figure 1A), suggesting that these cells differentiated along the myogenic pathway. Comparative immunofluorescence (IF) analysis for myosin heavy chain (MHC) expression, a marker of terminal skeletal muscle differentiation, in SJRHB013757_G1C cells grown in parallel in DMEM and NB medium confirmed this pro-differentiation effect of the DMEM condition (Figure 1D). In contrast, cells in NB medium generally remained small and stress-fiber free and did not upregulate muscle differentiation markers (Figure 1C-E).

The growth factors especially enhanced growth of aRMS cells, while in eRMS they had less effect or affected cell viability even negatively, such as in case of SJRHB012_RC cells on uncoated plates or in combination with gelatin-coating (Figure 1C, right panel). Interestingly, correlation of effects of growth factors on cell viability with genomic data revealed that among the eRMS especially the Ras-pathway mutant ones were not affected (Table 1). Finally, in three cases, the procedure failed to generate cancer cell cultures where outgrowth of mouse cells was observed (data not shown).

Taken together, these initial analyses revealed dramatic differences in behavior of cultures from individual RMS tumors in different culture conditions as well as some heterogeneity in requirements among the different tumors. However, taking into account both cell viability and morphology, NB based conditions in combination with Matrigel-coating represent in many cases the optimal condition identified.

Evaluation of the long-term proliferation capacity of rhabdomyosarcoma cells cultured in NB and DMEM-based conditions

In order to validate the superior performance of NB medium, we next compared DMEM and NB based conditions on the long-term proliferation rate of RTCs. We monitored the cell numbers of 2 ARMS (SJRHB010463_X16C, SJRHB013759_X1C) and 4 ERMS (SJRHB012_RC, SJRHB13758_X1C, SJRHB13758_X2C and RMS_ZH04_XC) cultures over a period of 1-2 months by counting cell numbers at every passage (Figure 2A). Interestingly, we found that in 5 out of 6 cases (~83%), NB-derived cells continuously proliferated with an exponential growth rate regardless of the passage number, whereas cell counts in DMEM were decreasing over time starting already from an early time point on passage 1 or 2 (Figure 2A). Only SJRHB13758_X2C cells, harboring a TP53 mutation (table 1) could be easily propagated also in DMEM with a growth kinetic indistinguishable from the one in NB medium, reflecting the high take-rate and aggressiveness of this particular tumor observed *in vivo* (Figure 2A and data not shown). Interestingly we observed, in DMEM cultures of two tumors (SJRHB012_RC and SJRHB012_SC) that a small number of cells resisted these suboptimal growth conditions and continued to proliferate, first forming outgrowing clones (DMEM_clones), which then could be propagated to confluent monolayers within 1-2 months (Suppl. Figure 1A). When transplanted into mice, both NB-derived cells and DMEM_clones from SJRHB012_RC were tumorigenic (engraftment in 5/5 mice) and displayed similar growth kinetics (Suppl. Figure 1B, left panel). In contrast, only 2/4 (50%) of DMEM_clones and all NB-derived cells (4/4) from SJRHB012_SC engrafted in mice (Suppl. Figure 1B, right panel). Thus, an *in vitro* selection and/or adaptation process is required for DMEM_clones to re-gain a proliferative status that is not always maintained *in vivo*.

To determine the components in the DMEM mixture, which are detrimental to cell fitness, we repeated the proliferation assay by seeding cells from four tumors in DMEM or NB based medium supplemented one-by-one with B27, FBS or the combination of both (Figure 2B). This approach revealed that FBS is the component that negatively affects the growth of all RTC cultures, both in DMEM and NB medium. Interestingly however, in one of the tested cases (SJRHB013759_X1C) this toxic effect was completely reverted by co-addition of B-27 and the combination generated even a synergistic pro-proliferative effect, which was more prominent in NB than DMEM based medium (Figure 2B). Hence, albeit our empiric attempts underscore the difficulty to generalize culture conditions, they clearly identify serum as the main undesirable component for RTCs.

In parallel, we also validated the effects of the growth factors in order to identify which of them is responsible for the detected biological effects. For that, we determined the proliferation rate of selected growth factor-activated (SJRHB013759_X1C) and -inhibited (SJRHB012_RC) RTC cultures under all possible growth factor permutations in NB medium (Figure 2C). In case of SJRHB012_RC bFGF inhibited cell proliferation and induced a drastic change in cell morphology (Figure 2C and Suppl. Figure 1D). Despite resembling myogenic differentiation, this phenotype

was not associated with MHC upregulation (Suppl. Figure 1D). In contrast, proliferation of SJRHB013759_X1C cells was strongly induced by bFGF, while EGF had only a small inductive effect, which was additive with the one from bFGF in combination tests (Figure 2C, lower panel).
In summary, these results indicate that selected culture conditions identified through our platform outperform conventional cell line protocols, which are highly detrimental to most RTCs due to the presence of FBS. Furthermore, we confirmed the growth factor susceptibility in a subset of RTC cultures and uncovered a tumor-suppressive role of bFGF in a single case.

Genomic and histological characterization of matched PDX and RTCs.

In order to confirm the tumor nature of the cultured cells and to elucidate if the applied culture conditions exert a selection pressure, we performed comparative DNA copy number analysis of matched PDX tumors and RTCs using array-CGH. Overall, we detected a high level of concordance between PDXs and RTCs (Figure 3A and Suppl. Figure 2A). Furthermore, DAPI-staining of cell nuclei, allowing discrimination of mouse from human cells based on different staining patterns revealed maximally 14.5% mouse cells in the cultures (Suppl. Figure 2B). Taken together, these data confirm that all RTC cultures indeed represent cancer cells and that they are genomically stable in NB-based medium. Nevertheless, in accordance with previous studies, we also noticed some small differences in DNA copy numbers between PDX and corresponding RTCs (Figure 3A). This was even more pronounced for DMEM_clones. For instance, SJRHB012_SC DMEM_clone was characterized by a unique loss in chromosome 4 and gain in chromosome 2, consistent with a selection process or acquisition of additional genetic alterations upon DMEM culture (Figure 3A, lower panel).
Although several studies demonstrated that PDX models retain most of the molecular and histopathologic characteristics of the primary tumors, little is known about the phenotype of tumors generated with matched cells propagated *in vitro*, particularly in case of RMS. To address this issue, we generated s.c. xenograft tumors using cells from RTC cultures (cell-derived xenografts; CDX) and compared their histological characteristics with the one from PDX and original patient tumors, if available. For that, tumor sections were assessed for cell morphology by haematoxylin and eosin (H&E) staining or for presence of cells with skeletal muscle differentiation by immunohistochemical detection of Desmin and Myogenin. This analysis revealed that both PDX and CDX retain RMS features phenocopying the tumor architecture and the degree of myogenic differentiation of the primary tumor (Figure 3B). Altogether, these findings showed that NB-derived cells maintain most of the copy number changes of their parental PDX and faithfully recapitulate tumor histology when transplanted *in vivo*.

***In vitro* compound screen with RTCs informs on pharmacological vulnerabilities of individual tumors**

Based on the low mutational burden of RMS tumors, we next asked whether our established RTC cultures represent a suitable pre-clinical model to unveil actionable drug targets in individual tumors. Therefore, we developed an *in vitro* proof-of-concept high-throughput screen employing a compound library containing 204 drugs. This contains both Food and Drug administration (FDA)-approved drugs and small molecules in clinical development, together covering a range of functional classes of targets, as well as standard chemotherapeutics used for RMS therapy (Suppl. Table 3). A panel of 15 RMS cell cultures including 8 RTCs (5 ERMS and 3 ARMS), 3 DMEM_clones and 4 commonly used cell lines (2 ERMS and 2 ARMS) were treated for 72h with a final drug concentration of 500 nM. We used WST-1 assay as read-out for cell viability and generated a hit map depicting drug responses based on the percentage of living cells relative to DMSO control (Figure 4A). Overall, 70/204 (~34%) of the drugs decreased cell viability more than 20% in at least one sample. Unsupervised hierarchical clustering analysis using the response data revealed that all PAX3-FOXO1 positive samples clustered together, while in case of ERMS different subgroups were found (Suppl. Figure 3). This findings mirror the different genetic landscape characterizing the two RMS subtypes as well as the larger heterogeneity of ERMS tumors [4] At the level of individual drugs, different response patterns were detected. A first set of drugs showed general toxicity (at least 40% reduction in cell viability in a majority of the cell cultures) including proteasome inhibitors (4), HSP90 antagonists (2), anti-PI3K agents (2), compounds interfering with the apoptotic machinery (Obatoclax and YM155), the dual ALK/IGF1R inhibitor AZD3463, and the mTOR inhibitor Torin 2. Other drugs showed more specific activity patterns. Among them are 3 out of 4 Akt inhibitors including GSK690693, Afuresertib and Ipatasertib, which especially affected aRMS samples, while among ERMS samples only two RAS^{WT} RTCs (SJRHB012_RC and SJRHB012_SC) but not the corresponding clones were highly sensitive (Figure 4A). Determination of IC_{50} values of GSK690693 and Afuresertib revealed sensitivities at therapeutically applicable concentrations of 95-281 nM and 196-212 nM, respectively for these compounds in two aRMS RTCs (Figure 4B). Notably, a small group of drugs was especially active in RTCs compared to cell lines. These include anti-topoisomerase chemotherapeutics (doxorubin and etoposide) in ARMS, the menin-MLL inhibitor MI-2 and ponatinib in ERMS (Figure 4A).

At the level of individual tumor samples, some exceptional behaviors were detected such as the resistance of the PAX7-FOXO1 fusion positive tumor (SJRHB013757_G1C) against all proteasome inhibitors (4), Volasertib (PLK1 inhibitor) and YM155 (survivin inhibitor) (Figure 4A). This finding again underscores the relevance of personalized drug profiles. Finally, strong degree of overlap between two DMEM CLONES derived from the same PDX was observed, further corroborating their distinct phenotype (Figure 4A and Suppl. Figure 3A).

As proof-of-principle for reproducibility of our discovery drug platform, we validated additional compounds anticipated to have a general (Verdinexor and YM155) or individual (ABT-263 and Idasunutlin) activity (Figure 4B and Suppl. Figure 3B). The IC-50 values were in general accordance to the predicted cell viability scores (Figure 4B and Suppl. Figure 3B, lower panels). It is worth mentioning that Idasanutlin exhibited a strong activity in all TP-53^{wt} RTCs tested but failed in 1/2 of RMS cell lines with an intact TP-53, presumably as consequence of an *in vitro* selection and/or adaptation process required to establish traditional cell lines (Figure 4B and Suppl. Figure 3B).

In sum, our unbiased drug screen revealed the need of using functional assays to interrogate druggable targets, which cannot be fully captured across the limited set of RMS cell lines available or dictated by genomic-based predictions.

Discussion

Historically, cancer cell lines have been routinely used as model system to study the biology of cancer. Given their versatility for high-throughput approaches, they have been adopted as pre-clinical platforms to readily identify therapeutic targets and test anti-cancer strategies. Despite the great promise of cell line-based screening programs, only few identified agents have met a clinical success [20]. Additionally, the current paucity of tumor-derived cell lines highlights a major shortcoming for modeling inter-patient cancer heterogeneity [17]. This is particularly relevant for the rare pediatric tumors, including RMS, where cancer research continues to rely on a limited panel of cell lines established decades ago [21-23]. This low success rate of cell cultivation might reflect the inability of traditional serum-containing media to adequately mimic the physiological environment of living tissues [24]. An alternative strategy to overcome *in vitro* limitations is represented by PDX models. Recent studies in RMS, have shown that PDX faithfully recapitulate molecular and phenotypic features of the original tumor biopsies and are currently employed in drug testing programs to prioritize effective agents for childhood cancers [15, 19, 25]. However, the narrow PDX populations representative of each tumor type and the restricted number of therapeutics that can be evaluated annually constitute critical caveats in current drug discovery and development pipelines.

To tackle this situation, in the present work we have established a large collection of PDX-derived RTCs using a serum-free culture method that preserves niche factor requirements, patient-specific genomic alterations, proliferative capacity and tumorigenic ability. By contrast, we observed a general difficulty to propagate cells in serum-containing media, consistent with the low rate of establishment of cancer cell lines achieved in the past with standard culture protocols [24]. In our hands, the presence of serum exhibited a strong anti-proliferative effect, induced profound morphological changes and in some cases promoted terminal skeletal muscle differentiation. Similar results have been documented for primary glioblastoma, neuroblastoma and ovarian

tumor cells, suggesting that this might be a general phenomenon [26-28]. We speculate that the multitude of variable components of the serum might not properly recapitulate the fluid that cells are exposed to in their natural milieu [29]. Accordingly, 2 out of 3 successful examples of serum-derived cells in our settings were associated with a clonal outgrowth reminiscent of cells undergoing growth crisis before re-gaining a proliferative status [26, 30]. The selection pressure imposed by this culture condition resulted in the emergence of de novo genetic aberrations and in one case limited the tumorigenic potential of the cultured cells. This occurrence resembles the loss of tumorigenicity observed in primary glioblastoma cells exposed to serum [26]. Albeit future experiments are needed to unravel the growth inhibitor factors of the serum and clarify the stress-induced growth arrest, recent studies have suggested that both senescence and differentiation can take place [27, 31]. It is also worth mentioning that we were unable to generate RTCs in three cases, where we detected outgrowth of mouse cells, indicating that further attempts to refine our culture conditions will be necessary to increase the array of RMS cell types *in vitro*. Furthermore, our *in vitro* "culture discovery platform" revealed that semisolid culture conditions (with matrigel or gelatin) are highly beneficial for the growth of RTCs, probably by mimicking the cell-extracellular matrix (ECM) contacts occurring *in vivo* and thus limiting the plastic adaptation. We also describe unpredictable GF sensitivities and identified bFGF as the crucial factor affecting the growth of both GF-stimulated and GF-inhibited cells. This is in line with the importance of FGF signaling in RMS [32, 33]. Whether specific genetic alterations might account for this heterogeneity of response remains elusive. Alternatively, it is possible that tumors originated from different sites in the body, are exposed to distinct microenviroments to which they adapt. Accordingly, it was shown that, colorectal tumor organoids displayed individual dependencies on niche factors that might reflect their original anatomic site, tumor stage and genomic background [34]. Finally, we have shown a broad spectrum of responses to different class of agents across our set of RTCs derived from patients with distinct clinical course and RMS subtype. With the goal in mind to identify compounds of potential clinical benefit for individual patients, we were able to capture not only expected drug activities (i.e. idasanutlin in TP-53^{wt} samples) but also exquisite patient-specific sensitivities (i.e. ABT-263) or refractory responses (i.e. preteasome inhibitors) that could not be anticipated based solely on genomic data. We also discovered a subset of patients with an AKT responsive phenotype as demonstrated by the clear overlap of several AKT inhibitors. These latter are currently investigated in phase I/II clinical trials for adult malignancies [35]. Despite evidences suggesting that AKT iper-phosphorylation (AKT ser473) predicts poor overall survival in RMS, little attention has been focused on the mTOR/AKT axis blockade so far [36]. Instead, our findings indicate that *in vitro* drug profiling is a suitable approach to pre-select RMS sub-groups who may benefit from anti-AKT therapies. Since identification of "druggable" mutations in RMS does not always match therapeutic utility [37], we propose that functional testing would

complement current genome-based technologies or other diagnostic tools (i.e. BH3 profiling [38, 39]) to precisely infer drug activity for precision medicine.

To our knowledge our data provide the first systematic characterization of culture methods for efficient derivation and maintenance of RTCs *in vitro* and demonstrate the adverse effect of serum-based protocols. We also outline the feasibility of using RTCs to functionally inform on personalized treatment strategies and in a clinically relevant time frame.

Materials and Methods

Patient-derived samples

The PDX samples SJRHB012_R, SJRHB012_S, SJRHB013758_X1, SJRHB013758_X2, SJRHB010463_X16, SJRHB013759_X1 and SJRHB013757_G1 were obtained from St. Jude Children's Research Hospital (USA) [15]. RMS_ZH04_X was generated from a tiny tumor biopsy collected at the Mumbai Children's Research Hospital in agreement with local institutional ethical regulations and implanted subcutaneously in NOD scid gamma (NSG) mice. Once tumors reached a size of ~1cm^3, xenografts were harvested and dissociated for cell derivation and PDX propagation. For multiple *in vivo* passages, PDX were either implanted as tumor pieces or injected as cell suspension subcutaneously in NSG mice. A description of the PDX lines used in this study can be found in Suppl. Table S1.

Tumor dissociation

PDXs were minced with scalpel, suspended in 2 ml digestion buffer containing 1x HBSS (Sigma Aldrich), 200 U/ml Dnase1 (Stemcell Technologies or Roche Diagnostics), 1 mM $MgCl_2$, 200 ug/ml Liberase (Roche Diagnostics) and incubated at 37°C for 20-30 minutes. Cells were resuspended in 18 ml of Dulbecco's Modified Eagle Medium supplemented with 10% fetal bovine serum (heat inactivated), filtered through 70 um cell strainer and centrifuged at 300 g for 5 minutes. Finally, the cell pellet was washed once with PBS before cell counting. For freezing procedures, digested PDXs or minced tumors were cryo-preserved in either FBS (heat inactivated) plus 10% DMSO or Cryostor (Stemcell Technologies).

Culture screen

1-2 hours before mouse sacrifice and PDX collection, 18 wells of a 96-well plate were pre-coated with 2% gelatin (Sigma Aldrich) for 40-60 minutes at 37˚C. Afterwards, 18 additional wells were pre-coated with 10% matrigel (in neurobasal medium) (Corning) for 40-60 minutes at room temperature. Hence, PDX were dissociated in single cell suspensions and counted by using a mini automated cell counter (ORFLO). For cell seeding, 30.000 cells per well were plated in

triplicates by using a multichannel pipette before cell viability was assessed 1-3 weeks later by WST-1 assay (Roche Diagnostics) according to the manufacturer's instructions.

Xenograft studies

For establishment of cell-derived xenografts (CDXs), $5x10^6$ cells were suspended in 100 ul PBS and injected subcutaneously (s.c.) in NOD scid gamma (NSG) mice. Tumor size was determined by digital calliper measurements of 2 diameters (d1, d2) in right angles. Total tumor volumes were calculated by the formula $V = (4/3)\pi r3$; $r = (d1 + d2)/4$. Mice were euthanized once tumors reached the maximum allowable size (1 cm^3) or with weight loss over 20% than baseline (body weight was monitored daily through the course of each experiment).

Cell culture and cell proliferation

RD (ATCC, Manassas, VA, USA), RHJT, RH36 and RH4 cells (kindly provided by Peter Houghton, The Research Institute at Nationwide Children's Hospital, Columbus OH) were cultured on uncoated plates in DMEM supplemented with 10% fetal bovine serum (heat inactivated), 1% L-glutamine and 1% penicillin-streptomycin. RTCs were cultured in Neurobasal medium (Thermo Fisher Scientific) supplemented with 1% glutaMAX (Thermo Fisher Scientific), 1% penicillin-streptomycin, 2x B27 (Thermo Fisher Scientific), bFGF (20ng/ml, Peprotech) and EGF (20ng/mL, Peprotech). Only SJRHB012_RC cells were maintained without GF supply. Medium was replaced tree times a week. Plates were pre-coated with either 10% matrigel (Corning) for 40-60 minutes at room temperature or 2% gelatin (Sigma Aldrich) for 40-60 minutes at 37˚C, according to the optimal culture conditions per each RTC described in the text. All cells were cultured in 5% CO2 at 37°C.

For proliferation assay, cells were seeded in duplicate for each culture condition and split at the indicated time points by using either accutase (Sigma Aldrich) or trypsin (1:1 with PBS). The cumulative number per each condition was calculated by multiplying the average number of cells by the spitting ratio. Data are presented as percentage of day 0 in either linear or logarithmic scale.

Drug screen

Cells were seeded in triplicate on flat-bottomed, white 384-well plates and after 24h medium was replaced before treatment start. Each compound (10 mM stock solution dissolved in DMSO) was pre-diluted with medium the day of the experiment at 10 uM concentration and 1 ul of this solution was added manually to each well containing 19 ul of medium to achieve a final concentration of 500 nM. DMSO was used as vehicle control. WST-1 assay was performed at 72h time point. The average number of leaving cells for each triplicate was normalized to untreated cells (vehicle

control) and data are shown as percentage of control. The drug library containing 204 drugs was purchased from Selleck and details are shown in Supp. Table 3.

For drug validation, cells were plated in triplicates on flat-bottomed, white 384-well plates at cell densities ranging between 3000 to 10000 cells depending on the cell type used. 24h after cell seeding, medium was replaced and drug was added by using HPD300 digital dispenser at concentrations indicated in each figure. 72h after treatment WST-1 assay (Roche Diagnostics) was performed according to the manufacturer's instructions. The following compounds were further validated: idasanutlin, afuresertib, GSK690693, ABT-263, YM155, verdinexor and AZ-20 (Selleck).

Immunofluorescence

SJRHB013757_G1C and SJRHB012_SC cells were grown on tissue culture slides (Corning) pre-coated with 10% matrigel or 2% gelatin, respectively. After washing once with PBS, cells were fixed with 4% formalin for 15 minutes, washed again with PBS before adding 0.1 M Glycin (in PBS) for 5 minutes. After three washing steps with PBS, cells were permeabilized with 0.1% Triton X-100 (in PBS) for 15 minutes, blocked for additional 15 minutes in PBS containing 4% horse serum and 0.1% Triton X-100 (blocking buffer) and incubated overnight with primary monoclonal myosin heavy chain antibody (1:400 in blocking buffer, DSHB) at 4ºC. The day after, cells were washed three times with PBS and incubated with Alexa-488 (or Alexa-594) labelled donkey anti-mouse secondary antibody (Invitrogen) diluted 1:250 in PBS plus 4% horse serum for 60 minutes at room temperature before three additional washing steps. Finally, slides were dipped in water and nuclei stained with DAPI (Vector Laboratories). Images were acquired by using a fluorescence microscope (Zeiss Axio Observer).

Immunohistochemistry

Following mouse sacrifice and tumor collection, tissue was fixed in paraformaldehyde overnight, and stored in 70% EtOH at +4°C until embedment. Staining was performed on 3μm thick sections from blocks of formalin-fixed, paraffin-embedded (FFPE) tissue at the department of Pathology (University of Zurich) as previously described [40]. The following antibodies were used: DESMIN (Dako, M076029, dilution 1:20) and MYOGENIN (Novocastra,Leica, PA0226, dilution 1:20).

aCGH analysis

Genomic DNA was extracted using the DNAse® Blood&Tissue Kit **(#**69506) following the manufacturer's instructions. The aCGH assay was performed using the CytoScan™ HD Array Kit according to the manufacturer's protocol (Affymetrix, Thermo Fisher Scientific, MA, USA). The raw data of each single sample was analyzed with the Chromosome Analysis Suite (ChAS) software (Version 3.1.1.27, Affymetrix).

References

1. Hanahan, D. and R.A. Weinberg, *The hallmarks of cancer.* Cell, 2000. **100**(1): p. 57-70.
2. Jemal, A., et al., *Annual Report to the Nation on the Status of Cancer, 1975-2014, Featuring Survival.* J Natl Cancer Inst, 2017. **109**(9).
3. De Giovanni, C., et al., *Molecular and cellular biology of rhabdomyosarcoma.* Future Oncol, 2009. **5**(9): p. 1449-75.
4. Shern, J.F., et al., *Comprehensive genomic analysis of rhabdomyosarcoma reveals a landscape of alterations affecting a common genetic axis in fusion-positive and fusion-negative tumors.* Cancer Discov, 2014. **4**(2): p. 216-31.
5. Barr, F.G., *Gene fusions involving PAX and FOX family members in alveolar rhabdomyosarcoma.* Oncogene, 2001. **20**(40): p. 5736-46.
6. Pappo, A.S., et al., *Survival after relapse in children and adolescents with rhabdomyosarcoma: A report from the Intergroup Rhabdomyosarcoma Study Group.* J Clin Oncol, 1999. **17**(11): p. 3487-93.
7. Gey, G., W.D. Coffman, and M.T. Kubicek. *Tissue culture studies of the proliferative capacity of cervical carcinoma and normal epithelium*. in *Cancer research*. 1952. AMER ASSOC CANCER RESEARCH PO BOX 11806, BIRMINGHAM, AL 35202.
8. Daniel, V.C., et al., *A primary xenograft model of small-cell lung cancer reveals irreversible changes in gene expression imposed by culture in vitro.* Cancer Res, 2009. **69**(8): p. 3364-73.
9. Romer, J. and T. Curran, *Targeting medulloblastoma: small-molecule inhibitors of the Sonic Hedgehog pathway as potential cancer therapeutics.* Cancer Res, 2005. **65**(12): p. 4975-8.
10. Lee, J., et al., *Tumor stem cells derived from glioblastomas cultured in bFGF and EGF more closely mirror the phenotype and genotype of primary tumors than do serum-cultured cell lines.* Cancer Cell, 2006. **9**(5): p. 391-403.
11. Ince, T.A., et al., *Characterization of twenty-five ovarian tumour cell lines that phenocopy primary tumours.* Nat Commun, 2015. **6**: p. 7419.
12. Sausville, E.A. and A.M. Burger, *Contributions of human tumor xenografts to anticancer drug development.* Cancer Res, 2006. **66**(7): p. 3351-4, discussion 3354.
13. Hidalgo, M., et al., *Patient-derived xenograft models: an emerging platform for translational cancer research.* Cancer Discov, 2014. **4**(9): p. 998-1013.
14. Byrne, A.T., et al., *Interrogating open issues in cancer precision medicine with patient-derived xenografts.* Nat Rev Cancer, 2017. **17**(4): p. 254-268.
15. Chen, X., et al., *Targeting oxidative stress in embryonal rhabdomyosarcoma.* Cancer Cell, 2013. **24**(6): p. 710-24.
16. Norris, R.E. and P.C. Adamson, *Challenges and opportunities in childhood cancer drug development.* Nat Rev Cancer, 2012. **12**(11): p. 776-82.
17. Sharma, S.V., D.A. Haber, and J. Settleman, *Cell line-based platforms to evaluate the therapeutic efficacy of candidate anticancer agents.* Nat Rev Cancer, 2010. **10**(4): p. 241-53.
18. Liu, X., et al., *Conditional reprogramming and long-term expansion of normal and tumor cells from human biospecimens.* Nat Protoc, 2017. **12**(2): p. 439-451.
19. Stewart, E., et al., *Orthotopic patient-derived xenografts of paediatric solid tumours.* Nature, 2017. **549**(7670): p. 96-100.
20. Shoemaker, R.H., *The NCI60 human tumour cell line anticancer drug screen.* Nat Rev Cancer, 2006. **6**(10): p. 813-23.
21. Hinson, A.R., et al., *Human rhabdomyosarcoma cell lines for rhabdomyosarcoma research: utility and pitfalls.* Front Oncol, 2013. **3**: p. 183.
22. Hazelton, B.J., et al., *Characterization of cell lines derived from xenografts of childhood rhabdomyosarcoma.* Cancer Res, 1987. **47**(16): p. 4501-7.
23. McAllister, R.M., et al., *Cultivation in vitro of cells derived from a human rhabdomyosarcoma.* Cancer, 1969. **24**(3): p. 520-6.

24. Giard, D.J., et al., *In vitro cultivation of human tumors: establishment of cell lines derived from a series of solid tumors.* J Natl Cancer Inst, 1973. **51**(5): p. 1417-23.
25. Houghton, P.J., et al., *The pediatric preclinical testing program: description of models and early testing results.* Pediatric blood & cancer, 2007. **49**(7): p. 928-940.
26. Lee, J., et al., *Tumor stem cells derived from glioblastomas cultured in bFGF and EGF more closely mirror the phenotype and genotype of primary tumors than do serum-cultured cell lines.* Cancer cell, 2006. **9**(5): p. 391-403.
27. Persson, C.U., et al., *Neuroblastoma patient-derived xenograft cells cultured in stem-cell promoting medium retain tumorigenic and metastatic capacities but differentiate in serum.* Sci Rep, 2017. **7**(1): p. 10274.
28. Ince, T.A., et al., *Characterization of twenty-five ovarian tumour cell lines that phenocopy primary tumours.* Nature communications, 2015. **6**.
29. Baker, M., *Reproducibility: Respect your cells!* Nature, 2016. **537**(7620): p. 433-5.
30. Loo, D.T., et al., *Extended culture of mouse embryo cells without senescence: inhibition by serum.* Science, 1987. **236**: p. 200-203.
31. Kumar, R., et al., *Induction of senescence in primary glioblastoma cells by serum and TGFbeta.* Sci Rep, 2017. **7**(1): p. 2156.
32. Vl, J.G.T., et al., *Identification of FGFR4-activating mutations in human rhabdomyosarcomas that promote metastasis in xenotransplanted models.* The Journal of clinical investigation, 2009. **119**(11): p. 3395.
33. Wachtel, M., et al., *FGFR4 signaling couples to Bim and not Bmf to discriminate subsets of alveolar rhabdomyosarcoma cells.* International journal of cancer, 2014. **135**(7): p. 1543-1552.
34. Fujii, M., et al., *A Colorectal Tumor Organoid Library Demonstrates Progressive Loss of Niche Factor Requirements during Tumorigenesis.* Cell Stem Cell, 2016. **18**(6): p. 827-38.
35. Fruman, D.A. and C. Rommel, *PI3K and cancer: lessons, challenges and opportunities.* Nat Rev Drug Discov, 2014. **13**(2): p. 140-56.
36. Petricoin, E.F., et al., *Phosphoprotein pathway mapping: Akt/mammalian target of rapamycin activation is negatively associated with childhood rhabdomyosarcoma survival.* Cancer research, 2007. **67**(7): p. 3431-3440.
37. Rarivomanana, M., et al., *[Botryoid rhabdomyosarcoma of the urogenital sinus. Apropos of 1 case in an 11 month old child].* Bull Soc Pathol Exot, 2000. **93**(1): p. 29-30.
38. Montero, J., et al., *Drug-induced death signaling strategy rapidly predicts cancer response to chemotherapy.* Cell, 2015. **160**(5): p. 977-89.
39. Chonghaile, T.N., et al., *Pretreatment mitochondrial priming correlates with clinical response to cytotoxic chemotherapy.* Science, 2011. **334**(6059): p. 1129-1133.
40. Böhm, M., et al., *Helicase CHD4 is an epigenetic coregulator of PAX3-FOXO1 in alveolar rhabdomyosarcoma.* The Journal of clinical investigation, 2016. **126**(11): p. 4237.

Figure legends

Figure 1. Identification of culture medium requirements for RTCs

(A) Model used to generate an RTC-based pre-clinical platform. Briefly, established PDXs were collected and dissociated to derive RTCs, which were then seeded on a 96-well plate format under different culture conditions (see text) before WST-1 assay was performed. Next, the proliferation rate of cells under standard and selected culture protocol was monitored together with aCGH analysis. Finally, a patient-specific drug profile was applied trough a high-throughput drug screen followed by *in vivo* validation of the top candidates on the original PDX. (B) Cell culture screen results of indicated RTCs. Blue and orange graph bars indicate absence or presence of supplemented growth factors (GFs), respectively (mean ± sd). (C) Representative bright-field images of SJRHB013757_G1C and SJRHB010463_X16C taken before WST-1 assay. Scale bar 200 μm. (D) IF analysis for expression of myosin heavy chain (MHC) in SJRHB013757_G1C cells under DMEM or PCM (primary culture medium, NB condition) conditions. Dapi was used for staining the nuclei. Scale bar 100 μm. (E) Representative bright-field images of SJRHB012_RC in presence or absence of GF on uncoated or gelatin-coating conditions. Scale bar 200 μm.

Table 1. Table indicating known genetic alterations of the RTCs used in the present study and the effect of GF on cell fitness. The GF ratio (+GF/-GF) was calculated for cells cultured under NB conditions and on Matrigel for all cell types but SJRHB012_RC and SJRHB013758_X1C where cell viability of cells cultured on gelatin was considered.

Figure 2. Proliferation rate of RTCs cultured under DMEM or NB conditions

(A) Proliferation rate of RTCs cultured under DMEM (black line) on uncoated plates and NB (red line) on Matrigel (RMS_ZH04_XC, SJRHB010463_X16C, SJRHB013759_X1C and SJRHB13758_X2C) or gelatin-coated plates (SJRHB13758_X1C and SJRHB012_RC). Cell number was normalized to day of seeding and is expressed in a logarithmic scale. (mean ± sd). (B) Growth curves of RTCs over time under indicated culture conditions (mean ± sd). Please note that “NB” in these graphs indicates neurobasal medium supplemented with 1% glutammax and 1% penicillin-streptomycin but without B-27. (C) Assessment of GF dependency upon long-term proliferation of GF-inhibited (upper panel) and GF-stimulated cells (lower panel). Each data point is expressed as percentage of day 0 (mean ± sd). On the right side of each graph, representative bright-field images taken at passage 3 are shown. Scale bar 100X magnification.

Figure 3. Copy number variants analysis of RTCs and histological characterization of xenografts

(A) Copy-number variants (CNVs) analysis of RMS_ZH04 (upper panel), SJRHB012_R (middle panel) and SJRHB012_S (lower panel) for the original PDXs and corresponding NB-derived RTCs or DMEM clones. (B, left panel) Formalin-fixed paraffin-embedded (FFPE) sections of RMS_ZH04 primary tumor, corresponding PDX and RTC-derived xenografts were stained for H&E (Hematoxylin and Eosin), DESMIN and MYOGENIN. (B, middle and right panel) FFPE sections of SJRHB012_R and SJRHB012_S PDX and matched RTC- or DMEM clone-derived xenografts. Staining for H&E, DESMIN and MYOGENIN is shown. Scale bar 200X magnification.

Figure 4. Pharmacological screen on RTCs and RMS cell lines

(A) Heat map depicting the activity of indicated agents used at final concentration of 500 nM across the RMS cell panel. RMS subtype, fusion status and cell type (RTC or cell line) are shown above each column. Each color in the heat map indicates the percentage of leaving cells relative to vehicle control: 0-30% (red), 30-60% (orange), 60-80% (light blue) and >80% (dark blue). (B, upper panel) Cell viability of indicated RTCs or cell lines treated for 72h with increasing concentrations of each drug (ABT-263, afuresertib, GSK690693, and idasanutlin) (mean ± sd; N=3). (B, lower panel) Table indicating corresponding IC-50 values (Black: undefined, Blue: >1uM, orange: 0.25-1uM and red: 0-0.25 uM) calculated by WST-1 assay. Subtype and TP-53 status for each cell type are also specified.

Supplemental Figures

Supplemental Table 1.

A description of the PDX lines and corresponding RTCs used in the present study. Information regarding the subtype, anatomic site, and type of treatment (if any) of the original tumors are shown.

Supplemental Figure 1 (relative to figure 1 and 2).

(A) Representative bright-field images of RTCs cultivated in NB or DMEM conditions. Outgrowing dmem_clones are also shown for SJRHB012_SC and SJRHB012_RC (upper panel). Images were taken at 40X or 100X magnification. (B) Tumor growth kinetic of SJRHB012_RC (left panel) and SJRHB012_SC (right panel) xenografts derived from matched NB cells (red line) or dmem_clones (black line). (C) Representative bright-field images of SJRHB012_RC, SJRHB012_SC and RMS-ZH04_XC cells at passage 3 under indicated culture conditions. Scale bar 100X magnification. (D, upper panel) Representative light-microscopy images of SJRHB012_RC at passage 1 (7 days from day of plaiting) in presence or absence of indicated

GF. (D, lower panel) IF for MYOSIN HEAVY CHAIN (MHC) expression in SJRHB012_RC cells at the same time point. Dapi was used to stain the nuclei. Images show overly of DAPI and MHC staining. Scale bar 50 μm.

Supplemental Figure 2 (relative to figure 3).

(A) Copy-number variants (CNVs) analysis of SJRHB13758 PDX and corresponding RTCs under NB or DMEM. (B) Table depicting the percentage of mouse cells detected by DAPI staining of indicated RTCs.

Supplemental Figure 3 (relative to figure 4).

(A) Clustering analysis of the drug response profile shown in figure 4. The activity of the compounds (row) is shown for each sample (column). (B, upper panel) Cell viability of indicated RTCs or cell lines treated for 72h with increasing concentrations of each drug (AZ20, YM155, verdinexor, idasanutlin) (mean ± sd). (B, lower panel) Table indicating corresponding IC-50 values (Black: undefined, Blue: >1uM, orange: 0.25-1uM and red: 0-0.25 uM) calculated by WST-1 assay. Subtype and TP-53 status for each cell type are also specified.

Figure 1

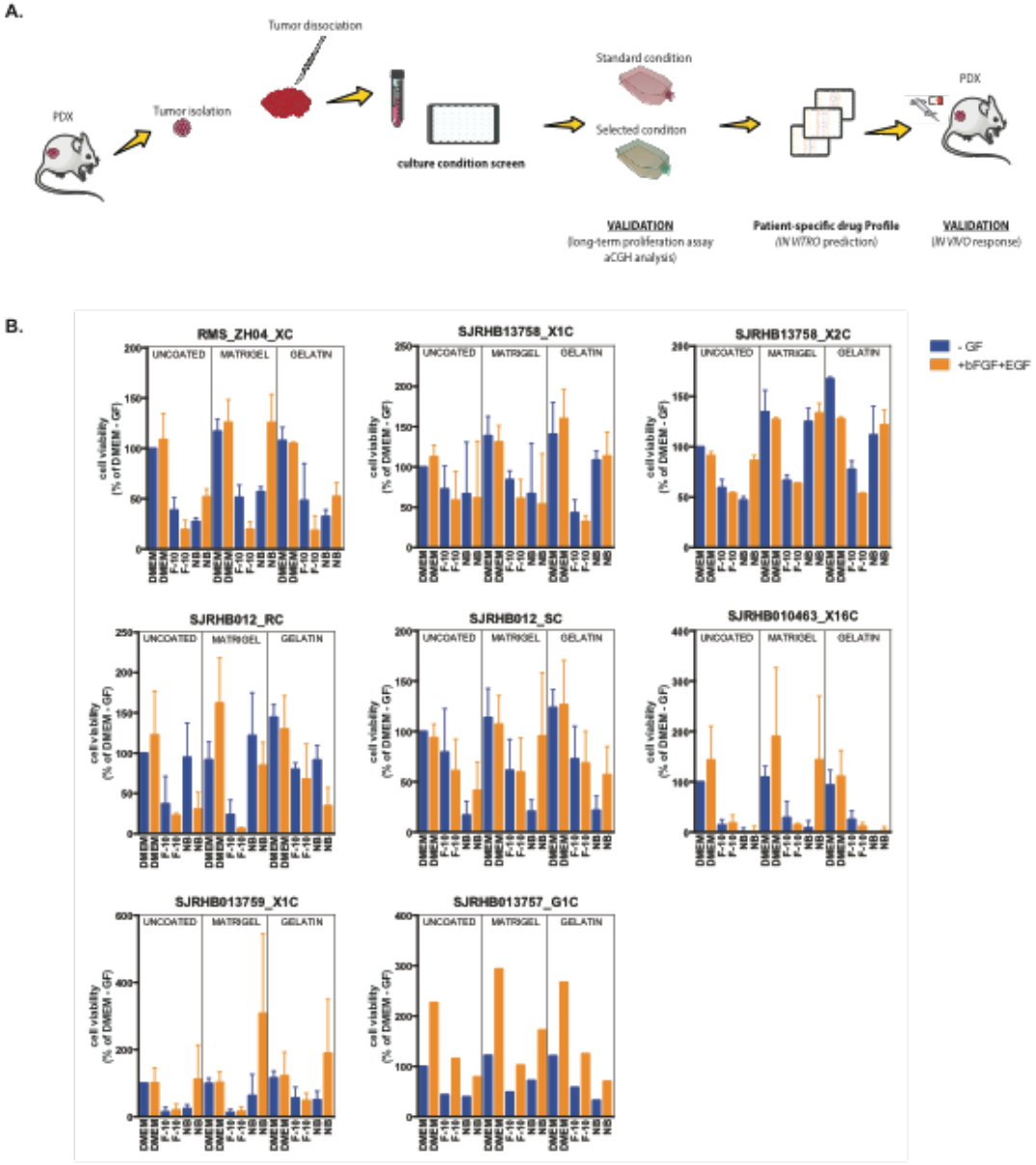
A.
PDX
Tumor isolation
Tumor dissociation
culture condition screen
Standard condition
Selected conditon
PDX
VALIDATION
(long-term proliferation assay
aCGH analysis)
Patient-specific drug Profile
(IN VITRO prediction)
VALIDATION
(IN VIVO response)
B.
RMS_ZH04_XC
SJRHB13758_X1C
SJRHB13758_X2C
SJRHB012_RC
SJRHB012_SC
SJRHB010463_X16C
SJRHB013759_X1C
SJRHB013757_G1C
UNCOATED
MATRIGEL
GELATIN
cell viability
(% of DMEM - GF)
- GF
+bFGF+EGF
C.
SJRHB013757_G1C
DMEM (+GF)
NB (+GF)
UNCOATED
SJRHB010463_X16C
DMEM (+GF)
NB (+GF)
MATRIGEL
D.
SJRHB013757_G1C
E.
SJRHB012_RC
NB (-GF)
NB (+GF)
UNCOATED
NB (-GF)
NB (+GF)
GELATIN

Table 1

SAMPLE	MUTATIONS	GF EFFECT (RATIO +GF/-GF)
SJRHB010463_X16C	PAX3-FOXO1, FGFR1	17.2
SJRHB013759_X1C	PAX3-FOXO1	4.9
SJRHB012_SC	CARD11, A2ML1	4.63
SJRHB013757_G1C	PAX7-FOXO1	2.4
RMS_ZH04_XC	Unknown	2.2
SJRHB013758_X1C	**HRAS**, NOTCH3	1
SJRHB013758_X2C	**HRAS**, TP53	1.1
SJRHB012_RC	CARD11, NF1, A2ML1	0.38

Figure 2

A.

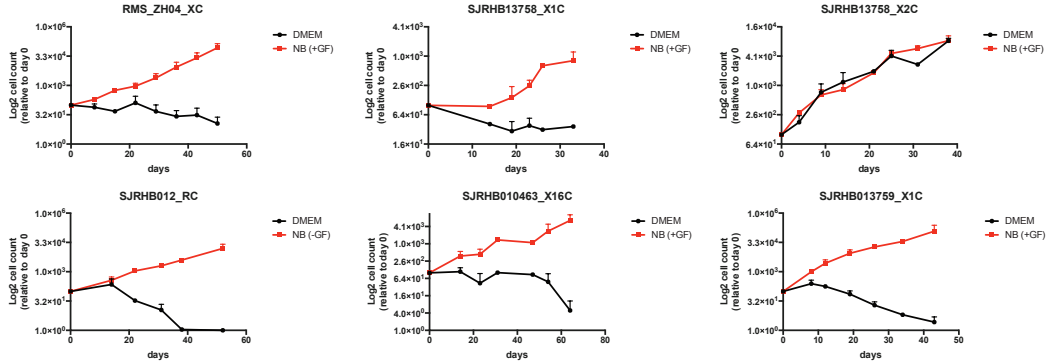
RMS_ZH04_XC
SJRHB13758_X1C
SJRHB13758_X2C
SJRHB012_RC
SJRHB010463_X16C
SJRHB013759_X1C
Log2 cell count (relative to day 0)
days
DMEM
NB (+GF)
NB (-GF)

B.

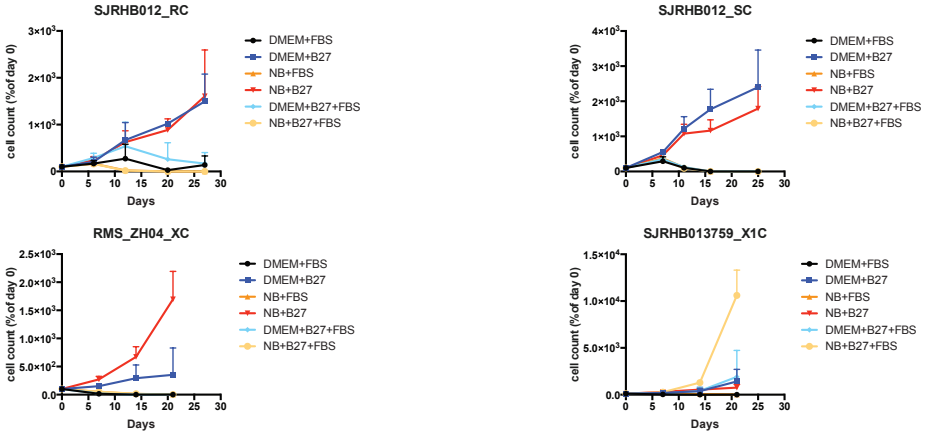
SJRHB012_RC
SJRHB012_SC
RMS_ZH04_XC
SJRHB013759_X1C
cell count (%of day 0)
Days
DMEM+FBS
DMEM+B27
NB+FBS
NB+B27
DMEM+B27+FBS
NB+B27+FBS

C.

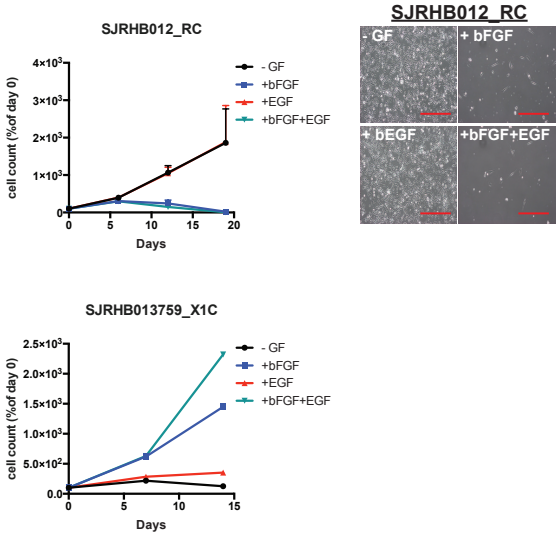
SJRHB012_RC
SJRHB013759_X1C
cell count (%of day 0)
Days
- GF
+bFGF
+EGF
+bFGF+EGF
SJRHB012_RC
- GF
+ bFGF
+ bEGF
+bFGF+EGF

Figure 3

A.

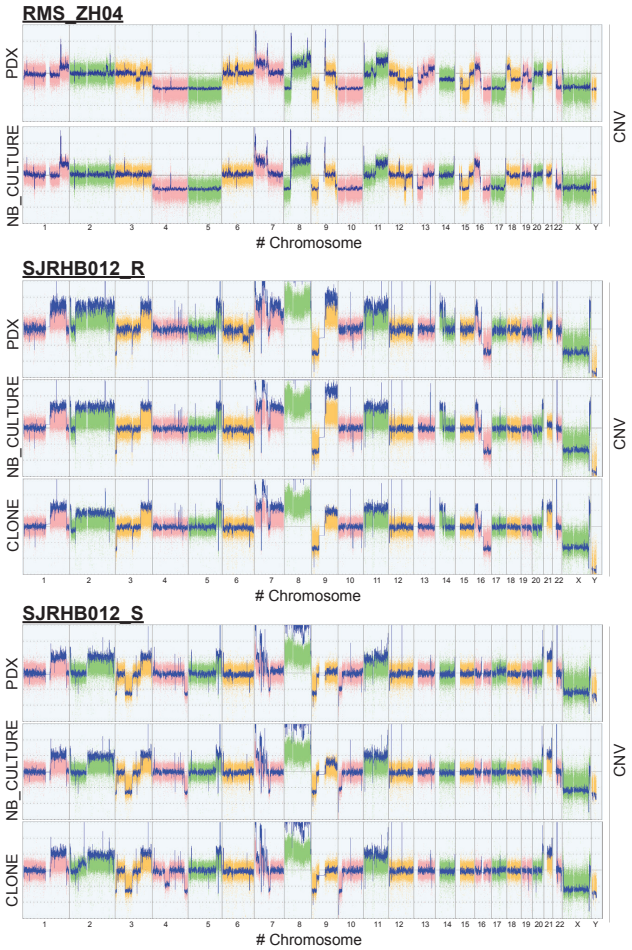
RMS_ZH04
PDX
NB_CULTURE
CNV
Chromosome
SJRHB012_R
PDX
NB_CULTURE
CLONE
CNV
Chromosome
SJRHB012_S
PDX
NB_CULTURE
CLONE
CNV
Chromosome

B.

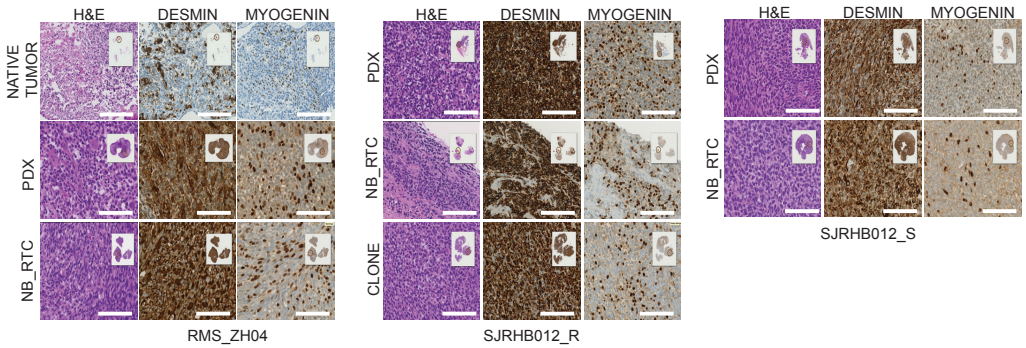
H&E
DESMIN
MYOGENIN
NATIVE TUMOR
PDX
NB_RTC
RMS_ZH04
H&E
DESMIN
MYOGENIN
PDX
NB_RTC
CLONE
SJRHB012_R
H&E
DESMIN
MYOGENIN
PDX
NB_RTC
SJRHB012_S

Figure 4

A.

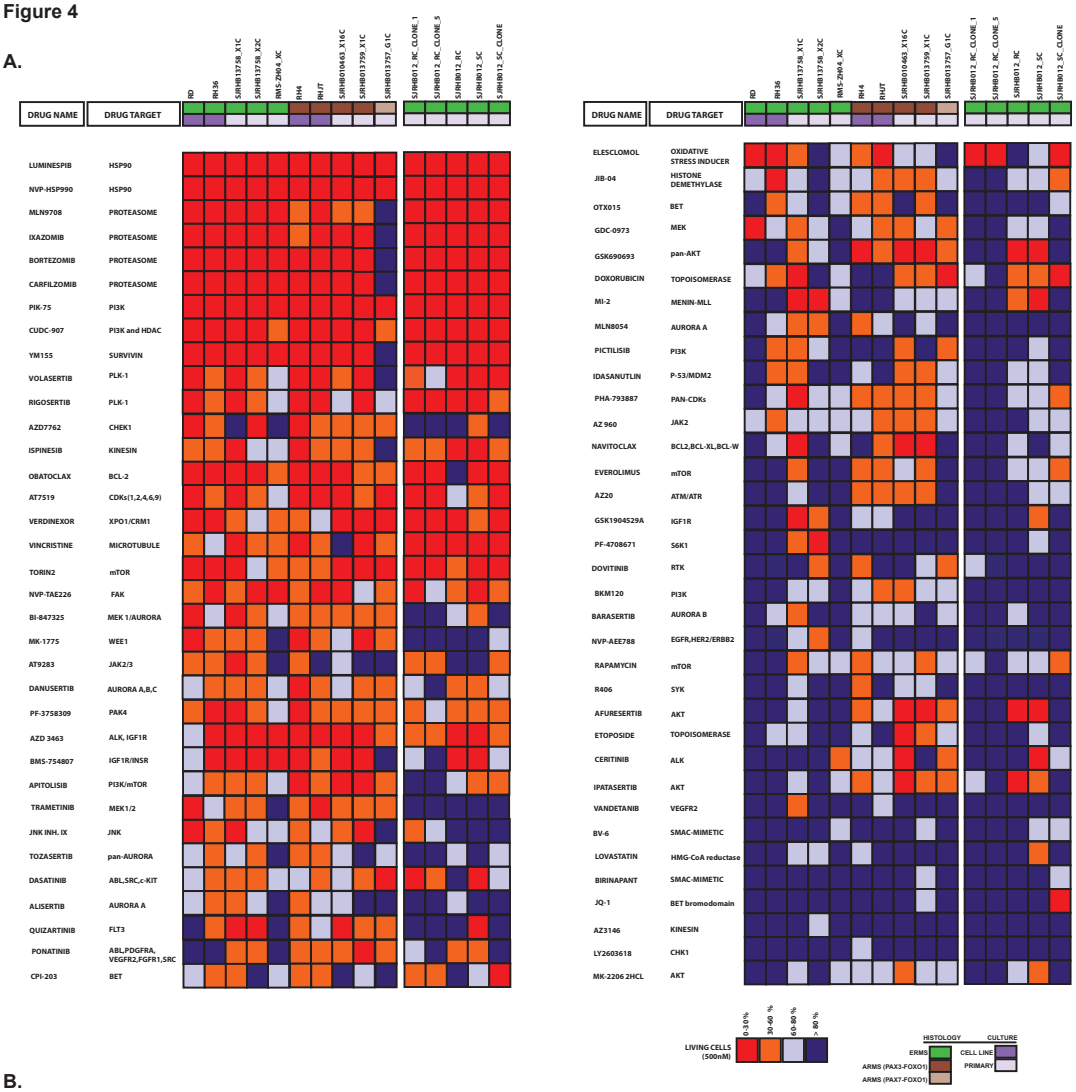

B.

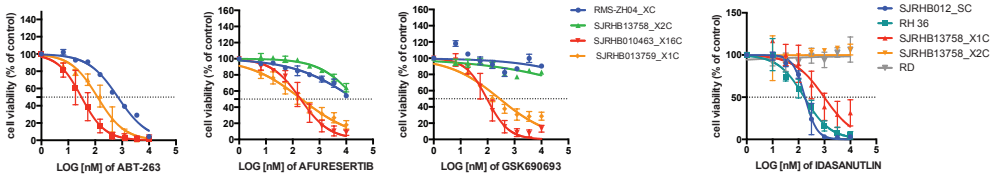

NAME	SUBTYPE	TP-53 STATUS	IC50 (uM) AFURESERTIB	IC50 (uM) GSK690693	IC50 (uM) ABT-263	IC50 (uM) IDASANUTLIN
RMS_ZH04_XC	ERMS	UNKNOWN	20.556	UNDEFINED	0.694	
SJRHB13758_X2C	ERMS	MUT	23.230	UNDEFINED		UNDEFINED
SJRHB010463_X16C	ARMS	WT	0.196	0.095	0.031	
SJRHB013759_X1C	ARMS	WT	0.212	0.281	0.122	
SJRHB13758_X1C	ERMS	WT				0.977
RD	ERMS	MUT				UNDEFINED
SJRHB012_SC	ERMS	WT				0.177
RH36	ERMS	WT				0.166

IC-50 (uM)
Undefined
>1
0.25-1
0-0.25

Suppl. Table 1

PDX	PRIMARY CULTURE	PRIMARY SITE	PATIENT (#)	SUBTYPE	ORIGIN	PRE-TREATED
SJRHB012_R	SJRHB012_RC	Prostate	# 2	ERMS	St. Jude Children's Research Hospital	Doxorubicin Etoposide
SJRHB012_S	SJRHB012_SC	Pelvic	# 2	ERMS	St. Jude Children's Research Hospital	Doxorubicin Etoposide
SJRHB013758_X1	SJRHB013758_X1C	Abdomen	# 3	ERMS	St. Jude Children's Research Hospital	No
SJRHB013758_X2	SJRHB013758_X2C	Unknown	# 3	ERMS	St. Jude Children's Research Hospital	Yes, 21 weeks chemo
RMS_ZH04_X	RMS_ZH04_XC	Unknown	# 4	ERMS	University Children's Hospital Zurich	Yes
SJRHB010463_X16	SJRHB010463_X16C	Unknown	# 5	ARMS (PAX3-FOXO1)	St. Jude Children's Research Hospital	No
SJRHB013759_X1	SJRHB013759_X1C	Unknown	# 6	ARMS (PAX3-FOXO1)	St. Jude Children's Research Hospital	No
SJRHB013757_G1	SJRHB013757_G1C	Unknown	# 7	ARMS (PAX7-FOXO1)	St. Jude Children's Research Hospital	No

Suppl.Figure 1

A.

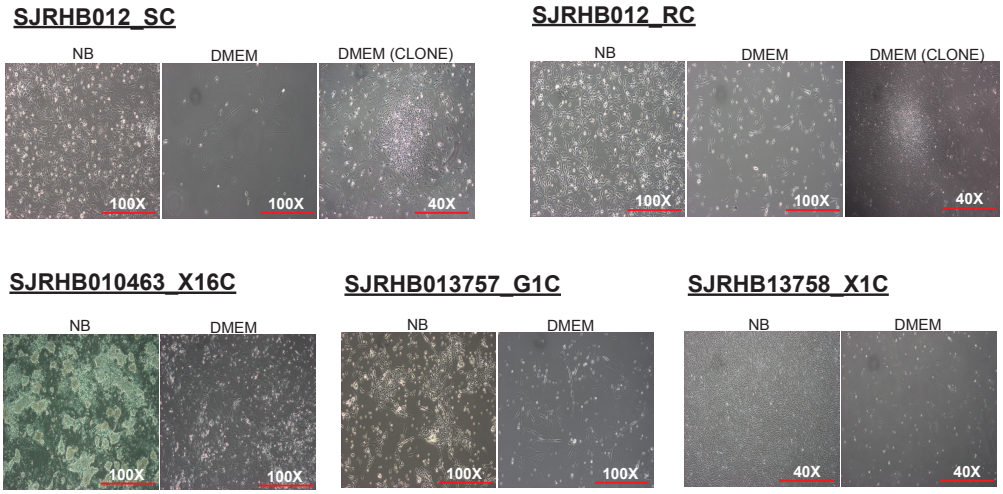

B.

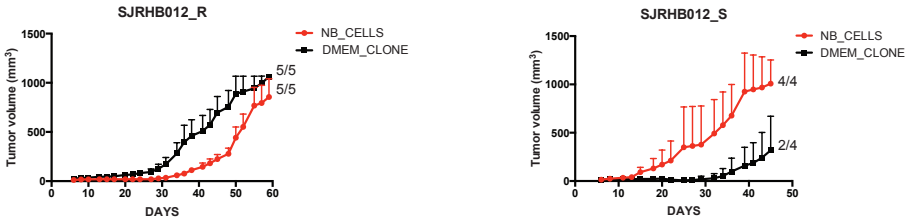

C.

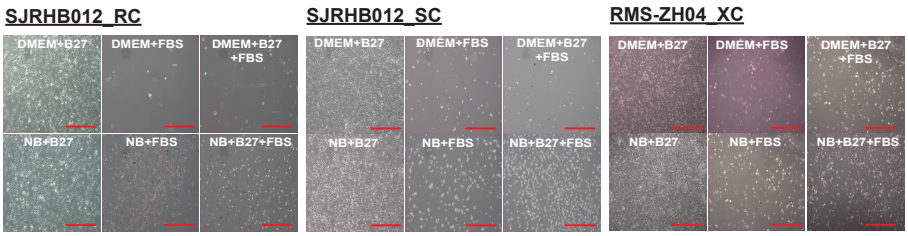

D.

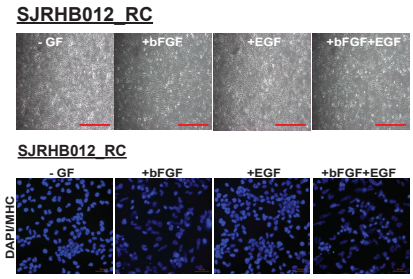

Suppl.Figure 2

A.

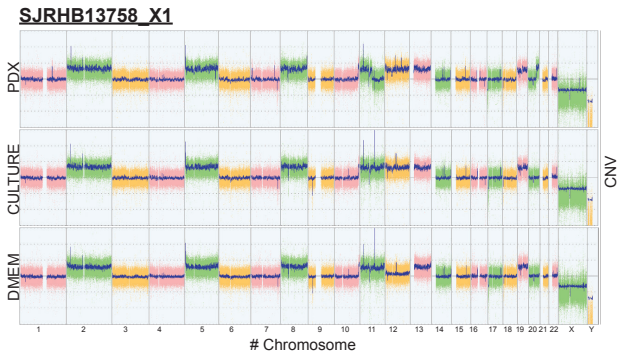

B.

SAMPLE	MOUSE CELLS (%)
SJRHB010463_X16C	Not performed
SJRHB013759_X1C	<1
SJRHB012_SC	<1
SJRHB013757_G1C	<1
RMS_ZH04_XC	8
SJRHB013758_X1C	14.5
SJRHB013758_X2C	<1
SJRHB012_RC	<1

Supp. Figure 3

A.

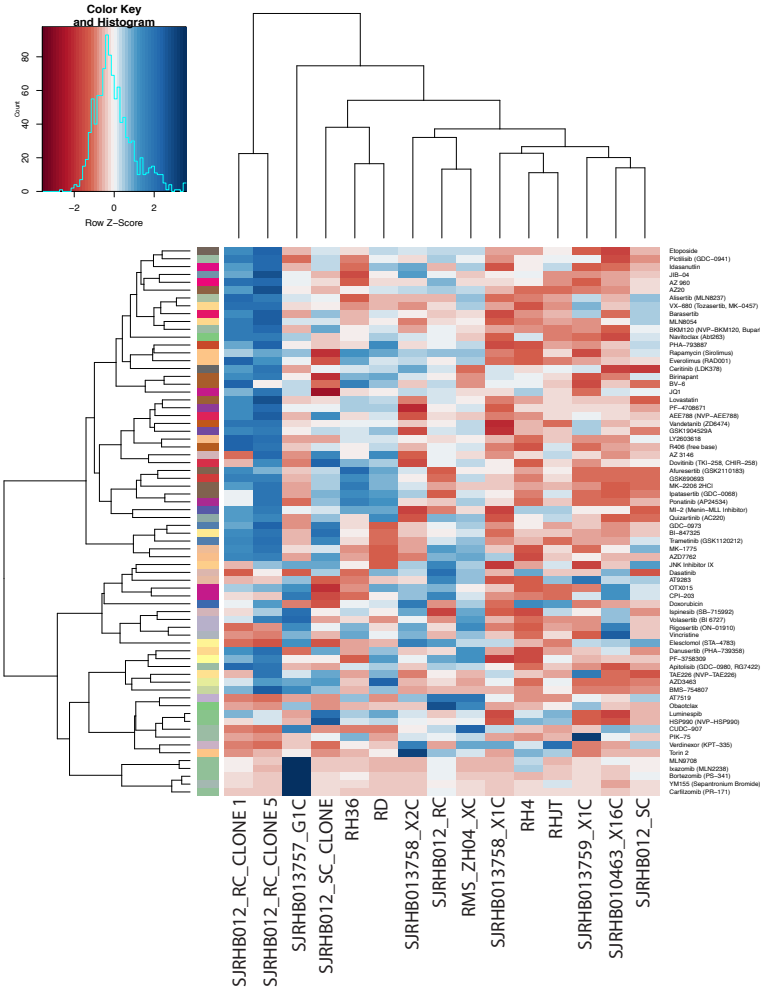

B.

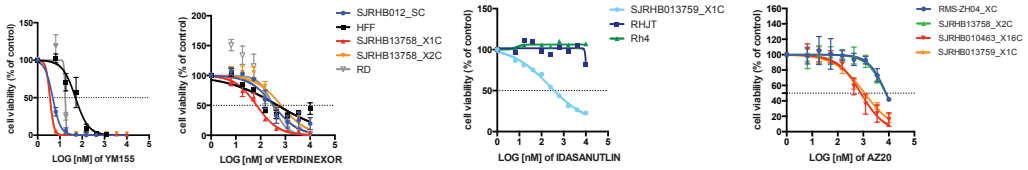

NAME	SUBTYPE	TP-53 STATUS	IC50 (uM) AZ20	IC50 (uM) YM155	IC50 (uM) VERDINEXOR	IC50 (uM) IDASANUTLIN
RMS_ZH04_XC	ERMS	UNKOWN	7.796			
SJRHB010463_X16C	ARMS	WT	0.803			
SJRHB13758_X2C	ERMS	MUT	7.477	0.0035	0.679	
SJRHB013759_X1C	ARMS	WT	1.125			0.224
HFF	NORMAL CELLS	WT		0.05	0.487	
SJRHB13758_X1C	ERMS	WT		0.0036	0.069	
RD	ERMS	MUT		0.017	0.317	
SJRHB012_SC	ERMS	WT		0.0048	0.331	
RH4	ARMS	MUT				UNDEFINED
RHJT	ARMS	WT				UNDEFINED

Suppl. Table 2

		SJRHB010463_X16C	SJRHB013759_X1C	RMS-ZH04_XC	SJRHB013757_G1C	SJRHB13758_X1C	SJRHB13758_X2C	SJRHB012_RC	SJRHB012_SC
NO COATING									
-	DMEM	100	100	100	100	100	100	100	100
+	DMEM	143.28633	100.66277	108.745225	226.5206	112.6048667	91.35102	122.6057572	93.80551414
-	F-10	14.33978825	14.40550567	38.68501	43.65427	72.64595333	59.281345	36.92284888	79.38370446
+	F-10	18.13584625	20.26559633	19.416395	115.6674	58.70552667	54.04034	22.79631607	61.04767599
-	NB	0.43415545	24.00341667	27.3079	39.43107	66.70999	47.061345	94.74028925	16.88459187
+	NB	1.4654645	111.5079967	52.03451	79.12473	61.3214	86.42069	30.45999425	41.35088759
MATRIGEL									
-	DMEM	109.3724025	99.07643	117.01555	121.7506	138.7735	134.79435	91.68912643	113.7840817
+	DMEM	190.1150525	102.04987	125.9591	230.4375	131.1431333	126.95085	162.1196676	107.2259965
-	F-10	28.90856025	12.96668667	51.43482	49.0372	84.16536333	66.808995	23.81132526	61.31859762
+	F-10	14.4909775	15.86510967	19.63866	102.6477	60.79662	63.774855	6.243846331	59.46330499
-	NB	8.377257	63.12761	57.02533	71.94749	66.90718667	125.25335	121.8345388	20.62598575
+	NB	143.7415725	307.92	125.7676	172.2101	54.00627667	133.70855	84.96755659	95.44013311
GELATIN									
-	DMEM	93.52682	115.2651633	107.7371	120.9847	140.58068	167.48	144.494349	123.7064537
+	DMEM	110.9570425	121.5720967	104.84925	267.046	160.1919	127.87035	129.9856156	126.562512
-	F-10	25.111923	55.67869333	48.340285	58.20569	43.15438333	77.620855	80.06798513	72.7524233
+	F-10	11.551761	48.17922333	18.5549485	124.9672	32.37836333	53.725055	67.74864823	68.54139239
-	NB	-1.552923125	49.98456333	32.287195	32.47265	108.4531233	111.80429	91.4576457	21.63124264
+	NB	2.88213725	188.87067	52.327215	70.4814	113.5296067	121.8352	34.61986302	57.0184661

CELL VIABILITY

0-100

100-200

200-310

Suppl. Table 3

Catalog No.	Product Name	Target
S1005	**Axitinib**	VEGFR, PDGFR, c-Kit
S1023	**Erlotinib HCl (OSI-744)**	EGFR
S1042	**Sunitinib Malate**	VEGFR, PDGFR, c-Kit, Flt
S1060	**Olaparib (AZD2281, Ku-0059436)**	PARP
S1082	**Vismodegib (GDC-0449)**	Hedgehog, P-gp
S1119	**Cabozantinib (XL184, BMS-907351)**	VEGFR, c-Met, Flt, Tie-2, c-Kit
S1164	**Lenvatinib (E7080)**	VEGFR
S1267	**Vemurafenib (PLX4032, RG7204)**	Raf
S1524	**AT7519**	CDK
S1570	**KU-60019**	ATM
S2061	**Lovastatin**	HMG-CoA Reductase
S1006	**Saracatinib (AZD0530)**	Src, Bcr-Abl
S1025	**Gefitinib (ZD1839)**	EGFR
S1046	**Vandetanib (ZD6474)**	VEGFR
S1065	**GDC-0941**	PI3K
S1092	**KU-55933 (ATM Kinase Inhibitor)**	ATM
S1120	**Everolimus (RAD001)**	mTOR
S1168	**Valproic acid sodium salt (Sodium valproate)**	GABA Receptor, HDAC
S1362	**Rigosertib (ON-01910)**	PLK
S1525	**MK-1775**	Wee1
S1574	**BIRB 796 (Doramapimod)**	p38 MAPK
S2151	**LDE225 (NVP-LDE225,Erismodegib)**	Smoothened
S1007	**FG-4592**	HIF
S1028	**Lapatinib (GW-572016) Ditosylate**	EGFR, HER2
S1047	**Vorinostat (SAHA, MK0683)**	HDAC
S1067	**SB431542**	TGF-beta/Smad
S1093	**GSK1904529A**	IGF-1R
S1124	**BMS-754807**	IGF-1R
S1171	**CYC116**	Aurora Kinase, VEGFR
S1378	**Ruxolitinib (INCB018424)**	JAK
S1526	**Quizartinib (AC220)**	Flt
S1575	**RO4929097**	Y-Secretase
S2163	**PF-4708671**	S6 Kinase
S1011	**Afatinib (BIBW2992)**	EGFR
S1029	**Lenalidomide (CC-5013)**	TNF-alpha
S1048	**VX-680 (Tozasertib, MK-0457)**	Aurora Kinase
S1068	**Crizotinib (PF-02341066)**	c-Met, ALK
S1100	**MLN8054**	Aurora Kinase
S1130	**YM155 (Sepantronium Bromide)**	Survivin
S1180	**XAV-939**	Wnt/beta-catenin
S1396	**Resveratrol**	Sirtuin
S1532	**AZD7762**	Chk
S1577	**Tie2 kinase inhibitor**	Tie-2
S2180	**MLN2238**	Proteasome

S1013	**Bortezomib (PS-341)**	Proteasome
S1033	**Nilotinib (AMN-107)**	Bcr-Abl
S1049	**Y-27632 2HCl**	ROCK
S1069	**AUY922 (NVP-AUY922)**	HSP
S1107	**Danusertib (PHA-739358)**	Aurora Kinase, FGFR, Bcr-Abl, c-RET, Src
S1133	**Alisertib (MLN8237)**	Aurora Kinase
S1193	**Thalidomide**	Others
S1452	**Ispinesib (SB-715992)**	Kinesin
S1533	**R406 (free base)**	Syk
S1782	**Azacitidine**	DNA/RNA Synthesis
S2181	**MLN9708**	Proteasome
S1014	**Bosutinib (SKI-606)**	Src
S1035	Pazopanib HCl	
S1052	**Elesclomol (STA-4783)**	HSP
S1070	**PHA-665752**	c-Met
S1113	**GSK690693**	Akt
S1134	**AT9283**	Bcr-Abl, JAK, Aurora Kinase
S1200	**Decitabine**	DNA/RNA Synthesis
S1486	**AEE788 (NVP-AEE788)**	EGFR, Flt, VEGFR, HER2
S1534	**Org 27569**	Cannabinoid Receptor
S1802	**Acadesine**	AMPK
S2198	**SGI-1776 free base**	Pim
S1004	**Veliparib (ABT-888)**	PARP
S1021	**Dasatinib**	Src, Bcr-Abl, c-Kit
S1040	**Sorafenib Tosylate**	VEGFR, PDGFR, Raf
S1055	**Enzastaurin (LY317615)**	PKC
S1078	**MK-2206 2HCl**	Akt
S1116	**Palbociclib (PD-0332991) HCl**	CDK
S1153	**Roscovitine (Seliciclib,CYC202)**	CDK
S1233	**2-Methoxyestradiol (2-MeOE2)**	HIF
S1490	**Ponatinib (AP24534)**	Bcr-Abl, VEGFR, FGFR, PDGFR, Flt
S1567	**Pomalidomide**	TNF-alpha, COX
S2013	**PF-573228**	FAK
S1018	**Dovitinib (TKI-258, CHIR-258)**	c-Kit, FGFR, Flt, VEGFR, PDGFR
S1039	**Rapamycin (Sirolimus)**	mTOR
S1053	**Entinostat (MS-275)**	HDAC
S1075	**SB216763**	GSK-3
S1114	**JNJ-38877605**	c-Met
S1147	**Barasertib (AZD1152-HQPA)**	Aurora Kinase
S1205	**PIK-75**	PI3K, DNA-PK
S1487	**PHA-793887**	CDK
S1541	**EX 527 (Selisistat)**	Sirtuin
S1971	**Nicorandil**	Others
S2214	**AZ 960**	JAK
S7638	*LDC1267*	Axl
S7656	*CPI-360*	Histone Methyltransferase

S7665	*CH5183284 (Debio-1347)*	FGFR
S7679	*YK-4-279*	DNA/RNA Synthesis
S7693	*AZD6738*	ATM/ATR
S7707	*Verdinexor (KPT-335)*	CRM1
S7748	*EPZ015666*	Histone Methyltransferase
S7799	*Pexmetinib (ARRY-614)*	p38 MAPK
S7818	*Pexidartinib (PLX3397)*	CSF-1R
S7843	*BI-847325*	MEK
S7906	*PFI-4*	Epigenetic Reader Domain
S7910	*Epacadostat (INCB024360)*	IDO
S8031	**NSC 23766**	Rac
S8044	**BMS-345541**	IκB/IKK
S8057	**Pacritinib (SB1518)**	JAK
S2235	**Volasertib (BI 6727)**	PLK
S2673	**Trametinib (GSK1120212)**	MEK
S2742	**PHA-767491**	CDK
S2820	**TAE226 (NVP-TAE226)**	FAK
S3021	**Rimonabant**	Cannabinoid Receptor
S7050	**AZ20**	ATM/ATR
S7097	**HSP990 (NVP-HSP990)**	HSP (e.g. HSP90)
S7152	**C646**	Histone Acetyltransferase
S7281	*JIB-04*	Histone demethylases
S7440	**LEE011**	CDK
S7574	*GSK-LSD1 2HCl*	Histone Demethylase
S2243	**Degrasyn (WP1130)**	DUB, Bcr-Abl
S2680	**Ibrutinib (PCI-32765)**	Src
S2759	**CUDC-907**	HDAC, PI3K
S2824	**TPCA-1**	IKK
S4001	**Cabozantinib malate (XL184)**	
S7061	*GSK126*	Histone Methyltransferase
S7106	**AZD3463**	ALK
S7153	**10058-F4**	c-Myc
S7294	*PFI-2*	Histone Methyltransferase
S7461	**LDC000067**	CDK
S7581	*GSK J1*	Histone Demethylase
S2247	**BKM120 (NVP-BKM120, Buparlisib)**	PI3K
S2686	**NVP-BSK805 2HCl**	JAK
S2761	**NVP-BVU972**	c-Met
S2853	**Carfilzomib (PR-171)**	Proteasome
S4054	**Spironolactone**	Androgen Receptor
S7062	**EPZ5676**	Methyltransferase
S7128	**EPZ-6438**	Histone Methyltransferase
S7173	**AVL-292**	BTK
S7304	**CPI-203**	Epigenetic Reader Domain
S7462	**PI-1840**	Proteasome
S7587	**INCB024360**	IDO
S2475	**Imatinib (STI571)**	PDGFR,c-Kit, v-Abl

S2696	**GDC-0980 (RG7422)**	mTOR, PI3K
S2773	**SB705498**	TRPV
S2871	**T0070907**	PPAR
S4901	**JNK-IN-8**	Free Base
S7070	**GSK J4 HCl**	Others
S7129	**PYR-41**	E1 Activating
S7234	**IOX1**	Histone demethylases
S7307	**GSK2606414**	PERK
S7508	**JNK Inhibitor IX**	JNK
S7591	*BRD4770*	Histone Methyltransferase
S2606	**Mifepristone**	Estrogen/progestogen Receptor
S2697	**A-769662**	AMPK
S2789	**Tofacitinib (CP-690550,Tasocitinib)**	JAK
S2912	**WZ811**	CXCR
S4902	**QNZ (EVP4593)**	NF-κB
S7083	**LDK378**	ALK
S7130	**PR-619**	DUB
S7237	**OG-L002**	Histone demethylases
S7330	**6H05**	Rho
S7519	*GNF-5837*	Trk receptor
S7597	**BV-6**	IAP
S2626	**LY2603618**	Chk
S2719	**AMG-900**	Aurora Kinase
S2807	**Dabrafenib (GSK2118436)**	Raf
S2919	**IOX2**	HIF
S5001	**Tofacitinib (CP-690550) Citrate**	JAK
S7085	**IWP-2**	Wnt/beta-catenin
S7132	**P5091 (P005091)**	DUB
S7256	**SGC-CBP30**	Epigenetic Reader Domain
S7332	**K-Ras(G12C) inhibitor 9**	Rho
S7521	*Afuresertib (GSK2110183)*	Akt
S7611	*EI1*	Histone Methyltransferase
S2221	**Apatinib**	VEGFR
S2660	**MK-0752**	Gamma-secretase
S2731	**AZ 3146**	Kinesin
S2817	**Torin 2**	mTOR
S3012	**Pazopanib**	VEGFR
S7040	**AZD3514**	Androgen Receptor
S7094	**PF-3758309**	PAK
S7145	**AZD1080**	GSK-3
S7265	**MM-102**	Histone Methyltransferase
S7360	**OTX015**	BET
S7570	*UNC0379*	Histone Methyltransferase
S2638	**NU7441 (KU-57788)**	DNA-PK, PI3K
S2730	**Crenolanib (CP-868596)**	PDGFR
S2808	**GDC-0068**	Akt
S2925	**Evacetrapib (LY2484595)**	CETP

S7010	**GDC-0152**	IAP
S7087	**GSK2334470**	PDK-1
S7138	**BMS-833923**	Hedgehog/Smoothened
S7257	**CNX-774**	BTK
S7337	**SH-4-54**	STAT
S7554	*GDC-0994*	ERK
S7618	*MI-2 (Menin-MLL Inhibitor)*	Histone Methyltransferase
KISPI001	GDC-0973	MEK
KISPI002	Fenretinide	Unknown
KISPI003	JQ-1	BRD4
KISPI004	Birinapant	IAP
KISPI005	Doxorubicin	topoisomerase II
KISPI006	Etoposide	topoisomerase II
KISPI007	Vincristine	Microtubule
KISPI008	Idasanutlin	MDM2-P53
KISPI009	iBET	BRD
KISPI010	ABT-263	BCL-2,BCL-XL,BCL-W
KISPI011	Obatoclax	BCL-2
KISPI012	Dynosaur	DYNAMIN
KISPI013	Dynamo	

6.2. Manuscript 2

BCL-XL Inhibition Sensitizes Patient-Derived Recurrent Rhabdomyosarcoma Cells To Standard Chemotherapy.

[1]Manzella G., [1]Römmele M. and [1]Schäfer B.W.

[1] Department of Oncology, University Children's hospital of Zurich, Switzerland

Manuscript in preparation

Personal contribution: I performed all experiments except mice xenograft studies, which were performed by Römmele M. (Figure 6B).

I was further responsible for conception and design, statistical analysis, data interpretation as well as writing and formatting of this manuscript.

Introduction

While childhood cancers are generally uncommon, they represent the first cause of disease-related death in children (≤20 years old) [1]. The mainstay of therapy for pediatric patients with solid tumors consists of surgery, radiotherapy and standard chemotherapy. Although such approach remains one of the greatest examples of success in the clinic, cancer is still fatal for approximately 90,000 children and adolescents every year worldwide [2, 3].

Rhabdomyosarcoma (RMS) is the most common soft-tissue sarcoma in children and includes two main subtypes named alveolar (ARMS) and embryonal (ERMS) RMS. The traditional first-line chemotherapy regimen is based on the VAC/VAI protocol, which combines vincristine, actinomycin D and cyclophosphamide or ifosfamide [4]. Despite advances in RMS care, cure rates have reached a plateau over the last three decades [5, 6]. Presently, 30% of RMS patients continue to experience relapse disease with a median surivival of only ~10 months from the time of first recurrence [7, 8]. The treatment plan for this group of patients is not well defined and in most of the cases intensification of chemotherapy (with the addition of topoisomerase I and II antagonists) is applied [4]. It was estimated that even when response occurs, one third of the survivors experience at least one severe or life threatening effect such as organ dysfunctions or development of second malignant neoplasms (SMNs) [9-11]. Hence, resistance to cytotoxic chemotherapeutics followed by long-term sequelae represent a major challenge for the achievement of a complete cure.

One possibility to counteract chemoresistance and limit aggressive therapies is to define new combinatorial treatments strategies. However, a priori identification of druggable interaction networks is hindered by the relative homogenous genetic landscape of RMS and therefore functional pre-clinical platforms are urgently needed [12, 13]. Recently, we and others have shown the feasibility of using RMS PDX models and primary cultures (RPCs) to guide personalized therapeutic strategies (manuscript 1 and [14, 15]).

In the present study, we modeled chemorefractory disease by taking advantage of RPCs derived from diagnostic/relapse pairs of ERMS tumors. We first confirmed that our *in vitro* culture conditions preserved the differential chemo-response in recurrent compared to diagnostic RPCs of the same patient. We then employed *in vitro* high-throughput drug screens to identify chemosensitizing compounds for patients with poor outcome. Among the top scoring drugs, we discovered the BH3-mimetic ABT-263, which was further validated *in vivo* on the original PDX. Mechanistic studies revealed that ABT-263/standard chemotherapy exploits the BCL-XL/MCL-1 axis and in a NOXA-dependent manner in recurrent ERMS. Altogether, we discovered new combinatorial therapeutic modalities that might be evaluated in clinical trials as escape routes for patients where responses to conventional treatments are not long lasting.

Results

Characterization of chemo-resistant/sensitive ERMS models.

To discover mechanisms of sensitization to standard-of-care therapies in ERMS, we adopted a pre-clinical platform, which combines PDXs and matched primary cultures (RPCs) derived from pre-treatment and post-relapse tumor biopsies of the same patient (Figure 1A and manuscript 1). Of note, our *in vitro* model closely preserves the molecular and phenotypic heterogeneity observed in the primary tumors and PDXs (manuscript 1). Hence, we asked weather RPCs from relapse and diagnostic patients displayed a different sensitivity to conventional chemo-therapeutics. To this end, we performed dose escalation experiments following 72h treatment with a panel of agents (doxorubicin, etoposide, actinomycin D and vincristine) commonly used for the management of RMS patients and also according to the available clinical information of the samples we employed in the current study (Figure 1B and 1C and manuscript 1). WST-1 assay was used as read-out of cell viability and data were normalized to vehicle control. Interestingly, we observed a clear refractory response for SJRHB13758_X2C (relapse cells from patient #3) to both topoisomerase II targeting agents ($IC50_{doxrubicin}$ > 33.8 fold, $IC50_{etoposide}$ > 39.9 fold) and to etoposide only ($IC50_{etoposide}$ > 3.3 fold) for SJRHB012_ZC (relapse cells from patient #2) when compared to the corresponding diagnostic RPCs (Figure 1B and 1C). Moreover, vincristine exhibited mostly a cytostatic effect in either diagnostic or recurrent cells and no difference was observed in the response to actinomycin D (Suppl.Figure 1A). Such response profile is partially consistent with the treatment regimen initially applied to the patients (manuscript 1).

Altogether, we validated the chemoresistant phenotype of recurrent RPCs, which we selected as model to unravel new combinatorial options for patients with poor outcome.

A drug screening approach identifies ABT-263 as potential novel sensitizer of standard chemotherapy in ERMS.

Failure of conventional treatment for high-risk group ERMS patients remains a major unsolved clinical problem to date. Therefore, to identify “ready to use” sensitizing drugs towards standard chemotherapy, we combined a drug library containing 204 FDA-approved drugs or compounds in clinical development (500 nM) with standard cytotoxic agents (doxorubicin ~IC-20 or etoposide, ~IC-30) in SJRHB13758_X2C cells which served as recurrent and resistant model of ERMS (Figure 1A). Cell viability was assessed 72 hours post-treatment and top hits were filtered by considering only drugs showing at least 40% reduction of cell survival in combination compared to single treatment. Based on these criteria, we identified only few candidates in each combinatorial screen (3 drugs in combination with etoposide and 6 with doxorubicin), of which 5 out of 9 target growth factor signaling followed by cell death pathways (2 out of 9) (Figure 2A). Nevertheless, we focused our attention on ABT-263, a multiple BCL-2/BCL-XL/BCL-W inhibitor

(orally available), for several reasons: 1) it was the only candidate shared between the 2 screen results, 2) it has already entered into clinical trials for different cancer entities [16-19], 3) we reasoned that interfering directly with the apoptotic machinery might overcome the limitations of upstream kinase inhibitors 4) and its chemosensitizer function has not been explored in RMS yet. Therefore, we initially tested the single agent activity of ABT-263 in a panel of ERMS cells including primary cultures (RPCs), RD cell line and normal primary human foreskin fibroblasts (HFF). Cells were treated for 72 hours with increasing concentrations of the drug (Figure 2B, upper panel). Cell viability results revealed that relapse cells were generally poor responsive to the drug (IC-50: 1-69-14.63 uM) whereas no effect was observed in HFF cells. In contrast, a strong response was detected for SJRHB13758_X1C (diagnostic cells from patient #3) showing an IC50 in the nanomolar range (~150 nM) (Figure 2B, lower panel). To unravel this discrepancy in the drug-response we performed protein analysis for both pro-survival and pro-apoptotic BCL-2 family members in ABT-263-naive and -resistant cells but we were unable to correlate the expression of these proteins with the response to the inhibitor (Figure 2C). However, BCL-XL, BCL-2, MCL-1, BAK, BIM and NOXA were widely expressed across the cell types examined although to different levels. Only BAX could not be detected in SJRHB13758_X2C cells, a feature previously shown to be associated with chemo-resistant tumors [20, 21].

In sum, these findings suggest that ABT-263 has a limited single agent activity across ERMS recurrent cells but represents a potential 'partner' compound of conventional therapy.

Treatment with ABT-263 restores chemo-sensitivity in ERMS recurrent cells

In order to validate our screen results, we performed combinatorial treatments in various ERMS relapse cells with ABT-263 (250 nM and 500 nM) and a set of chemotherapeutics (i.e. doxorubicin, etoposide and vincristine) tested in an 8-point dose-response curve. Again cell viability was normalized to vehicle control per each data point. As expected, ABT-263 alone showed a negligible effect on cell survival (ranging between 6.72% to 32.5% reduction) whereas the combination with standard chemotherapy was highly effective across 3 different recurrent cell types (Figure 3A and Supp. Figure 2A). Calculation of the combination index (CI) revealed a strong synergistic effect of ABT-263 with doxorubicin and vincristine and to a lesser extent with etoposide (Suppl. Figure 2B). To demonstrate the cytotoxic activity of the ABT-263/standard chemotherapy combination, we monitored caspase 3/7-activity upon co-treatment of ABT-263 with doxorubicin (3-6 hours time point), vincristine (9 hours time point) and etoposide (24-48 hours time point) (Figure 3B and Suppl.Figure 2C). Our analysis revealed that both SJRHB13758_X2C and SJRHB012_ZC cells showed an elevated cell death in co-treatment experiments reaching between ~2- and ~10- fold increase when compared to ABT-263 alone. These findings were further corroborated by western blot analysis, which showed increased protein levels of known apoptotic markers such as cleaved PARP and CASPASE 3 in co-treated

cells (Figure 3C and Suppl.Figure 2D). Taken together, these data indicate that ABT-263 enhances the effect of conventional chemotherapeutics by augmenting cell death in recurrent RPCs.

NOXA partially mediates ABT-263/standard chemotherapy-induced cell death

Next, we investigated which pro-apoptotic player is engaged by ABT-263/standard chemotherapy. To this aim, we used a lentiviral-based crispr-Cas9 system to knock-out two main BH3-only proteins namely BIM (1 sgRNA) and NOXA (2 sgRNAs), which are well known antagonistic partners of the pro-survival BCL-2 family members (Figure 4A, left panel). Cells transduced with a scramble sgRNA sequence were used as negative control. Silencing was validated on protein level by western blot 7 days after transduction (Supp. Figure 3A, right panel). We then assessed the caspase activity upon short-term co-treatment of ABT-263 with conventional chemotherapeutics (Figure 4B and Suppl. Figure 3A). Unlike BIM knock-out, NOXA depletion significantly impaired the cooperative effect of ABT-263 with either vincristine or doxorubicin when compared to scramble control cells (Suppl. Figure 3A and Figure 4B). Accordingly, NOXA protein levels were transiently and shortly (6-9 h) upregulated upon exposure to these cytotoxic agents (Figure 4D). This is consistent with the pick of cell death achieved at these early time points in co-treatment experiments (Figure 3B). However, although ablation of NOXA could still counteract the effect of ABT-263/vincristine at later time points (72h), it was no longer sufficient to affect the cytotoxic activity of ABT-263/doxorubicin (Figure 4C). Therefore, late compensatory mechanisms might take place to mediate the combinatorial effect of ABT-263/doxorubicin. Additionally, the regulation of NOXA is likely to be independent from P53, since SJRHB13758_X2C cells do not express a functional P-53 as demonstrated by the lack of activity of idasunutlin, a MDM2 antagonist (Supp. Figure 3B). In contrast, the corresponding diagnostic cells, which harbor a TP-53^{wt} were rather sensitive (IC50 ~1uM). In sum, these findings suggest that NOXA is a functional mediator of ABT-263/standad chemotherapy-induced cell death.

ABT-263/stadard chemotherapy blocks the BCL-XL/MCL-1 axis

With the idea that the apoptotic machinery is altered by ABT-263/standard chemotherapy, we embarked on identifying which pro-survival factors are implicated in this interaction. First, we sought to determine the specific target of ABT-263 by using selective inhibitors of either BCL-2 (ABT-199 or venetoclax) or BCL-XL (A-1331852) at concentrations of 500 nM and 1uM each (Figure 5A). Upon 24h co-treatment with increasing concentrations of cytotoxic agents (doxorubicin or vincristine), we found that only BCL-XL inhibition could phenocopy the effect of ABT-263 (Figure 5A and Suppl. Figure 4A). Accordingly, crispr/Cas9-mediated down-regulation of BCL-XL by 2 independent sgRNAs sensitized SJRHB13758_X2C cells to vincristine-induced cell death at the same time point (24h) (Figure 5B and Suppl. Figure 4B). In contrast, depletion of

BCL-2, MCL-1 and BCL-W did not exhibit any effect pointing to BCL-XL as the main BCL-2 pro-survival member mediating the ABT-263 response (Figure 5B and Suppl. Figure 4B). Next, we attempted to dissect the potential anti-apoptotic factor affected by the standard chemotherapy. To this aim, we exposed the established knock-out cells to increasing concentrations of ABT-263 and assessed cell viability 24h later. Remarkably, only cells lacking MCL-1 were highly sensitive to the drug, corroborating previous reports (Figure 5C) [22]. Thus we reasoned that MCL-1, which is well known to be specifically engaged by NOXA represents a good candidate target of chemotherapy. To pursue this hypothesis, we analyzed MCL-1 protein levels upon doxorubicin treatment with or without ABT-263 in both SJRHB13758_X2C and SJRHB012_ZC recurrent cells. Notably, this analysis revealed a striking down-regulation of MCL-1 expression upon chemotherapy exposure in both RPCs (Suppl. Figure 4C). Only minor effects were observed for BCL-XL or BCL-2 expression, indicating that this is not a general cytotoxicity induced by doxorubicin (Suppl. Figure 4C). Hence, these data suggest a model where BCL-XL and MCL-1 are the two major factors mounting the anti-apoptotic response in recurrent ERMS cells. To demonstrate that this is a vulnerable axis, we pharmacologically inhibited both BCL-XL and MCL-1 by using specific inhibitors (MCL1i and BCL-XLi) tested at 4 different concentrations. Impressively, this drug pair showed a sever growth inhibition and exhibited a strong synergistic effect in three recurrent RPCs, mimicking the ABT-263/standard chemotherapy (Figure 5D and Suppl. Figure 4D). Altogether, we showed that simultaneous blockade of BCL-XL and MCL-1 is particularly effective in recurrent RPCs and might be exploited by ABT-263 and the standard-of-care therapy.

Assessment of BCL-XL expression and response to ABT-263/stadard chemotherapy *in vivo*

Based on the chemosensitization effect of ABT-263-mediated inhibition of BCL-XL, we aimed to confirm the clinical relevance of BCL-XL in a large cohort. Therefore, we analyzed BCL-XL mRNA levels from two independent datasets of primary RMSs publicly available through the R2 platform (Figure 6A). As control, we used normal skeletal muscle tissues. Consistent with the importance of BCL-XL in our RPCs, we found a statistical significant increase of BCL-XL expression in RMS tumors compared to control samples, whereas BCL-2 and BCL-W were significantly down regulated (Figure 6A). These findings prompted us to evaluate the functional role of BCL-XL in a pre-clinical *in vivo* model of RMS resistant to conventional therapies. Hence, we tested whether BCL-XL blockade sensitizes a chemorefractory and fast-growing PDX (SJRHB13758_X2) to doxorubicin *in vivo*. Since selective BCL-XL antagonists are still in early pre-clinical development, we chose ABT-263, which is already in clinical evaluation. To this end, immunocompromised NOD scid gamma (NSG) mice were engrafted subcutaneusly with $1*10^6$ dissociated tumor cells from the original SJRHB13758_X2 PDX. Mice with palpable tumors (~100 mm^3) were randomized

to 4 groups (6 mice each): vehicle, ABT-263 treatment, doxorubicin arm and combination. Additionally, to limit the risk of thrombocytopenia associated with ABT-263 administration, we used a therapy schedule that reduces both doses (80 mg/Kg) and time of treatment (three days a week) compared to previous reports (Figure 6B, left panel). However, after only one cycle of therapy, mice had to be scarified due to doxorubicin-induced body weight loss. In contrast, no overt toxicities were detected in vehicle or ABT-263 cohorts. In this short time frame when we could monitor tumor growth, we observed a trend for a reduced tumor kinetic in the combination arm compared to single agent or vehicle groups although it did not reach statistical significance (Figure 6B, right panel). Taken together, these data suggest that BCL-XL is generally over-expressed in RMS patients and its inhibition represents a promising strategy to couple with first-line therapies. However, establishment of less aggressive treatment protocols are needed to assess the long-term effect of such combination in pre-clinical settings.

Discussion

Standard chemotherapy regimens are routinely applied for the management of RMS patients leading to extraordinary cure rates in low-risk groups. Unfortunately, the outcome for patients who experience metastasis and/or relapse disease remains dismal. The estimated long-term event-free survival (EFS) rate for this category is in the range of 15% to 35%, and no further progress has been made in the last decades [23]. Different combinations of dubulking agents including VAC/VAI, VAC plus topoisomerase inhibitors or VAC plus carboplatin failed to show substantial clinical benefit in previous clinical trials [23]. Hence, the search of novel combinatorial options is highly warranted in the field. To this end, in the present study we performed an unbiased chemo-sensitizing screen by combining standard-of-care therapeutics and a targeted compound library in a chemoresistant relapsed RPC model. We identified ABT-263 as the top-scoring drug capable of restoring vulnerability to a wide range of cytotoxic agents (i.e. doxorubicin, etoposide and vincristine).

ABT-263 resembles the structure of the BH3-only BAD, thus is designed to induce apoptosis by neutralizing the pro-survival function of the BCL-2 family members BCL-2, BCL-XL and BLC-W [24]. Such BH3-mimetic (ABT-263 or its predecessor ABT-737) has been previously shown to potentiate the efficacy of a variety of clinically relevant compounds in a large set of cancer entities [24-29]. However, its role in the context of sensitization to first-line chemotherapy in RMS remains elusive. Here, we provide compelling evidence that ABT-263 augments the cytotoxicity of conventional chemotherapeutics in two different recurrent RPC models regardless of the TP-53 status. Strong single agent activity for ABT-263 was detected in only 1 out of 5 RMS cell types tested, corroborating the *in vivo* findings of the pediatric preclinical testing program (PPTP) [30].

From a mechanistic standpoint, we show that the pro-apoptotic BH3-only NOXA mediates, at least in part, the combinatorial effect of ABT-263/standard chemotherapy.

NOXA is known to specifically bind to MCL-1 but not BCL-XL or BCL-2 [31], and down-regulation of MCL-1 sensitizes cells to ABT-263 (Figure 5C and [22, 32]). Consequently NOXA knock-out significantly reduced the ABT-263-induced cell death and thus mitigated its chemosensitization effect, probably by re-enforcing MCL-1 function and/or stability. On the other hand, single chemotherapy treatment induced a transient up-regulation of NOXA and a dramatic down-regulation of MCL-1. The time window when this latter occurred (between 3h and 9h), correlated with the pick of cell death observed in co-treatment experiments. Notably, BCL-XL or BCL-2 protein levels were not affected. Hence, we hypothesize that the chemotherapy-induced perturbation of the steady-state levels of NOXA strongly affects the MCL-1-mediated sensitivity to ABT-263. Cells with a MCL-1 blockade would then rely on either BCL-2 or BCL-XL to survive, thus their inhibition by ABT-263 will lead to cell death. Such model is supported by the fact that (i) chemotherapy-mediated down-regulation of MCL-1 has been documented in cancer [27, 33], (ii) NOXA can promote MCL-1 degradation [34] and (iii) NOXA over-expression can sensitize cells to BH3-mimetics [35, 36]. Although BIM has also been proposed as a key determinant of the sensitivity to ABT-263 [37], we did not find any cell death alteration in BIM knock-out cells treated with either ABT-263 alone or with chemotherapy. However, we cannot rule out the involvement of NOXA-independent mechanisms since depletion of NOXA did not completely abrogate the ABT-263/chemotherapy effect. Importantly, the RPC model used (SJRHB13758_X2C) harbor mutant TP-53 and does not respond to the MDM2/P53 inhibitor idasanutlin. Since NOXA is a well-known P53 target [38], it remains subject of further studies to unravel the mode of regulation of NOXA in this context.

Following a model where chemotherapy blocks MCL-1, we also dissected the direct target of ABT-263. We found that inhibition of BCL-XL is likely to contribute to the cooperativity of ABT-263 with standard chemotherapy. This has been proven by the increased sensitivity of RPCs towards doxorubicin and/or vincristine upon pharmacological and genetic interference of BCL-XL. In contrast, BCL-2 appeared to be largely dispensable for the observed phenotype. This underscores a new function for BCL-XL in ERMS besides its well-recognized role as modulator of the anti-apoptotic function of PAX3-FOXO1 in ARMS [39]. Finally, we demonstrated that simultaneous inhibition of BCL-XL and MCL-1 by selective targeting compounds phenocopies the combinatorial effect of ABT-263/standard chemotherapy. Thus, this axis represents a “druggable” vulnerability in recurrent RPCs resembling the strong genetic and pharmacological interaction of BCL-XL and MCL-1 recently shown in chronic myeloid leukemia (CML) but with only minor effects in normal counterparts [40]. However, it is noteworthy that pre-clinical and phase II studies with ABT-263 as single agent revealed that thrombocytopenia is a major drawback that limits dose escalation [41]. Hence we attempted to translate our findings in a clinically relevant *in vivo* model

by taking into consideration the on-target toxicities associated with ABT-263. However, we noticed a severe body weight loss in mice due to doxorubicin administration that was no additive in presence of the BH3-mimetic (data not shown). Although we used doses of chemotherapy that are considered low in mice (2mg/Kg), it is possible that mouse strain, gender, age, and administration route might have contributed to this unexpected phenotype. Nevertheless, in the short time frame available for treatment (1 week) we observed a clear trend for a tumor growth reduction in the co-treatment compared to single agents or vehicle control. This will motivate us to establish safer treatment schedules to test this therapeutic combination for a longer time period *in vivo*.

In conclusion, we demonstrated that our previously established pre-clinical platform (manuscript 1) is amenable to capture novel combinatorial options for recurrent RMS patients where responses to conventional therapies are failing. As proof-of-principle, we describe ABT-263 to be a novel sensitizer toward standard chemotherapy in ERMS and provide mechanistic insights into their mode of action.

Materials and Methods

Patient-derived samples

ERMS PDX samples SJRHB012_X, SJRHB012_Y, SJRHB012_Z, SJRHB013758_X1 and SJRHB013758_X2 were obtained from the St. Jude Children's Research Hospital (USA) and processed according to the procedures reported previously in. [15] and (manuscript 1). A description of the PDX lines used in this study can be found in manuscript 1 (Supp. Table 1).

Xenograft studies and *in vivo* treatments

$1x10^6$ cells from dissociated SJRHB013758_X2 PDX were suspended in 100 ul of PBS and injected subcutaneously in male NOD scid gamma (NSG) mice. Once tumors reached a size of around 100 mm^3, mice were randomized to vehicle (control group), ABT-263 only, standard chemotherapy only (doxorubicin) and combinatorial treatment arm (6 animals per group). Treatments schedules are indicated in the figure legends. ABT-263 (ApexBio) was dissolved in a mixture of 10% EtOH, 30% PEG-400 (Lipoid) and 60% phosal 50 PG (Sigma Aldrich) and was given orally 1.5 h after standard chemotherapy for combination experiments. Compound solution was prepared fresh before drug administration and any remaining solution was routinely stored at +4°C for no longer than 1 week after dissolving. Doxorubicin (Sandoz) was injected intravenously (i.v.) and stored at +4°C. Tumor size was determined by digital calliper measurements of 2 diameters (d1, d2) in right angles. Total tumor volumes were calculated by the formula $V = (4/3)\pi r3$; $r = (d1 + d2)/4$. Mice were euthanized once tumors reached the maximum allowed size

(1000 mm^3) or with weight loss over 20% than baseline (body weight was monitored daily through the course of each experiment).

Cell culture, cell viability and chemicals

RD (ATCC, Manassas, VA, USA), HEK293T (ATCC, LGC Promochem, Molsheim, France) and HFF (purchased from System Biosciences, CA, US) cells were cultured in Dulbecco's modified Eagle's medium supplemented with 10% fetal bovine serum (heat inactivated), 1% L-glutamine and 1% penicillin-streptomycin. RPCs were maintained as previously described (manuscript 1). All cells were cultured in 5% CO2 at 37°C. For cell viability, cells were plated in triplicates or duplicates in 96 or 384-well plates at cell densities optimized per each cell type (Supplemental Table S1). 24h after cell seeding, medium was replaced and drug was added by using HPD300 digital dispenser at concentrations indicated in each figure. After treatment (at various time points), WST-1 assay (Roche Diagnostics) was performed according to the manufacturer's instructions. A list of the compound details used in this study is available in (Supplemental table S3 manuscript 1).

Drug screen

3000 SJRHB013758_X2C cells were seeded in duplicate in 384-well plate and after 24 h medium was changed before treatment start. Each compound (10 mM stock solution dissolved in DMSO) was pre-diluted with medium the day of the experiment at 10 uM concentration and 1 ul of this solution was added manually to 19 ul of medium per well to achieve a final concentration of 500 nM. Finally, either doxorubicin (IC-20) or etoposide (IC-30) were added by using HPD300 digital dispenser. DMSO and water solution containing 0.3% tween 20 (Sigma Aldrich) were used as vehicle controls for etoposide and doxorubicin, respectively. WST-1 assay was performed at 72 h time point and cell viability for each well was normalized to untreated cells (vehicle control) and data are shown as percentage of control. The drug library containing 204 drugs was purchased from Selleck and details are shown in (Supplemental table S3 manuscript 1).

Caspase 3/7-activity assay

Cells were seeded in white 384-well plates with clear bottom (Greiner Bio-One). Caspase activity was determined at indicated time points by Caspase-Glo 3/7 Assay (Promega) according to the manufacturer's instructions. Luminescence was measured using the multidetection microplate reader Synergy HT (Bio-Tek Instruments).

Western blotting

Total protein from cell lysates was extracted using RIPA buffer (50 mM TrisCl (pH 7.5), 150 mM NaCl, 1% NP-40, 0.5% Na-deoxycholate, 1 mM EGTA, 0.1% SDS, 50 mM NaF, 10 mM sodium

β-glycerolphosphate, 5 mM sodium pyrophosphate, 1 mM sodium orthovanadate and supplemented with Complete Mini Protease Inhibitor Cocktail (Roche). To load equal amounts of proteins per sample, relative protein quantification was calculated using the Pierce BCA protein Assay Kit (Thermo Fisher Scientific, LuBioScience). Proteins were separated using NuPAGE 4%–12% Bis-Tris SDS–PAGE pre-cast gels (Life Technologies) for about 1-1.5 hours at 120 V (constant voltage) and transferred to nitrocellulose membranes (GE Healthcare Life Sciences) for 3 h at 33 V. After blocking with 5% milk powder in TBS/0.1% Tween for 50 minutes, membranes were incubated overnight at 4°C with the primary antibody. The day after, membranes were washed twice with TBS/0.1% Tween and incubated with secondary antibody for 50 minutes. After 2 additional washing steps, the specific proteins were detected by using Amersham ECL Detection reagent (GE Healthcare Life Sciences) or SuperSignal West Femto Maximum Sensitivity Substrate (Thermo Scientific). A description of the antibodies used throughout the study can be found in (Supplemental table S2).

Expression analysis using R2 database

All data used are accessible through the open access platform R2 for visualization and analysis of the microarray data (http://r2.amc.nl). The following datasets were used: Normal Muscle Skeletal-Asmann-40-MAS5.0-u133p2, tumor Rhabdomyosarcoma-Davicioni-147-MAS5.0-u133a, tumor Rhabdomyosarcoma-Schafer-30-MAS5.0-u133a.

Statistics

Data analysis was performed using GraphPad Prism (version 6). Significance was calculated using Student's t-test (unpaired, two tailed) or multiple t-test. For BCL-XL expression from RMS and normal tissue datasets, one-way ANOVA was used for multiple comparisons. Differences were considered statistically different if $P<0.05$. The number of biological replicates (N) per each experiment is indicated in the figure legends. Drug interaction was analyzed by using the Chou-Talalay method [42]. A visualized shiny app to evaluate drug-drug interaction was used to calculate the combination index (CI) and is freely available from https://github.com/pampernickel/drTools. CI>1 indicates antagonism, 1-0.8 additivity and <0.8 synergism.

Supplemental methods:

Plasmids, transfection methods and lentiviral transduction

pLentiCRISPR-EGFP (empty backbone) (Addgene # 75159) and pLentiCRISPR-tagBFP (empty backbone) (Addgene # 75160) were a gift from Beat Bornhauser. SgRNAs (sequences are listed in Supplemental table S3) targeting exon regions shared across all the predicted isoforms for the

selected gene were designed by using the online CRISPR design tool (http://crispr.mit.edu/) and top candidates with a score over 80 were chosen. For cloning, double-stranded sgRNA oligos were inserted into pLentiCRISPR vectors by digestion with ESP3I (Thermo Scientific) and ligation with a T4 ligase (Themo Scientific). For lentiviral particle production, pVSV-G, pMDL, pREV (kindly provided by Oliver Pertz, Department of Biomedicine, University of Basel, Switzerland) and pLentiCRISPR vectors were co-transfected into HEK293T cells using calciumphosphate. 48h after transfection, the virions from supernatant cultures were collected and concentrated using Amicon Ultra tubes (Ultracel 100k, Millipore). SJRHB013758_X2C cells were transduced with LentiCRISPR constructs at MOI of 0.7-0.9 and 24h after medium was changed. 7 days post-transduction polyclonal sgRNA-expressing cells were used for experiments.

References

1. Ries, L.A.G., et al., *Cancer incidence and survival among children and adolescents: United States SEER Program 1975-1995.* Cancer incidence and survival among children and adolescents: United States SEER Program 1975-1995., 1999.
2. Mackall, C.L., *In search of targeted therapies for childhood cancer.* Front Oncol, 2011. **1**: p. 18.
3. Norris, R.E. and P.C. Adamson, *Challenges and opportunities in childhood cancer drug development.* Nat Rev Cancer, 2012. **12**(11): p. 776-82.
4. Van Gaal, J.C., et al., *Building the bridge between rhabdomyosarcoma in children, adolescents and young adults: the road ahead.* Critical reviews in oncology/hematology, 2012. **82**(3): p. 259-279.
5. Smith, M.A., et al., *Declining childhood and adolescent cancer mortality.* Cancer, 2014. **120**(16): p. 2497-506.
6. Hettmer, S., et al., *Rhabdomyosarcoma: current challenges and their implications for developing therapies.* Cold Spring Harbor perspectives in medicine, 2014. **4**(11): p. a025650.
7. Pappo, A.S., et al., *Survival after relapse in children and adolescents with rhabdomyosarcoma: A report from the Intergroup Rhabdomyosarcoma Study Group.* J Clin Oncol, 1999. **17**(11): p. 3487-93.
8. Hayes-Jordan, A. and R. Andrassy, *Rhabdomyosarcoma in children.* Curr Opin Pediatr, 2009. **21**(3): p. 373-8.
9. Mattke, A.C., et al., *Does the time-point of relapse influence outcome in pediatric rhabdomyosarcomas?* Pediatric blood & cancer, 2009. **52**(7): p. 772-776.
10. Oeffinger, K.C., et al., *Chronic health conditions in adult survivors of childhood cancer.* N Engl J Med, 2006. **355**(15): p. 1572-82.
11. Geenen, M.M., et al., *Medical assessment of adverse health outcomes in long-term survivors of childhood cancer.* JAMA, 2007. **297**(24): p. 2705-15.
12. Shern, J.F., et al., *Comprehensive genomic analysis of rhabdomyosarcoma reveals a landscape of alterations affecting a common genetic axis in fusion-positive and fusion-negative tumors.* Cancer Discov, 2014. **4**(2): p. 216-31.
13. Vogelstein, B., et al., *Cancer genome landscapes.* Science, 2013. **339**(6127): p. 1546-58.
14. Stewart, E., et al., *Orthotopic patient-derived xenografts of paediatric solid tumours.* Nature, 2017. **549**(7670): p. 96-100.
15. Chen, X., et al., *Targeting oxidative stress in embryonal rhabdomyosarcoma.* Cancer Cell, 2013. **24**(6): p. 710-24.

16. Gandhi, L., et al., *Phase I study of Navitoclax (ABT-263), a novel Bcl-2 family inhibitor, in patients with small-cell lung cancer and other solid tumors.* J Clin Oncol, 2011. **29**(7): p. 909-16.
17. Roberts, A.W., et al., *Substantial susceptibility of chronic lymphocytic leukemia to BCL2 inhibition: results of a phase I study of navitoclax in patients with relapsed or refractory disease.* Journal of Clinical Oncology, 2011. **30**(5): p. 488-496.
18. Wilson, W.H., et al., *Navitoclax, a targeted high-affinity inhibitor of BCL-2, in lymphoid malignancies: a phase 1 dose-escalation study of safety, pharmacokinetics, pharmacodynamics, and antitumour activity.* Lancet Oncol, 2010. **11**(12): p. 1149-59.
19. Rudin, C.M., et al., *Phase II study of single-agent navitoclax (ABT-263) and biomarker correlates in patients with relapsed small cell lung cancer.* Clin Cancer Res, 2012. **18**(11): p. 3163-9.
20. Krajewski, S., et al., *Reduced expression of proapoptotic gene BAX is associated with poor response rates to combination chemotherapy and shorter survival in women with metastatic breast adenocarcinoma.* Cancer Res, 1995. **55**(19): p. 4471-8.
21. Kang, S.Y., et al., *Low expression of Bax predicts poor prognosis in patients with locally advanced esophageal cancer treated with definitive chemoradiotherapy.* Clin Cancer Res, 2007. **13**(14): p. 4146-53.
22. Van Delft, M.F., et al., *The BH3 mimetic ABT-737 targets selective Bcl-2 proteins and efficiently induces apoptosis via Bak/Bax if Mcl-1 is neutralized.* Cancer cell, 2006. **10**(5): p. 389-399.
23. Hawkins, D.S., et al., *Children's Oncology Group's 2013 blueprint for research: Soft tissue sarcomas.* Pediatr Blood Cancer, 2013. **60**(6): p. 1001-8.
24. Tse, C., et al., *ABT-263: a potent and orally bioavailable Bcl-2 family inhibitor.* Cancer Res, 2008. **68**(9): p. 3421-8.
25. Faber, A.C., et al., *Assessment of ABT-263 activity across a cancer cell line collection leads to a potent combination therapy for small-cell lung cancer.* Proc Natl Acad Sci U S A, 2015. **112**(11): p. E1288-96.
26. Preuss, E., et al., *Pan-mammalian target of rapamycin (mTOR) inhibitor AZD8055 primes rhabdomyosarcoma cells for ABT-737-induced apoptosis by down-regulating Mcl-1 protein.* J Biol Chem, 2013. **288**(49): p. 35287-96.
27. Chen, J., et al., *The Bcl-2/Bcl-XL/Bcl-w inhibitor, navitoclax, enhances the activity of chemotherapeutic agents in vitro and in vivo.* Molecular cancer therapeutics, 2011: p. molcanther. 0415.2011.
28. Anderson, G.R., et al., *PIK3CA mutations enable targeting of a breast tumor dependency through mTOR-mediated MCL-1 translation.* Science translational medicine, 2016. **8**(369): p. 369ra175-369ra175.
29. Nakajima, W., et al., *Combination with vorinostat overcomes ABT-263 (navitoclax) resistance of small cell lung cancer.* Cancer Biol Ther, 2016. **17**(1): p. 27-35.
30. Lock, R., et al., *Initial testing (stage 1) of the BH3 mimetic ABT-263 by the pediatric preclinical testing program.* Pediatric blood & cancer, 2008. **50**(6): p. 1181-1189.
31. Chen, L., et al., *Differential targeting of prosurvival Bcl-2 proteins by their BH3-only ligands allows complementary apoptotic function.* Molecular cell, 2005. **17**(3): p. 393-403.
32. Dai, Y. and S. Grant, *Targeting multiple arms of the apoptotic regulatory machinery.* Cancer Res, 2007. **67**(7): p. 2908-11.
33. Wong, M., et al., *Navitoclax (ABT-263) reduces Bcl-xL mediated chemo-resistance in ovarian cancer models.* Molecular cancer therapeutics, 2012: p. molcanther. 0693.2011.
34. Willis, S.N., et al., *Proapoptotic Bak is sequestered by Mcl-1 and Bcl-xL, but not Bcl-2, until displaced by BH3-only proteins.* Genes & development, 2005. **19**(11): p. 1294-1305.
35. Tahir, S.K., et al., *Influence of Bcl-2 family members on the cellular response of small-cell lung cancer cell lines to ABT-737.* Cancer Res, 2007. **67**(3): p. 1176-83.
36. Wesarg, E., et al., *Targeting BCL-2 family proteins to overcome drug resistance in non-small cell lung cancer.* Int J Cancer, 2007. **121**(11): p. 2387-94.
37. Faber, A.C., et al., *Assessment of ABT-263 activity across a cancer cell line collection leads to a potent combination therapy for small-cell lung cancer.* Proceedings of the National Academy of Sciences, 2015. **112**(11): p. E1288-E1296.

38. Oda, E., et al., *Noxa, a BH3-only member of the Bcl-2 family and candidate mediator of p53-induced apoptosis.* Science, 2000. **288**(5468): p. 1053-8.
39. Margue, C.M., et al., *Transcriptional modulation of the anti-apoptotic protein BCL-XL by the paired box transcription factors PAX3 and PAX3/FKHR.* Oncogene, 2000. **19**(25): p. 2921-9.
40. Han, K., et al., *Synergistic drug combinations for cancer identified in a CRISPR screen for pairwise genetic interactions.* Nat Biotechnol, 2017. **35**(5): p. 463-474.
41. Letai, A., *Apoptosis and Cancer.* Annual Review of Cancer Biology, 2017. **1**: p. 275-294.
42. Chou, T.-C., *Drug combination studies and their synergy quantification using the Chou-Talalay method.* Cancer research, 2010. **70**(2): p. 440-446.

Figure legends

Figure 1. Characterization of the response towards chemotherapeutic agents in pairs of diagnostic/recurrent ERMS RPCs.

(A) Model used to study chemosensitization mechanisms in ERMS. Tumor biopsies taken from the patient at the diagnosis and relapse were implanted in mice to generate PDXs. Freshly derived RPCs were used to test the response towards standard chemotherapy. Hence, high-throughput drug screens were performed on chemoresistant RPCs to identify potential chemo-sensitizers. (B and C) Viability assay in pairs of diagnostic (blue)/relapse (black) RPCs from patient #2 (B) and patient #3 (C) treated for 72h with doxorubicin (upper panel) and etoposide (lower panel)(mean ± SD; N=3). Graph bars indicate the corresponding IC-50 values for each drug (mean ± SEM). *$P \leq 0.05$; **$P \leq 0.01$; **$P \leq 0.001$; NS, not significant.

Figure 2. A drug screen approach identifies ABT-263 as sensitizer to standard chemotherapy in ERMS.

(A) Drug screen results showing the top hit compounds that modulate the sensitivity of doxorubicin (light green circle) and etoposide (light blue circle). The common candidate (ABT-263) is highlighted in the intersection. Black and red bars indicate the effect of the inhibitors as single agent and in combination, respectively. (B) Dose titration curves for ABT-263 performed in ERMS cells (N=3) and HFF (human foreskin fibroblasts) (N=2) after 72h treatment (left panel) (mean ± SD). The IC-50 values are shown for each cell type (lower panel). (C) Western blot analysis showing expression of indicated proteins in HFF and ERMS cells. β-ACTIN was used as loading control.

Figure 3. ABT-263 synergizes with conventional therapy to induce cell death in ERMS recurrent samples.

(A) Viability of ERMS recurrent cells treated with increasing concentrations of etoposide, doxorubicin and vincristine as single arm treatment (black) or in combination with ABT-263 (500nM and 250 nM, dark and light blue lines, respectively) for 72h. The cell type used is shown above each graph. (Mean ± SD; N=2-3). (B) Caspase 3/7-activity assay performed in SJRHB13758_X2C (upper and lower panel) and SJRHB012_ZC (middle panel) following treatment with the indicated chemotherapeutics with or without ABT-263. (Mean ± SD; N=3). (C) Western blot analysis showing protein levels of PARP, cleaved PARP and cleaved CASPASE 3 in SJRHB13758_X2C (upper and lower panel) and SJRHB012_ZC (middle panel) after short-term exposure to single or combinatorial treatments with the indicated compounds. GAPDH was used as loading control.

Figure 4. ABT-263 sensitizes ERMS cells to chemotherapy via NOXA.

(A) Representation of the experimental workflow aimed at the identification of the BH3-only protein mediating the effect of ABT-263/chemotherapy. (B) Caspase 3/7 assay performed on SJRHB13758_X2C NOXA$^{-/-}$ upon treatment with vincristine (VCR) (upper panel) and doxorubicin (lower panel) with or without ABT-263 (500nM and 250nM) at the indicated time points. (Mean ± SD; N=3);*P≤0.05; **P≤0.01; ***P≤0.001; ****P≤0.0001. (C) WST-1-assay performed on SJRHB13758_X2C NOXA$^{-/-}$ upon treatment with vincristine (VCR) (left panel) and doxorubicin (right panel) with or without ABT-263 (500nM and 250nM) at the indicated time points. (Mean ± SD; N=3-4;) *P≤0.05; **P≤0.01; ***P≤0.001; ****P≤0.0001. (D) SJRHB13758_X2C treated with either vincristine (left) or doxorubicin (right) for 3,6,9,24 and 48 hours (h), were collected at time points for western blot. NOXA and GAPDH protein levels are shown.

Figure 5. Chemotherapy and ABT-263 target MCL-1 and BCL-xl, respectively.

(A, left panel) Cell viability analysis of SJRHB13758_X2C cells co-treated with ABT-199 (BCL-2i) and doxorubicin (upper panel, N=2) or vincristine (lower panel, N=3) for 24h (mean ± SD). (A, right panel) Cell viability analysis of SJRHB13758_X2C cells co-treated with A-1331852 (BCL-XLi) and doxorubicin (upper panel, N=3) or vincristine (lower panel, N=3) for 24h (mean ± SD). A schematic view depicting the strategy used is shown on the left of each graph. (B) Schematic representation showing the approach used to identify the target of chemotherapy (left panel). Indicated protein levels from scramble control (sg_SC), MCL-1, BCL-2 and BCL-XL knock-out cells (sg1 and sg2) are shown. β-ACTIN was used as loading control. (C) Cell viability performed on SJRHB13758_X2C knock-out cells for BCL-2, BCL-XL, BCL-W and MCL-1 upon treatment with ABT-263 for 24h. (Mean ± SD; N=2-3). (D) Dual inhibition of MCL-1 and BCL-XL via MCL-1i (A-1210477) and BCL-XLi (A-1331852), respectively (left panel). SJRHB13758_X2C and SJRHB012_ZC cells were treated with increasing concentrations of BCL-XLi and MCL-1i for 72h before cell viability was analyzed (right panel). (Mean ± SD; N=3).

Figure 6. Clinical relevance of BCL-XL and *in vivo* treatment with ABT-263/doxrubicin.

(A) Expression analysis for BCL-XL, BCL-2 and BCL-w for two different RMS collections (N=147 and N=30) and normal skeletal muscle tissues (N=40). (B) Treatment plan for *in vivo* assessment of ABT-263/doxorubcin (left panel) and tumor growth of mice (n=6) treated with vehicle, ABT-263 (80mg/Kg orally), doxorubicin (2 mg/kg i.v.) or ABT-263 plus doxorubicin (right panel). Tumor growth is expressed as percentage of tumor volume at day of randomization before treatment start (Mean±SEM).

Supplemental Figures

Figure S1 (related to Figure 1). Characterization of the response towards chemotherapeutic agents in pairs of diagnostic/recurrent ERMS primary cultures.

(A) Cell viability assay of diagnostic (blue)/relapse (black) cells derived from patient #3 upon 72h treatment with the indicated cytotoxic agents (mean ± SD). Histogram graphs represent IC-50 values for each drug (mean ± SEM, N=2). NS, not significant.

Figure S2 (related to Figure 3). ABT-263 synergizes with conventional therapy to induce cell death in ERMS recurrent samples.

(A) Cell viability analysis of RD cell line co-treated with increasing concentrations of doxorubicin with or without ABT-263 (250nM and 500nM) for 72h (mean ± SD, N=3). (B) Calculation of the combination index (CI) for SJRHB13758_X2C and SJRHB012_Z cells upon 72h co-treatment with ABT-263 and indicated chemotherapeutics at various concentrations. CI>1 indicates antagonism (red), 1-08 additivity (dark green) and <0.8 synergism (light green). (C) Caspase 3/7-activity assay performed on SJRHB012_ZC and SJRHB13758_X2C cells co-treated with ABT-263 and etoposide at 24h and 48h, respectively. (Mean ± SD; N=3). (D) Time course analysis of protein levels from SJRHB13758_X2C cells treated with vincristine (0.1 and 1uM), ABT-263 (500nM) or both at indicated time points (h). GAPDH was used as loading control.

Figure S3 (related to Figure 4). ABT-263 sensitizes ERMS cells to chemotherapy via NOXA.

(A, left panel) Caspase 3/7-activity assay performed in SJRHB13758_X2C cells transduced with sgSC (control) or sgBIM and treated for 24h with vincristine alone or in combination with ABT-263 (250 and 500nM) (mean ± SD, N=3). (A, right panel) Western blot analysis for validation of NOXA and BIM down-regulation at protein level. β-ACTIN was used as loading control. (B) Dose response curve of SJRHB13758_X1C (diagnostic, blue line) and SJRHB13758_X1C (relapse, black line) cells exposed to increasing concentrations of idasanutlin (mean ± SD; N=3). Corresponding IC-50 values per each sample are indicated in the table.

Figure S4 (related to Figure 5). Chemotherapy and ABT-263 target MCL-1 and BCL-xl, respectively.

(A) Cell viability analysis of SJRHB_ZC (left panel) and SJRHB_YC (right panel) cells co-treated with A-1331852 (BCL-XLi) and chemotherapeutics (doxorubicin or vincristine) for 24h (mean ± SD; N=2-3). (B) Experimental model used to identify the target of ABT-263 (left panel). SJRHB13758_X2C cells containing sgRNAs targeting BCL-XL (N=4), BCL-2 (N=2), MCL-1 (N=2), BCL-W (N=2) and scramble control (SC, N=4) were treated with different concentrations of vincristine (VCR) 7 days after transduction. Caspase 3/7-activity assay was performed 24h after treatment start. (Mean ± SD; *$P \leq 0.05$; ns, not significant). (C) Western blot analysis showing the

expression of indicated proteins after treatment with ABT-263 and/or doxorubicin in SJRHB13758_X2C and SJRHB_ZC cells at the indicated time points. β-ACTIN was used as loading control. (D) Cell viability analysis of co-treated SJRHB_YC cells with increasing concentrations of BCL-XLi and MCL-1i for 72h (Mean ± SD; N=3).

Figure 1

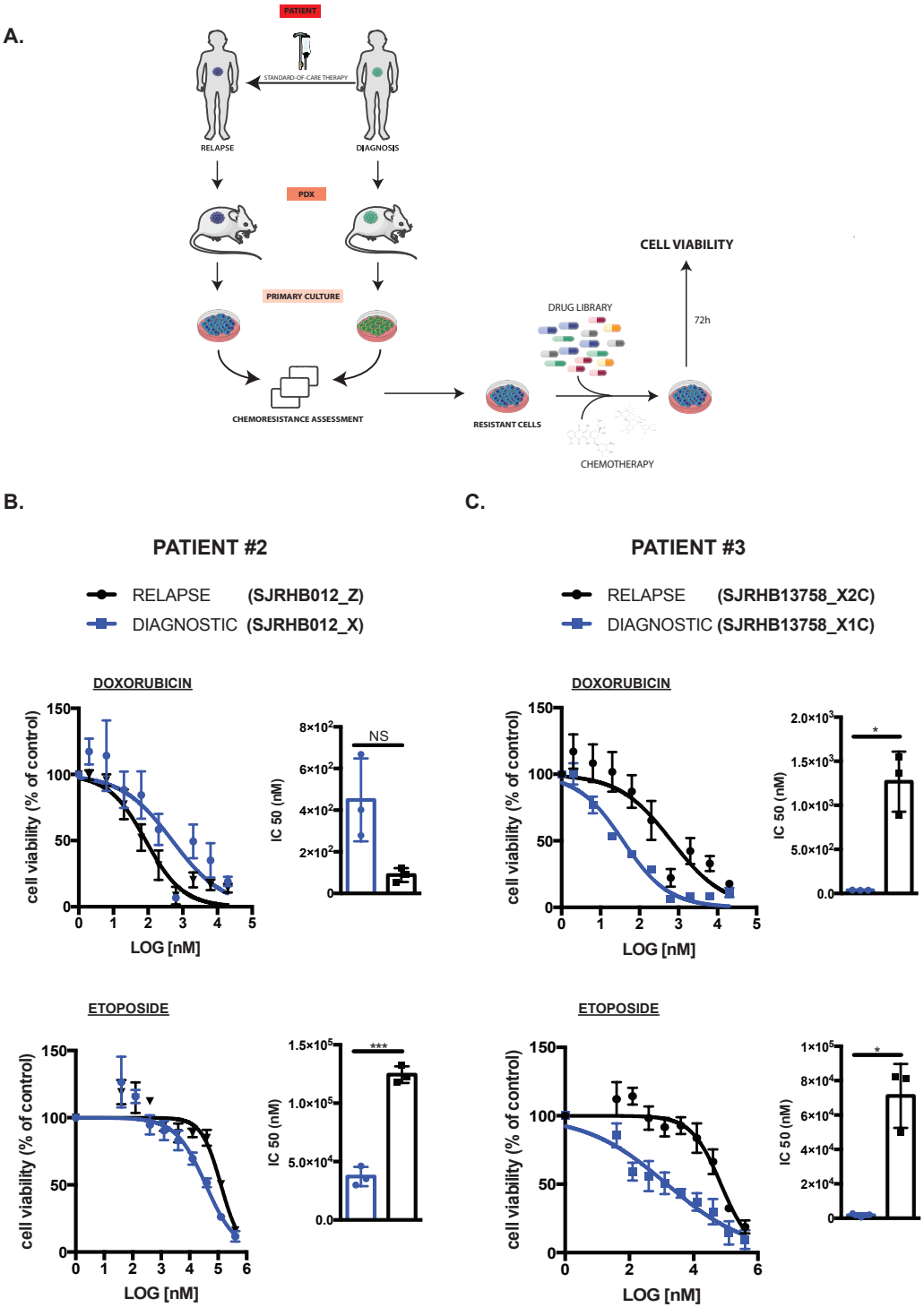
A.
PATIENT
STANDARD-OF-CARE THERAPY
RELAPSE
DIAGNOSIS
PDX
PRIMARY CULTURE
CHEMORESISTANCE ASSESSMENT
RESISTANT CELLS
DRUG LIBRARY
CHEMOTHERAPY
72h
CELL VIABILITY
B.
PATIENT #2
RELAPSE (SJRHB012_Z)
DIAGNOSTIC (SJRHB012_X)
DOXORUBICIN
cell viability (% of control)
LOG [nM]
IC 50 (nM)
NS
ETOPOSIDE
***
C.
PATIENT #3
RELAPSE (SJRHB13758_X2C)
DIAGNOSTIC (SJRHB13758_X1C)
DOXORUBICIN
*
ETOPOSIDE
*

Figure 2

A.

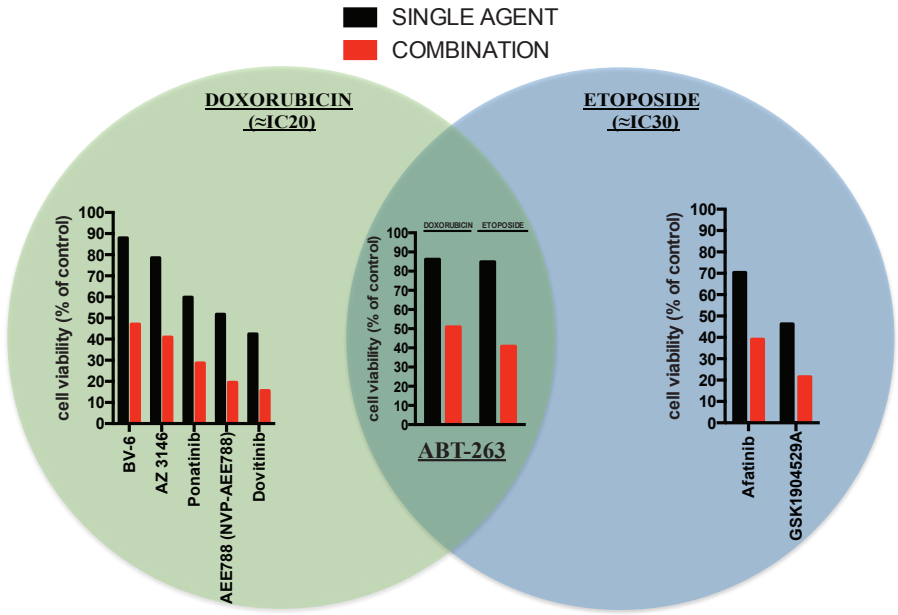

B.

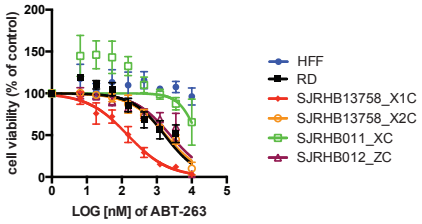

NAME	CELL TYPE	SAMPLE	IC50 (uM) ABT-263
FIBROBLASTS (HFF)	PRIMARY	NON-TUMOR	Inactive
RD	CELL LINE	RELAPSE	1.69
SJRHB13758_X1C	PRIMARY	DIAGNOSTIC	0.15
SJRHB13758_X2C	PRIMARY	RELAPSE	1.82
SJRHB012_ZC	PRIMARY	RELAPSE	2.45
SJRHB011_XC	PRIMARY	RELAPSE	14.63

C.

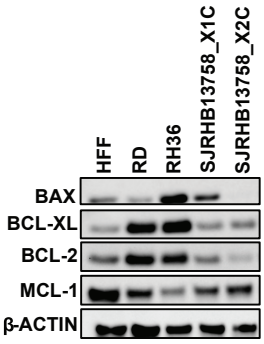

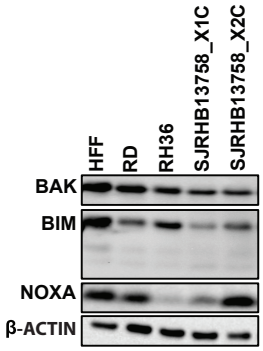

Figure 3

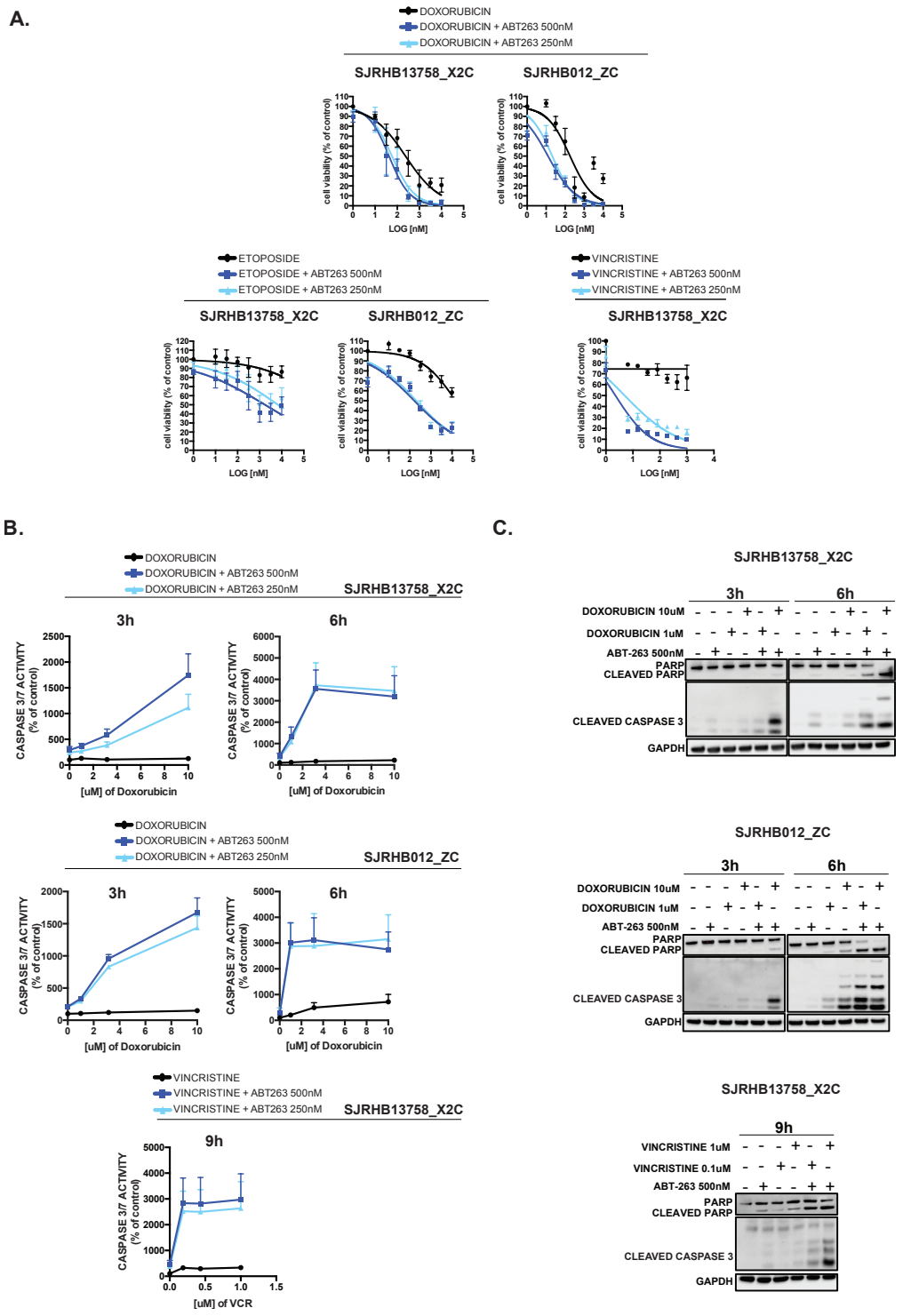
A.
DOXORUBICIN
DOXORUBICIN + ABT263 500nM
DOXORUBICIN + ABT263 250nM
SJRHB13758_X2C
SJRHB012_ZC
cell viability (% of control)
LOG [nM]
ETOPOSIDE
ETOPOSIDE + ABT263 500nM
ETOPOSIDE + ABT263 250nM
VINCRISTINE
VINCRISTINE + ABT263 500nM
VINCRISTINE + ABT263 250nM
B.
CASPASE 3/7 ACTIVITY (% of control)
[uM] of Doxorubicin
3h
6h
9h
[uM] of VCR
C.
DOXORUBICIN 10uM
DOXORUBICIN 1uM
ABT-263 500nM
VINCRISTINE 1uM
VINCRISTINE 0.1uM
PARP
CLEAVED PARP
CLEAVED CASPASE 3
GAPDH

Figure 4

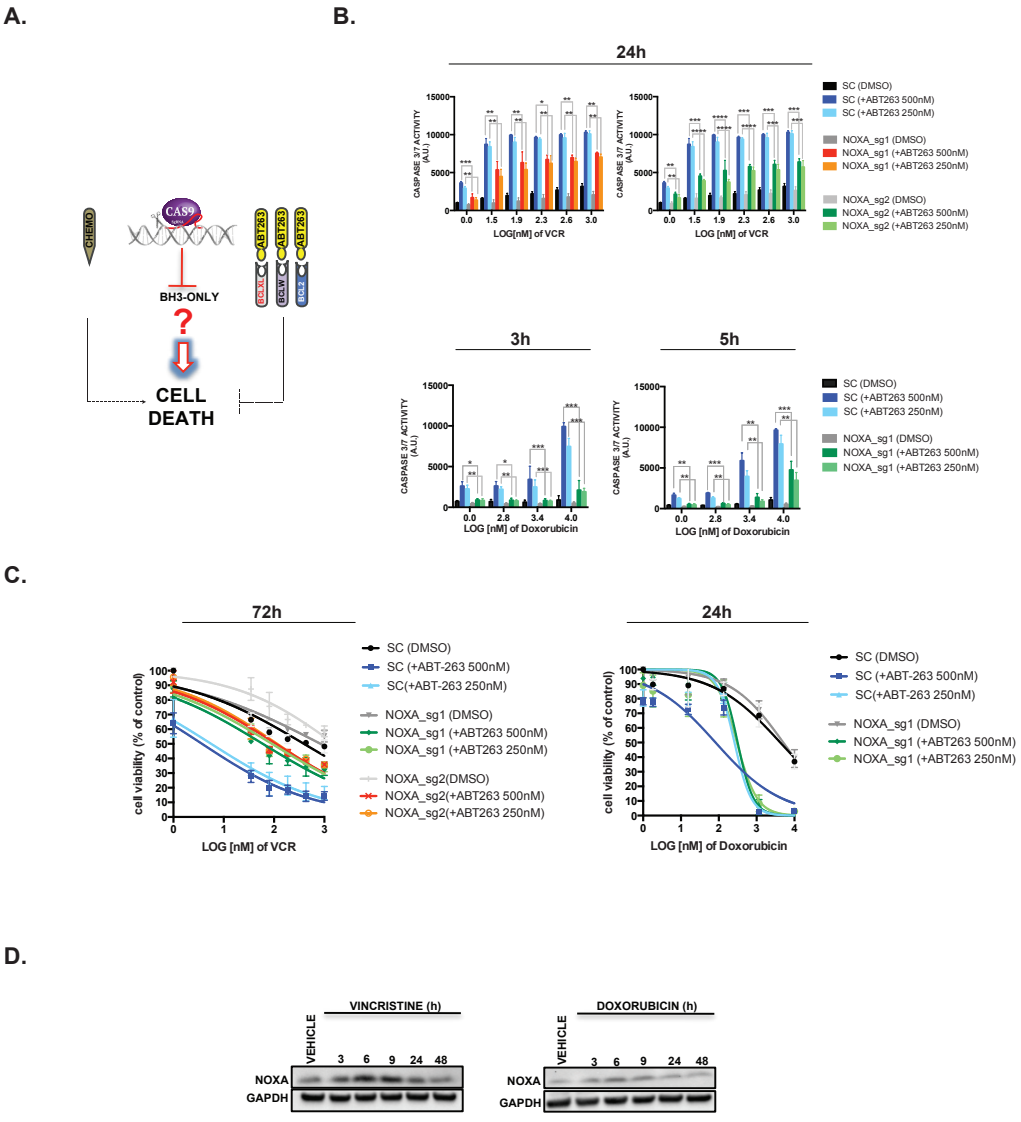
A.
B.
C.
D.
CHEMO
CAS9
BH3-ONLY
ABT263
CELL DEATH
24h
3h
5h
SC (DMSO)
SC (+ABT263 500nM)
SC (+ABT263 250nM)
NOXA_sg1 (DMSO)
NOXA_sg1 (+ABT263 500nM)
NOXA_sg1 (+ABT263 250nM)
NOXA_sg2 (DMSO)
NOXA_sg2 (+ABT263 500nM)
NOXA_sg2 (+ABT263 250nM)
CASPASE 3/7 ACTIVITY (A.U.)
LOG[nM] of VCR
LOG [nM] of VCR
LOG [nM] of Doxorubicin
72h
24h
cell viability (% of control)
SC (+ABT-263 500nM)
SC(+ABT-263 250nM)
NOXA_sg2(DMSO)
NOXA_sg2(+ABT263 500nM)
NOXA_sg2(+ABT263 250nM)
VINCRISTINE (h)
DOXORUBICIN (h)
VEHICLE
3 6 9 24 48
NOXA
GAPDH

Figure 5

A.

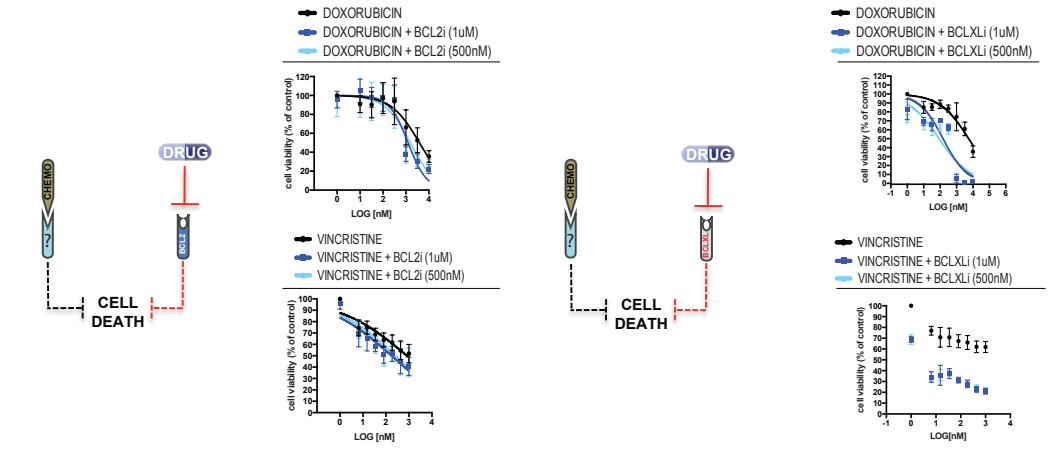

B.

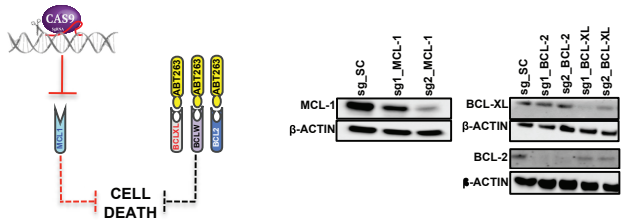

C.

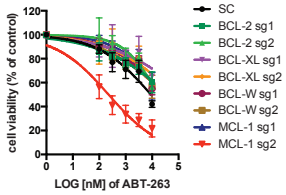

D.

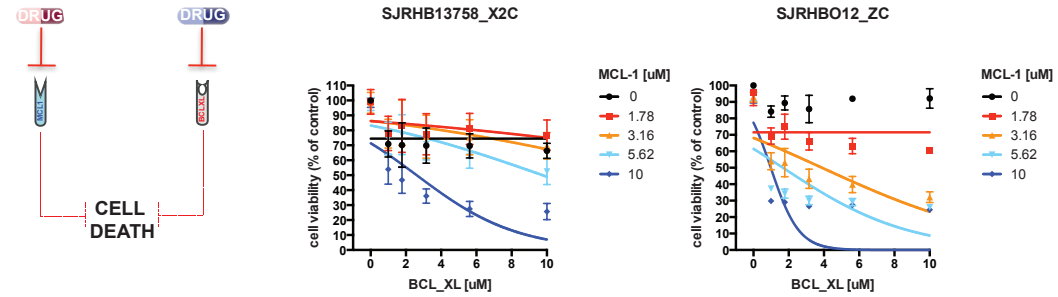

Figure 6

A.

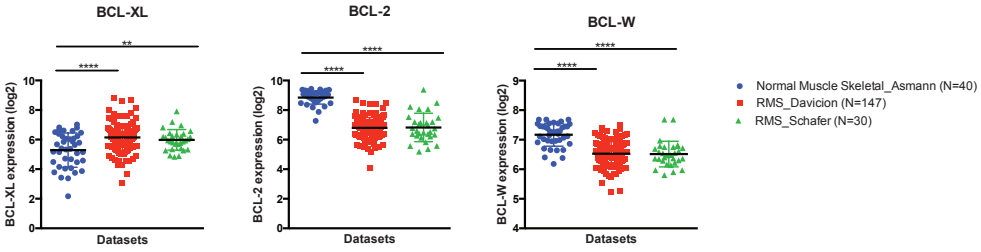
BCL-XL
BCL-2
BCL-W
BCL-XL expression (log2)
BCL-2 expression (log2)
BCL-W expression (log2)
Datasets
Normal Muscle Skeletal_Asmann (N=40)
RMS_Davicion (N=147)
RMS_Schafer (N=30)

B.

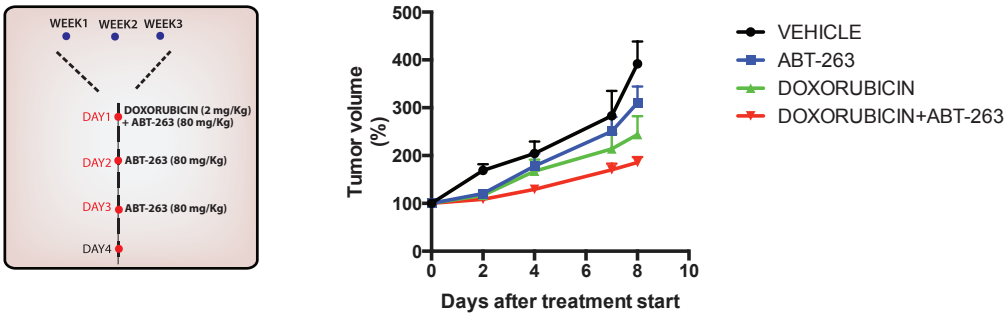
WEEK1
WEEK2
WEEK3
DAY1
DOXORUBICIN (2 mg/Kg)
+ ABT-263 (80 mg/Kg)
DAY2
ABT-263 (80 mg/Kg)
DAY3
ABT-263 (80 mg/Kg)
DAY4
Tumor volume (%)
Days after treatment start
VEHICLE
ABT-263
DOXORUBICIN
DOXORUBICIN+ABT-263

.

Supplemental Figure 1

A.

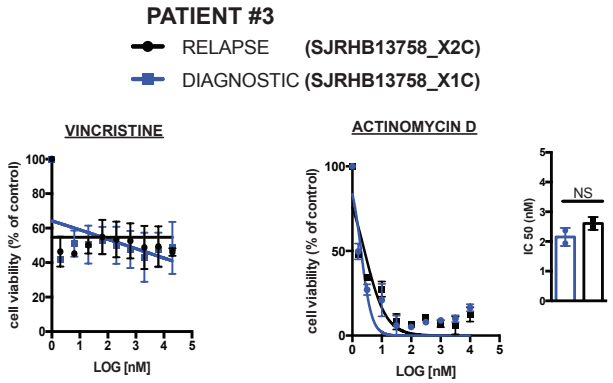

Supplemental Figure 2

A.

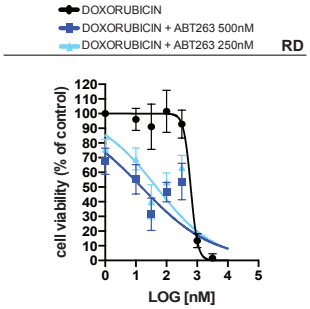

B.

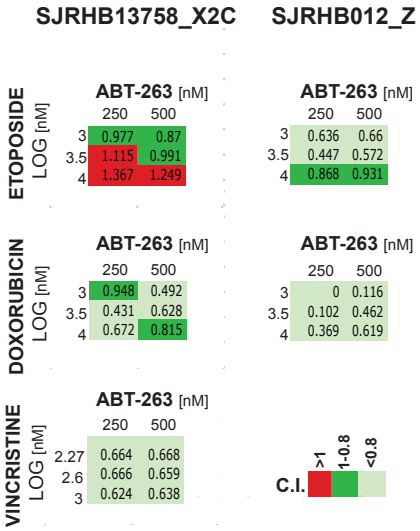

C.

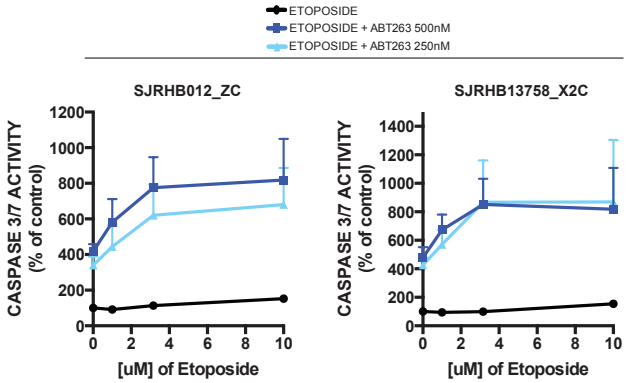

D.

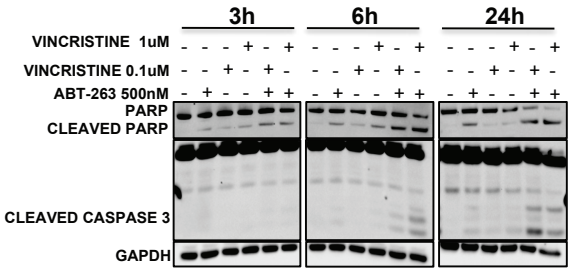

Supplemental Figure 3

A.

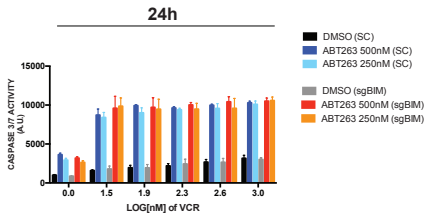

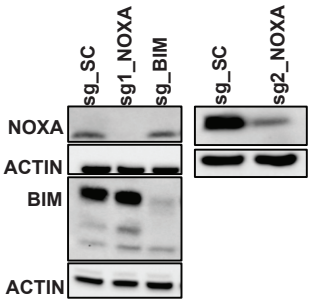

B.

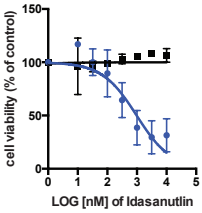

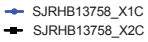

NAME	SAMPLE	P-53 STATUS	IC50 (uM) IDASANUTLIN
SJRHB13758_X1C	DIAGNOSTIC	WT	0.977
SJRHB13758_X2C	RELAPSE	MUTATED	INACTIVE

Supplemental Figure 4

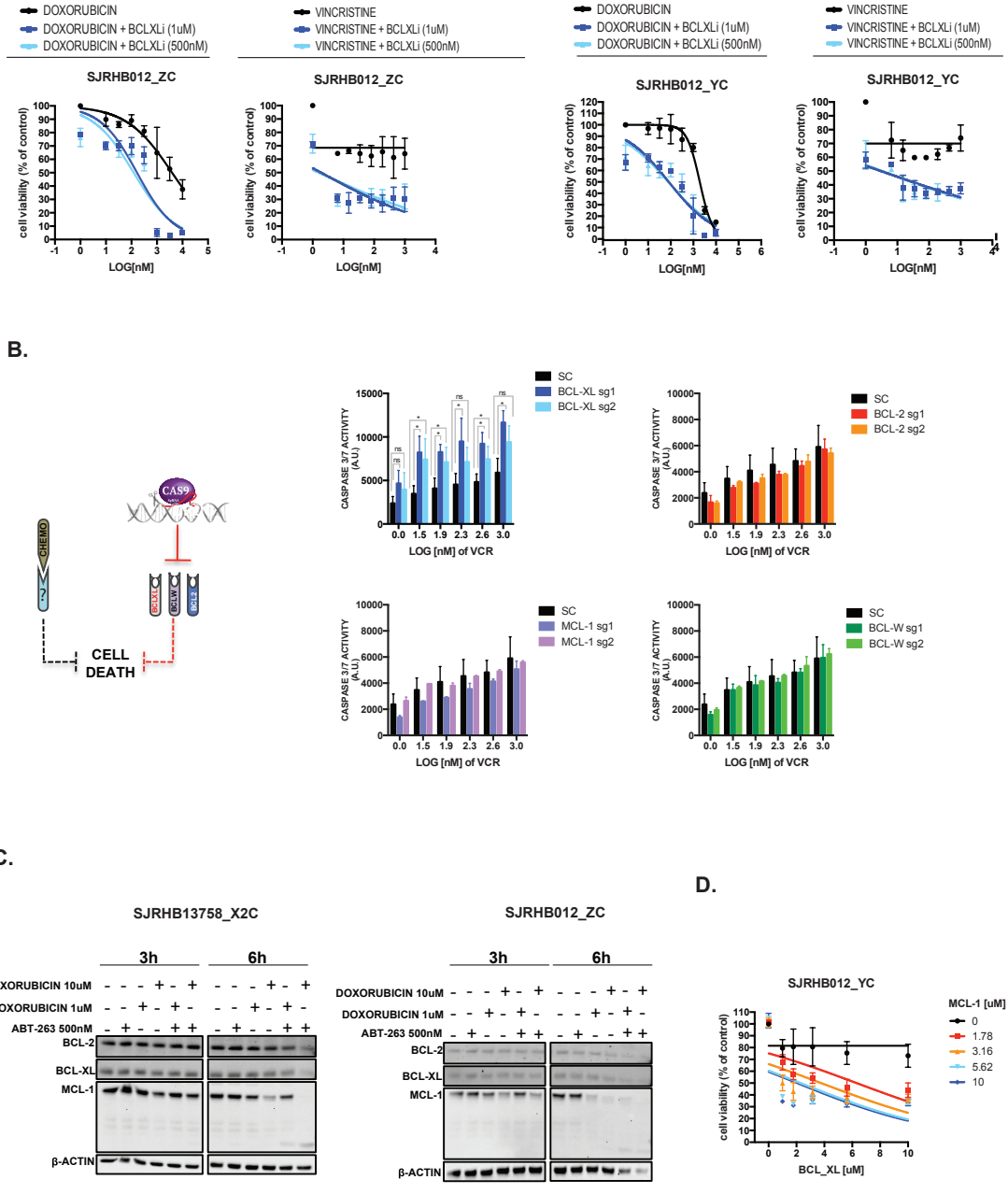

Supplemental Table S1

Cell type	384-well plate	Volume (ul) for 384-well plate	Pre-coated	96-well plate	Volume (ul) for 96-well plate	Pre-coated
RD	2000	20	No	not performed	not performed	not performed
HFF	2000	20	No	not performed	not performed	not performed
SJRHB012_X	4000	20	Yes, 2 % gelatin	10000	100	Yes, 0.2% gelatin
SJRHB012_Y	12000	20	Yes, 2 % gelatin	not performed	not performed	not performed
SJRHB012_Z	3000	20	Yes, 2 % gelatin	10000	100	Yes, 0.2% gelatin
SJRHB13758_X1C	4000	20	Yes, 2 % gelatin	15000	100	Yes, 0.2% gelatin
SJRHB13758_X2C	3000	20	Yes, 2 % gelatin	10000	100	Yes, 0.2% gelatin

Supplemental Table S2

PRIMARY ANTIBODIES

Detected Protein	Applications	Molecular Weight (kDa)	Species	Clonality	Dilution	Catalog Number (#)	Company
BAX	WB	20	Rabbit	Monoclonal	1:1000	5023S	Cell signaling
BCL-XL	WB	28	Rabbit	Polyclonal	1:1000	2762S	Cell signaling
BCL-2	WB	26	Mouse	Monoclonal	1:1000	M0887	Dako
MCL-1	WB	40	Rabbit	Monoclonal	1:1000	5453T	Cell signaling
β-ACTIN[1]	WB	45	Mouse	Monoclonal	1:1000	12262S	Cell signaling
BAK	WB	25	Rabbit	Monoclonal	1:1000	6947S	Cell signaling
BIM	WB	23-15-12	Rabbit	Monoclonal	1:1000	2933S	Cell signaling
NOXA	WB	10	Rabbit	Monoclonal	1:1000	14766S	Cell signaling
PARP	WB	89-116	Rabbit	Polyclonal	1:1000	9542S	Cell signaling
CLEAVED CASPASE 3	WB	17-19	Rabbit	Monoclonal	1:1000	9664P	Cell signaling
GAPDH	WB	37	Rabbit	Monoclonal	1:1000	2118S	Cell signaling

SECONDARY ANTIBODIES

Anti-Mouse IgG[1]	WB				1:2500	7076S	Cell signaling
Anti-Rabbit IgG[1]	WB				1:2500	7074S	Cell signaling

[1] HRP-conjugated

Abbreviations:

HRP- Horseradish peroxidase
WB- Western Blotting

Supplemental Table S3

GENE	sgRNA sequence (de-PAM-end)	Backbone vector used
SCRAMBLE	GCACTACCAGAGCTAACTCA	pLentiCRISPR-EGFP (Addgene, #75159) andpLentiCRISPR-tagBFP (Addgene, #75160)
MCL-1 sg1	CTCAAAAGAAACGCGGTAAT	pLentiCRISPR-EGFP (Addgene, #75159)
MCL-1 sg2	TGGAGACCTTACGACGGGTT	pLentiCRISPR-EGFP (Addgene, #75159)
BCL-XL sg1	CAGTGGCTCCATTCACCGCG	pLentiCRISPR-EGFP (Addgene, #75159)
BCL-XL sg2	GGGTTGCCATTGATGGCACT	pLentiCRISPR-EGFP (Addgene, #75159)
BCL-2 sg1	GAGAACAGGGTACGATAACC	pLentiCRISPR-EGFP (Addgene, #75159)
BCL-2 sg2	GTCGCAGAGGGGCTACGAGT	pLentiCRISPR-EGFP (Addgene, #75159)
BCL-w sg1	ATGAGTTCGAGACCCGCTTC	pLentiCRISPR-EGFP (Addgene, #75159)
BCL-w sg2	GACCTGGGTGAAGCGTTGTT	pLentiCRISPR-EGFP (Addgene, #75159)
NOXA sg1	ACGCTCAACCGAGCCCCGCG	pLentiCRISPR-tagBFP (Addgene, #75160)
NOXA sg2	TCGAGTGTGCTACTCAACTC	pLentiCRISPR-tagBFP (Addgene, #75160)
BIM sg	TGGTTGAAGGCCTGGCAAGG	pLentiCRISPR-tagBFP (Addgene, #75160)

6.3. Manuscript 3

Pharmacological Blockade of The Hedgehog Signaling Enhances the Cytotoxicity of Conventional Chemotherapeutics

[1]Manzella G., [1]Kottarathil T. and [1]Schäfer B.W.

[1] Department of Oncology, University Children's hospital of Zurich, Switzerland

Manuscript in preparation

Personal contribution: I performed experiments in figure 1A, 1B, 1C, 3A, 3B and Suppl. Figure 2A. Kottarathil T. performed all the rest.

I was further responsible for data interpretation, writing and formatting of this manuscript.

Introduction

Rhabdomyosarcoma (RMS) is the most frequent soft-tissue sarcoma in children, accounting for about 4-8 % of all pediatric tumors. RMS comprises embryonal rhabdomyosarcoma (ERMS, 60%), alveolar Rhabdomyosarcoma (ARMS, 20%) and other subtypes (20%), showing different histological, genetic and clinical features [1]. Indeed, 70-80% of the alveolar subtype is characterized by specific chromosomal translocations which lead to the generation of PAX3/PAX7-FOXO1 fusion proteins, considered clinically relevant in the aetiology and prognosis of the disease [2, 3]. ERMS is the most common subtype of RMS and has frequent loss of heterozygosity (LOH) and loss of imprinting (LOI) at 11p15.5 locus. It is mostly diagnosed in the head, neck and genitourinary region of children and rarely metastasises even if the overall survival for patients with recurrent disease is less than 30% [4, 5]. To date, chemotherapy, radiotherapy and surgery are the current treatments for RMS. Despite improvements in the survival rate of patients with localized disease, the outcome for high-risk groups remains poor [6]. One of the approaches used in the clinic to overcome this poor prognosis includes intensive chemotherapy given the better tolerability of children compared to adults. However, these treatments are often associated with long-term side effects such as secondary malignancies and organ dysfunctions [7]. Therefore, there is a need to improve current therapies, for example by looking at new targets involved in the aetiology and maintenance of RMS [8]. To this end, a valid avenue is offered by embryonic signalling pathways such as Notch, Wnt and Hedgehog, mainly active during embryogenesis but often deregulated in cancer, with a high propensity for childhood malignancies [9, 10]. Among these, Hedgehog (Hh) is the most studied signalling pathway in ERMS. In physiological conditions, Hh signalling is activated by three mammalian ligand variants SHH, IHH and DHH, which bind to the negative regulator, patched (PTCH) receptor. This leads to the de-repression of smoothened (SMO) co-receptor, which can accumulate on the mammalian primary cilium and release the downstream GLI (GLI1, GLI2 and GLI3) transcription factors from suppressed of fused (SUFU) inhibition. GLI1 is the main effector of Hh signalling, while GLI3 is mostly a repressor and GLI2 can behave as repressor and activator. Three main reasons underscore the importance of Hh in ERMS tumorigenesis. First, individuals with germline mutations in Ptch1 (Gorline syndrome) are predisposed to ERMS [11, 12]. Second, Hh gain-of-function gene expression signature is highly prevalent in human primary ERMS tumors [13-15]. Third, GLI1 over-expression and/or genetic inactivation of Sufu have been reported in ERMS [14]. These observations together with the relevant role of Hh in the generation and maintenance of stem cell pools during embryogenesis, suggest a key role in ERMS pathogenesis. According to this, we have previously shown the existence of high tumorigenic sub-populations with cancer stem cell (CSC)-like proprieties in ERMS [16] and the key role of Hh in modulating these self-renewal compartments [17]. Since CSCs are also known to drive relapse disease, we reasoned

that targeting Hh signalling in combination with conventional therapies might represent a valid avenue to counteract chemoresistance.

Here, we show that Hh signalling is iper-activated in three independent recurrent PDX models compared to matched diagnostic samples. Consequently, chemical inhibition of upstream (SMO) as well as downstream (GLI) Hh players strongly improves the effects of standard chemotherapeutics. Although this represents a promising approach, further investigations on the mechanism of action of anti-Hh compounds are required since we were unable to recapitulate the pharmacological effects by genetic means.

Results

Hh signaling is over-activated in relapse PDX samples

In our previous study we showed that Hh signaling is an important driver of stemness in ERMS tumor-initiating cells (TICs), which are also considered to be responsible for chemoresistance [17, 18]. Therefore, we took advantage of our recently described pairs of diagnostic/recurrent PDX samples to study whether relapse disease can be associated with changes in Hh signaling activity (manuscript1). To test this, we evaluated the expression of Hh target genes (GLI1, HHIP and PTCH1) by quantitative real-time PCR (qRT-PCR) for each of these paired models (derived from three ERMS patients) and compared the mRNA levels ($2^{-\Delta CT}$) between diagnostic and relapse tumors (Figure 1 A). Remarkably, all recurrent samples had increased expression of GLI1 (between 2.62- to 8.59- fold) and HHIP (between 5.6- to 12- fold) whereas PTCH1 was up-regulated only in relapsed patient #1 (> 3.18 fold change) and patient #2 (> 1.47-fold). Accordingly, immunoblot analysis confirmed GLI1 over-expression (ranging from 2.35 to 15.64 fold change) in all recurrent PDXs relative to diagnostic samples within the same patient (Figure 1 B). Next, to further investigate the functional contribution of Hh pathway to chemoresistance *in vitro*, we derived diagnostic (SJRHB011_YC) and recurrent (SJRHB011_XC) primary cultures from patient #1 (PDX) and tested whether the *in vitro* system recapitulates the same expression pattern observed *in vivo*. As expected, qRT-PCR analysis revealed increased expression of GLI1, HHIP and PTCH1 in SJRHB011_XC compared to SJRHB011_YC at similar extends as *in vivo* (Figure 1 C, upper panel). Furthermore, GLI1 protein expression was also increased similarly to the initial paired PDX sample (Figure 1 C, lower panel). Since Hh is a ligand-based pathway, we asked whether increased Hh signaling activation in relapsed cells is associated with higher ligand expression. To this aim, we analyzed mRNA levels of SHH, IHH and DHH by qRT-PCR and found that both DHH and SHH are relatively higher in SJRHB011_XC compared to SJRHB011_YC cells although the basal levels were consistently low (Figure 1 D). In sum, these results indicate an Hh gain-of-function gene expression signature in recurrent samples, which is

conserved also in one example of paired PDX-derived cells, leading us to investigate further the role of Hh pathway in the context of chemo-resistance.

Pharmacological inhibition of Hh signaling sensitizes ERMS cells to standard chemotherapy

The observed aberrant activity of Hh pathway in recurrent ERMS samples prompted us to explore the functional relationship between Hh machinery and resistance to conventional treatment in ERMS. We used SJRHB011_XC and RD (relapse cell line) as *in vitro* culture system to model relapse disease. We then inhibited Hh signaling by a pharmacological approach using GANT61 and GDC-0449 inhibitors targeting GLI1/2 and SMO, respectively. We verified the on-target effect of these compounds by immunoblot for GLI1, which is the main target to be affected if Hh pathway is modulated. Both GDC-0449 and GANT61 treatment led to a downregulation of GLI1 protein of ~50% compared to vehicle control (Figure 2 A). Next, we performed cell viability assays on cells treated with either increasing amounts of Hh inhibitors (GANT-61 and GDC-0449) or co-treated with de-bulking agents at EC-50 concentrations. We selected three different cytotoxic drugs namely doxorubicin, a topoisomerase II inhibitor, actinomycin D, a DNA intercalator affecting mRNA synthesis and vincristine, a microtubule destabilizer, which are all wildly used in up-front treatments of ERMS patients. According to our previous findings, Hh signaling inhibition does not affect cell survival in both SJRHB011_XC and RD cells at concentrations up to 5 uM of GANT61 and 20 uM of GDC-0449 (Figure 2 B and S1 A, B and C). In contrast, we observed a dose dependent increased sensitivity to actinomycin D in presence of the Hh antagonists compared to the single arm treatments. Similarly, GANT61 could sensitize relapse ERMS cells to vincristine whereas GDC-0449 was less effective. Finally, only the highest concentration of GANT61 (5uM) was sufficient to significantly increase the sensitivity towards doxorubicin in RD cells and only a trend was observed in SJRHB011_XC although it was not statistical significant (Figure 2 B, S1 A). Taken together these results suggest that both SMO- and GLI-mediated pharmacological inhibition increase the cytotoxicity of standard chemotherapeutics in recurrent ERMS cells.

Genetic modulation of Hh signaling does not alter chemo-sensitivity in ERMS recurrent cells

To further study the Hh-mediated chemo-sensitization, we took advantage of the Crispr/Cas9-genome editing tool to generate ERMS recurrent cells with low and high Hh signaling activity by knocking out GLI1 ($GLI1^{-/-}$) and SUFU ($SUFU^{-/-}$), respectively. Western blot analysis showed efficient protein depletion in both SJRHB011_XC (Figure 3 A) and RD (Figure S2 A) upon transduction with lenti-Crispr vectors containing sgRNAs directed against the respective targets. Importantly, GLI1 inactivation was accompanied by a down-regulation of GLI1 itself and HHIP at

mRNA levels in both SJRHB011_XC (Figure 1 B) and RD (Figure S2 B) cells confirming a positive and negative feedback loop, respectively. However, we cannot rule out the possibility that indel mutations could affect the stability of GLI1 mRNA. On the other hand, qRT-PCR analysis demonstrated a clear up-regulation of the Hh targets in SJRHB011_XC SUFU$^{-/-}$ cells (Figure 3B) followed by increased GLI1 protein expression (Figure 3A, lower panel). Similar results were obtained for RD cells (Figure S2 A and B). Next, we verified that genetic manipulation of Hh signaling did not alter cell viability in ERMS cells resembling the phenotype observed following treatment with Hh-antagonists as single agents (Figure 3C and S2 C). Hence, to assess if this holds true also for the combination with conventional chemotherapeutics we monitored cell viability upon treatment of Hh "low" and "high" cells with Actinomycin D and vincristine, which showed the best combinatorial effect with Hh inhibitors (Figure 2 B, S1 A, B and C). Surprisingly, either SUFU or GLI1 knock-out did not affect the response of ERMS cells towards these cytotoxic drugs with only a modest increased sensitivity towards vincristine in RD cells (Figure 3 A and S2 D). Therefore, our results indicate that specific modulation of GLI1 by genetic means is not sufficient to regulate the response to standard de-bulking agents in ERMS cells highlighting a discrepancy with chemical-mediated GLI1 inhibition.

Discussion

Over-activation of Hh pathway is a common event occurring in cancer and has been associated with the onset of several cancer entities including ERMS [19, 20]. This latter appears to be hierarchically organized where Hh-regulated CSCs boost tumorigenesis by promoting 'stemness' features [17, 18] . Because CSCs are often spared by conventional cytotoxic agents, in the present study we investigated the role of Hh signaling in the context of chemoresistance, a devastating phenomenon in clinical oncology. Here, we show a dramatic upregulation of Hh target genes (GLI1, HHIP and PTCH1) in ERMS PDXs compared to matched diagnostic samples from three independent patients. This correlates with early findings showing that aberrant Hh signaling activity predicts poor overall survival in ERMS population [14, 21]. Interestingly, among the GLI family members, GLI1 was the only transcription factor to be consistently over-expressed in relapsed samples, whereas only minor changes were observed for GLI2 and GLI3 (Figure 1 and data not shown). Although the role of these latter is not well understood in RMS and warrants deeper investigations, we have previously shown that GLI1 is a critical driver of tumor-initiating populations (TIPs) and might represent a potential biomarker for patient stratification [17].

To functionally characterize the Hh-mediated effect on chemoresistance, we used primary cultures from patient #1, and demonstrated that *in vitro* the expression pattern of Hh targets was retained as in the original PDX (Figure 1C). The increased activity in relapsed cells correlated with upregulation of Hh ligands (DHH and SHH) indicating an ongoing autocrine signaling. This

corroborates our previous findings where up-regulation of Hh target genes in CSC-enriched conditions (rhabdospheres) was associated with increased ligand expression [17]. Similarly, a recent report has shown that genetic down-regulation of Hh ligands in RMS cells decreased tumor growth at similar extent as inactivation of GLI1 [22]. Consistent with this, genetic aberrations of Hh components occur in only a minority of RMS cases [4, 20, 23, 24].

If chemoresistance relies on de-regulation of Hh signaling, then its inhibition would sensitize cells to debulking agents. Our data revealed that the viability of RMS recurrent cells was significantly decreased by combining anti-Hh compounds with a wide range of chemotherapeutics such as doxorubicin, actinomnycin D and vincristine. Generally, the chemo-sensitization effect was more pronounced with the GLI antagonist GANT-61, which prompted us to explore the GLI1 dependency by genetic means. Surprisingly, GLI1 knock-out did not recapitulate chemical inhibition in two *in vitro* recurrent models. Yet, complete protein depletion of SUFU, a direct endogenous inhibitor of the GLI transcription factors, did not alter chemo-response as well. Thus, it is unluckily that GLI2 and/or GLI3 would compensate for GLI1 down-regulation, at least in this context. Instead, we speculate that either GDC-0449 or GANT-61, might affect additional signaling cascades besides Hh inhibition. For instance, inhibition of both Hh and AKT/mTOR has been proposed as mechanism underling the GANT-61-mediated regression of RMS xenografts and as means to enhance the effect of vincristine [25]. Consequently, it is not surprising the synergistic effect observed in RMS cells upon double blockade of Hh signaling and the PI3K axis [26]. Furthermore, a systematic gene expression profile in RMS cells treated with GDC-0449 revealed a strong induction of the UPR response as potential off-target effects [22]. Given the on-target mixed responses elicited by the Hh inhibitors in RMS cells, a more systematic characterization of the mode of action of such compounds will clarify the observed discrepancy between chemical and genetic inhibition of Hh signaling in RMS.

In conclusion, our data highlight a clear association between Hh signaling activation and relapse disease, confirming the prognostic relevance of this developmental pathway in RMS. Although further studies are needed to clarify the functional role of Hh-mediated chemoresistance, our work provides the rationale for using Hh antagonists in combination with first-line therapies in RMS.

Materials and Methods

Patient-derived samples, cell culture and treatments

PDX samples were processed as previously described (manuscript 1). RD (ATCC, Manassas, VA, USA), HEK293T (ATCC, LGC Promochem, Molsheim, France) SJRHB011_X and SJRHB011_Y cells were cultured in Dulbecco's modified Eagle's medium supplemented with 10% fetal bovine serum, 1% L-glutamine and 1% penicillin-streptomycin. All cells were cultured in 5% CO2 at 37°C.

For drug treatments, 8000 cells/well were seeded in 96-well plates in quadruplicate. 24h after, medium was replaced and drug was added either manually or by using HPD300 digital dispenser at concentrations indicated in each figure. 72h later, cell viability was assessed by WST-1 assay, according to the manufacturer's instructions. All drugs were dissolved in DMSO, which was used as vehicle control.

GANT-61 (Tocris Biosciences), GDC-0449 (Selleck Chemicals), doxorubicin (Sandoz), vincristine (Selleck Chemicals) and actinomycin D (Sigma-Aldrich) were used at the indicated concentrations. For dose response curves of chemotherapeutics as single agent or in combinations, serial dilutions were performed.

Western Blot, lentiviral production and generation of knock-out cells

As recently described in manuscript 2. Information regarding the antibodies and sgRNAs used in the study can be found in suppl. Table 1 and suppl. Table 2, respectively.

Quantitative Real-time PCR

Total RNA was extracted using RNeasy Mini Kit (Quiagen) following manufacturer's recommendations. Genomic DNA contamination was removed using RNase-free Dnase (Quiagen). RNA concentration and purity was evaluated using NanoDrop ND-1000.cDNA synthesis was carried out using High Capacity cDNA Reverse Transcription kit (Life technologies) according to manufacturer's instructions. Quantitative Real-Time PCR (qRT-PCR) was performed using commercially available mastermix and TaqMan® Gene Expression Assays (Life technologies; assay IDs are listed in the Suppl. Table 3) at standard conditions on an ABI 7900 HT Real-Time PCR machine and the data was analyzed with SD software (Applied Biosystems, Life Technologies). Absolute and relative expression levels were calculated using the ΔΔCt method and normalized to HMBS or GAPDH.

Statistical analysis

Data analysis was performed using GraphPad Prism (version 6). Significance was calculated using Student's t-test (unpaired, two tailed). Differences were considered statistically different if $P<0.05$. The number of biological replicates (N) per each experiment is indicated in the figure legends.

References

1. Belyea, B., et al., *Embryonic signaling pathways and rhabdomyosarcoma: contributions to cancer development and opportunities for therapeutic targeting.* Sarcoma, 2012. **2012**: p. 406239.
2. Dagher, R. and L. Helman, *Rhabdomyosarcoma: an overview.* Oncologist, 1999. **4**(1): p. 34-44.
3. Hawkins, D.S., A.A. Gupta, and E. Rudzinski, *What's New in the Biology and Treatment of Pediatric Rhabdomyosarcoma?* Current opinion in pediatrics, 2014. **26**(1): p. 50.
4. Chen, X., et al., *Targeting oxidative stress in embryonal rhabdomyosarcoma.* Cancer Cell, 2013. **24**(6): p. 710-24.
5. De Giovanni, C., et al., *Molecular and cellular biology of rhabdomyosarcoma.* Future Oncol, 2009. **5**(9): p. 1449-75.
6. Oberlin, O., et al., *Prognostic factors in metastatic rhabdomyosarcomas: results of a pooled analysis from United States and European cooperative groups.* J Clin Oncol, 2008. **26**(14): p. 2384-9.
7. Landier, W. and S. Bhatia, *Cancer survivorship: a pediatric perspective.* Oncologist, 2008. **13**(11): p. 1181-92.
8. Wachtel, M. and B.W. Schafer, *Targets for cancer therapy in childhood sarcomas.* Cancer Treat Rev, 2010. **36**(4): p. 318-27.
9. Takebe, N., et al., *Targeting cancer stem cells by inhibiting Wnt, Notch, and Hedgehog pathways.* Nat Rev Clin Oncol, 2011. **8**(2): p. 97-106.
10. Manzella, G. and B.W. Schafer, *Interfering with Hedgehog Pathway: New Avenues for Targeted Therapy in Rhabdomyosarcoma.* Curr Drug Targets, 2016. **17**(11): p. 1228-34.
11. Gorlin, R.J. and R.W. Goltz, *Multiple nevoid basal-cell epithelioma, jaw cysts and bifid rib. A syndrome.* N Engl J Med, 1960. **262**: p. 908-12.
12. Gorlin, R.J., *Nevoid basal cell carcinoma (Gorlin) syndrome: unanswered issues.* J Lab Clin Med, 1999. **134**(6): p. 551-2.
13. Paulson, V., et al., *High-resolution array CGH identifies common mechanisms that drive embryonal rhabdomyosarcoma pathogenesis.* Genes Chromosomes Cancer, 2011. **50**(6): p. 397-408.
14. Zibat, A., et al., *Activation of the hedgehog pathway confers a poor prognosis in embryonal and fusion gene-negative alveolar rhabdomyosarcoma.* Oncogene, 2010. **29**(48): p. 6323-30.
15. Rubin, B.P., *Bioinformatic mining of gene expression datasets identifies ETV1 as a critical regulator of oncogenesis in gastrointestinal stromal tumors.* Cancer Cell, 2010. **18**(5): p. 407-8.
16. Walter, D., et al., *CD133 positive embryonal rhabdomyosarcoma stem-like cell population is enriched in rhabdospheres.* PLoS One, 2011. **6**(5): p. e19506.
17. Satheesha, S., et al., *Targeting hedgehog signaling reduces self-renewal in embryonal rhabdomyosarcoma.* Oncogene, 2016. **35**(16): p. 2020-30.
18. Walter, D., et al., *CD133 positive embryonal rhabdomyosarcoma stem-like cell population is enriched in rhabdospheres.* PLoS One, 2011. **6**(5): p. e19506.
19. Hahn, H., et al., *Rhabdomyosarcomas and radiation hypersensitivity in a mouse model of Gorlin syndrome.* Nat Med, 1998. **4**(5): p. 619-22.
20. Tostar, U., et al., *Deregulation of the hedgehog signalling pathway: a possible role for the PTCH and SUFU genes in human rhabdomyoma and rhabdomyosarcoma development.* J Pathol, 2006. **208**(1): p. 17-25.
21. Pressey, J.G., et al., *Hedgehog pathway activity in pediatric embryonal rhabdomyosarcoma and undifferentiated sarcoma: a report from the Children's Oncology Group.* Pediatr Blood Cancer, 2011. **57**(6): p. 930-8.
22. Almazan-Moga, A., et al., *Ligand-dependent Hedgehog pathway activation in Rhabdomyosarcoma: the oncogenic role of the ligands.* Br J Cancer, 2017.
23. Bridge, J.A., et al., *Novel genomic imbalances in embryonal rhabdomyosarcoma revealed by comparative genomic hybridization and fluorescence in situ hybridization: an*

intergroup rhabdomyosarcoma study. Genes, Chromosomes and Cancer, 2000. **27**(4): p. 337-344.
24. Calzada-Wack, J., et al., *Analysis of the PTCH coding region in human rhabdomyosarcoma.* Hum Mutat, 2002. **20**(3): p. 233-4.
25. Srivastava, R.K., et al., *GLI inhibitor GANT-61 diminishes embryonal and alveolar rhabdomyosarcoma growth by inhibiting Shh/AKT-mTOR axis.* Oncotarget, 2014. **5**(23): p. 12151-65.
26. Graab, U., H. Hahn, and S. Fulda, *Identification of a novel synthetic lethality of combined inhibition of hedgehog and PI3K signaling in rhabdomyosarcoma.* Oncotarget, 2015. **6**(11): p. 8722-35.

Figure legends

Figure 1. Expression of Hh target genes in diagnostic and relapse samples.

(A) GLI1, HHIP and PTCH1 mRNA levels ($2^{-\Delta CT}$) assessed by quantitative PCR (qPCR) in diagnostic (black bar) and relapsed (blue bar) PDX pairs. Patient #1 (diagnostic: N=1, relapse: N=2), patient #2 (diagnostic: N=2, relapse: N=3), patient #3 (diagnostic: N=3, relapse: N=3) (mean±sd). (B) Western Blot analysis showing GLI1 protein levels in diagnostic and relapse PDX samples. TUBULIN was used as loading control. Relative protein quantification is shown for each blot. (C, upper panel) Expression levels ($2^{-\Delta CT}$) of GLI1, HHIP and PTCH1 in diagnostic and relapse primary cultures derived from patient #1 assessed by qPCR (mean±sd; N=3). (C, lower panel) GLI1 protein levels assessed by western blot analysis in the same samples. Relative protein quantification is also shown. TUBULIN was used as loading control. (D) Assessment of Hh ligands (IHH, DHH and SHH) expression by qPCR in primary cultures (diagnostic and relapse cells) derived from patient #1 (mean±sd; N=3).

Figure 2. Chemical inhibition of Hh signaling increases the activity of standard chemo-therapeutics.

(A) Protein levels analysis of GLI1 upon treatment with GANT61 (left panel) and GDC-0449 (right panel) assessed by western blot. TUBULIN was used as loading control. Relative protein quantification is also shown. (B) Cell viability analysis upon co-treatment of Hh antagonists (GANT61 and GDC-0449) with doxorubicin (left panel), actinomycin (right panel) and vincristine (VCR) (lower panel) in SJRHB011_XC cells. Data are expressed as percentage (%) of living cells relative to vehicle control (mean±sd; N=3-4).

Figure 3. Inhibition of Hh signaling components by genetic means does not influence chemo-sensitivity.

(A) Assessment of GLI1 or SUFU knock-out efficiency in SJRHB011_XC cells transduced with a lentiCrispr vector containing sgRNAs targeting either GLI1 (sgB_GLI1 and sgC_GLI1) or SUFU (sgC_SUFU and sgA_SUFU). A scramble sgRNA sequence (SC) was used as negative control. (B) Hh target genes (GLI1, HHIP and PTCH1) mRNA levels ($2^{-\Delta CT}$) assessed by quantitative PCR (qPCR) in GLI1 or SUFU knock-out cells (mean±sd; N=3). (C) Cell viability assessed by WST-1 in SC, GLI1 and SUFU knock-out cells. Each data point is expressed as percentage of living cells relative to vehicle control (mean±sd; N=3). (D) Dose response curve of GLI1 and SUFU knock-out cells following treatment with increasing concentrations of either actinomycin (left panel) or vincristine (right panel) (mean±sd; N=4).

Supplemental Figures

Supplemental Figure 1 (relative to Figure 2).

(A, B and C) Cell viability analysis upon co-treatment of Hh antagonists (GANT61 and GDC-0449) with doxorubicin (A), actinomycin (B) and vincristine (VCR) (C) in RD cell line. Data are expressed as percentage (%) of living cells relative to vehicle control (mean±sd; N=3).

Supplemental Figure 2 (relative to Figure 3)

(A) Assessment of GLI1 or SUFU knock-out efficiency in RD cell line transduced with a lentiCrispr vector containing sgRNAs targeting either GLI1 (sgA_GLI1, sgB_GLI1 and sgC_GLI1) or SUFU (sgA_SUFU and sgC_SUFU). A scramble sgRNA sequence (SC) was used as negative control. (B) Hh target genes (GLI1, HHIP and PTCH1) mRNA levels ($2^{-\Delta CT}$) assessed by quantitative PCR (qPCR) in GLI1 or SUFU knock-out cells (RD) (mean±sd; N=3). (C) Cell viability assessed by WST-1 in SC, GLI1 and SUFU knock-out cells (RD). Each data point is expressed as percentage of living cells relative to vehicle control (mean±sd; N=3). (D) Dose response curve of GLI1 and SUFU knock-out cells (RD) following treatment with increasing concentrations of either actinomycin (left panel) or vincristine (right panel) (mean±sd; N=4).

Figure 1

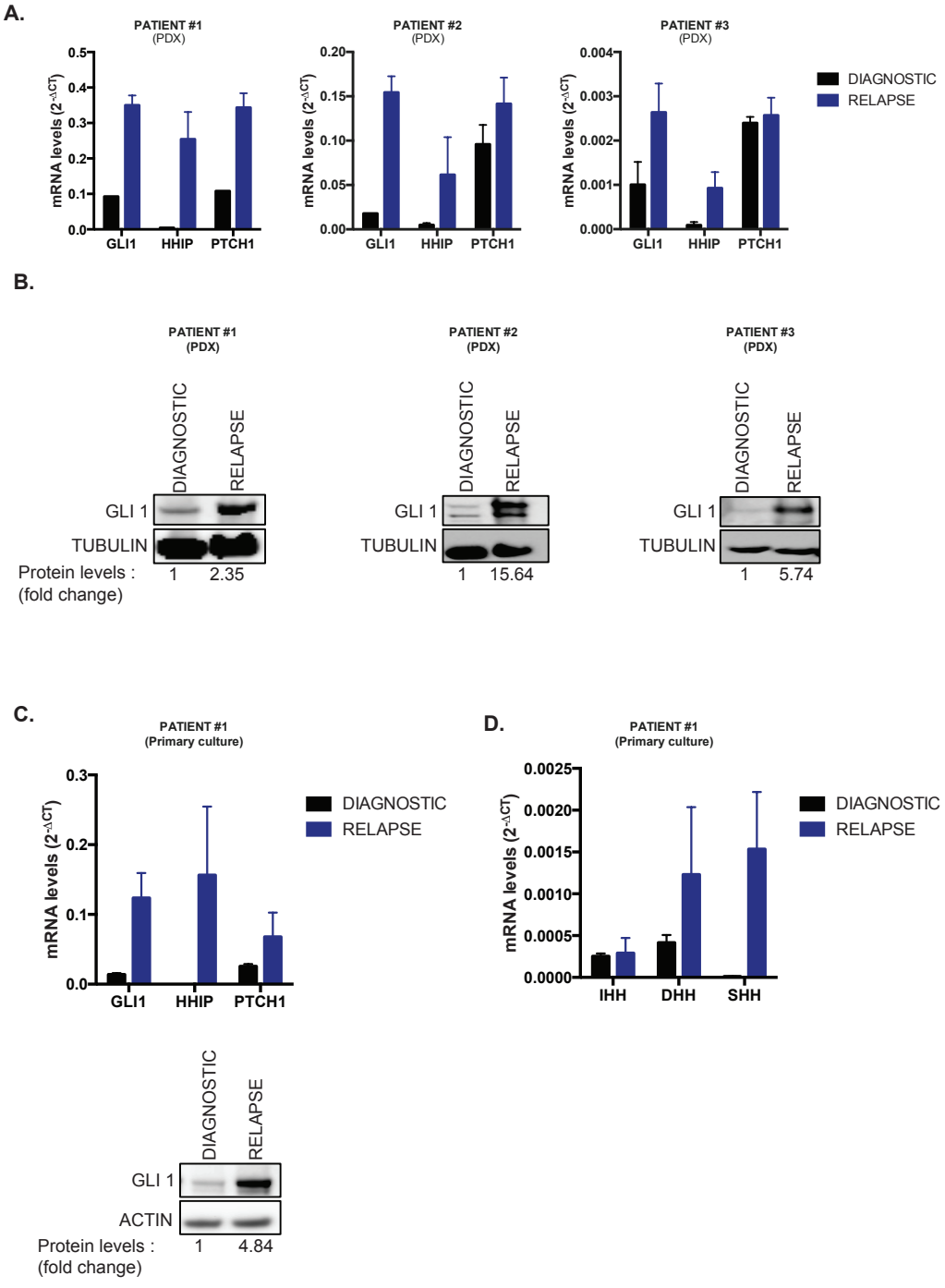
A.
PATIENT #1
(PDX)
PATIENT #2
(PDX)
PATIENT #3
(PDX)
mRNA levels (2^-ΔCT)
GLI1
HHIP
PTCH1
DIAGNOSTIC
RELAPSE
B.
PATIENT #1
(PDX)
PATIENT #2
(PDX)
PATIENT #3
(PDX)
DIAGNOSTIC
RELAPSE
GLI 1
TUBULIN
Protein levels :
(fold change)
1
2.35
1
15.64
1
5.74
C.
PATIENT #1
(Primary culture)
mRNA levels (2^-ΔCT)
GLI1
HHIP
PTCH1
DIAGNOSTIC
RELAPSE
GLI 1
ACTIN
Protein levels :
(fold change)
1
4.84
D.
PATIENT #1
(Primary culture)
mRNA levels (2^-ΔCT)
IHH
DHH
SHH
DIAGNOSTIC
RELAPSE

Figure 2

A.

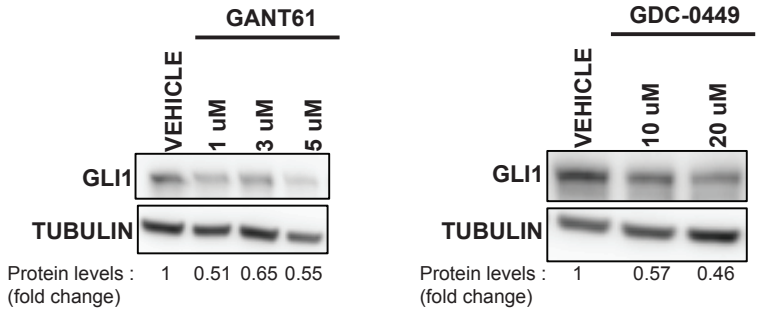
GANT61
VEHICLE
1 uM
3 uM
5 uM
GLI1
TUBULIN
Protein levels : 1 0.51 0.65 0.55
(fold change)
GDC-0449
VEHICLE
10 uM
20 uM
GLI1
TUBULIN
Protein levels : 1 0.57 0.46
(fold change)

B.

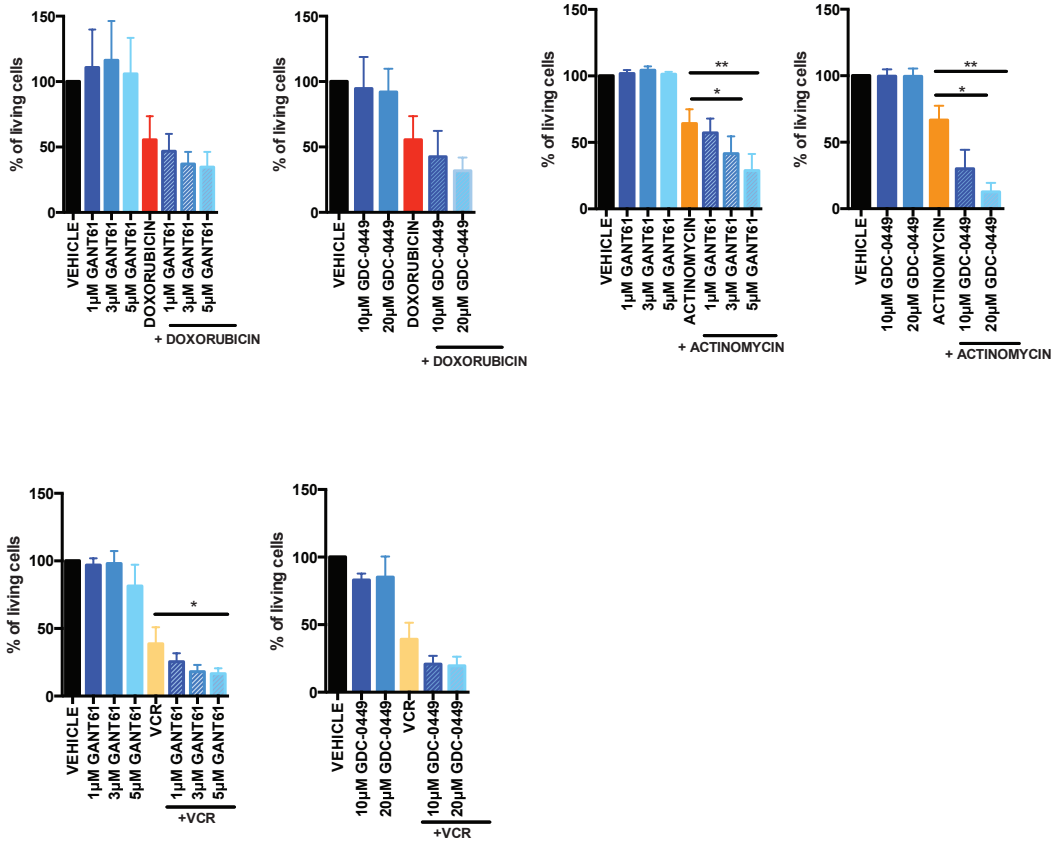
% of living cells
VEHICLE
1μM GANT61
3μM GANT61
5μM GANT61
DOXORUBICIN
+ DOXORUBICIN
10μM GDC-0449
20μM GDC-0449
ACTINOMYCIN
+ ACTINOMYCIN
VCR
+VCR

Figure 3

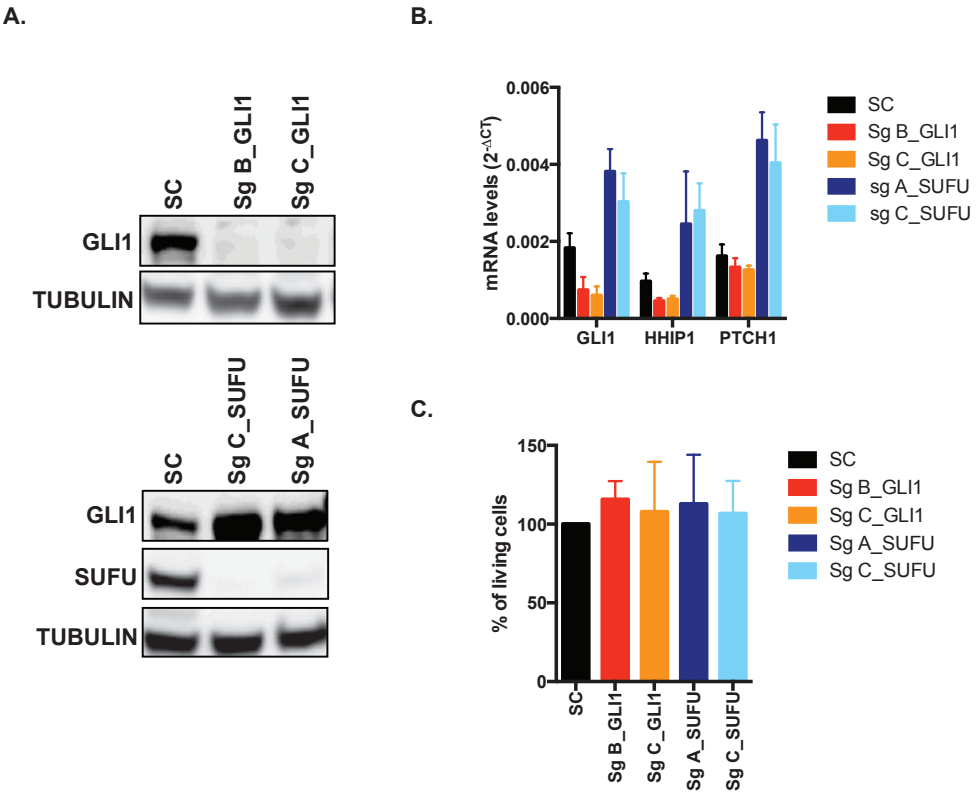
A.
SC
Sg B_GLI1
Sg C_GLI1
GLI1
TUBULIN
SC
Sg C_SUFU
Sg A_SUFU
GLI1
SUFU
TUBULIN
B.
mRNA levels (2^-ΔCT)
0.006
0.004
0.002
0.000
GLI1
HHIP1
PTCH1
SC
Sg B_GLI1
Sg C_GLI1
sg A_SUFU
sg C_SUFU
C.
% of living cells
150
100
50
0
SC
Sg B_GLI1
Sg C_GLI1
Sg A_SUFU
Sg C_SUFU
SC
Sg B_GLI1
Sg C_GLI1
Sg A_SUFU
Sg C_SUFU
D.
ACTINOMYCIN
cell viability (% of control)
LOG [nM]
SC
sg B_GLI1
sg C_GLI1
sg A_SUFU
sg C_SUFU
VINCRISTINE
cell viability (% of control)
LOG [nM]
SC
sg B_GLI1
sg C_GLI1
sg A_SUFU
sg C_SUFU

Supp. Figure 1

A.

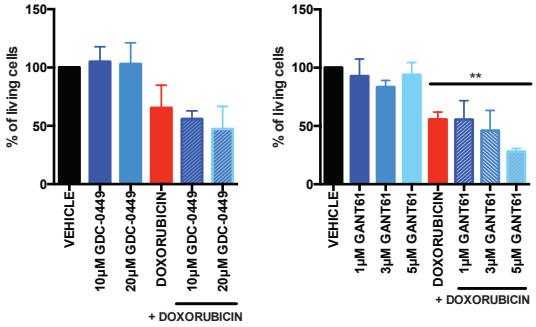

B.

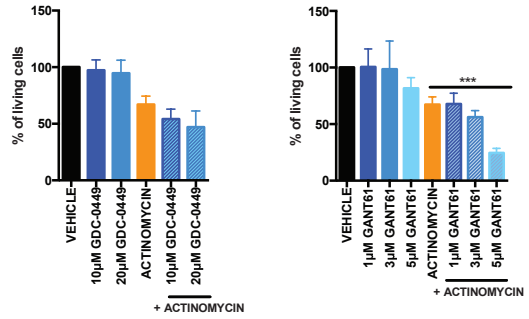

C.

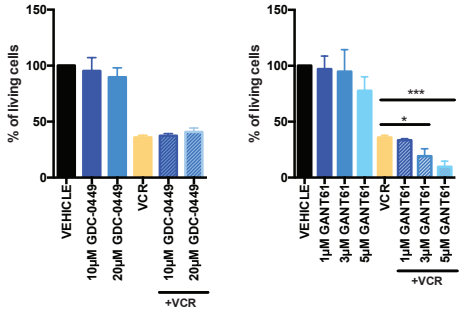

Supp. Figure 2

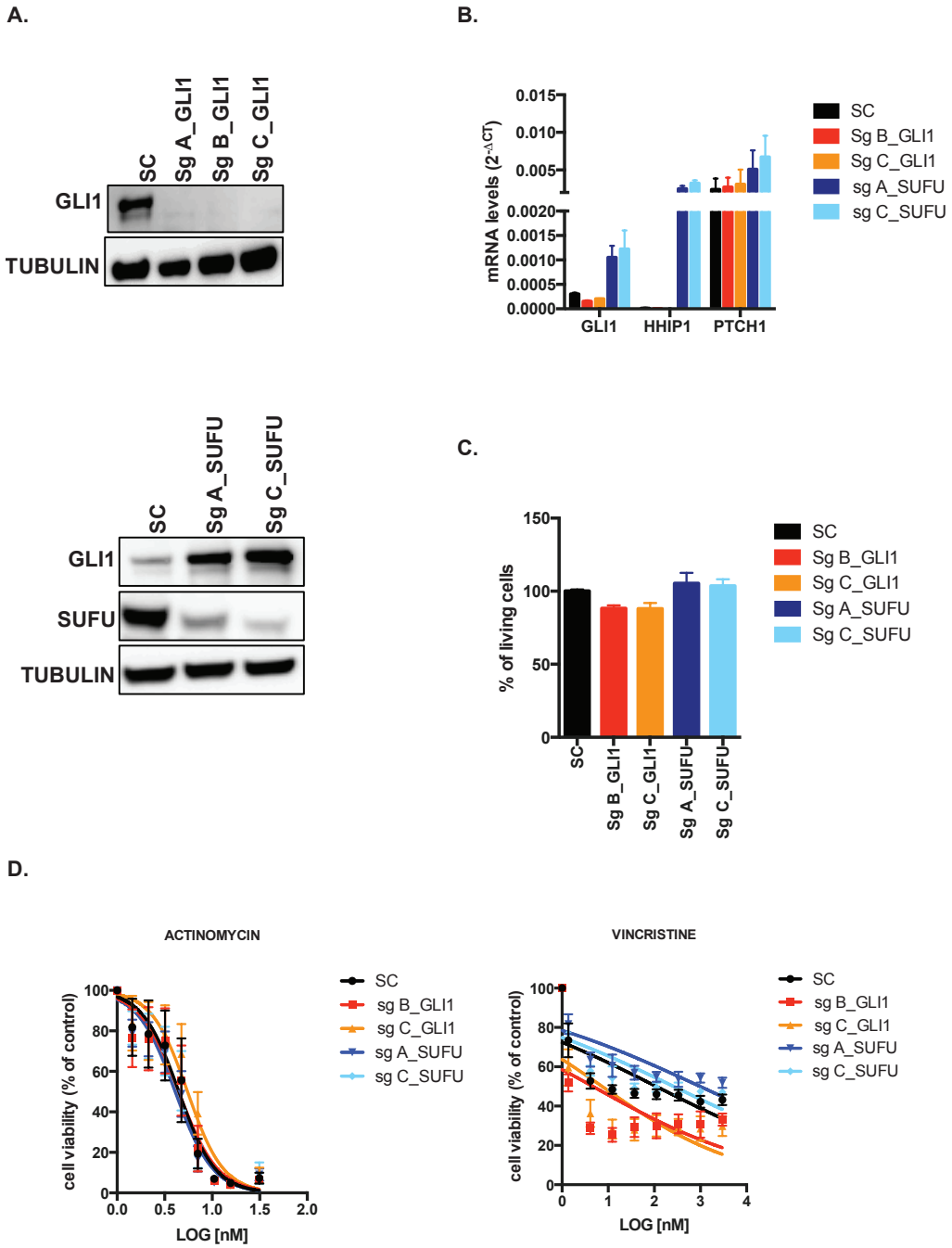

Suppl. Table 1

PRIMARY ANTIBODIES

Detected Protein	Applications	Molecular Weight (kDa)	Species	Clonality	Dilution	Catalog Number (#)	Company
GLI1	WB	133	Rabbit	Polyclonal	1:1000	2534	Cell signaling
SUFU	WB	54	Rabbit	Monoclonal	1:1000	2522	Cell signaling
α-TUBULIN	WB	50	Mouse	Monoclonal	1:5000	T-9026	Sigma Aldrich
β-ACTIN	WB	45	Rabbit	Monoclonal	1:1000	4970	Cell signaling

SECONDARY ANTIBODIES

Anti-Mouse IgG[1]	WB				1:2500	7076S	Cell signaling
Anti-Rabbit IgG[1]	WB				1:2500	7074S	Cell signaling

[1] HRP-conjugated

Abbreviations:

HRP- Horseradish peroxidase
WB- Western Blotting

Suppl. Table 2

GENE	sgRNA sequence (de-PAM-end)	Backbone vector used
SCRAMBLE	GCACTACCAGAGCTAACTCA	pLentiCRISPR-V2 (Addgene, #52961)
sgA_GLI1	ATCCCACATCCTCAGTCCCG	pLentiCRISPR-V2 (Addgene, #52961)
sgB_GLI1	ACATGCTGGTTGGCAAGTGC	pLentiCRISPR-V2 (Addgene, #52961)
sgC_GLI1	TGTATGAAACTGACTGCCGT	pLentiCRISPR-V2 (Addgene, #52961)
sgA_SUFU	CTAACATAGTCCAAGGGGTC	pLentiCRISPR-V2 (Addgene, #52961)
sgC_SUFU	AGCCCGTGCAGACACCCTTT	pLentiCRISPR-V2 (Addgene, #52961)

Suppl. Table 3

List of TaqMan®-probe based gene expression assays used in the study.

Gene	Species	TaqMan® Gene Expression Assay ID
HMBS	Human	Hs00609297_m1
GAPDH	Human	Hs02758991_g1
GLI1	Human	Hs01110766_m1
PTCH1	Human	Hs00181117_m1
HHIP	Human	Hs01011008_m1
SHH	Human	Hs00179843_m1
IHH	Human	Hs00745531_s1
DHH	Human	Hs00368306_m1

6.4. Additional studies

Targeting hedgehog signaling reduces self-renewal in embryonal rhabdomyosarcoma.

S Satheesha[1,4], G Manzella[1,4], A Bovay[1], E A Casanova[1], P K Bode[1,2], R Belle[1], S Feuchtgruber[3], P Jaaks[1], N Dogan[1], E Koscielniak[3] and B W Schäfer[1]

[1]Department of Oncology and Children's Research Center, University Children's Hospital, Zurich, Switzerland

[2]Institute of Surgical Pathology, University Hospital Zurich, Zurich, Switzerland

[3]Department of Oncology/Hematology/Immunology, Olgahospital, Klinikum Stuttgart, Stuttgart, Germany

Correspondence: Professor BW Schäfer, Department of Oncology and Children's Research Center, University Children's Hospital, Steinwiessstrasse 75, 8032 Zurich, Switzerland. E-mail: Beat.Schaefer@kispi.uzh.ch

[4]These authors contributed equally to the work.
Received 16 October 2014; Revised 14 April 2014; Accepted 19 June 2015
Advance online publication 20 July 2015

Manuscript published

I was responsible for collection of the data and data analysis: Figure 1a, 1b, 1d, 2b, 3f-j, 4 e-f, Suppl.Figure 1e-l, Suppl.Figure 2 a-c, Suppl. Figure 4b, 4c, 4i, Suppl. Figure 8a-b and Suppl. Figure 9f.

Abstract

Current treatment regimens for rhabdomyosarcoma (RMS), the most common pediatric soft tissue cancer, rely on conventional chemotherapy, and although they show clinical benefit, there is a significant risk of adverse side effects and secondary tumors later in life. Therefore, identifying and targeting sub-populations with higher tumorigenic potential and self-renewing capacity would offer improved patient management strategies. Hedgehog signaling has been linked to the development of embryonal RMS (ERMS) through mouse genetics and rare human syndromes. However, activating mutations in this pathway in sporadic RMS are rare and therefore the contribution of hedgehog signaling to oncogenesis remains unclear. Here, we show by genetic loss- and gain-of-function experiments and the use of clinically relevant small molecule modulators that hedgehog signaling is important for controlling self-renewal of a subpopulation of RMS cells *in vitro* and tumor initiation *in vivo*. In addition, hedgehog activity altered chemoresistance, motility and differentiation status. The core stem cell gene NANOG was determined to be important for ERMS self-renewal, possibly acting downstream of hedgehog signaling. Crucially, evaluating the presence of a subpopulation of tumor-propagating cells in patient biopsies identified by GLI1 and NANOG expression had prognostic significance. Hence, this work identifies novel functional aspects of hedgehog signaling in ERMS, redefines the rationale for its targeting as means to control ERMS self-renewal and underscores the importance of studying functional tumor heterogeneity in pediatric cancers.

Introduction

Rhabdomyosarcoma (RMS) comprises of a heterogeneous set of neoplasms that possess features of halted skeletal muscle differentiation and is the most common pediatric soft tissue cancer. The two major histological subtypes, embryonal (ERMS) and alveolar, differ in their molecular cytogenetic profiles, clinical presentations and prognosis. ERMS accounts for about 70% of RMS cases and possesses a relatively more complex genomic landscape with frequent alterations within the RAS pathway.[1, 2, 3] Currently, pre-treatment histology and initial clinical presentation guide risk stratification to determine therapy intensity. Although a majority of ERMS patients have good prognosis, clinical benefit from current treatments has reached a plateau and prognosis is dismal for high-risk metastatic ERMS patients.[2] Therefore, there is an urgent need to implement rationally selected targeted treatment options to reduce rate of relapse, therapy burden and improve clinical outcome.

Hedgehog pathway, a master developmental signaling system, is commonly activated in sporadic ERMS.[4, 5, 6, 7] Canonical hedgehog pathway is a ligand-activated signaling system with three ligand variants—Sonic (SHH), Indian (IHH) and Desert hedgehog (DHH). The secreted ligands bind to the extracellular domain of the Patched (PTCH) receptor leading to the release of the receptor Smoothened (SMO). SMO then translocates to the primary cilium to activate the downstream signaling cascade that involves relieving inhibition of Suppressor of Fused (SUFU) on activity of the GLI transcription factors. The ligands available for activation can be titrated by the transmembrane Hedgehog-interacting protein (HHIP). There are three GLI transcription factors, of which GLI1 is the most potent transactivator. Low-level gains in the GLI1 genomic region have been noted in ERMS patients.[5]The expression of GLI target genes, which include components of the hedgehog pathway such as GLI1, PTCH1 and HHIP, can be used to study pathway activation status.[8, 9]

Recent data suggest that ERMS is a hierarchically organized tumor.[10, 11, 12] At present, little is known about the pathways used to maintain self-renewal and tumorigenic properties of ERMS tumor-propagating cells (TPCs). In the present study, using small molecules and various genetic approaches, we show that hedgehog signaling modulates ERMS TPC features of self-renewal and tumor initiation. We describe additional novel roles played by this pathway in determining ERMS chemoresistance, invasion and differentiation, and identify NANOG as a functionally important self-renewal gene that could be downstream of the pathway, previously unknown in any soft tissue sarcoma. Importantly, we show that functional intra-tumoral heterogeneity identified by the presence of hedgehog-active TPC markers in ERMS patients is clinically relevant.

Results

Hedgehog signaling is necessary for ERMS self-renewal and efficient tumorigenesis

We analyzed the expression of hedgehog pathway components in ERMS sphere cultures that are enriched in de-differentiated, self-renewing and highly tumorigenic cells.[11] Quantitative PCR (qPCR) analysis revealed that the expression of hedgehog target genes was upregulated in ERMS spheres (Figure 1a and Supplementary Figures 1a and c) and xenografts from ERMS cell lines and patient-derived tumors (Figure 1b and Supplementary Figures 1d and f) compared with adherent cultures. The addition of hedgehog agonist SAG1.3 during primary sphere formation led to enhanced secondary sphere formation (RD: +50% and RH36: +170%; Figure 1c) indicating that activating the hedgehog pathway could increase self-renewal in ERMS cells. Similarly, the use of two independent siRNAs against SUFU led to significantly increased sphere-initiating ability (Figure 1d and Supplementary Figures 1g and i). To exclude any extraneous effects of sphere media components on hedgehog pathway activation, ERMS adherent cells were treated with SAG1.3 prior to plating in sphere media. Again, treatment led to a dose-dependent increase in sphere initiation without affecting cell cycle profile or viability (Figure 1e and Supplementary Figures 1j and l).

We performed single cell cloning of RD cell line that showed heterogeneous expression of GLI1 to isolate subpopulations with varying levels of hedgehog pathway activity. All the 29 clones analyzed also showed heterogeneous GLI1 expression (data not shown), indicating that the pathway is dynamically controlled. We performed sphere-initiation studies using two clones (Clones E8 and H3) that had fewer $GLI1^{high}$ cells than bulk RD cells and Clone F2 that was enriched in $GLI1^{high}$ cells (Supplementary Figures 2a and b). Clone E8 and Clone H3 had significantly lower spherogenicity (by 50% and 40%, respectively) and Clone F2 had increased sphere-initiating capacity (+30%; Supplementary Figure 2c) highlighting that a population-intrinsic level of hedgehog signaling could determine self-renewal capacity.

To study the role of hedgehog pathway activation in more detail, we generated stable cell lines that overexpressed full-length GLI1 (pCMV-GLI1). At the endogenous level, we could detect the more stable shorter isoform of GLI1 (~130 kDa; Figure 1f) reportedly derived from the 160kDa full-length protein.[13] pCMV-GLI1 cells showed an increased expression of downstream targets, PTCH1 and HHIP, compared with the control (Figure 1f and Supplementary Figures 2d and e). We also found the expression of PGDFRA, a known hedgehog target gene that was previously implicated in ERMS biology,[14, 15] to be increased (Supplementary Figures 2d and e). pCMV-GLI1 cells possessed enhanced primary sphere-forming and colony-forming abilities (Figures 1g and h and Supplementary Figure 2f). When plated for secondary sphere formation, the relative increase in sphere-initiation capacity became more apparent (RD: +87% and RH36: +230%) indicating improved self-renewal. Importantly, pCMV-GLI1 cells displayed significantly faster

tumor growth rate when injected orthotopically in NOD/SCID mice (Figures 1i and j). The xenografts retained GLI1 overexpression (Supplementary Figure 2g) and were confirmed to be of ERMS histotype (Supplementary Figure 3). Taken together, the active hedgehog pathway in ERMS cells leads to higher self-renewal and increased tumor-initiating capacity.

Next, we inhibited the hedgehog pathway both pharmacologically and genetically. ERMS cells treated with SMO inhibitor GDC-0449 or GLI inhibitor GANT61 during primary sphere formation showed decreased sphere numbers (Figure 2a and Supplementary Figure 4a). GDC-0449 treatment led to an 88% decrease in secondary sphere formation for RD cells and RH36 cells showed no spheres formation. GANT61 treatment was more potent because no viable cells were available for secondary sphere formation from either cell line. Using two independent siRNAs against GLI1 in adherent cells significantly decreased sphere initiation (Figure 2b and Supplementary Figures 4b and c). Next, cells were treated with inhibitors (also including the SMO inhibitor LDE-225) under adherent conditions and then plated for sphere formation. Dose-dependent decrease in sphere initiation was observed with all drugs (Figure 2c and Supplementary Figure 4d). Treatments did not alter cell cycle profile or viability status of the cells (Supplementary Figures 4e and h). Pre-treatment of RD cells with GANT61 *in vitro*led to slower tumor initiation *in vivo* owing to reduced hedgehog pathway activity at the time of engraftment (Figures 2d and e and Supplementary Figures 4i–k).

To study the long-term effects of inhibition, we generated stable cell lines that overexpressed SUFU (pCMV-SUFU) to inhibit GLI activity directly or expressed shRNA against SMO (shSMO) to inhibit the canonical ligand-based hedgehog signaling. Both inhibitory systems led to decreased target gene expression (Figures 2f and g and Supplementary Figures 5a and e). Adherent colony-forming ability, sphere initiation and renewal were markedly decreased by either hedgehog-inhibition strategies (Figures 2h and i and Supplementary Figures 5f and g). Although no significant changes occurred in proliferation or cell cycle profiles (Supplementary Figures 5h and n and data not shown), significant decrease in tumor growth kinetics was observed *in vivo* (Figures 2j–m). Impressively, RD cells showed no palpable tumor growth in the majority of hedgehog-inhibited xenografts at the time when the controls reached maximum allowed tumor volumes. While tumor initiation rate was 100% for control cells, only three out of five mice and three out of seven mice injected with pCMV-SUFU and shSMO cells, respectively, eventually developed tumors. Taken together, the inhibition of hedgehog pathway reduces *in vitro* self-renewal and *in vivo* tumor initiation.

Pathway activation seemed to be largely ligand-based because inhibition of either receptor-mediated or GLI-based hedgehog signaling led to similar and comparable effects on self-renewal and tumorigenesis. Accordingly, we found increased expression of hedgehog ligands DHH and IHH in RH36 spheres and xenografts (Supplementary Figures 6a and c), and of DHH in RD cells (Supplementary Figures 6b and d) compared with adherent cultures. Also, patient-derived

xenograft (PDX) samples showed higher expression of both (RH70) or IHH ligand (RH73) *in vivo* (Supplementary Figures 6e and f). DHH and IHH were also found to be the most commonly expressed hedgehog ligands in ERMS patient tumors, with on average a higher expression of DHH (Supplementary Figures 6g and h). Surprisingly, SHH was expressed only in a minority of tumor biospies and not at all in adherent cell lines, sphere cultures, xenografts or murine skeletal muscle. Additionally, using species-specific qPCR probes, we could determine that ligand-based signaling was occurring in an autocrine manner with a minor inverse-paracrine contribution from the stroma within xenografts (Supplementary Figures 6k and n). Therefore, ligand-based hedgehog signaling is active in ERMS and seems to increase under conditions of self-renewal and *in vivo* tumorigenesis and, importantly, is necessary for TPC functionality.

Hedgehog signaling alters chemoresistance, differentiation status and cell motility of ERMS cells

TPCs might also be responsible for tumor recurrence by being more resistant to chemotherapeutic treatments.[16] To test this notion, we treated our stable cells with serial dilutions of irinotecan or doxorubicin that are currently used in clinical management. We observed on average higher IC_{50} values for pCMV-GLI1 cells compared with a control indicating that cells with increased hedgehog activity are more resistant (Table 1). Conversely, cells with inhibited pathway were more sensitive to conventional drugs. Interestingly, treatment of wild-type RD cells with increasing doses of irinotecan also enhanced sphere-initiating capacity, which could be rescued by combined treatment with hedgehog inhibitor LDE-225 (Supplementary Figures 7a and b). This implies that high-dose chemotherapy treatment currently used in clinical management could enrich for hedgehog-active TPCs.

Next, we evaluated the effect of hedgehog signaling on ERMS differentiation. Expression of PAX7 is highest in muscle stem cells, while committed muscle progenitor cells express MYOGENIN. Therefore, expression of these proteins provides a convenient readout to assess the differentiation status. Indeed, the expression of these markers was mutually exclusive also in ERMS cells indicating that the differentiation programs present during normal myogenesis are also active in the pathological state (Figure 3a and Supplementary Figure 7c). pCMV-GLI1 cells possessed increased $PAX7^+$ cells and concomitantly fewer $MYOGENIN^+$ cells (Figures 3a–c and Supplementary Figure 7c), whereas inhibition of the pathway induced differentiation as evidenced by a reduction in the percentage of $PAX7^+$ and gain in $MYOGENIN^+$ cells (Figures 3a and Supplementary Figures 7d and e). Treatment with small molecule modulators induced similar alterations in the differentiation status (Supplementary Figures 7f and i). Furthermore, significant increase in the expression of terminal muscle differentiation markers CKM and MYL1 was noted upon long-term treatment with GANT61 (Supplementary Figure 7j). These data suggest that activation of hedgehog signaling confers a more stem-like state, whereas pathway

inhibition induces differentiation. We could not find significant co-localization of PAX7 and GLI1 expression (data not shown) indicating that PAX7 may not be a direct target of GLI1. Rather, hedgehog pathway activation might induce de-differentiation by reducing the transcriptional activity of pro-differentiation muscle regulatory factors.[17]

A previous study evaluating *in vivo* tumor heterogeneity in a zebrafish model of ERMS reported that the Myogenin-expressing (differentiated) compartment had higher invasiveness.[12] Concordantly, we observed that the hedgehog-inhibited cells possessed increased ECM invasion capacity (Figures 3f and g and Supplementary Figure 8a). This effect was cell autonomous because coating the membrane filter with gelatin did not alter the results (Supplementary Figure 8a). Surprisingly, in the absence of a basement membrane matrix, the differentiated cells had much lower migratory ability (Figures 3h and i and Supplementary Figure 8b), indicating that matrix adhesion probably has an important role in determining cell motility in ERMS.

NANOG is functionally important for ERMS self-renewal

To identify genes that could be regulated by the hedgehog pathway in ERMS cells, we used a stem cell-focused qPCR-based screening approach interrogating 162 genes associated with developmental pathways and the stem cell phenotype. We found 147 genes to be reliably expressed (Ct value<35), of which 142 were common to both cell lines. Non-supervised hierarchical clustering identified genes either positively or negatively modulated by hedgehog signaling (Figure 3j). In general, we found more genes to be negatively regulated by the hedgehog signaling and among them were several components of TGF-β, Wnt and Notch (in RD cells; data not shown) signaling pathways. Interestingly, expression of the stem cell transcription factor NANOG was positively regulated by the hedgehog pathway in both ERMS cell lines studied. NANOG is a homeodomain-containing transcription factor essential for establishing pluripotency[18] with a known function in TPC maintenance in many adult cancers.[19] It has already been characterized as a GLI target gene in neural stem cells, medulloblastoma and glioblastoma neurospheres.[20, 21] Therefore, we chose to further study its role in ERMS.

First, we confirmed alterations in NANOG expression noted in the screen on additional samples (Supplementary Figures 9a and d). Next, ERMS cells were co-immunostained for GLI1 and NANOG. The expression of both proteins was found to be heterogeneous and strictly co-localized in both cell lines and primary cells from three PDX samples (Figure 4a and Supplementary Figures 9e and f). Upon GLI1 overexpression or SAG1.3 treatment, the percentage of NANOG-expressing cells increased significantly (Figures 4b and c and Supplementary Figures 10a and c). NANOG expression was higher in sphere cultures and xenografts than adherent cultures (Supplementary Figures 10d and g). These data indicate that NANOG expression correlates with hedgehog pathway activity, both in ERMS cells and patient samples, implying that it could be a target gene of the pathway in ERMS similar to observations in other cancers.

We also reduced NANOG expression in RD cells using transient and stable genetic means and both approaches led to decreased sphere formation (Figures 4d and e). Transient overexpression of NANOG significantly improved spherogenicity (Figures 4f and g). Importantly, ectopic NANOG expression in hedgehog-inhibited cells rescued the lowered self-renewal ability back to the level of controls, indicating that NANOG could act epistatic to hedgehog pathway (Figures 4f and g). We also noted that alteration in NANOG expression led to a concordant change in the expression of GLI1 (Supplementary Figures 11a and c), which could be either due to the effect on overall proportion of ERMS stem cell-like population marked by GLI1 expression or the direct modulation of GLI1 expression as previously reported in brain cancers.[21] Interestingly the expression of PDGFRA was also decreased upon NANOG knockdown (Supplementary Figure 11a). To evaluate the role of NANOG on self-renewal and tumor growth independently, we generated stable rescue lines where NANOG expression was decreased in GLI1 overexpressing cells (GLI1+shNANOG) and corresponding empty vector (pCMV+pLKO.1) or GLI1 overexpression only controls (GLI1+pLKO.1) (Supplementary Figures 11d and e). When both RD and RH36 rescue systems were allowed to form spheres, secondary sphere formation was increased significantly in the GLI1+pLKO.1 cells for both cell lines (RD: +108% and RH36: +59%) and impressively, NANOG knockdown rescued it back to almost control levels (Figures 4h and i). Additionally, the *in vivo* tumor growth rate of GLI1+shNANOG cells was significantly lower than control cells (Figure 4j and Supplementary Figures 11f and g). Taken together, NANOG emerges as a functionally important gene for TPC properties in ERMS that could act downstream of the hedgehog signaling.

GLI1 and NANOG expression has prognostic value for ERMS patients

Finally, we evaluated whether the expression of GLI1 and NANOG is clinically relevant. To this end, we performed a double-blind analysis of GLI1 and NANOG expression in a previously described set of tissue microarrays (TMA) with multiple tumor cores from 116 ERMS patient samples using immunohistochemistry.[22]Reliable protein expression status was obtained for 91 patients, most of whom were negative for both proteins. However, patients positive for one were in 80% of the cases also positive for the other. We observed that only tumor cells expressed GLI1 and NANOG and, importantly, the expression was heterogeneous as seen in cell cultures (Figure 5a and Supplementary Figure 11h). Correlation with clinical data revealed that the expression of GLI1 alone could predict significantly worse overall survival and a similar trend was observed for NANOG status (Figures 5b and c). These patients also tended to have worse event-free survival although the data did not reach statistical significance (Supplementary Figures 11i and j). Importantly, it was only when the patients were distinguished based on the presence of $GLI1^+$ and $NANOG^+$ cellular sub-populations within their tumors that we observed statistically significant worse event-free and overall survival (Figures 5d and e). The distribution of patient- and tumor-

related parameters was similar among patient subgroups. Chi-square tests revealed no significant differences between the groups (data not shown). Owing to low patient numbers, it was not possible to assess whether GLI1 and/or NANOG expression could be used as independent prognostic markers. Nevertheless, our analysis reveals that intra-tumoral heterogeneity represented by the expression of both GLI1 and NANOG can help identify a subset of ERMS patients with worse outcome and therefore is clinically relevant.

Discussion

Although previous studies have identified hedgehog signaling as a clinically relevant pathway in ERMS,[4, 5] its functional role in ERMS pathology and particularly its contribution to the hierarchical organization seen in ERMS has not been investigated. Here, we show that hedgehog pathway activity is an important determinant of ERMS 'stemness' features such as self-renewal and tumor initiation, as previously shown for other malignancies.[23] Therefore, clinical strategies for using hedgehog inhibitors in ERMS would need to accommodate the conceptual implications of the cancer stem cell model.[24, 25] For instance, tumor regression may not be an appropriate endpoint to estimate treatment efficacy, because the effect of hedgehog pathway modulation on ERMS pathology was not due to changes in cell cycle, cell viability or proliferation.

Pathway activation seems to be occurring primarily by autocrine secretion of IHH and/or DHH. This is in line with an earlier study ruling out SHH autocrine signaling in ERMS patients.[6] Pathway inhibition was effective at the level of SMO as well as of GLI, which could avoid emergence of cross talks converging on the GLI-code and resistance mechanisms in the clinics.[9] Furthermore, we found that modulating the pathway can alter sensitivity to generic drugs. Therefore, combination therapy with hedgehog inhibitors might allow the usage of lowered drug doses to reduce treatment-related morbidity.

Interestingly, our work suggests novel negative feedback mechanisms between hedgehog signaling and key muscle differentiation pathways, Wnt, Notch and TGFβ.[26, 27, 28] Previous reports show that inhibition of Notch and TGFβ and activation of Wnt could lead to ERMS differentiation.[7, 29, 30] Interestingly, activation of the Wnt pathway induced differentiation and reduced tumor initiation in a RAS-driven zebrafish ERMS model. The authors also identified the hedgehog inhibitor cyclopamine as one of the top drug candidates from a large-scale small molecular screen that could differentiate ERMS cells and reduce tumor growth *in vivo*.[31] This study supports our findings and further highlights crosstalk between 'stemness' pathways that could define ERMS TPC behavior. However, the more differentiated compartments are also likely to have important roles in tumor progression (this study and Ignatius *et al.*[12]).

Previously, PTCH1 mRNA expression in ERMS patients was shown to predict poor outcome.[4] Although PTCH1 mRNA expression correlates significantly with that of GLI1 mRNA (data not shown and Zibat *et al.*[4]), PTCH1 provides negative feedback cues into the pathway that

could obscure the final outcome on cellular self-renewal. Hence, PTCH1 protein expression status may not be a reliable predictor of prognosis. We reported that ERMS patients with CD133^{high} expression have poor overall survival,[11] but the functional role of CD133 protein is currently unclear. Also, the impact of other potential ERMS TPCs markers (FGFR3 (ref. 32) and MYF5 (ref. 12) on prognosis is unknown. We identify NANOG as a functionally important gene whose expression along with GLI1 could serve as novel prognostic indicators. Importantly, we detected clear GLI1-NANOG co-localization in ERMS PDX cells. However, we were unable to do so on the TMA tumor cores owing to the lack of serial sections. Interestingly, we observed heterogeneous expression of GLI1 and NANOG also within alveolar RMS patient tumor cores but without prognostic significance (data not shown). Therefore, the GLI1-NANOG TPC marking could be important specifically for ERMS patient stratification and further highlights the biological disparity between the two RMS variants.

Expression of transcription factors important for development of neural crest-derived mesenchymal and neural tissues, namely PAX6, PITX2 and LMX1B,[33, 34, 35] were positively regulated by the hedgehog pathway, whereas myogenic differentiation factors were downregulated. Therefore, GLI1-NANOG^{high} ERMS cells could possess a pre-myogenic multipotent phenotype reminiscent of neural crest or non-myogenic origin for ERMS. This is concordant with recent observations in hedgehog-activated mouse models, wherein ERMS 'cell of origin' was determined to be from either pre-somitic or non-muscle mesenchyme.[36, 37] ERMS cells expressing other potential TPC markers have been described to be restricted to the skeletal muscle lineage.[10, 32, 38] It is therefore possible that different ERMS TPC subpopulations with varying differentiation potentials are concomitantly present within tumors. The hierarchical relationship between these potential compartments and their relative importance for ERMS tumorigenicity is yet to be determined and warrants further research.

It is likely that the hedgehog-active TPC phenotype is a widespread feature because activation of RAS signaling is common in ERMS[1, 3] and is known to have a positive influence on hedgehog signaling.[39] Interestingly, also, the loss of p53 can increase GLI-NANOG signaling in stem cells and TPCs of neural origin.[20, 21] The cell lines used in this study represent these genetic backgrounds (RD: NRAS^{Q61H}; p53^{R248V} and RH36: HRAS^{Q61K}). Hence, hedgehog-driven targeting could be of broad interest in sporadic ERMS. Our study highlights that phenotypic and functional tumor heterogeneity could have significance for clinical management of ERMS patients and suggests hedgehog inhibition as a treatment strategy aimed at reducing the rate of relapse for a long-term cure.

Materials and Methods

Patient-derived samples

Early passages of ERMS PDX samples RH70 (SJRHB011_Y), RH72 (SJRHB013_X) and RH73 (SJRHB011_X) were obtained from St. Jude Children's Research Hospital (USA) and previously described in detail in.[1] All patient tissue specimens used only for RNA extraction were obtained from the Swiss Pediatric Oncology Group (SPOG) Tumor Bank except ZH_ERMS, which was obtained from the Department of Pathology, University Hospital Zurich. The use of SPOG Tumor Bank tissue samples was approved by the Ethical Review Board of Zurich (Ref. No. StV-18/02). Written informed consent was obtained from each patient by the hospital that provided the tissue samples. The TMA used in this study included multiple tumor cores from 149 RMS patients (116 ERMS and 33 alveolar RMS) enrolled in the German soft-tissue sarcoma group (CWS) studies -81, -86, -91 and -96 as previously described.[22]

Orthotopic xenograft generation

RD (3×10^5cells/mouse) or RH36 (2.5×10^5cells/mouse) were injected into the femoral muscles of one leg of 4–6-week-old NOD.CB17-*Prkdc*^{scid} mice (NOD/SCID; Jackson Laboratory, Bar Harbor, ME, USA). Animals were chosen from either sex and were assigned randomly to different groups. Once tumor was palpable, size was determined every 4 days by measuring two diameters (d_1 and d_2) in right angles of both legs with a Vernier caliper until tumors reached the maximum allowed volume of 1000 cm^3 or followed for 120 days. Tumor volumes were calculated using the following formula: $V=[4/3 \times \pi \times 1/2(d_1+d_2)]_{injected\ leg}-[4/3 \times \pi \times 1/2(d_1+d_2)]_{control\ leg}$.

For PDX generation, dissociated cells were resuspended in matrigel (Corning, Amsterdam, Netherlands) at 1×10^4 cells/µl and 100 µl was injected as described above.

Freshly isolated xenografts were stored in RNAlater (Ambion, Huntingdon, Cambridgeshire, UK) for RNA extraction, snap-frozen in liquid N_2 for protein extraction or fixed in 4% paraformaldehyde **for imunohistochemistry. The experiments were conducted in a non-blind manner and approved by the veterinary office of Canton Zurich.**

Tumor dissociation

PDX samples were minced with scalpels and digested using Liberase DH (0.62 WU/ml; Roche, Rotkreuz, Switzerland) in buffer containing 1 × HBSS, 10 mM HEPES, 200 U/ml DNase (Roche) and 1 mM $MgCl_2$, at 37 °C for 70 min. The cells were pelleted, resuspended in Dulbecco's modified Eagle's media +10% fetal bovine serum and passed through a cell strainer to remove debris. Primary cells were plated and maintained in standard culture media for experiments.

Cell culture and treatments

Human ERMS cell lines RD (ATCC, Manassas, VA, USA), RH36, RH18 (both kindly provided by Peter Houghton, St. Jude's Children's Hospital, USA) and TTC442 (kindly provided by Timothy J. Triche, Children's Hospital Los Angeles, USA) were cultured in Dulbecco's modified Eagle's media supplemented with 10% fetal bovine serum, 2 mM L-glutamine and 100 U/ml penicillin-streptomycin. Sphere cultures were maintained as previously described.[11] The cell lines were authenticated by short tandem repeat analysis and regularly checked for mycoplasma contamination. For sphere formation, equal numbers of cells were plated at clonal density in Ultra-Low attachment plates (Corning). Primary spheres were dissociated using Accutase (Sigma-Aldrich, Buchs, Switzerland) and stained with Trypan Blue solution (Sigma-Aldrich) for counting. Equal numbers of viable sphere cells were plated for secondary sphere formation. For single cell cloning, RD cells were plated in 96-well plates in stringent single cell dilution (0.5 cell/well) in normal adherent culture media. After 16 h, the wells with single cells were marked and followed for viable colony formation. Upon reaching confluency, the cultures were propagated in larger plate formats. Drugs used included SMO inhibitors GDC-0449 and LDE-225 (Selleck, Munich, Germany), GLI inhibitor GANT61 (Tocris, Bristol, UK) and GLI activator SAG1.3 (Calbiochem, San Diego, CA, USA). For IC_{50} measurements of irinotecan (SN-38; Sigma-Aldrich) and doxorubicin (Sandoz, Rotkreuz, Switzerland), cells were plated in quadruplicate in 96-well plates and treated with five-step serial dilutions for 72 h in 10% fetal bovine serum media. Dimethyl sulfoxide (Sigma-Aldrich) was used as vehicle control except for SAG1.3 (diluted in water).

siRNA transfection

Adherent cells were transfected with Silencer select siRNAs (Ambion, Life technologies) against GLI1 (#1: s5814; #2: s5816), SUFU (#1: s28520; #2: s28521), NANOG (#1: s36649; #2: s36650) or scrambled control (Silencer Negative Control# 2) using Lipofectamine RNAiMAX (Invitrogen, Zug, Switzerland) at a final concentration of 10 nM. Sphere growth was initiated 24 h post transfection.

Cell viability, proliferation and clonogenic assays

To assess cell viability and proliferation, cells were plated in quadruplicate per condition in 96-well plates. After treatment, viability was measured using WST-1 (Roche). Cell proliferation was measured 24 h post plating using Cell Proliferation ELISA, BrdU (chemiluminescent) assay (Roche). Clonogenic assay was performed as described by Franken *et al.*[40] In brief, cells were seeded in dilution of 1 cell/µl in six-well plates in normal culture media. Media was changed every 3 days until colonies (>50 cells) were visible. Cells were fixed and stained using with Crystal

Violet staining solution (0.5% Crystal Violet and 6% gluteraldehye in water). Colonies were quantified using ImageJ software (version 1.47).

Quantitative PCR

Normal human skeletal muscle pooled RNA lysate, referred to as AdSkM_P, from five adults (R1234171_P) and individual RNA lysates from three fetal donors (R1244171; Lot # A503105, B505186, A508111) were purchased from (Amsbio, Lugano, Switzerland). Total RNA was extracted using RNeasy Mini Kit (Qiagen, Basel, Switzerland) with RNase-free DNase. Normal murine muscle RNA was extracted from femoral muscle of NOD/SCID mice. Complementary DNA synthesis was carried out using High-Capacity cDNA Reverse Transcription kit (Life Technologies, Zug, Switzerland). QPCR was performed using Taqman mastermix and Gene Expression Assays (Life Technologies; assay IDs are listed in Supplementary Table 1). Absolute and relative expression levels were calculated using the ΔΔCt method and normalized to HMBS (unless otherwise specified) or GAPDH. For screening, RT^2 Profiler PCR Arrays (Stem Cell Signaling (PAHS-047ZE) and Stem Cell Transcription Factors (PAHS-501ZE)) were purchased from Qiagen. Data analysis was performed using the RT^2 Profiler PCR Array Analysis web-based software (version 3.5). Non-supervised hierarchical clustering was performed using by dChip.

Western blotting and immunofluorescence

Total protein was extracted using RIPA buffer (50 mM Tris-Cl, pH 6.8, 100 mM NaCl, 1% Triton X-100, 0.1% SDS) supplemented with Complete Mini Protease Inhibitor Cocktail (Roche). Proteins were separated using NuPAGE gradient SDS–PAGE pre-cast gels (Life Technologies) and detected by chemiluminescence using Amersham ECL Detection reagent (GE Healthcare, Glattbrugg, Switzerland) or SuperSignal West Femto Maximum Sensitivity Substrate (Thermo Scientific, St Leon-Rot, Germany). For immunofluorescence, cells were fixed with 4% paraformaldehyde and incubated over night at 4 °C with primary antibodies. All the antibodies and further details are listed in Supplementary Table 2.

TMA scoring and data analysis

TMA was evaluated by a senior pathologist (PB). A minimum of two desmin-positive intact cores was required for the patient to be included in the analysis. At least three stained cells were required to label a patient as positive. Tumors from 91 ERMS and 23 alveolar RMS patients provided reliable GLI1 and NANOG expression status. Clinical data were analyzed independently by CWS study member (SF) who was blind to the hypothesis. Statistical analysis was performed using SPSS software (version 21, (IBM, Armonk, NY, USA)) based on all data available up to the cutoff date, 05.04.2013. Differences in survival rates were analyzed using the log-rank test.

Statistical analysis

Data were analyzed using GraphPad Prism (version 4.03). Significance was calculated using Student's *t*-test (unpaired, two-tailed), and if the variance was found to be significantly different by F-test, then Welch's correction was used. Normal distribution of data was assessed using D'Agostino and Pearson normality test. Mann–Whitney test was used to assess significance when data were non-parametric. Tumor growth curves were compared using two-way analysis of variance with Bonferroni *post hoc* tests. Only animals that showed tumor growth were included in the final analysis. $P<0.05$ was considered significant. The total sample size ('*n*') and biological replicates ('*N*') per condition per experiment are indicated in the figure legends. Each experiment was replicated at least twice. Data are represented as mean with s.d. as error bars unless otherwise mentioned. No power analysis was used to pre-determine sample size.

Conflict of interest

The authors declare no conflict of interest.

Acknowledgements

We highly appreciate St Jude's Children's Research Hospital for providing the ERMS PDX samples, Swiss Pediatric Oncology Group (SPOG) for providing ERMS patient tumor samples and the German Soft tissue sarcoma study group (CWS) for providing the TMA sections and performing the clinical data analysis. We are also grateful to Silvia Behnke (Sophistolab AG) and the technicians at the Institute of Surgical Pathology (University Hospital Zurich) for their excellent service. The work was supported by grants from Swiss National Science Fund (31003A-138460), Sciex (F-80016-02-01) and Cancer League Canton Zurich.

References

1. Chen X, Stewart E, Shelat AA, Qu C, Bahrami A, Hatley M *et al*. Targeting oxidative stress in embryonal rhabdomyosarcoma. *Cancer Cell* 2013; **24**: 710–724. | Article | PubMed | ISI | CAS |
2. Hawkins DS, Gupta AA, Rudzinski ER. What is new in the biology and treatment of pediatric rhabdomyosarcoma? *Curr Opin Pediatr* 2014; **26**: 50–56. | Article | PubMed |
3. Shern JF, Chen L, Chmielecki J, Wei JS, Patidar R, Rosenberg M *et al*. Comprehensive genomic analysis of rhabdomyosarcoma reveals a landscape of alterations affecting a common genetic axis in fusion-positive and fusion-negative tumors. *Cancer Discov* 2014; **4**: 216–231. | Article | PubMed | ISI | CAS |
4. Zibat A, Missiaglia E, Rosenberger A, Pritchard-Jones K, Shipley J, Hahn H *et al*. Activation of the hedgehog pathway confers a poor prognosis in embryonal and fusion gene-negative alveolar rhabdomyosarcoma. *Oncogene*2010; **29**: 6323–6330. | Article | PubMed | ISI | CAS |
5. Paulson V, Chandler G, Rakheja D, Galindo RL, Wilson K, Amatruda JF *et al*. High-resolution array CGH identifies common mechanisms that drive embryonal rhabdomyosarcoma pathogenesis. *Genes Chromosomes Cancer*2011; **50**: 397–408. | Article | PubMed | CAS |
6. Pressey JG, Anderson JR, Crossman DK, Lynch JC, Barr FG. Hedgehog pathway activity in pediatric embryonal rhabdomyosarcoma and undifferentiated sarcoma: a report

from the Children's Oncology Group. *Pediatr Blood Cancer* 2011; **57**: 930–938. | Article | PubMed |
7. Belyea B, Kephart JG, Blum J, Kirsch DG, Linardic CM. Embryonic signaling pathways and rhabdomyosarcoma: contributions to cancer development and opportunities for therapeutic targeting. *Sarcoma* 2012; **2012**: 406239. | Article | PubMed |
8. Hui CC, Angers S. Gli proteins in development and disease. *Annu Rev Cell Dev Biol* 2011; **27**: 513–537. | Article | PubMed | ISI | CAS |
9. Amakye D, Jagani Z, Dorsch M. Unraveling the therapeutic potential of the Hedgehog pathway in cancer. *Nat Med* 2013; **19**: 1410–1422. | Article | PubMed | ISI | CAS |
10. Langenau DM, Keefe MD, Storer NY, Guyon JR, Kutok JL, Le X *et al*. Effects of RAS on the genesis of embryonal rhabdomyosarcoma. *Genes Dev* 2007; **21**: 1382–1395. | Article | PubMed | ISI | CAS |
11. Walter D, Satheesha S, Albrecht P, Bornhauser BC, D'Alessandro V, Oesch SM *et al*. CD133 positive embryonal rhabdomyosarcoma stem-like cell population is enriched in rhabdospheres. *PLoS One* 2011; **6**: e19506. | Article | PubMed |
12. Ignatius MS, Chen E, Elpek NM, Fuller AZ, Tenente IM, Clagg R *et al*. In vivo imaging of tumor-propagating cells, regional tumor heterogeneity, and dynamic cell movements in embryonal rhabdomyosarcoma. *Cancer Cell*2012; **21**: 680–693. | Article | PubMed | ISI | CAS |
13. Stecca B, Ruiz i Altaba A. A GLI1-p53 inhibitory loop controls neural stem cell and tumour cell numbers. *EMBO J* 2009; **28**: 663–676. | Article | PubMed | ISI | CAS |
14. Mao J, Ligon KL, Rakhlin EY, Thayer SP, Bronson RT, Rowitch D *et al*. A novel somatic mouse model to survey tumorigenic potential applied to the Hedgehog pathway. *Cancer Res* 2006; **66**: 10171–10178. | Article | PubMed | ISI | CAS |
15. Ehnman M, Missiaglia E, Folestad E, Selfe J, Strell C, Thway K *et al*. Distinct effects of ligand-induced PDGFRalpha and PDGFRbeta signaling in the human rhabdomyosarcoma tumor cell and stroma cell compartments. *Cancer Res*2013; **73**: 2139–2149. | Article | PubMed | CAS |
16. Vidal SJ, Rodriguez-Bravo V, Galsky M, Cordon-Cardo C, Domingo-Domenech J. Targeting cancer stem cells to suppress acquired chemotherapy resistance. *Oncogene* 2014; **33**: 4451–4463. | Article | PubMed |
17. Voronova A, Coyne E, Al Madhoun A, Fair JV, Bosiljcic N, St-Louis C *et al*. Hedgehog signaling regulates MyoD expression and activity. *J Biol Chem*2013; **288**: 4389–4404. | Article | PubMed |
18. Theunissen TW, Silva JC. Switching on pluripotency: a perspective on the biological requirement of Nanog. *Philos Trans R Soc Lond B Biol Sci* 2011; **366**: 2222–2229. | Article | PubMed |
19. Wang ML, Chiou SH, Wu CW. Targeting cancer stem cells: emerging role of Nanog transcription factor. *Onco Targets Ther* 2013; **6**: 1207–1220. | PubMed |
20. Po A, Ferretti E, Miele E, De Smaele E, Paganelli A, Canettieri G *et al*. Hedgehog controls neural stem cells through p53-independent regulation of Nanog. *EMBO J* 2010; **29**: 2646–2658. | Article | PubMed | ISI | CAS |
21. Zbinden M, Duquet A, Lorente-Trigos A, Ngwabyt SN, Borges I, Ruiz i Altaba A. NANOG regulates glioma stem cells and is essential in vivo acting in a cross-functional network with GLI1 and p53. *EMBO J* 2010; **29**: 2659–2674. | Article | PubMed | ISI | CAS |
22. Wachtel M, Runge T, Leuschner I, Stegmaier S, Koscielniak E, Treuner J *et al*. Subtype and prognostic classification of rhabdomyosarcoma by immunohistochemistry. *J Clin Oncol* 2006; **24**: 816–822. | Article | PubMed | ISI | CAS |
23. Merchant AA, Matsui W. Targeting Hedgehog—a cancer stem cell pathway. *Clin Cancer Res* 2010; **16**: 3130–3140. | Article | PubMed | ISI | CAS |
24. Vermeulen L, de Sousa e Melo F, Richel DJ, Medema JP. The developing cancer stem-cell model: clinical challenges and opportunities. *Lancet Oncol*2012; **13**: e83–e89. | Article | PubMed |
25. Satheesha S, Schäfer BW. Cancer stem cells in pediatric sarcomas. In: Hayat MA (ed). *Stem Cells and Cancer Stem Cells: Therapeutic Applications in Disease and Injury* **vol. 11**. Springer:, Dordrecht, 2014, pp 111–126.

26. Brack AS, Conboy IM, Conboy MJ, Shen J, Rando TA. A temporal switch from notch to Wnt signaling in muscle stem cells is necessary for normal adult myogenesis. *Cell Stem Cell* 2008; **2**: 50–59. | Article | PubMed | ISI | CAS |
27. Kuang S, Gillespie MA, Rudnicki MA. Niche regulation of muscle satellite cell self-renewal and differentiation. *Cell Stem Cell* 2008; **2**: 22–31. | Article | PubMed | ISI | CAS |
28. von Maltzahn J, Chang NC, Bentzinger CF, Rudnicki MA. Wnt signaling in myogenesis. *Trends Cell Biol* 2012; **22**: 602–609. | Article | PubMed | ISI | CAS |
29. Raimondi L, Ciarapica R, De Salvo M, Verginelli F, Gueguen M, Martini C *et al*. Inhibition of Notch3 signalling induces rhabdomyosarcoma cell differentiation promoting p38 phosphorylation and p21(Cip1) expression and hampers tumour cell growth in vitro and in vivo. *Cell Death Differ* 2012; **19**: 871–881. | Article | PubMed |
30. Annavarapu SR, Cialfi S, Dominici C, Kokai GK, Uccini S, Ceccarelli S *et al*. Characterization of Wnt/beta-catenin signaling in rhabdomyosarcoma. *Lab Invest* 2013; **93**: 1090–1099. | Article | PubMed |
31. Chen EY, Deran MT, Ignatius MS, Grandinetti KB, Clagg R, McCarthy KM *et al*. Glycogen synthase kinase 3 inhibitors induce the canonical WNT/beta-catenin pathway to suppress growth and self-renewal in embryonal rhabdomyosarcoma. *Proc Natl Acad Sci USA* 2014; **111**: 5349–5354. | Article | PubMed | CAS |
32. Hirotsu M, Setoguchi T, Matsunoshita Y, Sasaki H, Nagao H, Gao H *et al*. Tumour formation by single fibroblast growth factor receptor 3-positive rhabdomyosarcoma-initiating cells. *Br J Cancer* 2009; **101**: 2030–2037. | Article | PubMed |
33. Gage PJ, Rhoades W, Prucka SK, Hjalt T. Fate maps of neural crest and mesoderm in the mammalian eye. *Invest Ophthalmol Vis Sci* 2005; **46**: 4200–4208. | Article | PubMed | ISI |
34. Buckingham M, Relaix F. The role of Pax genes in the development of tissues and organs: Pax3 and Pax7 regulate muscle progenitor cell functions. *Annu Rev Cell Dev Biol* 2007; **23**: 645–673. | Article | PubMed | ISI | CAS |
35. Liu P, Johnson RL. Lmx1b is required for murine trabecular meshwork formation and for maintenance of corneal transparency. *Dev Dyn* 2010; **239**: 2161–2171. | Article | PubMed |
36. Nitzki F, Zibat A, Frommhold A, Schneider A, Schulz-Schaeffer W, Braun T *et al*. Uncommitted precursor cells might contribute to increased incidence of embryonal rhabdomyosarcoma in heterozygous Patched1-mutant mice. *Oncogene* 2011; **30**: 4428–4436. | Article | PubMed |
37. Rajurkar M, Huang H, Cotton JL, Brooks JK, Sicklick J, McMahon AP *et al*. Distinct cellular origin and genetic requirement of Hedgehog-Gli in postnatal rhabdomyosarcoma genesis. *Oncogene* 2014; **33**: 5370–5378. | Article | PubMed | CAS |
38. Pressey JG, Haas MC, Pressey CS, Kelly VM, Parker JN, Gillespie GY *et al*. CD133 marks a myogenically primitive subpopulation in rhabdomyosarcoma cell lines that are relatively chemoresistant but sensitive to mutant HSV. *Pediatr Blood Cancer* 2013; **60**: 45–52. | Article | PubMed |
39. Stecca B, Mas C, Clement V, Zbinden M, Correa R, Piguet V *et al*. Melanomas require HEDGEHOG-GLI signaling regulated by interactions between GLI1 and the RAS-MEK/AKT pathways. *Proc Natl Acad Sci USA* 2007; **104**: 5895–5900. | Article | PubMed | CAS |
40. Franken NA, Rodermond HM, Stap J, Haveman J, van Bree C. Clonogenic assay of cells in vitro. *Nat Protoc* 2006; **1**: 2315–2319. | Article | PubMed | ISI | CAS |

Figure legends

Figure 1

Activation of hedgehog signaling increases self-renewal and tumorigenicity of ERMS cells. (a) Left panel: Expression levels of hedgehog signaling components in RD spheres (n=6; N=2) compared with adherent monolayer cultures (n=9; N=3) by quantitative PCR (Log10 scale). Right panel: Western Blot anaysis showing expression of indicated proteins in RD adherent and sphere cells. (b) GLI1 RNA expression levels (relative to HMBS) in patient-derived samples when grown as xenografts ('in vivo'; n=6, N=2) or dissociated and cultured as adherent cells ('in vitro'; n=6, N=2) determined by qPCR. (c) Sphere-initiation capacity of ERMS cells treated with hedgehog agonist SAG1.3 (500 nM) every 48 h (three rounds) during primary sphere formation and thereafter plated for secondary sphere formation in normal sphere media (n =9; N=3). (d) Sphere formation after siRNA-mediated knockdown of SUFU (10 nM) in RD adherent cells compared with scrambled control siRNA (N=2). (e) Sphere formation following 48 h treatment of ERMS adherent cultures with SAG1.3 (n=5; N =5). (f) Western blot analysis of indicated proteins in ERMS stable cell lines. Primary (1°) and secondary (2°) sphere formation measured in ERMS stable lines (g: RD; N=3 and h: RH36; N =3). (i) Tumor growth rate of RD-based stable lines pCMV-Empty (n=6/6) and pCMV-GLI1 (n=5/5) injected orthotopically in NOD/SCID mice. (j) Tumor growth rate of RH36-based stable lines pCMV-Empty (n=2/6) and pCMV-GLI1 (n=4/6) injected orthotopically in NOD/SCID mice. Error bars in i and j represent s.e.m. Each data point in the scatter plots represents a technical replicate with the line drawn at the mean. In bar graphs, data represent mean ±s.d. *Po0.05; **Po0.01; ***Po0.001; ****Po0.0001. FL, full-length.

Figure 2

Inhibition of hedgehog signaling decreases self-renewal and tumorigenicity of ERMS cells. (a) Sphere-initiation capacity of RD cells treated with small-molecule inhibitors GDC-0449 or GANT61 every 48 h (three rounds) during primary sphere formation and further plated for secondary sphere formation in normal sphere media (n=9; N= 3). § No viable cells were recovered for secondary sphere formation. (b) Sphere formation measured following siRNA (10 nM) mediated GLI1 knockdown in RD adherent cells (n=6; N=2). (c) Sphere-formation ability of RD adherent cells after 48 h treatment with hedgehog inhibitors (n=12, N =6 for GDC-0449 and GANT61; n=6, N=2 for LDE-225). Tumor growth rate (d) and tumor weight (e) of RD cells pre-treated in vitro with GANT61 (3μM) (n=5 per condition). Western blot analysis of indicated proteins in stable ERMS lines overexpressing tagged SUFU (f; Myc-DDK) and knockdown of SMO (g). Primary (1°) and secondary (2°) sphere formation measured in ERMS stable lines (h: N =2 per cell line; i: N=2-4 per cell line except 2° sphere formation). Tumor growth kinetics of hedgehog inhibited pCMV-SUFU (j: RD; n=3/5 and k: RH36; n=3/6) and control pCMV-Empty (j:

RD, n=5/5 and k: RH36, n=2/6) cells in NOD/ SCID mice. Tumor growth kinetics of hedgehog inhibited shSMO (l: RD, n=3/7 and m: RH36, n=6/7) and control pLKO.1 (l: RD, n=7/7 and m: RH36, n=7/7) cells in NOD/SCID mice. Error bars in d, e, j–m represent s.e.m. In bar graphs, data represent mean±s.d. *Po0.05; **Po0.01; ***Po0.001.

Figure 3

Hedgehog signaling alters the differentiation status and motility of ERMS cells. (a) Representative images of RD cells stained for PAX7 and MYOGENIN expression. All images were taken at × 400 magnification. Scale bar represents 20 μm. (b and d) Quantification of percentage of PAX7- or MYOGENIN-positive RD cells normalized to DAPI-stained nuclei counted per viewing field, using ImageJ (n=4). (c and e) Quantification of PAX7- or MYOGENIN-positive RH36 cells (n=5). (f and g) Total number of RD cells that could invade through matrigel-coated porous membrane filter towards a growth serum gradient over 48 h (n =3; N=3). (h and i) Relative migration of RD cells across porous membrane filter towards a growth serum gradient over 48 h (n=15; N=3). (j) Non-supervised hierarchical clustering of genes positively and negatively regulated by the hedgehog pathway common to both RD and RH36 cell lines. Each column represents the average RNA expression fold change for the labelled genes within the hedgehog-modulated stable cell line made relative to its respective empty vector control (n=2; N=2). *Po0.05, **Po0.01, ***Po0.001. Data represent mean±s.d.

Figure 4

Nanog is a functionally important target gene of hedgehog pathway in ERMS. (a) Representative images of RD cells co-stained for GLI1 and NANOG expression. All images were taken at × 400 magnification. Scale bar represents 20 μm. Quantification, using ImageJ, of NANOG-expressing cellular compartments normalized to DAPI-stained nuclei per viewing field in ERMS stable lines (b; N=2) and RD cells treated with SAG1.3 (500 nM) for 48 h (c; N=2). (d) Sphere formation in RD cells with stable knockdown of NANOG (shNANOG; N=3). (e) Sphere formation measured following siRNA (10 nM) mediated NANOG knockdown in RD adherent cells (N=2). (f and g) Primary sphere formation upon transient overexpression of NANOG in RD cells (n=12; N =2). Data represent mean±s.d. Secondary sphere formation in RD (h) and RH36 (i) rescue systems (N =3). (j) Tumor growth rate of RH36 cells in NOD/SCID mice (n=6/6 per cell line). Error bars represent s.e.m. *Po0.05, **Po0.01, ***Po0.001. ns, not significant.

Supplemental Figures

Supplemental Figure 1.

Analysis of ERMS spheres, xenografts and effect of transient activation of hedgehog pathway. mRNA expression of multiple hedgehog signaling components in RH36 (**a**; n=9; N=3 per cell type), TTC442 (**b**; n=6; N=2 per cell type) and fusion-negative RH18 (**c**; n=6; N=2 per cell type) spheres compared to adherent monolayer cultures by qPCR. (**d**) GLI1 mRNA expression levels (relative to HMBS) in indicated cell lines when grown as xenografts ("*in vivo*"; n=6, N=2) or cultured as adherent cells ("*in vitro*"; n=9, N=3) determined by qPCR. PTCH1 (**e**) and HHIP (**f**) mRNA expression levels relative to HMBS in indicated ERMS sample determined by qPCR (for PDX: n=6, N=2 per condition; for cell lines: n=6, N=2 for "*in vivo*" and n=9; N=3 for "*in vitro*"). (**g**) Western blotting for indicated proteins upon siRNA mediated knockdown of SUFU in RD adherent cells. (**h**) Sphere formation measured following siRNA (10nM) mediated SUFU knockdown in RH36 adherent cells (N=2). (**i**) SUFU protein expression in RH36 adherent cells after siRNA-mediated knockdown. Flow cytometry-based cell cycle profile estimation from Propidium Iodide staining of RD (**j**) and RH36 (**k**) cells treated with SAG1.3 for 48 hours (n=2; N=2 per cell line per condition). (**l**) Viability of ERMS cells, evaluated by WST assay, after 48 hours treatment with SAG1.3 (n=12; N=4). **P*<0.05, ***P*<0.01, ****P*<0.001, *****P*<0.0001. Data represent mean ± S.D. PDX – Patient-derived xenografts

Supplemental Figure 2.

Single cell cloning and effect of GLI1 over-expression on ERMS cells. (**a**) Representative images of bulk RD cells and three clonal cultures established from single cells immunostained for GLI1 expression. All images were taken at 200x magnification. Scale bar represents 50µm. (**b**) Western Blotting to assess overall GLI1 protein expression level in single cell clones compared to bulk RD cells. (**c**) Sphere forming ability of single cell clones relative to bulk cell line (N=2). The expression of target genes upon stable over-expression of GLI1 (pCMV-GLI1) in RD (**d**; n=10, N=5) and RH36 (**e**; n=12, N=4) compared to control cells (pCMV-Empty; set at baseline). Log_{10} scale. (**f**) Right panel: Colony forming ability of RD cells stably over-expressing GLI1 relative to empty vector transfected cells (N=4). Left panel: Representative images of the colonies stained with Crystal Violet in one well of a standard 6-well plate. (**g**) Western blotting for indicated proteins using lysates of xenografts from stable cell lines. **P*<0.05, ***P*<0.01, ****P*<0.001, *****P*<0.0001. Data represent mean ± S.D. ns - not significant

Supplemental Figure 3.

Immunohistochemical analysis of ERMS xenografts. Representative images of immunohistochemistry performed on formalin-fixed paraffin-embedded (FFPE) sections of

ERMS xenografts grown in NOD/SCID mice. The images for H&E (Hematoxylin and Eosin), Myogenin and Desmin images were taken at 200x magnification. Scale bar represents 50μm. The images for GLI1 staining were taken at 400x magnification. Scale bar represents 20μm. The presence of a few rhabdomyoblasts was noted within the xenografts. The xenografts had low differentiation with no visible strap cells. GLI1 staining was found to be heterogeneous within xenografts and the over-expression was more readily detected in case of RD. The RH36 pCMV-GLI1 xenograft contained more number of strongly positive GLI1 cells and in general the tumor appeared to be composed of more primitive looking cells.

Supplemental Figure 4.

Effect of hedgehog inhibition by synthetic small molecules on ERMS cells. (**a**) Sphere initiation for RH36 cells treated with small-molecule inhibitors GDC-0449 or GANT61 every 48h (3 rounds) during primary sphere formation and further plated for secondary sphere formation in normal media (n=6, N=2). # No spheres formed. **§** No viable cells were recovered for secondary sphere formation. (**b**) GLI1 protein expression is decreased upon siRNA-mediated knockdown in RD adherent cells. (**c**) Left panel: Sphere formation measured following siRNA (10nM) mediated GLI1 knockdown in RH36 adherent cells (N=2). Right panel: GLI1 protein reduction upon siRNA-mediated knockdown in RH36 adherent cells. (**d**) Sphere initiation of RH36 adherent cells pre-treated with hedgehog inhibitors (48 hours) (n=9, N=3 for GDC-0449 and GANT61; n=6, N=2 for LDE-225). Cell cycle profiles generated by flow cytometry-based measurement of Propidium Iodide staining of RD (**e**) and RH36 (**f**) cells treated with hedgehog inhibitors for 48 hours (n=2, N=2 per cell line per condition). Viability evaluated by WST assay, of RD (**g**) and RH36 (**h**) cells after 48 hours treatment with hedgehog inhibitor (n=12, N=4 for GDC-0449 and GANT61; n=6, N=2 for LDE-225). (**i**) Western blotting for GLI1 in RD adherent cells treated with 3μM GANT61 (48h). (**j**) Representative whole mounts of xenograft tumors formed by injecting RD cells either pre-treated with vehicle or GANT61 (3μM) for 48 hours *in vitro*. (**k**) Representative images of immunohistochemistry performed on FFPE sections of xenograft tumors formed by injecting RD cells either pre-treated with vehicle or GANT61 (3μM). The xenografts from GANT61 pre-treatment have fewer GLI1 strongly positive cells and lower desmin positivity. The images for H&E, Myogenin, Desmin and MIB1 were taken at 200x magnification. Scale bar represents 50μm. The images for GLI1 staining were taken at 400x magnification. Scale bar represents 20μm. **P*<0.05, ***P*<0.01, ****P*<0.001. Data represent mean ± S.D.

Supplemental Figure 5.

Effect of stable genetic hedgehog inhibition on ERMS cells. mRNA expression of hedgehog target genes in RD (**a**; n=6, N=2) and RH36 (**b**; n=3, N=1) cells over-expressing SUFU (pCMV-

SUFU) relative to empty vector control (pCMV-Empty), assessed by qPCR. mRNA expression of hedgehog target genes in RD (**c**; n=9, N=3) and RH36 (**d**; n=9, N=3) cells with stable knockdown of SMO (shSMO) relative to emtpy vector control (pLKO.1), assessed by qPCR. (**e**) Western blotting for indicated proteins in control and stable SMO knockdown ERMS cell lines (**f**) Right panel: Colony forming ability of pCMV-SUFU RD cells relative to pCMV-Empty cells (N=2). Left panel: Representative images of the Crystal Violet stained colonies in one well of a standard 6-well plate. (**g**) Right panel: Colony forming ability of shSMO RD cells relative to pLKO.1 cells (N=2). Left panel: Representative images of the Crystal Violet stained colonies formed in one well of a standard 6-well plate. (**h** and **i**) Cell proliferation measured by BrdU incorporation in RD cells (n=6, N=2). (**j**) Histogram plots of cell cycle profiles generated from Propidium Iodide (PI) staining of RD stable lines by flow cytometry. (**k** and **l**) Quantification of cell cycle stage distributions observed in RD cell lines with different hedgehog pathway status (n=2, N=2 per cell line). (**m** and **n**) Quantification of cell cycle stage distributions observed in RH36 cell lines with different hedgehog pathway status (n=2, N=2 per condition). **P*<0.05, ****P*<0.001. Data represent mean ± S.D. ns – not significant.

Supplemental Figure 6.

Cell autonomous ligand-based hedgehog pathway activation in ERMS. Relative mRNA expression level of hedgehog ligands in ERMS sphere cells (**a**: RH36; n=9, N=3 and **b**: RD; n=6, N=2) compared to adherent cells (**a**: RH36; n=9, N=3 and **b**: RD; n=9, N=3). Absolute RNA expression level of hedgehog ligands in ERMS xenografts (**c**: RH36; **d**: RD; n=12, N=4 per cell line) and their respective *in vitro* cultured cells (n=9, N=3 per cell line) normalized to housekeeping gene *HMBS*. (**e** and **f**) Absolute RNA expression level of hedgehog ligands in ERMS PDX samples when grown as tumors (“in vivo”) and when taken into culture as adherent cells (“in vitro”) normalized to HMBS (n=6; N=2 per condition per PDX sample). (**g**, **h** and **i**) QPCR for indicated hedgehog ligands performed on nine ERMS patient tumor samples. Data normalized to geometric mean of *HMBS* and *GAPDH*. (**j**) Scatter plot depicting data from panels **g**, **h** and **i** (excluding patient TB271). Each data point represents a single patient and the line represents median expression level in the cohort. Species-specific ligand RNA expression estimated in ERMS cell line-derived xenografts (**k**: RD; n=12, N=4 per condition and **l**: RH36; n=48, N=16 for human-specific probes; n=30, N=10 for mouse-specific probes). Expression of *Dhh* is higher within ERMS tumors (**m**: RD; n=12, N=4 and **n**: RH36; n=30, N=10) compared to normal murine skeletal muscle (n=6; N=2). Expression levels are normalized to *Gapdh*. **P*<0.05. *P*-value for **k** and **l** from Mann-Whitney test. Data represent mean ± S.D. FeSkM_P - Pool of Fetal Skeletal Muscle RNA (3 donors); AdSkM_P - Pool of Adult Skeletal Muscle RNA (5 donors); h - human; m – mouse; N.E. – Not Expressed, ns – not significant.

Supplemental Figure 7.

Effect of hedgehog pathway modulation on ERMS chemoresistance and differentiation. (**a**) Sphere initiation ability of RD cells treated for 48 hours with SN-38 (active metabolite of Irinotecan). Post-treatment equal number of viable cells were counted and plated at clonal density (n=9, N=3). (**b**) Sphere initiation ability of RD cells treated for 48 hours with SN-38 alone or in combination with SMO inhibitor LDE-225 (n=8, N=2). (**c** and **e**) Representative images of RH36 cells stained for PAX7 and MYOGENIN expression. (**d**) Representative images of RD cells stained for PAX7 and MYOGENIN expression. All images were taken at 400x magnification. Scale bar represents 20μm. Intra-cellular flow cytomtery for PAX7 or MYOGENIN positivity performed on RH36 cells treated for 48 hours with indicated concentrations of hedgehog inhibitors GDC-0449 (**f**), GANT61 (**g**) or agonist SAG1.3 (**h**) (n=2, N=2 per condition). (**i**) Percentage of PAX7- or MYOGENIN-positive RD cells treated for 48hrs with 3μM GANT61, normalized to DAPI stained nuclei counted per viewing field using ImageJ and made relative to vehicle treated cells (n=7). (**j**) The mRNA expression of indicated genes in RD cells after 6 days of treatment with GANT61, normalized to HMBS and made relative to expression in vehicle treated cells. The drug was replaced after 72 hours (n=3). **P*<0.05, ***P*<0.01, ****P*<0.001. Data represent mean ± S.D.

Supplemental Figure 8.

Effect of hedgehog pathway modulation on ERMS cell motility. Representative images of RD cells stained with Crystal Violet post-invasion (**a**) and post-migration (**b**) in trans-well assay. All images were taken at 200x magnification. Scale bar represent 50μm.

Supplemental Figure 9.

Confirmation of qPCR screen hit. NANOG RNA expression analysis using Taqman-based qPCR in pCMV-GLI1 (**a**: n=12, N=4), shSMO (**b**: n=9, N=3) and pCMV-SUFU (**c**: n=6, N=2) ERMS cells relative to their respective control cell lines. (**d**) Western blotting for NANOG protein expression (arrow) in control and SUFU-overexpressing ERMS cells. (**e**) Representative images of RH36 stable cells co-immunostained for GLI1 and NANOG expression. (**f**) Representative images of primary cells from ERMS PDX samples co-immunostained for GLI1 and NANOG expression. All images (**e** and **f**) were taken at 400x magnification. Scale bar represents 20μm. **P*<0.05. Data represent mean ± S.D.

Supplemental Figure 10.

Modulation of NANOG expression by hedgehog pathway activation. (**a**) NANOG expressing RH36 cells counted after 48hrs treatment with SAG1.3 (n=3). Representative images for RD (**b**) and RH36 (**c**) cells treated with SAG1.3 and stained for NANOG. All images were taken at 400x magnification. Scale bar represents 20μm. (**d**) NANOG RNA expression, normalized to HMBS, in RD xenografts (n=6, N=2) and adherent cultures (n=9, N=3). (**e**) NANOG expression in RH36 xenografts and adherent cells. Left panel: NANOG RNA expression normalized to HMBS in xenografts (n=6, N=2) and adherent cells (n=9, N=3). Right panel: Western blot showing expression of indicated proteins. (**f**) NANOG RNA expression in ERMS sphere cells relative to adherent cultures (n=6, N=2). (**g**) NANOG protein expression level (arrow) in ERMS adherent and sphere cells. **P*<0.05, ***P*<0.01. Data represent mean ± S.D.

Supplemental Figure 11.

Characterization of phenotype rescue cell lines and additional clinical data analysis. (**a**) Left panel: RNA expression analysis of indicated genes in RD cells with stable NANOG knockdown (shNANOG) relative to control (pLKO.1) (n=6, N=2). Right panel: Western Blot analysis of indicated proteins. (**b**) Left panel: RNA analysis of indicated genes upon siRNA-mediated NANOG knockdown (10nM; 48 hours) in RD adherent cells (n=6; N=2). Right panel: Western Blot analysis of indicated proteins upon siRNA-mediated NANOG knockdown in RD adherent cells. ***P*<0.01, ****P*<0.001 from Student's t-test. (**c**) Western Blot analysis of RD cells for indicated proteins upon transient overexpression of NANOG. Expression analysis to verify the stable cell lines generated from RD (**d**) and RH36 (**e**) cells with knockdown of NANOG in the presence of GLI1 over-expression (n=6; N=2). Data represent mean ± S.D. (**f**) Representative images of immunohistochemistry performed on FFPE sections of RH36 stable line xenografts grown in NOD/SCID mice. The images were taken at 200x magnification. Scale bar represents 50μm. (**g**) Western blot analysis of indicated proteins in RH36 xenografts. (**h**) Representative images of immunohistochemistry staining for GLI1 and NANOG within an ERMS patient tumor core. All images were taken at 400x magnification. Scale bar represents 20μm. Kaplan-Meier curve for event-free survival of 91 ERMS patients determined to be either negative (black line) or positive (grey line) for expression of GLI1 (**i**) or NANOG (**j**) alone. The *P*-values were generated using log-rank test.

Figure 1

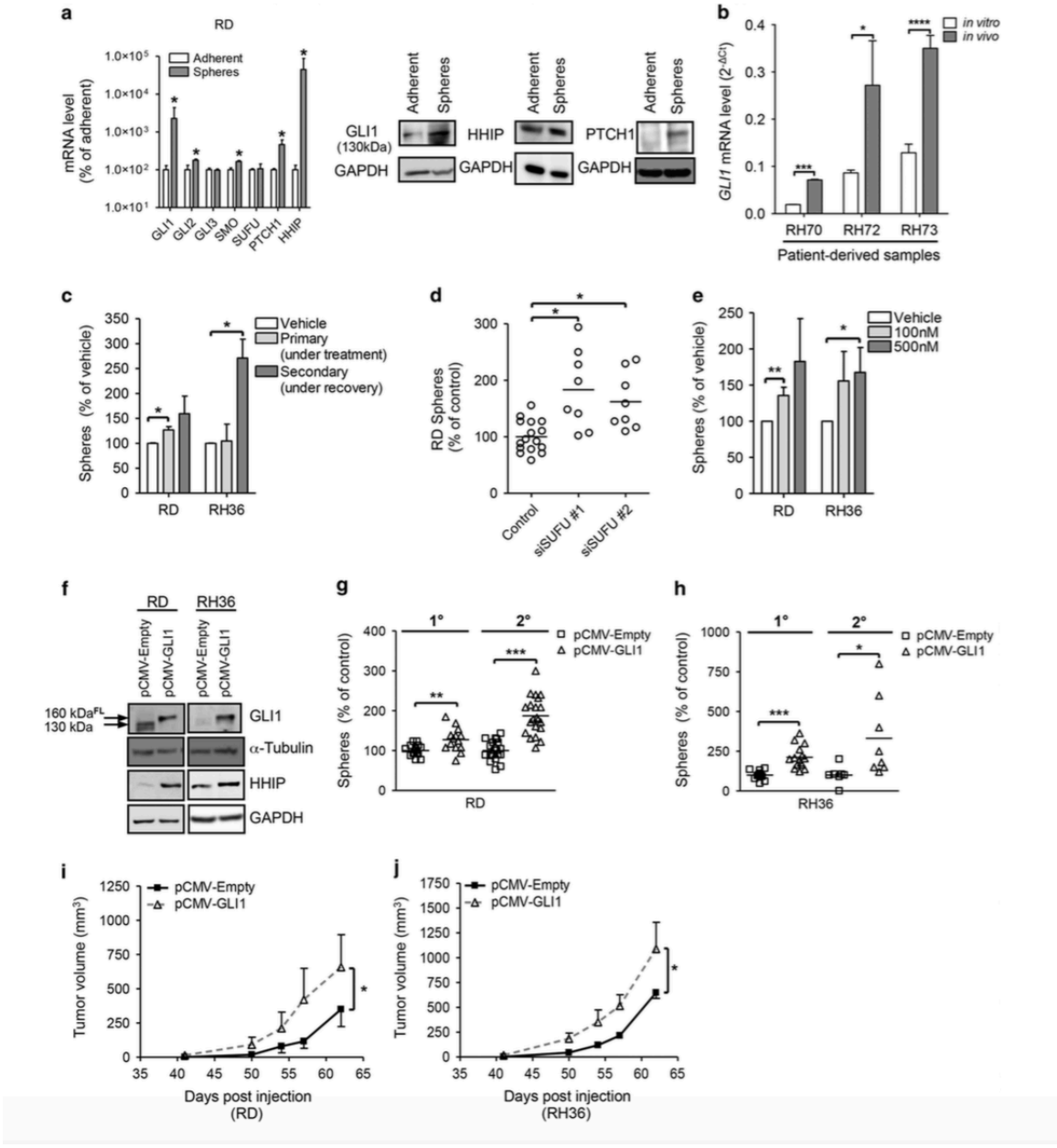
a
RD
Adherent
Spheres
mRNA level (% of adherent)
GLI1
GLI2
GLI3
SMO
SUFU
PTCH1
HHIP
GLI1 (130kDa)
GAPDH
b
in vitro
in vivo
GLI1 mRNA level (2-ΔCt)
RH70
RH72
RH73
Patient-derived samples
c
Vehicle
Primary (under treatment)
Secondary (under recovery)
Spheres (% of vehicle)
RD
RH36
d
RD Spheres (% of control)
Control
siSUFU #1
siSUFU #2
e
Vehicle
100nM
500nM
Spheres (% of vehicle)
f
RD
RH36
pCMV-Empty
pCMV-GLI1
160 kDaFL
130 kDa
GLI1
α-Tubulin
HHIP
GAPDH
g
1°
2°
pCMV-Empty
pCMV-GLI1
Spheres (% of control)
RD
h
RH36
i
Tumor volume (mm3)
Days post injection (RD)
j
Days post injection (RH36)

Figure 2

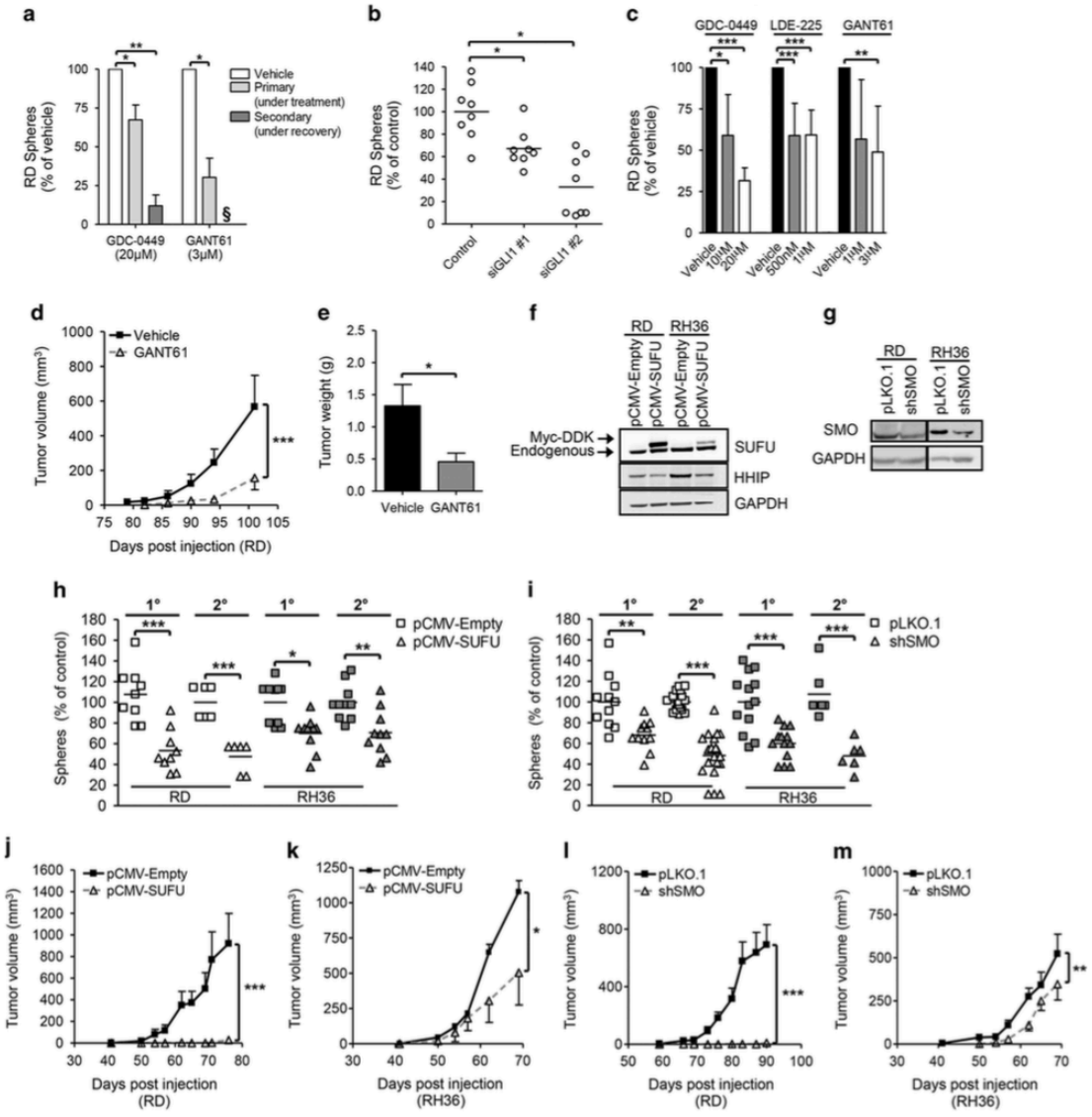
a
RD Spheres (% of vehicle)
Vehicle
Primary (under treatment)
Secondary (under recovery)
GDC-0449 (20μM)
GANT61 (3μM)
b
RD Spheres (% of control)
Control
siGLI1 #1
siGLI1 #2
c
GDC-0449
LDE-225
GANT61
RD Spheres (% of vehicle)
Vehicle
10nM
20nM
500nM
1nM
1nM
3nM
d
Tumor volume (mm³)
Vehicle
GANT61
Days post injection (RD)
e
Tumor weight (g)
Vehicle
GANT61
f
RD
RH36
pCMV-Empty
pCMV-SUFU
Myc-DDK
Endogenous
SUFU
HHIP
GAPDH
g
RD
RH36
pLKO.1
shSMO
SMO
GAPDH
h
Spheres (% of control)
1°
2°
pCMV-Empty
pCMV-SUFU
RD
RH36
i
Spheres (% of control)
pLKO.1
shSMO
RD
RH36
j
Tumor volume (mm³)
pCMV-Empty
pCMV-SUFU
Days post injection (RD)
k
Tumor volume (mm³)
pCMV-Empty
pCMV-SUFU
Days post injection (RH36)
l
Tumor volume (mm³)
pLKO.1
shSMO
Days post injection (RD)
m
Tumor volume (mm³)
pLKO.1
shSMO
Days post injection (RH36)

Table 1. Hedgehog pathway modulation alters chemoresistance of ERMS cells

Cell lines		*Mean absolute IC_{50} at 72 h (nM ± s.d.)*				*Phenotype*	
Parental	*Transgenic*	*Irinotecan (SN-38)*[a]	*Relative change in IC_{50}*[c,d]	*Doxorubicin*[b]	*Relative change in IC_{50}*[c,d]	*Hedgehog pathway activity*	*Relative resistance*
RH36	pCMV-Empty	11 ± 6		157 ± 84		Control	
	pCMV-GLI1	19 ± 15	↑ 73% (ns)	284 ± 205	↑ 81% (ns)	Increased	Increased
RD	pCMV-Empty	54 ± 30		186 ± 124		Control	
	pCMV-GLI1	94 ± 55	↑ 74% (*)	286 ± 249	↑ 54% (ns)	Increased	Increased
	pCMV-SUFU	37 ± 15	↓ 31% (ns)	139 ± 135	↓ 25% (ns)	Decreased	Decreased
RH36	pLKO.1	23 ± 15		221 ± 130		Control	
	shSMO	10 ± 5	↓ 56% (**)	105 ± 28	↓ 52% (*)	Decreased	Decreased
RD	pLKO.1	78 ± 36		198 ± 135		Control	
	shSMO	39 ± 16	↓ 50% (***)	177 ± 121	↓ 10% (ns)	Decreased	Decreased

Abbreviations: ERMS, embryonal rhabdomyosarcoma. [a]$N = 5$ for RD-based cell lines; $N = 4$ for RH36-based cell lines. [b]$N = 4$ for all cell lines . [c]'↑' – IC_{50} increased by; '↓' – IC_{50} decreased by. [d]In parenthesis are presented the statistical significance of the relative difference in the IC_{50} values: ns-not significant; *$P < 0.05$; **$P < 0.01$.

Figure 3

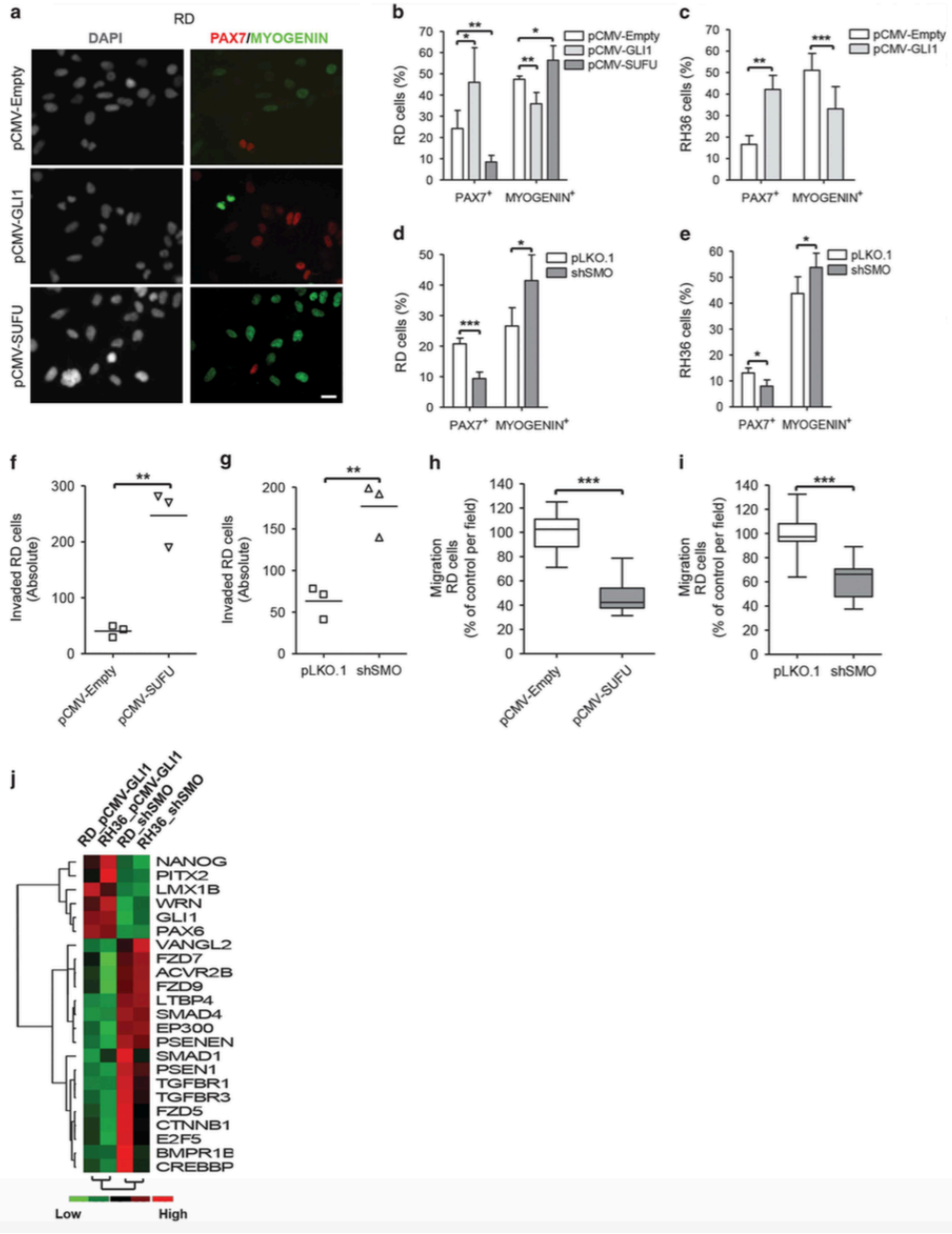
a
RD
DAPI
PAX7/MYOGENIN
pCMV-Empty
pCMV-GLI1
pCMV-SUFU
b
RD cells (%)
pCMV-Empty
pCMV-GLI1
pCMV-SUFU
PAX7+
MYOGENIN+
c
RH36 cells (%)
pCMV-Empty
pCMV-GLI1
PAX7+
MYOGENIN+
d
RD cells (%)
pLKO.1
shSMO
PAX7+
MYOGENIN+
e
RH36 cells (%)
pLKO.1
shSMO
PAX7+
MYOGENIN+
f
Invaded RD cells (Absolute)
pCMV-Empty
pCMV-SUFU
g
Invaded RD cells (Absolute)
pLKO.1
shSMO
h
Migration RD cells (% of control per field)
pCMV-Empty
pCMV-SUFU
i
Migration RD cells (% of control per field)
pLKO.1
shSMO
j
RD_pCMV-GLI1
RH36_pCMV-GLI1
RD_shSMO
RH36_shSMO
NANOG
PITX2
LMX1B
WRN
GLI1
PAX6
VANGL2
FZD7
ACVR2B
FZD9
LTBP4
SMAD4
EP300
PSENEN
SMAD1
PSEN1
TGFBR1
TGFBR3
FZD5
CTNNB1
E2F5
BMPR1B
CREBBP
Low
High

Figure 4

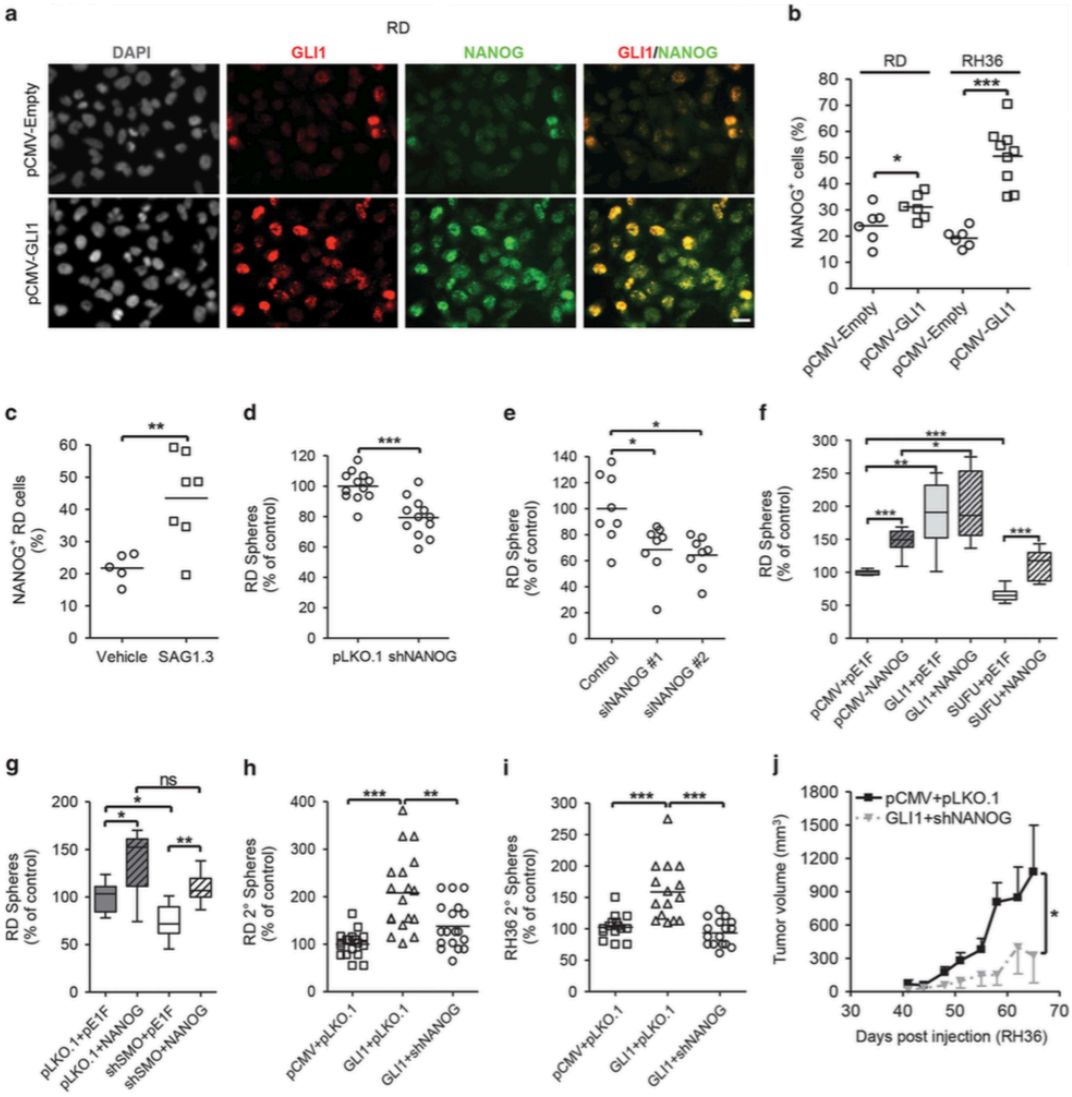
a
RD
DAPI
GLI1
NANOG
GLI1/NANOG
pCMV-Empty
pCMV-GLI1
b
RD
RH36
NANOG+ cells (%)
pCMV-Empty
pCMV-GLI1
pCMV-Empty
pCMV-GLI1
c
NANOG+ RD cells (%)
Vehicle
SAG1.3
d
RD Spheres (% of control)
pLKO.1
shNANOG
e
RD Sphere (% of control)
Control
siNANOG #1
siNANOG #2
f
RD Spheres (% of control)
pCMV+pE1F
pCMV-NANOG
GLI1+pE1F
GLI1+NANOG
SUFU+pE1F
SUFU+NANOG
g
RD Spheres (% of control)
ns
pLKO.1+pE1F
pLKO.1+NANOG
shSMO+pE1F
shSMO+NANOG
h
RD 2° Spheres (% of control)
pCMV+pLKO.1
GLI1+pLKO.1
GLI1+shNANOG
i
RH36 2° Spheres (% of control)
pCMV+pLKO.1
GLI1+pLKO.1
GLI1+shNANOG
j
pCMV+pLKO.1
GLI1+shNANOG
Tumor volume (mm3)
Days post injection (RH36)

Figure 5

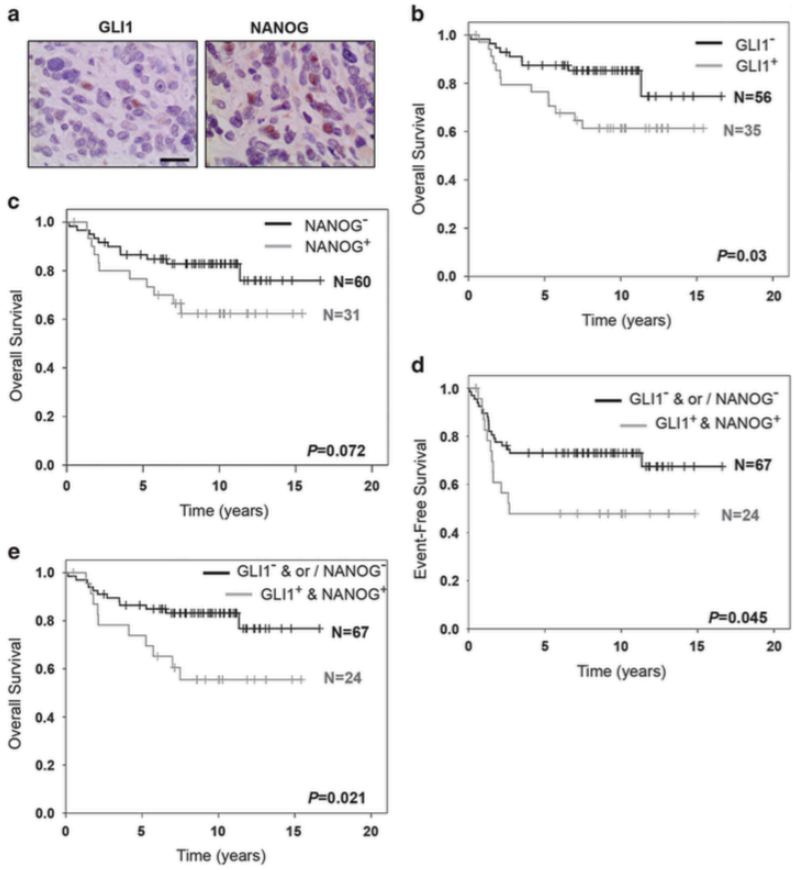
a
GLI1
NANOG
b
GLI1⁻
GLI1⁺
N=56
N=35
P=0.03
Overall Survival
Time (years)
c
NANOG⁻
NANOG⁺
N=60
N=31
P=0.072
Overall Survival
Time (years)
d
GLI1⁻ & or / NANOG⁻
GLI1⁺ & NANOG⁺
N=67
N=24
P=0.045
Event-Free Survival
Time (years)
e
GLI1⁻ & or / NANOG⁻
GLI1⁺ & NANOG⁺
N=67
N=24
P=0.021
Overall Survival
Time (years)

Supplementary materials

Transfection, transduction and generation of stable cell lines

The plasmids pCMV6-Entry (C-terminal Myc and DDK Tagged) referred to as pCMV-Empty, GLI1-transcript variant 1- Myc-DDK (referred to as pCMV-GLI1), SUFU-Myc-DDK tagged (referred to as pCMV-SUFU) were purchased from Origene. The plasmids pEGIP (26777; referred to as pE1F), and pSin-EF-Nanog-Pur (16578; over-expressing NANOG) were purchased from Addgene. All plasmid transfections were carried out using Lipofectamine® 2000 (Invitrogen) following manufacturer's instructions. Transduction of MISSION® TRC1.5 shRNA lentiviral particles (Sigma-Aldrich) - control (pLKO.1; SHC001V), TRCN0000014364 (shSMO) and TRCN0000004885 (shNANOG) - was carried out at MOI 1.5 in 1µg/ml Polybrene (Sigma-Aldrich) supplemented media. For stable cell line generation, plasmid transfected cells were continuously cultured in media supplemented 500 µg/ml G-418 antibiotic for 3-4 weeks and thereafter maintained in 100 µg/ml antibiotic media; viral transduced cells were continuously cultured in media supplemented with 1µg/ml Puromycin (Invivogen) for 10 days and thereafter maintained in 0.3 µg/ml antibiotic media. Stable pCMV-Empty and pCMV-GLI1 cells were transduced with pLKO.1 and shNANOG viral particles and selected with Puromycin as described above to generate stable phenotype rescue system. The effect of the expression of the transgene was regularly checked using qPCR and western blotting through the course of the experiments. Occasionally the stable lines were challenged with higher doses of antibiotics to ensure that the cell lines being propagated carried the transgene constructs.

Trans-well migration and invasion assays

Migration assays were carried out using BD Falcon™ cell culture inserts (BD Biosciences; 8µm pore size) in 24-well format. For invasion assays, BioCoat™ matrigel-coated inserts (BD Biosciences) or inserts coated manually with gelatin were used. Cells were maintained in 1% FBS media for 4hrs prior to plating and allowed to migrate over 24hrs or invade over 48hrs towards 10% FBS medium. The membrane was fixed with 4% paraformaldehyde (PFA; Carl Roth), cells stained with 0.05% Crystal Violet and visualized using Olympus CX41 microscope. Images were captured from 5 viewing fields across the membrane using INFINITY software (version 6, Lumenera). Cells were counted manually using ImageJ software (version 1.47).

Cell cycle analysis

Cells were fixed with ice-cold 70% ethanol and re-suspended in propidium iodide solution (1xPBS, 1% Triton X-100, 100mg/ml RNaseA, 1mg/ml Propidium Iodide solution) just before analysis. For intra-cellular staining, cells were fixed with cold 4% PFA and permeabilized with 0.2% Triton X-100. Antibodies used are indicated in Supplementary Table 2. Flow cytometry

was performed on a BD FACS Canto II instrument (BD Biosciences) using BD FACSDiva software. Data was analyzed with FlowJo software (version 7.6.1, TreeStar Inc.).

Immunohistochemistry

Cells were visualized using Leica 6000 DM epifluorescence microscope and images were captured using OpenLab software (version 3, Improvision). Cells stained only with conjugated-secondary antibodies were used as controls. Cell count estimation and image analysis was performed using ImageJ. Immunohistochemistry was performed on 3 µm thick sections from blocks of formalin-fixed, paraffin-embedded tissue at the Institute of Surgical Pathology (University Hospital Zurich). The procedure for detecting GLI1 and NANOG expression was optimized by Sophistolab AG (Eglisau, Switzerland) using an array containing a series of normal tissue and cancer tissues as controls. In brief, immunohistochemistry was performed according to manufacturer's guidelines on Leica BondMax instruments using Refine HRP-Kits (Leica DS9800) and buffer-solutions from Leica Microsystems Newcastle, Ltd. Slides were visualized using Zeiss Axioskop microscope. Images were captured and analyzed using Cell^{B} software (version 3.4; Olympus Soft Imaging Solutions GmbH).

Supplementary Table 1. List of TaqMan®-probe based gene expression assays used in the study.

Gene	Species	TaqMan® Gene Expression Assay ID
HMBS	Human	Hs00609297_m1
GAPDH	Human	Hs02758991_g1
GLI1	Human	Hs01110766_m1
GLI2	Human	Hs01119974_m1
GLI3	Human	Hs00609233_m1
PTCH1	Human	Hs00181117_m1
HHIP	Human	Hs01011008_m1
SMO	Human	Hs01090242_m1
SUFU	Human	Hs00171981_m1
SHH	Human	Hs00179843_m1
IHH	Human	Hs00745531_s1
DHH	Human	Hs00368306_m1
NANOG	Human	Hs02387400_g1
PDGFRA	Human	Hs00998018_m1
CKM	Human	Hs00176490_m1
MYL1	Human	Hs00984899_m1
Shh	Mouse	Mm00436528_m1
Dhh	Mouse	Mm01310203_m1
Ihh	Mouse	Mm00439613_m1
Gapdh	Mouse	Mm99999915_g1

Supplemental Table 2. Details of antibodies used in the study

Primary antibodies (Anti-human)[A]						
Detected protien (clone)	**Catalogue #**	**Company**	**Species**	**Clonality**	**Application**	**Dilution**
GLI1 (V812)	2534	Cell Signaling Technology	Rabbit	poly	WB	1/1000
HHIP (R-20)	sc-9408	Santa Cruz	Goat	poly	WB	1/100
SUFU (C81H7)	2522	Cell Signaling Technology	Rabbit	mono	WB	1/1000
SMO (N-19)	sc-6366	Santa Cruz	Goat	poly	WB	1/500
NANOG	ab21624	Abcam	Rabbit	poly	WB	1/500
NANOG (D73G4)	4903	Cell Signaling Technology	Rabbit	mono	WB	1/1000
GAPDH (D16H11)	5174	Cell Signaling Technology	Rabbit	mono	WB	1/10000
□-TUBULIN (DM1A)	T9026	Sigma-Aldrich	Mouse	mono	WB	1/40000
PAX7	PAX7	Developemtal Studies Hybridoma Bank	Mouse	mono	IF and IC-FC	1/50
MYOGENIN (M-225)	sc-576	Santa Cruz	Rabbit	poly	IF and IC-FC	1/1000
GLI1 (H-300)	sc-20687	Santa Cruz	Rabbit	poly	IF	1/100
NANOG (hNanog.2)	14-5768-82	eBioscience	Mouse	mono	IF	1/50
MYOGENIN (L026)	PA0226	Novocastra, Leica	Mouse	mono	IHC	1/20
DESMIN (D33)	M076029	Dako	Mouse	mono	IHC	1/20
MIB-1 (30-9)	-	Ventana, Roche	Rabbit	mono	IHC	Prediluted (Ventana, Roche)
GLI1 (H-300)	sc-20687	Santa Cruz	Rabbit	poly	IHC	1/75
NANOG (NNG-811)	ab62734	Abcam	Mouse	mono	IHC	1/2000
Secondary Antibodies[B]						
Detected species	**Catalogue no.**	**Company**	**Species**	**Conjugation**	**Application**	**Dilution**
Anti-Mouse IgG	7076	Cell Signaling Technology	Horse	HRP	WB	1/2000
Anti-Rabbit IgG	7074	Cell Signaling Technology	Goat	HRP	WB	1/2000
Anti-Goat IgG	A50-201P	Bethyl	Donkey	HRP	WB	1/2000
Anti-Mouse IgG	A21202	Life technologies	Donkey	Alexa Fluor-488	IF and IC-FC	1/500
Anti-Rabbit IgG	A21206	Life technologies	Donkey	Alexa Fluor-488	IF and IC-FC	1/500
Anti-Mouse IgG	A21203	Life technologies	Donkey	Alexa Fluor-594	IF	1/500
Anti-Rabbit IgG	A21207	Life technologies	Donkey	Alexa Fluor-594	IF	1/500

[1] Abbreviations: WB – Western Blotting, IF – Immunofluorescence, IC-FC – Intra-cellular Flow Cytometry, IHC – Immunohistochemistry, HRP – Horseradish peroxidise

[2] HRP-conjugated secondary antibodies for IHC were purchased pre-diluted in the reagents associated with the automated systems used for processing (see text).

Supplementary Figure 1

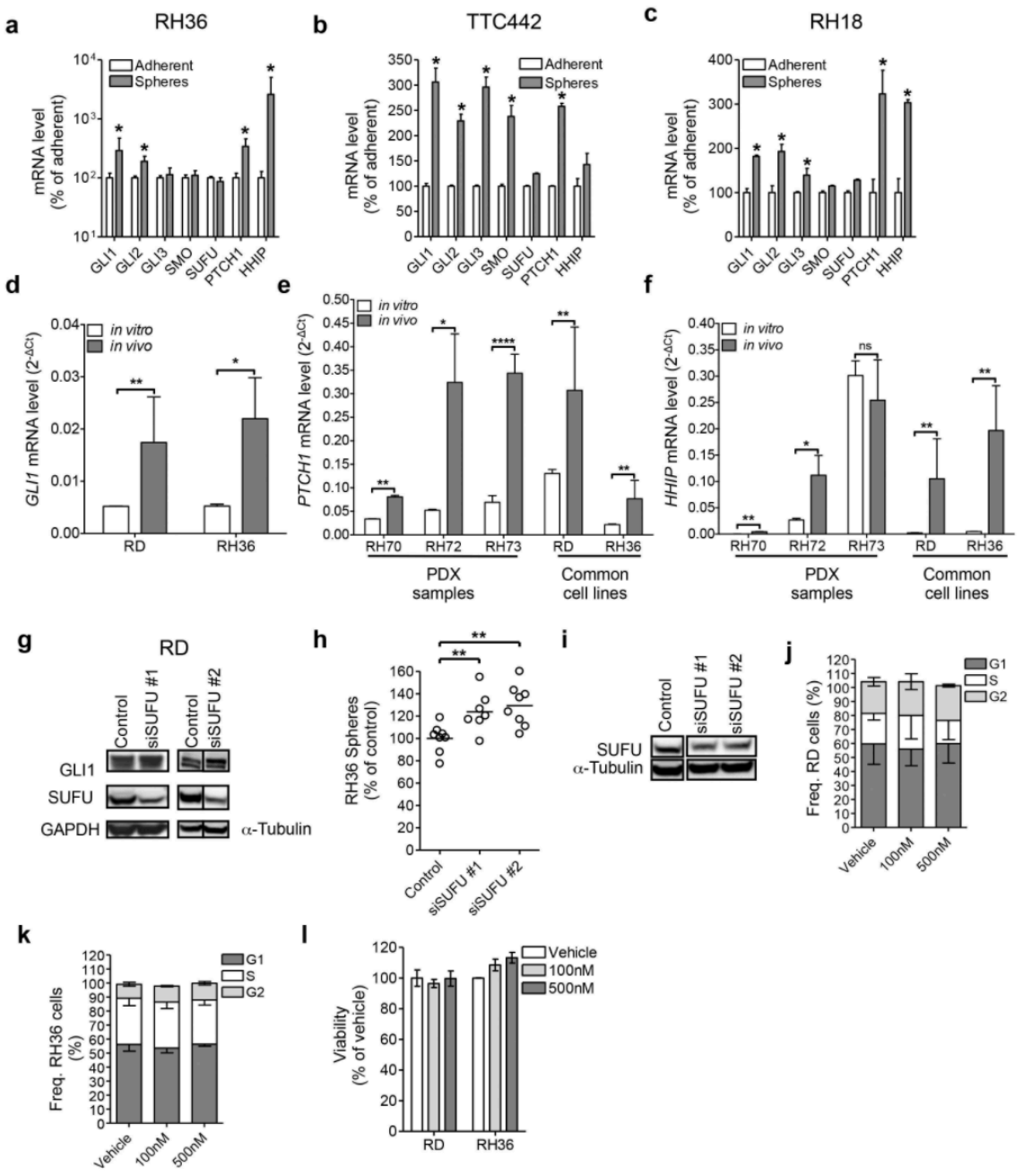

Supplementary Figure 2

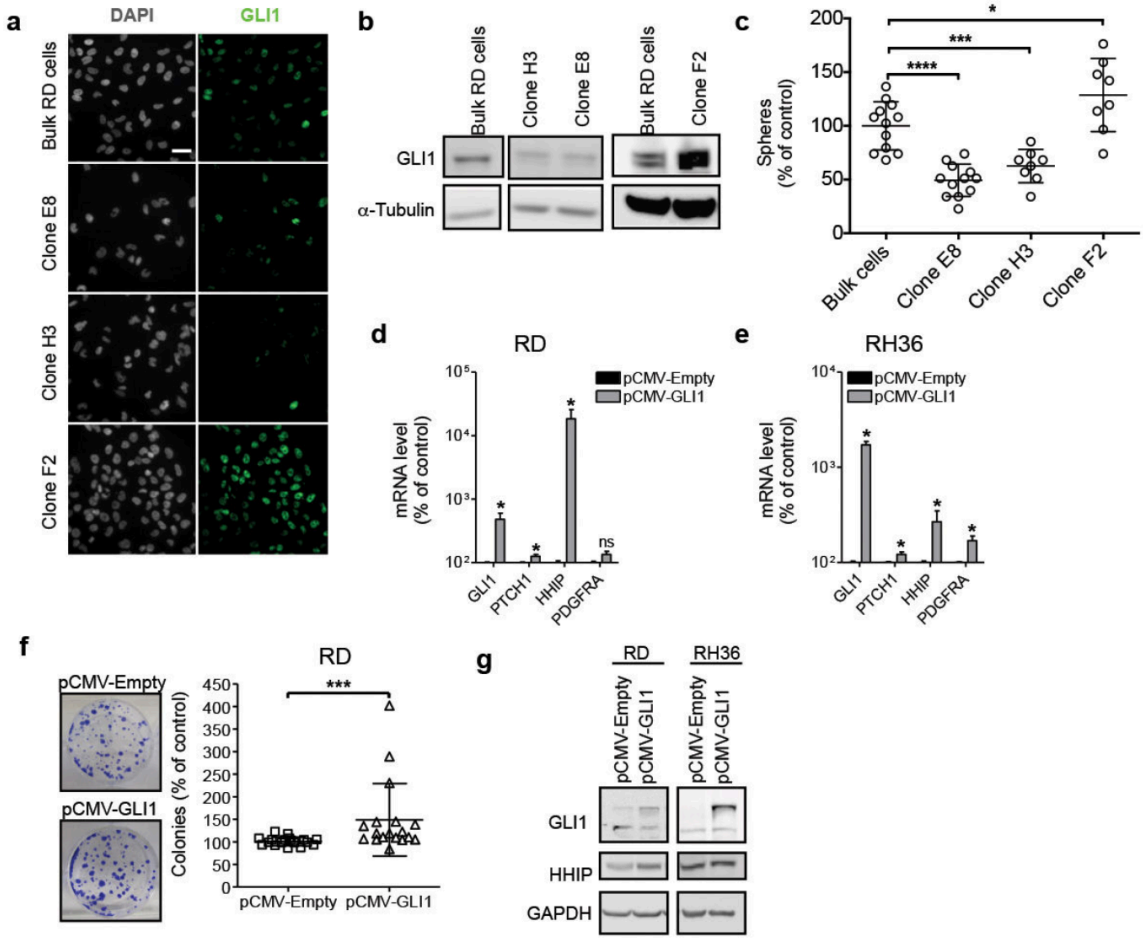

Supplementary Figure 3

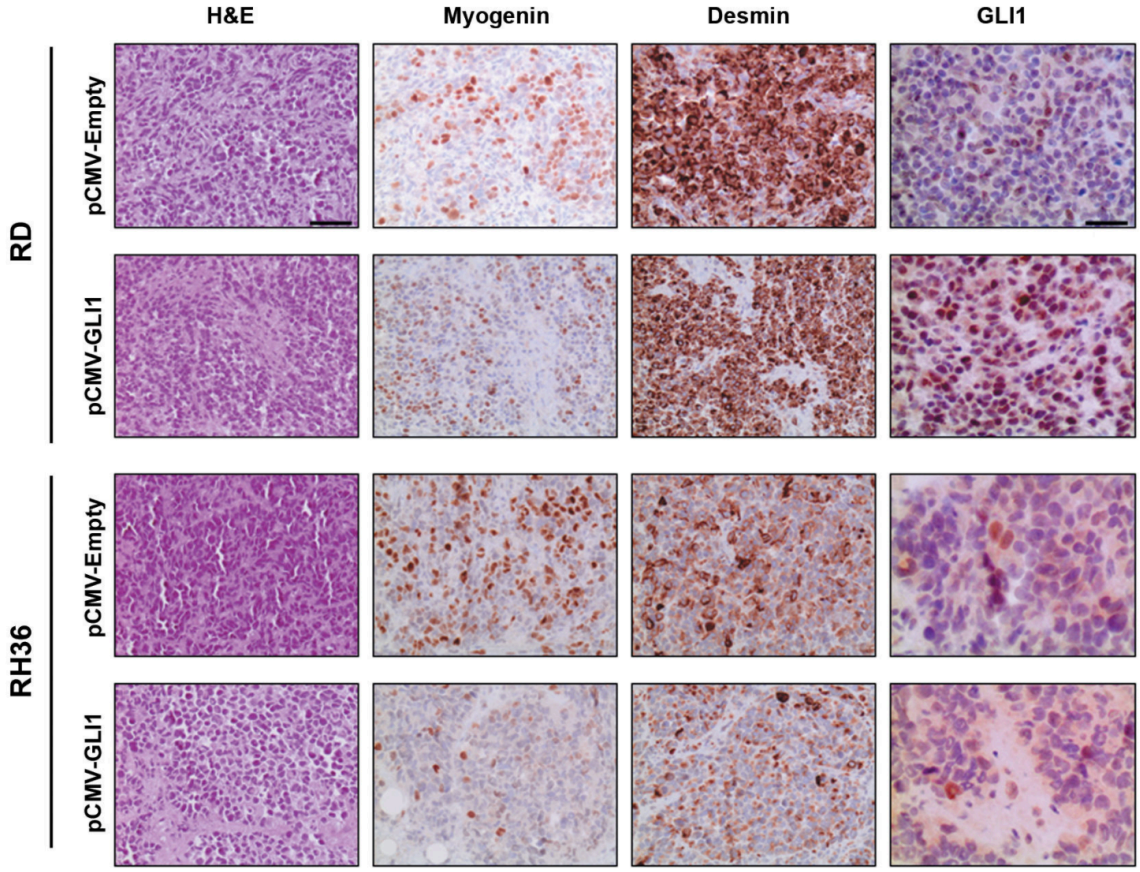

Supplementary Figure 4

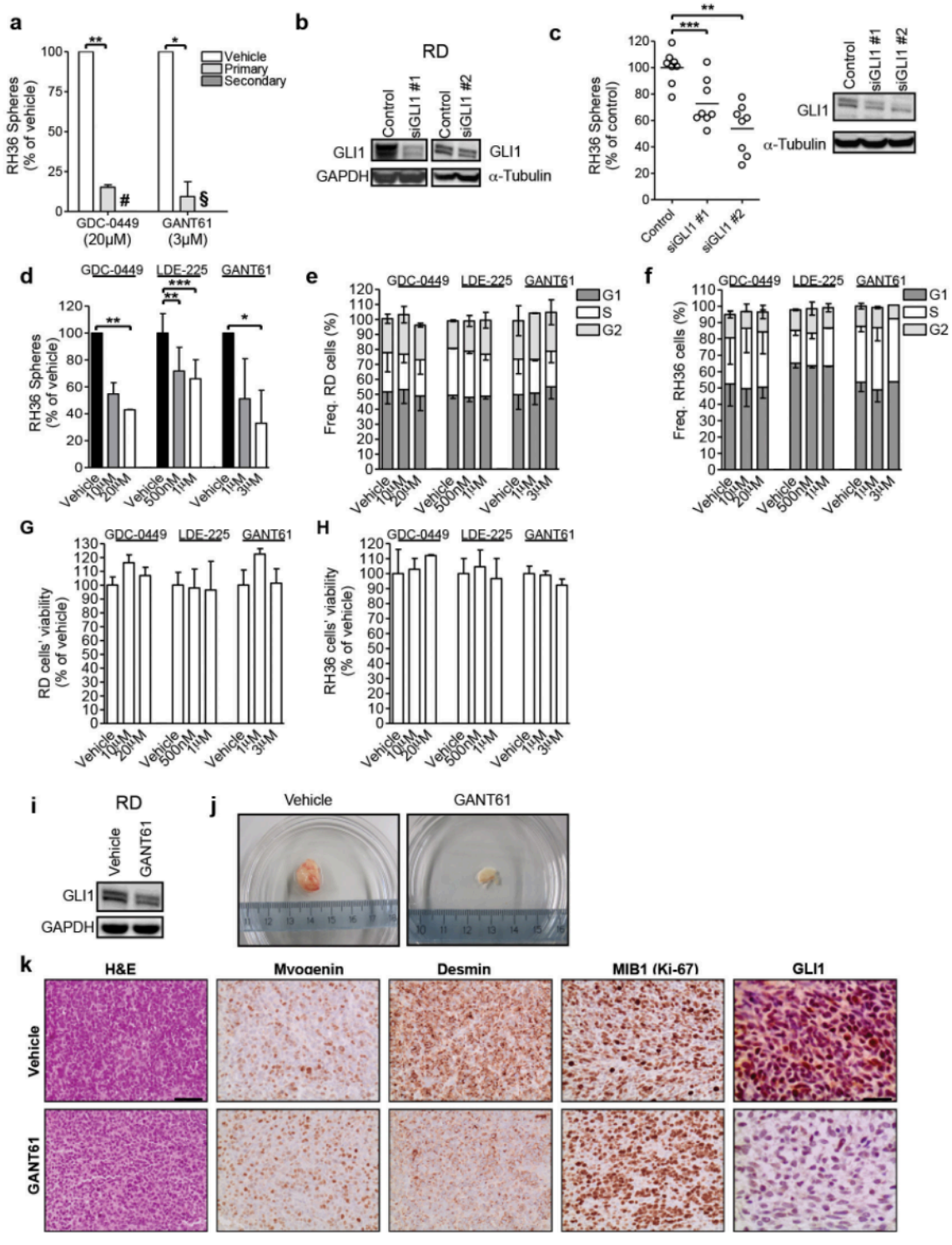

Supplementary Figure 5

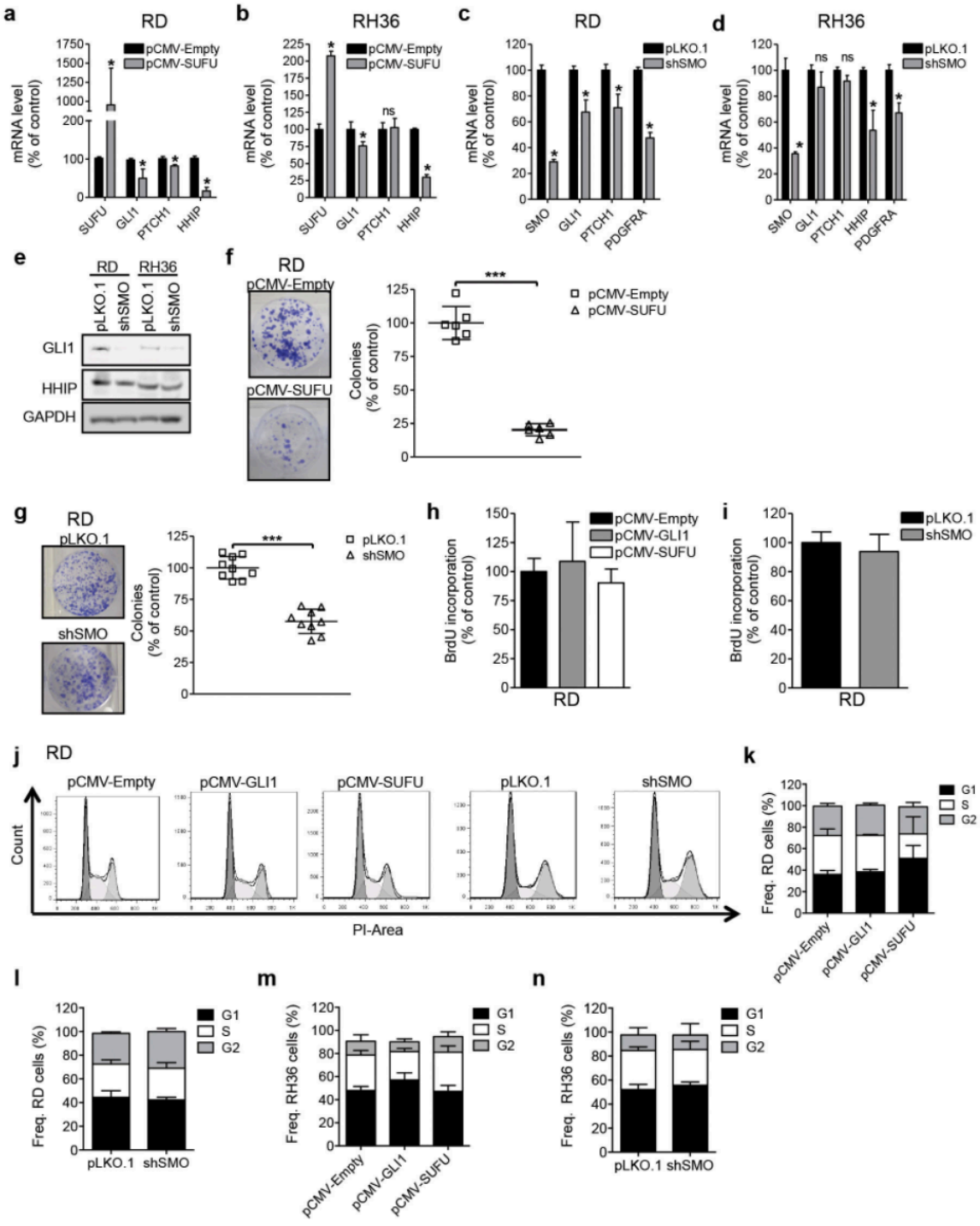

Supplementary Figure 6

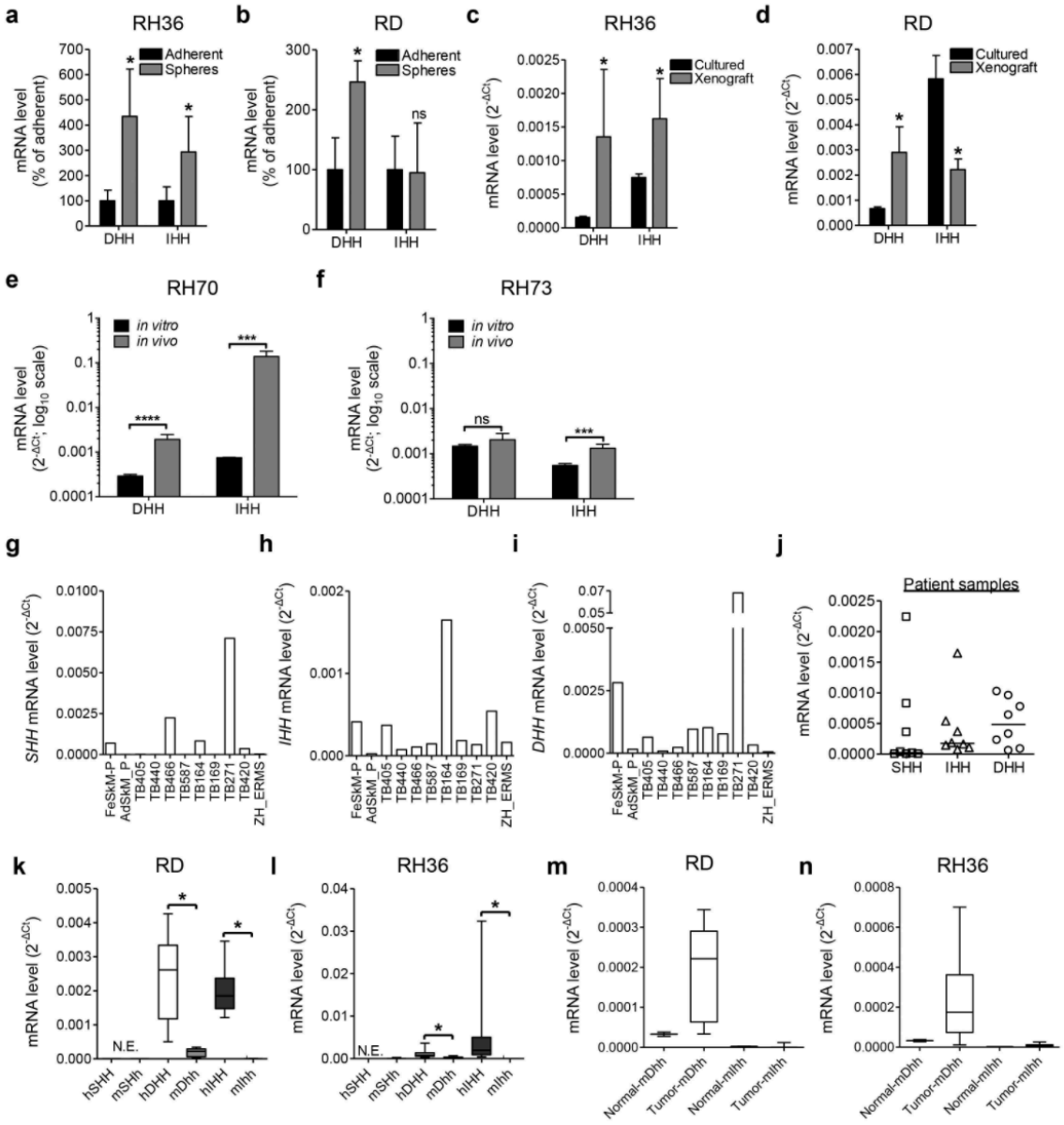

Supplementary Figure 7

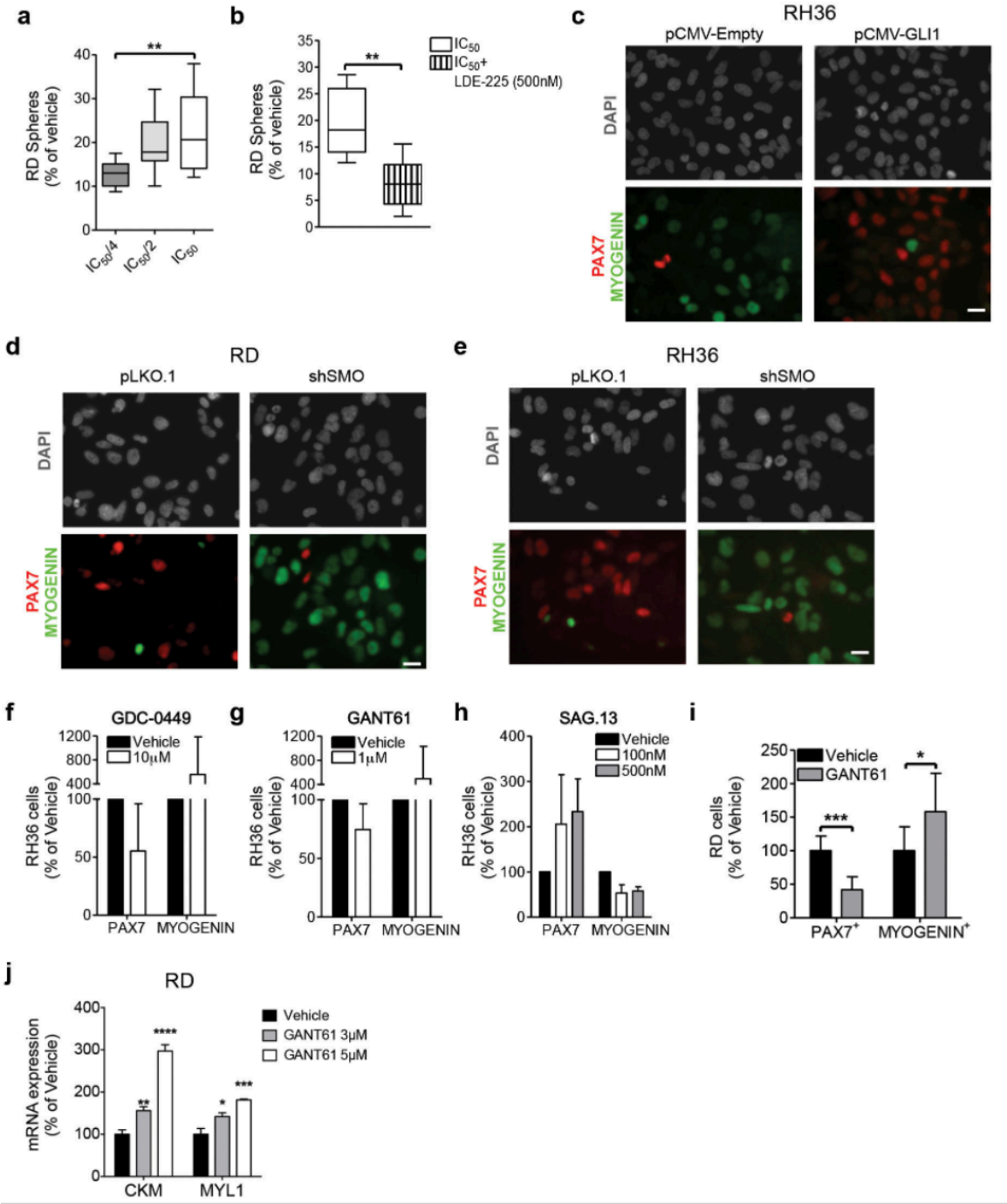

Supplementary Figure 8

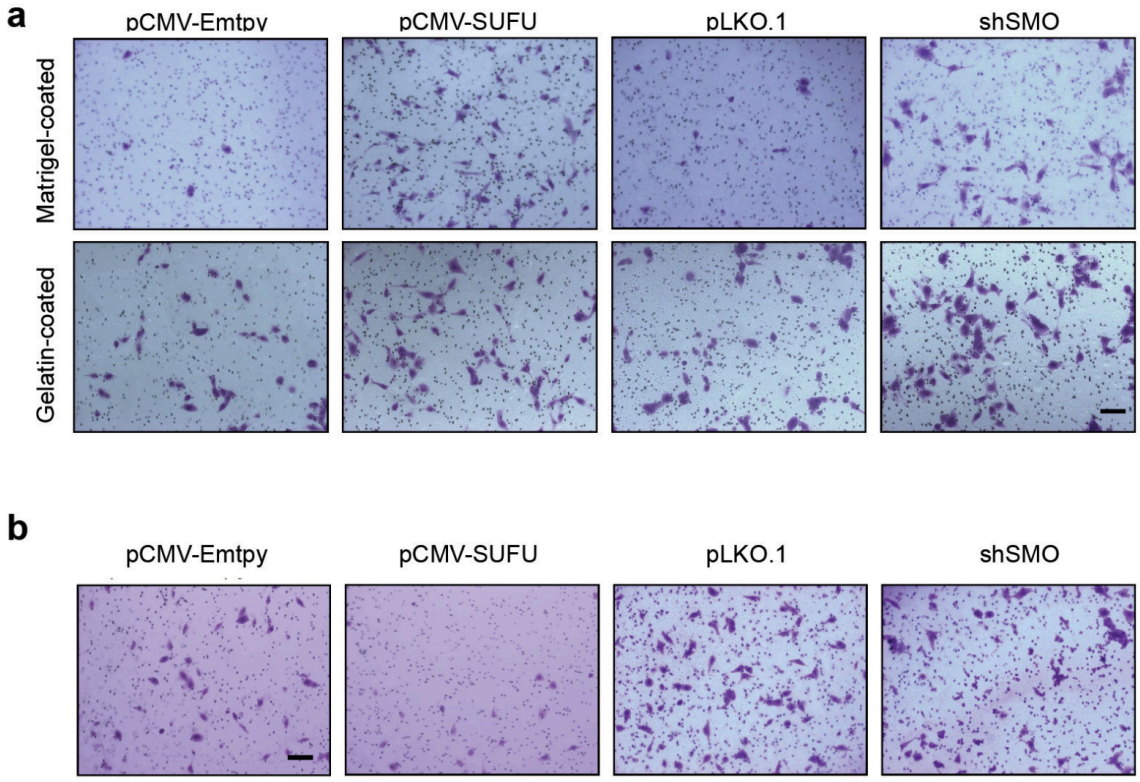

Supplementary Figure 9

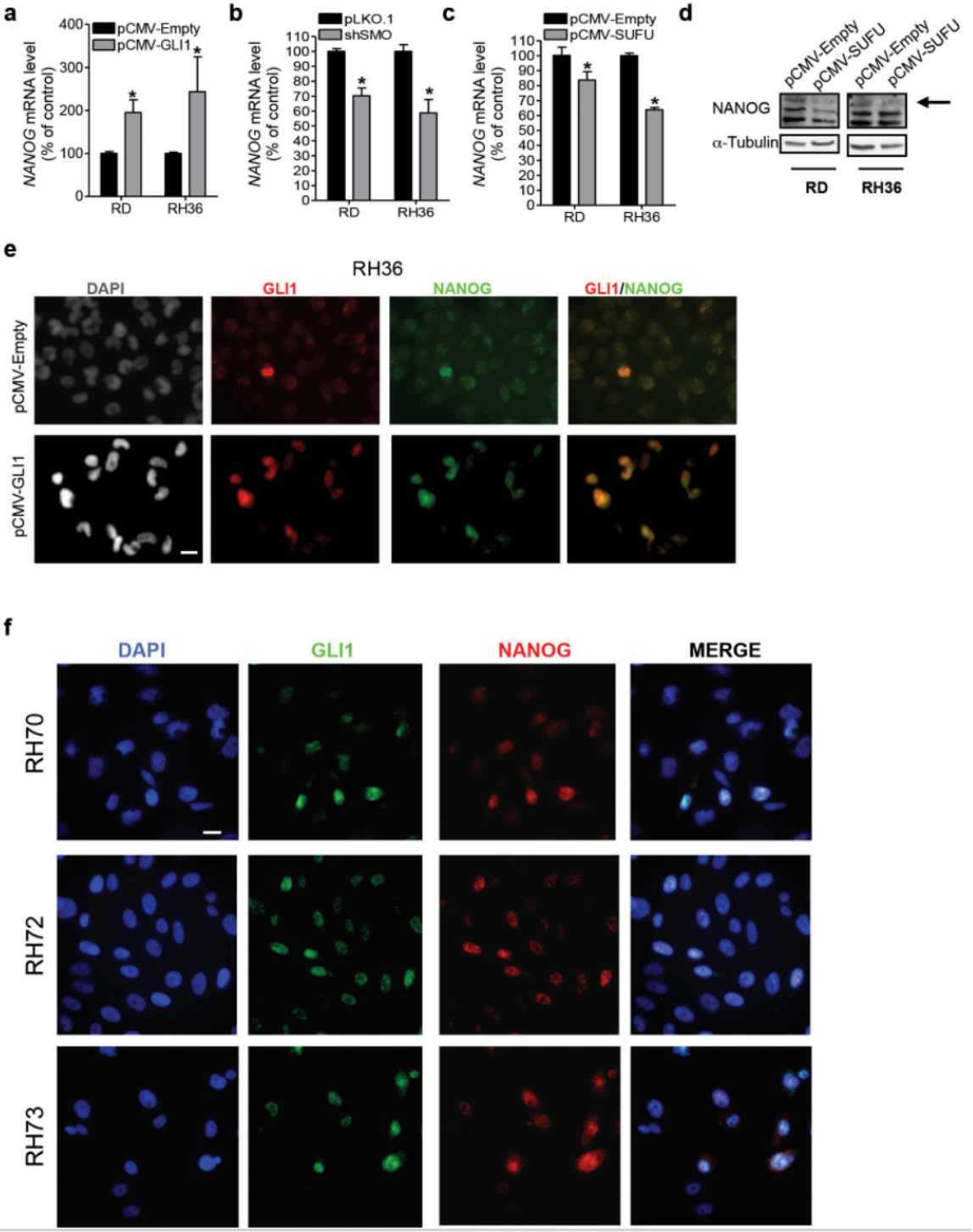

Supplementary Figure 10

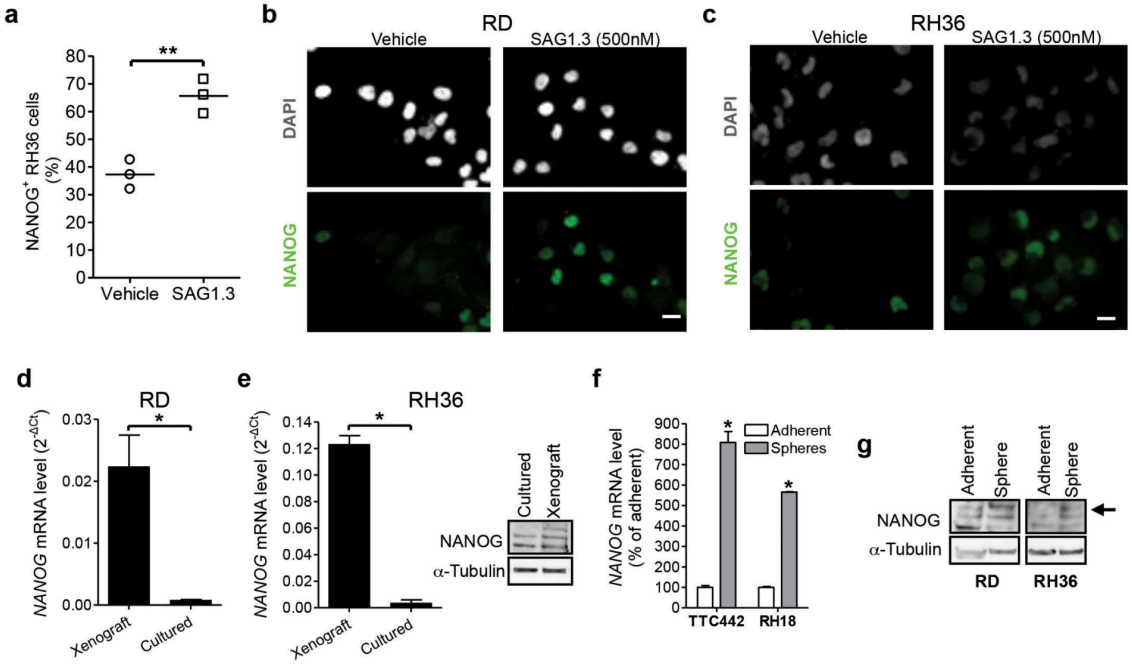

Supplementary Figure 11

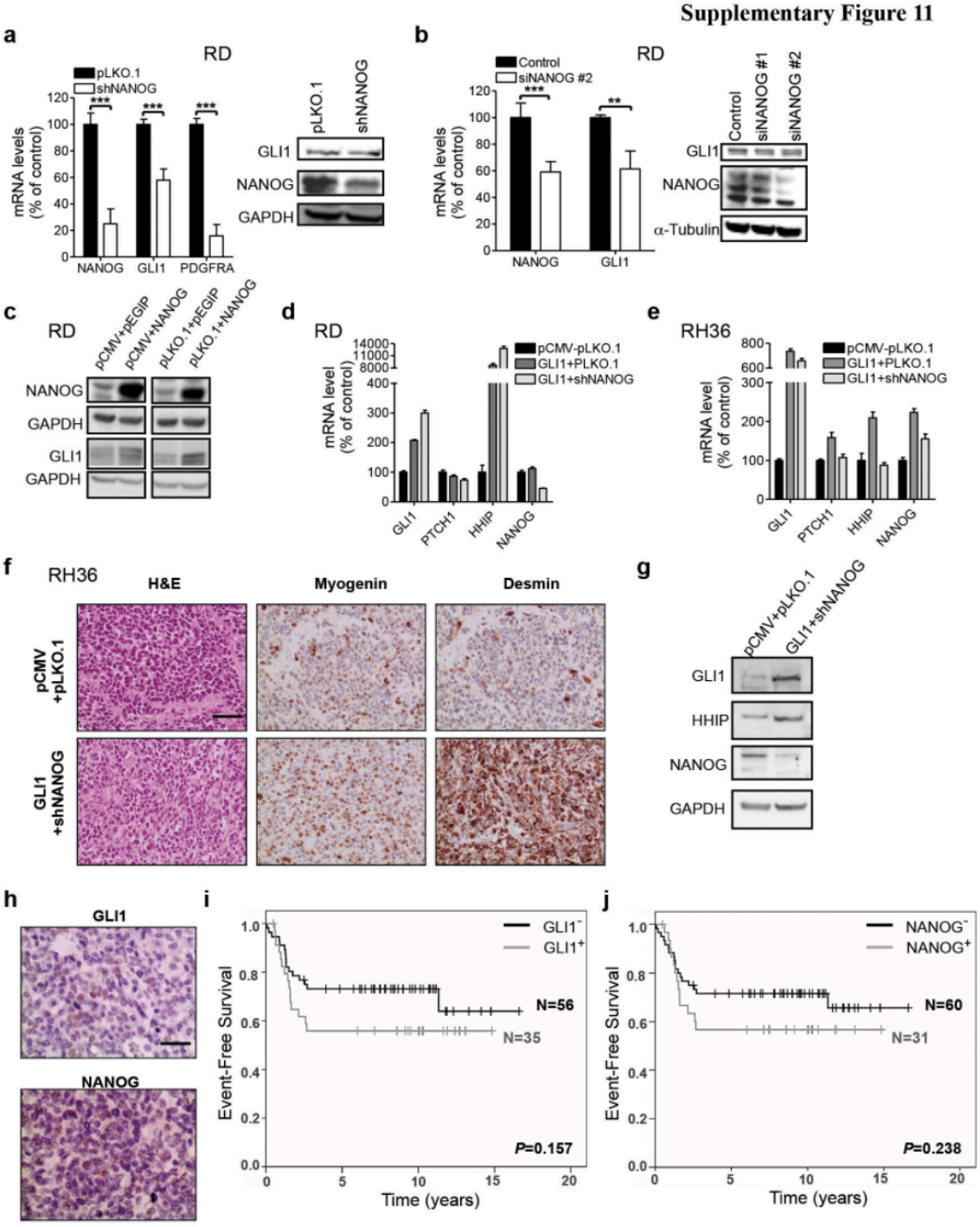

7. Discussion & Outlook

RMS accounts for the majority of soft-tissue sarcomas in children and multimodal treatment schedules including standard chemotherapy, surgery and radiotherapy remains the mainstay of therapy since almost half century. Although this treatment approach revolutionized the care of childhood cancers leading to impressive cure rates especially for paediatric acute lymphoblastic leukemia (5-years event-free survival approaching 80%), no further progress has been made over the last 20-30 years [236]. Importantly, only now we start recognizing the alarming cases of late morbidity following aggressive chemotherapy and radiotherapy cycles that are routinely applied since children tolerate much better than adults dose intensive cytotoxics [237]. Despite the great examples of novel targeted therapies approved for adult cancers in recent years, no molecularly-oriented drugs have entered the clinic for the management of RMS patients so far. This underlines critical issues associated with pediatric drug development, which does not meet the interest of the large financial markets. Indeed, childhood cancers represent only 1-2% of the global cancer burden, thus only a small fraction of patients might be enrolled in clinical trials. Yet, the relative success rate of standard treatments would confine the study population to relapse or metastatic groups only, who might not be a good “read-out window” to assess drug activity. Importantly, the general drug development pipeline of industry currently considers exclusively compounds that have already entered phase II studies for adult cancers [237]. However, such system might be misleading since the cancer spectrum in adulthood is largely dominated by carcinomas harboring a genetic landscape far more complex than pediatric tumors [7]. Thus, relevant targets for these latter will be completely underrepresented in adult malignancies.

To tackle this situation, in our studies we set out to develop a predictive and functional pre-clinical platform to inform on personalized treatment strategies for RMS patients. To this aim, we employed PDX models and systematic characterized culture conditions suitable for derivation and maintenance of RMS primary cultures (RPCs) (manuscript 1). Furthermore, we provide a proof-of-concept drug-testing program to identify patient-specific vulnerabilities or novel combinatorial options for patients refractory to the standard-of-care therapies (manuscript 1 and 2). These latter are associated with increased Hh output (manuscript 3), indicating that it might represent a potential bio-marker to capture patients with poor outcome or to monitor over time the risk of relapse of patients undergoing first-line treatments. A summary of the key findings of the present thesis is depicted in (Figure 17).

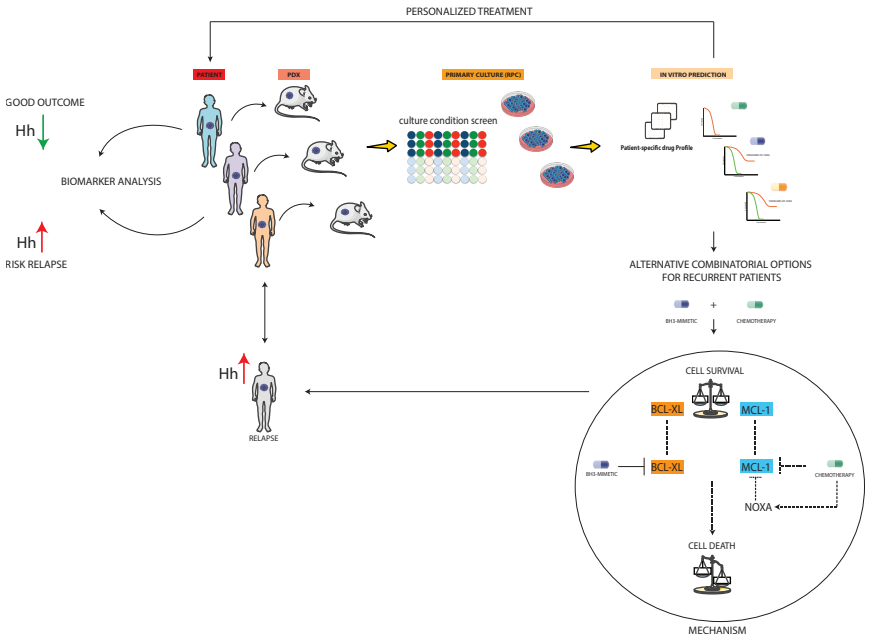

Figure 17. Overview of the main findings of the present thesis. The first aim of this project was to establish PDX models from RMS patients and characterize *in vitro* culture conditions to efficiently derive and maintain RMS primary cultures (RPCs) (manuscript 1). These latter were then employed for proof-of-concept high-throughput compound screens to identify patient-specific vulnerabilities (manuscript 1). Moreover, we describe a clear dependency of recurrent RPCs on BCL-XL and MCL-1 axis and their inhibition can be exploited by co-treatment with BH3-mimetics and standard chemotherapy. Finally, increased expression of Hh target genes correlated with relapsed disease in our cohort of PDX samples underscoring the clinical relevance of Hh pathway activity in RMS patients (manuscript 3).

7.1. Establishment of novel pre-clinical models of RMS

In our attempts to establish RMS patient-derived cells as reliable pre-clinical model of RMS, we developed a culture screen protocol to test a wide range of medium compositions and matrix requirements. Using a large panel of samples, we demonstrated, to our knowledge for the first time in RMS, a general negative effect of serum-containing media on the growth of RPCs. These findings might explain the very low success rate of cell line derivation achieved in the past for several solid and liquid cancer entities [238, 239]. Similar to others, we observed a serum-induced growth arrest accompanied by dramatic morphological changes that in some cases were associated with skeletal muscle differentiation [240, 241]. Although we do not know which component or mixture of factors present in the serum are responsible for this phenotype, we hypothesize that it might not adequately reflect the fluid that cells are exposed to in their natural environment. Interestingly, few RPCs could be propagated in presence of serum but this occurred either after a long adaptation period in culture (1-2 months) or for cells harboring TP-53 mutation (single case). *In vivo* tumorigenic assays revealed that 1 out of 2 serum-derived cells had impaired ability to generate tumors and aCGH analysis confirmed the presence of de-novo

genetic aberrations. Similar *in vitro* artifacts are frequently detected in traditional cancer cell lines, which often loose tumorigenicity or metastatic potential [240, 242]. In contrast, cells cultured in serum-free media, rapidly proliferated *in vitro* or *in vivo* and closely preserve most of the genetic aberrations and histological features of the original PDX. Furthermore, the use of serum replacements (B-27) can provide a more standardized system of cell culture, thus limiting the batch-to-batch variability of biological extracts.

Our systematic investigation of parameters for efficient *in vitro* cultivation of RPCs revealed that matrix support (matrigel or gelatin) is highly recommended and in some cases even necessary for cell viability. Probably, this might better model the pro-survival interactions between cancer cells and the extracellular matrix (ECM) occurring in vivo. Interestingly, the presence of growth factors (GFs) not always was beneficial for the growth of RPCs, highlighting the fact that generalization of culture conditions cannot always be applied. In line with this, we discovered in one case an unexpected growth inhibition of RPCs upon bFGF supply. Although we did not investigate the underlying molecular mechanism, previously studies demonstrated that bFGF-induced cell death is dependent on a sustained activation of $p38^{MAPK}$ in a panel of Ewing's sarcoma cell lines [243, 244].

Altogether, we uncovered culture condition requirements for derivation and maintenance of RPCs *in vitro,* which in the future might be translated directly on patient biopsies to minimize time for identification of clinically effective therapeutics.

7.2. Identification of novel pharmacological dependencies in RMS

Our study provides compelling evidence for using high-throughput drug screens in RPCs to capture patient-to-patient response variations that might guide personalized therapies. Indeed heterogeneous responses were observed for different agents in clinical development or already approved for other cancer types. For example, despite a general strong activity of different proteasome and PLK1 inhibitors across different patients, a single resistant case was identified with our platform. Such distinct pattern correlated with the presence of PAX7-FOXO1 translocation, which occurs in only a minority of ARMS patients. Although we cannot draw any conclusion on the potential involvement of PAX7-FOXO1 in this phenotype, our findings indicate that preliminary functional testing would be highly informative not only to identify effective compounds but also to avoid undesired side effects of unexpected inactive drugs. For example, bortezomib has become a standard-of care for relapse multiple myeloma (MM) and holds promise for several solid cancers, however dose-limiting toxicities and emergence of resistance remains a major concern [245, 246]. Among individual sensitivities, the BH3 mimetic ABT-263 exhibited a strong effect in three patients with IC-50 within the range of therapeutic doses (low nanomolar concentrations), further supporting the feasibility of our drug platform to nominate therapeutic candidates.

Impressively, clustering analysis of drug responses unveiled that cells harboring PAX3-FOXO1 fusion protein displayed a very similar pharmacological response pattern. Albeit, a larger panel of samples is required to correlate drug-response with PAX fusion status in RMS, we speculate that in addition to the distinct histological and genetic make-up of PFP and PFN, also specific pharmacological sensitivities might discriminate these two subtypes. This is not surprising since PFP and PFN are believed to eventually originate from different cell(s) of origin and to follow divergent models of tumorigenesis. According to this, mouse models experiments demonstrated that PFN mainly develop from adult muscle stem cells, which is consistent with the fact that PFN display a gene expression signature resembling satellite cell activation [174, 247]. In contrast, maturing myoblasts or terminally differentiated MyF-6-expressing cells have been reported as the origin of PFP tumors [170, 248]. Hence, the cellular context where the oncogenic event(s) occur might affect the molecular signature characterizing these two subgroups. In this regard, the RAS pathway is found frequently mutated exclusively in PFN [164], which mostly rely on the MEK/ERK axis. Similarly, we also observed a clear sensitivity to trametinib (MEK inhibitor) in RAS-mutated PFN cells. Controversy, an exquisite sensitivity to AKT inhibitors (3 out of 4) and everolimus (mTOR antagonist) was detected in PFP cells (mainly PAX3-FOXO1 fusion positive), suggesting a dependency on the mTOR/AKT axis. Although this might simply reflect the intact RAS status in these cells, two AKT consensus phosphorylation sites have been identified in the FOXO1 domain, thus corroborating a potential link between AKT and PAX3-FOXO1 [249]. This hypothesis is further supported by the fact that AKT can modulate the transcriptional activity of PAX3-FOXO1 to inhibit muscle differentiation in mouse ARMS cells. [250]. Finally, dose-response validations confirmed that the ATM/ATR inhibitor (AZ-20) was among the top drug candidates with a strong activity in PFP cells, which warrants further investigations.

7.3. Characterization of novel combination options for chemoresistant RMS

Although nowadays, resistance to conventional therapy remains a challenging clinical problem to overcome, novel therapeutic options have not been introduced into standard treatment regimens so far, which might be due at least in part to the lack of appropriate pre-clinical models. To fill this gap, we have generated a set of PDXs and matched RPCs derived from diagnostic/recurrent pairs of the same patient representing initial chemosensitive and subsequent chemoresistant disease. After validating the chemorefractory phenotype of relapse RPCs, we used these latter as system to identify sensitizers to standard chemotherapy. Hence, we describe the BH3-mimetic ABT-263 as a key pharmacological approach to bypass the apoptotic blockade of standard chemotherapy in high-risk group RMS samples. Mechanistically, the ABT-263/chemotherapy exploits the dual inhibition of BCL-XL and MCL-1 axis to restore programmed cell death in ERMS recurrent cells.

Resistance to apoptotic stimuli constitutes one of the hallmarks in cancer and provides an escape route to counteract the cytotoxic effect of conventional therapy [9, 10, 251]. Most chemotherapy drugs induce the intrinsic pathway of apoptosis, which is largely controlled by the BCL-2 proteins family. Consequently, imbalance between pro- and anti- apoptotic BCL-2 proteins has been shown to contribute to chemorefractory disease, although it remains poorly understood in RMS [251]. Among the BCL-2 pro-survival members, BCL-2, BCL-XL and MCL-1 are the most studied in cancer [252]. The oncogenic role of BCL-2 was initially described in follicular lymphomas as consequence of a t(14;18) translocation [253, 254]. Thereafter, over-expression of BCL-2 has been found in several solid and hematological cancers and has been shown to prevent chemotherapy-induced cell-death [255, 256]. Nevertheless, in our study pharmacological and genetic inhibition of BCL-2 appeared to be dispensable to sensitize RMS cells to both topoisomerase inhibitors (doxorubicin) and microtubule destabilizers (vincristine). Accordingly, by screening datasets of gene expression profiles, we did not find evidence of BCL-2 over-expression in RMS. In contrast, we found that mainly inhibition of BCL-XL mounts a chemosensitive response in recurrent ERMS. Although BCL-XL has been demonstrated to be transcriptional regulated by PAX3-FOXO1 and to mediate, at least in part, its anti-apoptotic response, no studies have addressed the functional role of BCL-XL in PFN tumors so far [257]. Our work corroborates previous findings showing the critical role of BCL-XL in the context of chemoresistance for other cancer entities [125, 258-260]. Albeit, BCL-XL targeting compounds represent an attractive strategy to incorporate in standard treatment protocols of RMS patients, severe sides effects have to be taken into account. In fact, because BCL-XL plays a pivotal role for survival in platelets, thrombocytopenia has been observed in pre-clinical mouse models and patients treated with ABT-263 [261, 262]. Therefore, re-design of new treatment schedules in pre-clinical settings is warranted to reverse these dose-limiting toxicities.

From a mechanistic standpoint we demonstrate that ABT-263/standard chemotherapy rely on the BCL-XL/MCL-1 axis, which is partially controlled by the pro-apoptotic BH3-only NOXA. Although MCL-1 depletion has been shown to sensitize cells to ABT-263, specific MCL-1 inhibitors are still in pre-clinical development [263, 264]. Here, we demonstrate that current debulking agents applied for the management of RMS patients can exploit MCL-1 inhibition. It is likely that this is not a direct effect but rather secondary to cell cycle regulation by chemotherapy. In fact, different studies have shown that MCL-1 protein stability undergoes a cell cycle-dependent regulation through post-translational modifications including phosphorylation and ubiquitination [265-267]. Additionally, also NOXA has been suggested to promote proteasomal degradation of MCL-1 and might provide the link between the chemo-mediated up-regulation of NOXA and downregulation of MCL-1 that we observe in our system [268]. Therefore, more experiments are needed in order to clarify the mode by which chemotherapy regulate MCL-1 in RMS.

7.4. Challenges of targeting Hh pathway in RMS[1]

Our data revealed that relapsed RMS tumors exhibit a strong up-regulation of Hh-targets (GLI1, HHIP and PTCH1) suggesting increased steady-state activity of the pathway. Such correlation is in agreement with previous studies showing that activation of Hh signaling is clinically relevant in PFN tumors [223, 269]. Therefore, assessment of Hh signaling status might help to identify specific subgroups of RMS with poor outcome and/or risk to relapse.

Given the importance of Hh signaling in modulating self-renewal and tumorigenicity of CSCs in ERMS, we reasoned that Hh^{high} chemo-resistant clones (CSCs) might be selected upon first-line treatments. Alternatively, iper-activation of the pathway following chemotherapy may promote a transition of chemo-sensitive cancer cells toward a resistant phenotype. These hypotheses are strengthened by the fact that we conducted a pairwise comparison of Hh target genes in individual PDX samples derived from tumors before chemotherapy and following chemo-relapse. Accordingly, our findings indicate that multi-strategy approaches including anti-Hh and bulk-reducing drugs may be more effective in tumor eradication, particularly for high-risk group patients.

Several inhibitors targeting different components of Hh molecular machinery are available to date (Figure 18). This includes ligand inhibitors (i.e, robotnikinin, 5E1 and MEDI-5304 neutralizing antibodies), Hh acyltransferase antagonists (i.e., RU-SKI 43), compounds against SMO (i.e., cyclopamine, Cur-61414, SANT1-4, LDE 225, GDC-0449, HPI 2-3, IPI 926, BMS-833923, ALLO1-2, Itraconazole), ciliogenesis inhibitors (CA1, CA2 and HPI-4) and GLI antagonists (i.e., GANT58, GANT61, HPI-1, forskolin and Arsenic Trioxide (ATO), glabrescione B) [270-272]. Currently, clinical trial strategies involving Hh pathway inhibitors include SMO antagonists, based on the success in preclinical models for different cancer types. In particular, GDC-0449 (or vismodegib) has been recently approved by US Food and Drug Administration (FDA) for the treatment of locally advanced and/or metastatic BCC [273-275]. Yet, LDE-225 alone and Vismodegib (Curis/Roche) in combination with a Notch inhibitor (R04929097) have entered into clinical trials for recurrent RMS and adult advanced RMS, respectively [276, 277]. This highlights the importance of studying developmental pathways in pediatric tumors, which might offer new options for future targeted therapies. However, deeper investigations on the mechanism of action of these compounds are needed since we could not recapitulate the pharmacological inhibition of Hh signaling by genetic means. For instance, GANT-61, an inhibitor of GLI activity has been reported to reduce RMS tumor growth in the chick chorioallantoic membrane (CAM) assay and in xenograft mouse models, but only at high concentrations [278-280]. Similarly, forskolin and betullic acid, two naturally occurring anti-Hh compounds have been shown to reduce proliferation or induce apoptosis in RMS although the effect was not specifically related to suppression of Hh pathway [281, 282]. Also, cyclopamine, a natural occurring compound targeting SMO, has been shown to be effective in reducing proliferation of RMS primary cells isolated from *Ptch+/-* mice or

human RMS cell lines *in vitro* [279, 283, 284]. Nevertheless, this effect is likely to be Hh-independent since our attempts to genetically modulate Hh signaling at different levels did not affect RMS cell growth (manuscript 3 and [269]). Thus we speculate that chemical inhibition of Hh signaling might also interfere with other signaling pathways. Such phenomenon has been shown to take place in RMS, where GANT-61 treatment could reduce tumor growth in mice by concomitant inhibition of Hh and AKT/mTOR signaling [285]. Hence, to clarify the specificity of the anti-Hh compounds and the dynamic changes of Hh pathway following chemotherapy we attempted to generate an endogenous GLI-reporter system by knocking-in a GFP into the GLI1 locus via the Crispr-Cas9 genome-editing tool (data not shown). Although we did not succeed, we emphasize the need of establishing new methods that enable to track the response of Hh-activating cells. Furthermore, such system would help to unravel the role of non-canonical Hh mediators in RMS, which have been shown as mechanism of resistance to SMO antagonists [286]. Therefore, it would open new avenues to interfere with down-stream Hh components since direct and specific targeting of transcription factors such as GLI1 remains a difficult task.

Finally, the therapeutic window of anti Hh compounds remains incompletely addressed in childhood cancers. This is an important caveat given the indispensable function of Hh signaling during development. Therefore, it is not unexpected to find that short-term blocking of Hh pathway in young mice resulted in severe and irreversible side effects, specifically in the bones [287]. Also, knockout for Ptch1 and Sufu as well as Gli1/Gli2 double mutants (lacking the DNA binding domain of Gli1 and Gli2) are not compatible with life in mice due to defects during neurogenesis and heart or lung abnormalities [217, 230, 288]. In contrast, mice homozygous for a Gli1 mutant allele have a normal phenotype suggesting that Hh inhibitors targeting specifically Gli1 might be well tolerated in children [288].

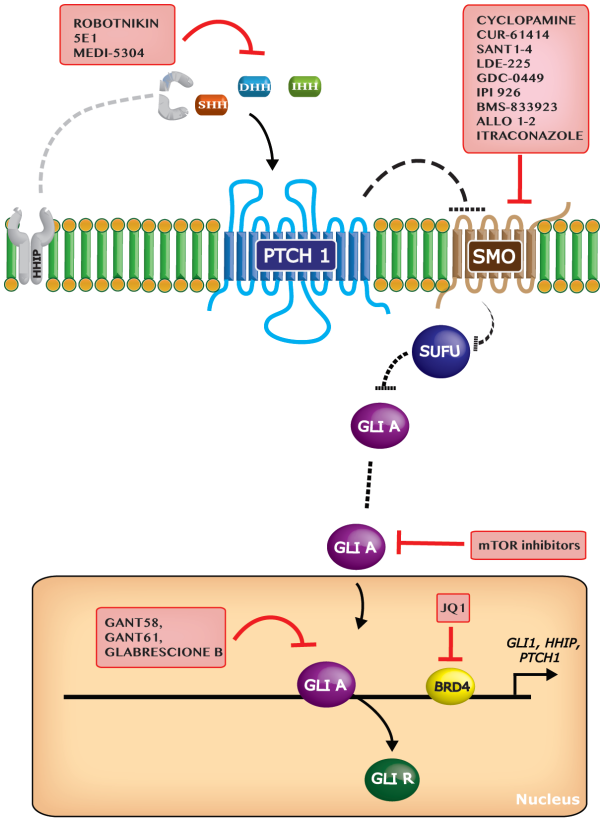

Figure 18. Targeting Hh Signaling. Schematic representation depicting Hh pathway and current inhibitors targeting both canonical and non-canonical Hh signaling activation in cancer

7.5. Conclusions

Over the last decades it has become increasingly clear that cancer is characterized by inter-individual heterogeneity, which is one of the main reasons for treatment failure. To address this problem, more patient-specific therapeutic approaches are necessary. One possibility takes advantage of comprehensive genomic profiling to detect cancer-specific, actionable driver oncogenes. Unfortunately, such genome-based drug selection is not feasible for tumors, which are driven by mutated but “undruggable” targets and have an otherwise low mutational burden, a characteristic of many pediatric sarcoma cancers such as rhabdomyosarcoma (RMS), in which fusion transcription factors are the main drivers of tumorigenesis. In this study we describe a complementary approach circumventing these problems by using patient-derived *in vitro* and *in vivo* model systems that enables direct drug-profiling of patient tumor cells. We also show the feasibility of such platform to identify effective drug pairs in patients where responses to standard-of-care therapies have been exhausted. Hence, we provide means to prioritize actionable drug targets and thus counteract the slow rate of drug development for children (Figure 19).

In conclusion, we believe that these findings will help to fill the existing gap between basic/translational science and clinical practice. Moreover, having established a large panel of

RPCs representative of a greater inter- and intra- patient heterogeneity, new biological questions underlining the biology of RMS can be addressed in the near future.

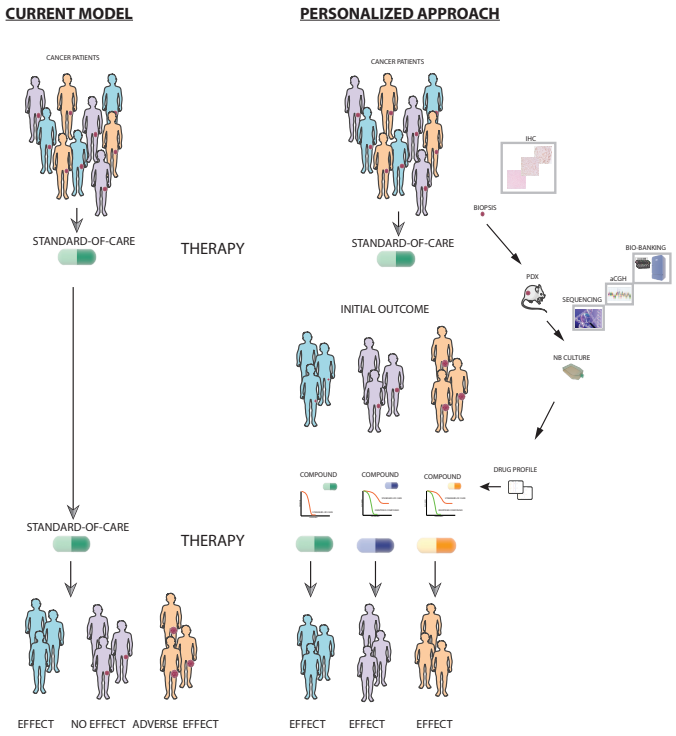

Figure 19. Precision medicine strategy for RMS patients. Drawing of the current model (left panel) and an alternative personalized strategy (right) for the management of RMS patients. In this latter, PDXs and RPCs will be generated in parallel during the course of the clinical trial to identify drug sensitivities in individual patients. Hence, at the time of assessment of the initial outcome, physicians will have information about the best treatment to apply for each patient or group of patients. This will limit the emergence of adverse effects or occurrence of 'no response'. Finally, the establishment of bio-banks with annotated information about genomic and gene expression data as well as drug profiles will help to discover novel bio-markers for future patient stratifications.

8. Bibliography

1. *Global Cancer Facts & Figures 3rd Edition.* Atlanta: American Cancer Society, 2015.
2. Bray, F., et al., *Global cancer transitions according to the Human Development Index (2008-2030): a population-based study.* Lancet Oncol, 2012. **13**(8): p. 790-801.
3. Downing, J.R., et al., *The Pediatric Cancer Genome Project.* Nat Genet, 2012. **44**(6): p. 619-22.
4. Pritchard-Jones, K. and R. Sullivan, *Children with cancer: driving the global agenda.* Lancet Oncol, 2013. **14**(3): p. 189-91.
5. Tomasetti, C. and B. Vogelstein, *Cancer etiology. Variation in cancer risk among tissues can be explained by the number of stem cell divisions.* Science, 2015. **347**(6217): p. 78-81.
6. Tomasetti, C., L. Li, and B. Vogelstein, *Stem cell divisions, somatic mutations, cancer etiology, and cancer prevention.* Science, 2017. **355**(6331): p. 1330-1334.
7. Vogelstein, B., et al., *Cancer genome landscapes.* Science, 2013. **339**(6127): p. 1546-58.
8. Hahn, W.C. and R.A. Weinberg, *Modelling the molecular circuitry of cancer.* Nat Rev Cancer, 2002. **2**(5): p. 331-41.
9. Hanahan, D. and R.A. Weinberg, *The hallmarks of cancer.* Cell, 2000. **100**(1): p. 57-70.
10. Hanahan, D. and R.A. Weinberg, *Hallmarks of cancer: the next generation.* Cell, 2011. **144**(5): p. 646-74.
11. Day, C.P., G. Merlino, and T. Van Dyke, *Preclinical mouse cancer models: a maze of opportunities and challenges.* Cell, 2015. **163**(1): p. 39-53.
12. Gillet, J.P., S. Varma, and M.M. Gottesman, *The clinical relevance of cancer cell lines.* J Natl Cancer Inst, 2013. **105**(7): p. 452-8.
13. Lucey, B.P., W.A. Nelson-Rees, and G.M. Hutchins, *Henrietta Lacks, HeLa cells, and cell culture contamination.* Arch Pathol Lab Med, 2009. **133**(9): p. 1463-7.
14. Culliton, B.J., *HeLa Cells: Contaminating Cultures around the World.* Science, 1974. **184**(4141): p. 1058-9.
15. Gey GO, C.W., Kubicek MT, *Tissue culture studies of the proliferative capacity of cervical carcinoma and normal epithelium.* Cancer Research, 1952. **12:264–265**

.

16. Freshney, R.I., *Culture of animal cells: a manual of basic technique*. 2000, New York: Wiley-Liss.
17. Cantor, J.R., et al., *Physiologic Medium Rewires Cellular Metabolism and Reveals Uric Acid as an Endogenous Inhibitor of UMP Synthase.* Cell, 2017. **169**(2): p. 258-272 e17.

18. Sharma, S.V., D.A. Haber, and J. Settleman, *Cell line-based platforms to evaluate the therapeutic efficacy of candidate anticancer agents.* Nat Rev Cancer, 2010. **10**(4): p. 241-53.
19. Nelson-Rees, W.A. and R.R. Flandermeyer, *Inter- and intraspecies contamination of human breast tumor cell lines HBC and BrCa5 and other cell cultures.* Science, 1977. **195**(4284): p. 1343-4.
20. Driscoll, J.S., *The preclinical new drug research program of the National Cancer Institute.* Cancer treatment reports, 1984. **68**(1): p. 63-76.
21. Voskoglou-Nomikos, T., J.L. Pater, and L. Seymour, *Clinical predictive value of the in vitro cell line, human xenograft, and mouse allograft preclinical cancer models.* Clinical Cancer Research, 2003. **9**(11): p. 4227-4239.
22. DeVita, V.T., Jr. and E. Chu, *A history of cancer chemotherapy.* Cancer Res, 2008. **68**(21): p. 8643-53.
23. Shoemaker, R.H., *The NCI60 human tumour cell line anticancer drug screen.* Nat Rev Cancer, 2006. **6**(10): p. 813-23.
24. Aref, A. and D. Barbie, *Ex Vivo Engineering of the Tumor Microenvironment*. 2017: Springer.
25. Mitra, A., L. Mishra, and S. Li, *Technologies for deriving primary tumor cells for use in personalized cancer therapy.* Trends Biotechnol, 2013. **31**(6): p. 347-54.
26. Lee, J., et al., *Tumor stem cells derived from glioblastomas cultured in bFGF and EGF more closely mirror the phenotype and genotype of primary tumors than do serum-cultured cell lines.* Cancer Cell, 2006. **9**(5): p. 391-403.
27. Hughes, P., et al., *The costs of using unauthenticated, over-passaged cell lines: how much more data do we need?* Biotechniques, 2007. **43**(5): p. 575-588.
28. Masters, J.R., *Human cancer cell lines: fact and fantasy.* Nat Rev Mol Cell Biol, 2000. **1**(3): p. 233-6.
29. Ince, T.A., et al., *Characterization of twenty-five ovarian tumour cell lines that phenocopy primary tumours.* Nat Commun, 2015. **6**: p. 7419.
30. Liu, X., et al., *Conditional reprogramming and long-term expansion of normal and tumor cells from human biospecimens.* Nat Protoc, 2017. **12**(2): p. 439-451.
31. Sachs, N. and H. Clevers, *Organoid cultures for the analysis of cancer phenotypes.* Curr Opin Genet Dev, 2014. **24**: p. 68-73.
32. Harrison, R.G., et al., *Observations of the living developing nerve fiber.* The Anatomical Record, 1907. **1**(5): p. 116-128.
33. Moscona, A. and H. Moscona, *The dissociation and aggregation of cells from organ rudiments of the early chick embryo.* Journal of anatomy, 1952. **86**(Pt 3): p. 287.
34. Simian, M. and M.J. Bissell, *Organoids: A historical perspective of thinking in three dimensions.* J Cell Biol, 2017. **216**(1): p. 31-40.
35. Lancaster, M.A. and J.A. Knoblich, *Organogenesis in a dish: modeling development and disease using organoid technologies.* Science, 2014. **345**(6194): p. 1247125.
36. Clevers, H., *Modeling Development and Disease with Organoids.* Cell, 2016. **165**(7): p. 1586-97.

37. van de Wetering, M., et al., *Prospective derivation of a living organoid biobank of colorectal cancer patients.* Cell, 2015. **161**(4): p. 933-45.
38. Gao, D., et al., *Organoid cultures derived from patients with advanced prostate cancer.* Cell, 2014. **159**(1): p. 176-87.
39. Huang, L., et al., *Ductal pancreatic cancer modeling and drug screening using human pluripotent stem cell- and patient-derived tumor organoids.* Nat Med, 2015. **21**(11): p. 1364-71.
40. Hubert, C.G., et al., *A Three-Dimensional Organoid Culture System Derived from Human Glioblastomas Recapitulates the Hypoxic Gradients and Cancer Stem Cell Heterogeneity of Tumors Found In Vivo.* Cancer Res, 2016. **76**(8): p. 2465-77.
41. Fujii, M., et al., *A Colorectal Tumor Organoid Library Demonstrates Progressive Loss of Niche Factor Requirements during Tumorigenesis.* Cell Stem Cell, 2016. **18**(6): p. 827-38.
42. Matano, M., et al., *Modeling colorectal cancer using CRISPR-Cas9-mediated engineering of human intestinal organoids.* Nature medicine, 2015. **21**(3): p. 256-262.
43. Fatehullah, A., S.H. Tan, and N. Barker, *Organoids as an in vitro model of human development and disease.* Nature cell biology, 2016. **18**(3): p. 246-254.
44. Yue, F., et al., *A comparative encyclopedia of DNA elements in the mouse genome.* Nature, 2014. **515**(7527): p. 355-64.
45. Bailey, M., Z. Christoforidou, and M.C. Lewis, *The evolutionary basis for differences between the immune systems of man, mouse, pig and ruminants.* Veterinary immunology and immunopathology, 2013. **152**(1): p. 13-19.
46. Le Magnen, C., A. Dutta, and C. Abate-Shen, *Optimizing mouse models for precision cancer prevention.* Nature Reviews Cancer, 2016. **16**(3): p. 187-196.
47. Hidalgo, M., et al., *Patient-derived xenograft models: an emerging platform for translational cancer research.* Cancer Discov, 2014. **4**(9): p. 998-1013.
48. Marangoni, E., et al., *A new model of patient tumor-derived breast cancer xenografts for preclinical assays.* Clin Cancer Res, 2007. **13**(13): p. 3989-98.
49. Zhang, X., et al., *A renewable tissue resource of phenotypically stable, biologically and ethnically diverse, patient-derived human breast cancer xenograft models.* Cancer Res, 2013. **73**(15): p. 4885-97.
50. Dong, X., et al., *Patient-derived first generation xenografts of non-small cell lung cancers: promising tools for predicting drug responses for personalized chemotherapy.* Clin Cancer Res, 2010. **16**(5): p. 1442-51.
51. Byrne, A.T., et al., *Interrogating open issues in cancer precision medicine with patient-derived xenografts.* Nat Rev Cancer, 2017. **17**(4): p. 254-268.
52. Malaney, P., S.V. Nicosia, and V. Dave, *One mouse, one patient paradigm: New avatars of personalized cancer therapy.* Cancer Lett, 2014. **344**(1): p. 1-12.
53. Gao, H., et al., *High-throughput screening using patient-derived tumor xenografts to predict clinical trial drug response.* Nature medicine, 2015. **21**(11): p. 1318-1325.
54. Zitvogel, L., et al., *Mouse models in oncoimmunology.* Nat Rev Cancer, 2016. **16**(12): p. 759-773.

55. Tentler, J.J., et al., *Patient-derived tumour xenografts as models for oncology drug development.* Nature reviews Clinical oncology, 2012. **9**(6): p. 338-350.
56. Frese, K.K. and D.A. Tuveson, *Maximizing mouse cancer models.* Nat Rev Cancer, 2007. **7**(9): p. 645-58.
57. Schonig, K., et al., *Stringent doxycycline dependent control of CRE recombinase in vivo.* Nucleic Acids Res, 2002. **30**(23): p. e134.
58. Lewandoski, M., *Conditional control of gene expression in the mouse.* Nat Rev Genet, 2001. **2**(10): p. 743-55.
59. Lakso, M., et al., *Targeted oncogene activation by site-specific recombination in transgenic mice.* Proc Natl Acad Sci U S A, 1992. **89**(14): p. 6232-6.
60. Hill, R., et al., *Selective evolution of stromal mesenchyme with p53 loss in response to epithelial tumorigenesis.* Cell, 2005. **123**(6): p. 1001-11.
61. Bhowmick, N.A., et al., *TGF-beta signaling in fibroblasts modulates the oncogenic potential of adjacent epithelia.* Science, 2004. **303**(5659): p. 848-51.
62. Coussens, L.M., et al., *MMP-9 supplied by bone marrow-derived cells contributes to skin carcinogenesis.* Cell, 2000. **103**(3): p. 481-90.
63. Smyth, M.J., et al., *Perforin-mediated cytotoxicity is critical for surveillance of spontaneous lymphoma.* Journal of Experimental Medicine, 2000. **192**(5): p. 755-760.
64. Cui, W., et al., *TGFβ1 inhibits the formation of benign skin tumors, but enhances progression to invasive spindle carcinomas in transgenic mice.* Cell, 1996. **86**(4): p. 531-542.
65. Visvader, J.E., *Cells of origin in cancer.* Nature, 2011. **469**(7330): p. 314-322.
66. Ji, H., et al., *The impact of human EGFR kinase domain mutations on lung tumorigenesis and in vivo sensitivity to EGFR-targeted therapies.* Cancer Cell, 2006. **9**(6): p. 485-95.
67. Politi, K., et al., *Lung adenocarcinomas induced in mice by mutant EGF receptors foundin human lung cancers respondto a tyrosine kinase inhibitor orto down-regulation of the receptors.* Genes & development, 2006. **20**(11): p. 1496-1510.
68. Lallemand-Breitenbach, V., et al., *Retinoic acid and arsenic synergize to eradicate leukemic cells in a mouse model of acute promyelocytic leukemia.* J Exp Med, 1999. **189**(7): p. 1043-52.
69. Clohessy, J.G. and P.P. Pandolfi, *Mouse hospital and co-clinical trial project--from bench to bedside.* Nat Rev Clin Oncol, 2015. **12**(8): p. 491-8.
70. Pinkel, D., et al., *Drug dosage and remission duration in childhood lymphocytic leukemia.* Cancer, 1971. **27**(2): p. 247-256.
71. Einhorn, L.H., *Testicular cancer as a model for a curable neoplasm: The Richard and Hinda Rosenthal Foundation Award Lecture.* Cancer Research, 1981. **41**(9 Part 1): p. 3275-3280.
72. Devita, V.T., et al., *Curability of Advanced Hodgkin's Disease with ChemotherapyLong-Term Follow-up of MOPP-Treated Patients at the National Cancer Institute.* Annals of Internal Medicine, 1980. **92**(5): p. 587-595.

73. Chisholm, R.H., et al., *Emergence of drug tolerance in cancer cell populations: an evolutionary outcome of selection, nongenetic instability, and stress-induced adaptation.* Cancer Res, 2015. **75**(6): p. 930-9.
74. Domingo-Domenech, J., et al., *Suppression of acquired docetaxel resistance in prostate cancer through depletion of notch- and hedgehog-dependent tumor-initiating cells.* Cancer Cell, 2012. **22**(3): p. 373-88.
75. Gupta, P.B., et al., *Stochastic state transitions give rise to phenotypic equilibrium in populations of cancer cells.* Cell, 2011. **146**(4): p. 633-44.
76. Cara, S. and I.F. Tannock, *Retreatment of patients with the same chemotherapy: implications for clinical mechanisms of drug resistance.* Ann Oncol, 2001. **12**(1): p. 23-7.
77. Sharma, S.V., et al., *A chromatin-mediated reversible drug-tolerant state in cancer cell subpopulations.* Cell, 2010. **141**(1): p. 69-80.
78. Diaz, L.A., Jr., et al., *The molecular evolution of acquired resistance to targeted EGFR blockade in colorectal cancers.* Nature, 2012. **486**(7404): p. 537-40.
79. Bozic, I. and M.A. Nowak, *Resisting resistance.* 2017.
80. Bozic, I. and M.A. Nowak, *Timing and heterogeneity of mutations associated with drug resistance in metastatic cancers.* Proc Natl Acad Sci U S A, 2014. **111**(45): p. 15964-8.
81. Holohan, C., et al., *Cancer drug resistance: an evolving paradigm.* Nat Rev Cancer, 2013. **13**(10): p. 714-26.
82. Longley, D.B. and P.G. Johnston, *Molecular mechanisms of drug resistance.* J Pathol, 2005. **205**(2): p. 275-92.
83. Ward, P.S. and C.B. Thompson, *Metabolic reprogramming: a cancer hallmark even warburg did not anticipate.* Cancer cell, 2012. **21**(3): p. 297-308.
84. Dean, M., T. Fojo, and S. Bates, *Tumour stem cells and drug resistance.* Nature Reviews Cancer, 2005. **5**(4): p. 275-284.
85. Visvader, J.E. and G.J. Lindeman, *Cancer stem cells in solid tumours: accumulating evidence and unresolved questions.* Nat Rev Cancer, 2008. **8**(10): p. 755-68.
86. Beck, B. and C. Blanpain, *Unravelling cancer stem cell potential.* Nat Rev Cancer, 2013. **13**(10): p. 727-38.
87. Reya, T., et al., *Stem cells, cancer, and cancer stem cells.* Nature, 2001. **414**(6859): p. 105-11.
88. Hemmati, H.D., et al., *Cancerous stem cells can arise from pediatric brain tumors.* Proceedings of the National Academy of Sciences, 2003. **100**(25): p. 15178-15183.
89. Cozzio, A., et al., *Similar MLL-associated leukemias arising from self-renewing stem cells and short-lived myeloid progenitors.* Genes Dev, 2003. **17**(24): p. 3029-35.
90. Kumar, S.M., et al., *Acquired cancer stem cell phenotypes through Oct4-mediated dedifferentiation.* Oncogene, 2012. **31**(47): p. 4898.
91. Friedmann-Morvinski, D. and I.M. Verma, *Dedifferentiation and reprogramming: origins of cancer stem cells.* EMBO Rep, 2014. **15**(3): p. 244-53.

92. Blanpain, C., et al., *DNA-damage response in tissue-specific and cancer stem cells.* Cell Stem Cell, 2011. **8**(1): p. 16-29.
93. Chen, J., et al., *A restricted cell population propagates glioblastoma growth after chemotherapy.* Nature, 2012. **488**(7412): p. 522-6.
94. Chiu, P.P., H. Jiang, and J.E. Dick, *Leukemia-initiating cells in human T-lymphoblastic leukemia exhibit glucocorticoid resistance.* Blood, 2010. **116**(24): p. 5268-79.
95. Shlush, L.I., et al., *Tracing the origins of relapse in acute myeloid leukaemia to stem cells.* Nature, 2017. **547**(7661): p. 104-108.
96. Paul, C., et al., *Implications On Drug Resistance and Survival of ABCB1 Single Nucleotide Polymorphisms in Normal Karyotype De Novo AML*. 2009, Am Soc Hematology.
97. Li, J., et al., *Expression of MRP1, BCRP, LRP, and ERCC1 in advanced non-small-cell lung cancer: correlation with response to chemotherapy and survival.* Clin Lung Cancer, 2009. **10**(6): p. 414-21.
98. Warta, R., et al., *Association of drug transporter expression with mortality and progression-free survival in stage IV head and neck squamous cell carcinoma.* PLoS One, 2014. **9**(9): p. e108908.
99. Hilton, J., *Role of aldehyde dehydrogenase in cyclophosphamide-resistant L1210 leukemia.* Cancer Res, 1984. **44**(11): p. 5156-60.
100. Pal, D., O. Heidenreich, and J. Vormoor, *Dormancy Stems the Tide of Chemotherapy.* Cancer Cell, 2016. **30**(6): p. 825-826.
101. Ghajar, C.M., et al., *The perivascular niche regulates breast tumour dormancy.* Nat Cell Biol, 2013. **15**(7): p. 807-17.
102. Duan, C.W., et al., *Leukemia propagating cells rebuild an evolving niche in response to therapy.* Cancer Cell, 2014. **25**(6): p. 778-93.
103. Ebinger, S., et al., *Characterization of Rare, Dormant, and Therapy-Resistant Cells in Acute Lymphoblastic Leukemia.* Cancer Cell, 2016. **30**(6): p. 849-862.
104. Vermeulen, L., et al., *The developing cancer stem-cell model: clinical challenges and opportunities.* Lancet Oncol, 2012. **13**(2): p. e83-9.
105. Tomiyasu, H. and H. Tsujimoto, *Comparative aspects of molecular mechanisms of drug resistance through ABC transporters and other related molecules in canine lymphoma.* Veterinary Sciences, 2015. **2**(3): p. 185-205.
106. Ni Chonghaile, T., et al., *Pretreatment mitochondrial priming correlates with clinical response to cytotoxic chemotherapy.* Science, 2011. **334**(6059): p. 1129-33.
107. Cory, S., et al., *Targeting BCL-2-like proteins to kill cancer cells.* Trends in Cancer, 2016. **2**(8): p. 443-460.
108. Letai, A., *Apoptosis and Cancer.* Annual Review of Cancer Biology, 2017. **1**: p. 275-294.
109. Evan, G.I. and K.H. Vousden, *Proliferation, cell cycle and apoptosis in cancer.* Nature, 2001. **411**(6835): p. 342-8.
110. Vo, T.-T., et al., *Relative mitochondrial priming of myeloblasts and normal HSCs determines chemotherapeutic success in AML.* Cell, 2012. **151**(2): p. 344-355.

111. Stamelos, V.A., C.W. Redman, and A. Richardson, *Understanding sensitivity to BH3 mimetics: ABT-737 as a case study to foresee the complexities of personalized medicine.* J Mol Signal, 2012. **7**(1): p. 12.
112. Teixeira, C., J.C. Reed, and M.A. Pratt, *Estrogen promotes chemotherapeutic drug resistance by a mechanism involving Bcl-2 proto-oncogene expression in human breast cancer cells.* Cancer Res, 1995. **55**(17): p. 3902-7.
113. Miyashita, T. and J.C. Reed, *bcl-2 gene transfer increases relative resistance of S49.1 and WEHI7.2 lymphoid cells to cell death and DNA fragmentation induced by glucocorticoids and multiple chemotherapeutic drugs.* Cancer Res, 1992. **52**(19): p. 5407-11.
114. Konopleva, M., et al., *The anti-apoptotic genes Bcl-XL and Bcl-2 are over-expressed and contribute to chemoresistance of non-proliferating leukaemic CD34+ cells.* British journal of haematology, 2002. **118**(2): p. 521-534.
115. Wei, M.C., et al., *Proapoptotic BAX and BAK: a requisite gateway to mitochondrial dysfunction and death.* Science, 2001. **292**(5517): p. 727-730.
116. Levine, A.J., *p53, the cellular gatekeeper for growth and division.* Cell, 1997. **88**(3): p. 323-31.
117. Nakano, K. and K.H. Vousden, *PUMA, a novel proapoptotic gene, is induced by p53.* Mol Cell, 2001. **7**(3): p. 683-94.
118. Oda, E., et al., *Noxa, a BH3-only member of the Bcl-2 family and candidate mediator of p53-induced apoptosis.* Science, 2000. **288**(5468): p. 1053-8.
119. Villunger, A., et al., *p53- and drug-induced apoptotic responses mediated by BH3-only proteins puma and noxa.* Science, 2003. **302**(5647): p. 1036-8.
120. Stilgenbauer, S., et al., *Venetoclax in relapsed or refractory chronic lymphocytic leukaemia with 17p deletion: a multicentre, open-label, phase 2 study.* Lancet Oncol, 2016. **17**(6): p. 768-78.
121. Konopleva, M., et al., *Efficacy and Biological Correlates of Response in a Phase II Study of Venetoclax Monotherapy in Patients with Acute Myelogenous Leukemia.* Cancer Discov, 2016. **6**(10): p. 1106-1117.
122. Souers, A.J., et al., *ABT-199, a potent and selective BCL-2 inhibitor, achieves antitumor activity while sparing platelets.* Nat Med, 2013. **19**(2): p. 202-8.
123. Tse, C., et al., *ABT-263: a potent and orally bioavailable Bcl-2 family inhibitor.* Cancer Res, 2008. **68**(9): p. 3421-8.
124. Chen, J., et al., *The Bcl-2/Bcl-XL/Bcl-w inhibitor, navitoclax, enhances the activity of chemotherapeutic agents in vitro and in vivo.* Molecular cancer therapeutics, 2011: p. molcanther. 0415.2011.
125. Wong, M., et al., *Navitoclax (ABT-263) reduces Bcl-xL mediated chemo-resistance in ovarian cancer models.* Molecular cancer therapeutics, 2012: p. molcanther. 0693.2011.
126. Faber, A.C., et al., *Assessment of ABT-263 activity across a cancer cell line collection leads to a potent combination therapy for small-cell lung cancer.* Proc Natl Acad Sci U S A, 2015. **112**(11): p. E1288-96.
127. Stewart, M.L., et al., *The MCL-1 BH3 helix is an exclusive MCL-1 inhibitor and apoptosis sensitizer.* Nature chemical biology, 2010. **6**(8): p. 595-601.

128. Ries, L.A.G., et al., *Cancer incidence and survival among children and adolescents: United States SEER Program 1975-1995.* Cancer incidence and survival among children and adolescents: United States SEER Program 1975-1995., 1999.
129. Pizzo, P.A. and D.G. Poplack, *Principles and Practice of Pediatric Oncology*. 2011: Wolters Kluwer Health/Lippincott Williams & Wilkins.
130. Mirabello, L., R.J. Troisi, and S.A. Savage, *International osteosarcoma incidence patterns in children and adolescents, middle ages and elderly persons.* International Journal of Cancer, 2009. **125**(1): p. 229-234.
131. Mitelman, F., B. Johansson, and F. Mertens, *The impact of translocations and gene fusions on cancer causation.* Nat Rev Cancer, 2007. **7**(4): p. 233-45.
132. Norris, R.E. and P.C. Adamson, *Challenges and opportunities in childhood cancer drug development.* Nat Rev Cancer, 2012. **12**(11): p. 776-82.
133. Mackall, C.L., *In search of targeted therapies for childhood cancer.* Front Oncol, 2011. **1**: p. 18.
134. Oeffinger, K.C., et al., *Chronic health conditions in adult survivors of childhood cancer.* N Engl J Med, 2006. **355**(15): p. 1572-82.
135. Sultan, I., et al., *Comparing adult and pediatric rhabdomyosarcoma in the surveillance, epidemiology and end results program, 1973 to 2005: an analysis of 2,600 patients.* J Clin Oncol, 2009. **27**(20): p. 3391-7.
136. Newton, W.A., Jr., et al., *Classification of rhabdomyosarcomas and related sarcomas. Pathologic aspects and proposal for a new classification--an Intergroup Rhabdomyosarcoma Study.* Cancer, 1995. **76**(6): p. 1073-85.
137. Arndt, C.A. and W.M. Crist, *Common musculoskeletal tumors of childhood and adolescence.* N Engl J Med, 1999. **341**(5): p. 342-52.
138. Parham, D.M., et al., *Immunohistochemical study of childhood rhabdomyosarcomas and related neoplasms. Results of an Intergroup Rhabdomyosarcoma study project.* Cancer, 1991. **67**(12): p. 3072-80.
139. Dias, P., et al., *Myogenic regulatory protein (MyoD1) expression in childhood solid tumors: diagnostic utility in rhabdomyosarcoma.* Am J Pathol, 1990. **137**(6): p. 1283-91.
140. Dodd, S., M. Malone, and W. McCulloch, *Rhabdomyosarcoma in children: a histological and immunohistochemical study of 59 cases.* J Pathol, 1989. **158**(1): p. 13-8.
141. Kumar, S., et al., *Myogenin is a specific marker for rhabdomyosarcoma: an immunohistochemical study in paraffin-embedded tissues.* Modern Pathology, 2000. **13**(9): p. 988.
142. Tsokos, M., et al., *Rhabdomyosarcoma. A new classification scheme related to prognosis.* Arch Pathol Lab Med, 1992. **116**(8): p. 847-55.
143. Crist, W.M., et al., *Intergroup rhabdomyosarcoma study-IV: results for patients with nonmetastatic disease.* J Clin Oncol, 2001. **19**(12): p. 3091-102.
144. Oberlin, O., et al., *Prognostic factors in metastatic rhabdomyosarcomas: results of a pooled analysis from United States and European cooperative groups.* J Clin Oncol, 2008. **26**(14): p. 2384-9.
145. Barr, F.G., et al., *Genetic heterogeneity in the alveolar rhabdomyosarcoma subset without typical gene fusions.* Cancer Res, 2002. **62**(16): p. 4704-10.

146. Matsumura, T., et al., *Advantage of FISH analysis using FKHR probes for an adjunct to diagnosis of rhabdomyosarcomas.* Virchows Arch, 2008. **452**(3): p. 251-8.
147. Davicioni, E., et al., *Molecular classification of rhabdomyosarcoma—genotypic and phenotypic determinants of diagnosis: a report from the Children's Oncology Group.* The American journal of pathology, 2009. **174**(2): p. 550-564.
148. Williamson, D., et al., *Fusion gene–negative alveolar rhabdomyosarcoma is clinically and molecularly indistinguishable from embryonal rhabdomyosarcoma.* Journal of Clinical Oncology, 2010. **28**(13): p. 2151-2158.
149. Lawrence, W., Jr., et al., *Prognostic significance of staging factors of the UICC staging system in childhood rhabdomyosarcoma: a report from the Intergroup Rhabdomyosarcoma Study (IRS-II).* J Clin Oncol, 1987. **5**(1): p. 46-54.
150. Lawrence, W., Jr., et al., *Pretreatment TNM staging of childhood rhabdomyosarcoma: a report of the Intergroup Rhabdomyosarcoma Study Group. Children's Cancer Study Group. Pediatric Oncology Group.* Cancer, 1997. **80**(6): p. 1165-70.
151. Smith, L.M., et al., *Which patients with microscopic disease and rhabdomyosarcoma experience relapse after therapy? A report from the soft tissue sarcoma committee of the children's oncology group.* Journal of clinical oncology, 2001. **19**(20): p. 4058-4064.
152. Van Gaal, J.C., et al., *Building the bridge between rhabdomyosarcoma in children, adolescents and young adults: the road ahead.* Critical reviews in oncology/hematology, 2012. **82**(3): p. 259-279.
153. Wolden, S.L., et al., *Indications for radiotherapy and chemotherapy after complete resection in rhabdomyosarcoma: A report from the Intergroup Rhabdomyosarcoma Studies I to III.* Journal of clinical oncology, 1999. **17**(11): p. 3468-3475.
154. Abramson, D.H. and C.M. Notis, *Visual acuity after radiation for orbital rhabdomyosarcoma.* Am J Ophthalmol, 1994. **118**(6): p. 808-9.
155. Paulino, A.C. and B.Z. Fowler, *Secondary neoplasms after radiotherapy for a childhood solid tumor.* Pediatr Hematol Oncol, 2005. **22**(2): p. 89-101.
156. Hettmer, S., et al., *Rhabdomyosarcoma: current challenges and their implications for developing therapies.* Cold Spring Harbor perspectives in medicine, 2014. **4**(11): p. a025650.
157. Wilbur, J.R., *Combination chemotherapy for embryonal rhabdomyosarcoma.* Cancer chemotherapy reports, 1974. **58**(2): p. 281.
158. Pappo, A.S., et al., *Survival after relapse in children and adolescents with rhabdomyosarcoma: A report from the Intergroup Rhabdomyosarcoma Study Group.* J Clin Oncol, 1999. **17**(11): p. 3487-93.
159. Schmid, P., et al., *Phase II Randomized Preoperative Window-of-Opportunity Study of the PI3K Inhibitor Pictilisib Plus Anastrozole Compared With Anastrozole Alone in Patients With Estrogen Receptor-Positive Breast Cancer.* J Clin Oncol, 2016. **34**(17): p. 1987-94.

160. Hayes, F.A., et al., *Long-term survival in patients with Ewing's sarcoma relapsing after completing therapy.* Med Pediatr Oncol, 1987. **15**(5): p. 254-6.
161. Mattke, A.C., et al., *Does the time-point of relapse influence outcome in pediatric rhabdomyosarcomas?* Pediatric blood & cancer, 2009. **52**(7): p. 772-776.
162. Wachtel, M., et al., *Gene expression signatures identify rhabdomyosarcoma subtypes and detect a novel t(2;2)(q35;p23) translocation fusing PAX3 to NCOA1.* Cancer Res, 2004. **64**(16): p. 5539-45.
163. Davicioni, E., et al., *Identification of a PAX-FKHR gene expression signature that defines molecular classes and determines the prognosis of alveolar rhabdomyosarcomas.* Cancer research, 2006. **66**(14): p. 6936-6946.
164. Shern, J.F., et al., *Comprehensive genomic analysis of rhabdomyosarcoma reveals a landscape of alterations affecting a common genetic axis in fusion-positive and fusion-negative tumors.* Cancer Discov, 2014. **4**(2): p. 216-31.
165. Seki, M., et al., *Integrated genetic and epigenetic analysis defines novel molecular subgroups in rhabdomyosarcoma.* Nat Commun, 2015. **6**: p. 7557.
166. Sorensen, P.H., et al., *PAX3-FKHR and PAX7-FKHR gene fusions are prognostic indicators in alveolar rhabdomyosarcoma: a report from the children's oncology group.* J Clin Oncol, 2002. **20**(11): p. 2672-9.
167. Wachtel, M. and B.W. Schafer, *Unpeaceful roles of mutant PAX proteins in cancer.* Semin Cell Dev Biol, 2015. **44**: p. 126-34.
168. Bernasconi, M., et al., *Induction of apoptosis in rhabdomyosarcoma cells through down-regulation of PAX proteins.* Proceedings of the National Academy of Sciences, 1996. **93**(23): p. 13164-13169.
169. Scheidler, S., et al., *The hybrid PAX3-FKHR fusion protein of alveolar rhabdomyosarcoma transforms fibroblasts in culture.* Proceedings of the National Academy of Sciences, 1996. **93**(18): p. 9805-9809.
170. Keller, C., et al., *Alveolar rhabdomyosarcomas in conditional Pax3:Fkhr mice: cooperativity of Ink4a/ARF and Trp53 loss of function.* Genes Dev, 2004. **18**(21): p. 2614-26.
171. Shern, J.F., M.E. Yohe, and J. Khan, *Pediatric Rhabdomyosarcoma.* Crit Rev Oncog, 2015. **20**(3-4): p. 227-43.
172. Chen, X., et al., *Targeting oxidative stress in embryonal rhabdomyosarcoma.* Cancer Cell, 2013. **24**(6): p. 710-24.
173. Langenau, D.M., et al., *Effects of RAS on the genesis of embryonal rhabdomyosarcoma.* Genes & development, 2007. **21**(11): p. 1382-1395.
174. Rubin, B.P., et al., *Evidence for an unanticipated relationship between undifferentiated pleomorphic sarcoma and embryonal rhabdomyosarcoma.* Cancer cell, 2011. **19**(2): p. 177-191.
175. Soleimani, V.D. and M.A. Rudnicki, *New insights into the origin and the genetic basis of rhabdomyosarcomas.* Cancer cell, 2011. **19**(2): p. 157-159.
176. Hatley, M.E., et al., *A mouse model of rhabdomyosarcoma originating from the adipocyte lineage.* Cancer cell, 2012. **22**(4): p. 536-546.

177. Keller, C., et al., *Alveolar rhabdomyosarcomas in conditional Pax3: Fkhr mice: cooperativity of Ink4a/ARF and Trp53 loss of function.* Genes & development, 2004. **18**(21): p. 2614-2626.
178. Keller, C. and M.R. Capecchi, *New genetic tactics to model alveolar rhabdomyosarcoma in the mouse.* Cancer Res, 2005. **65**(17): p. 7530-2.
179. Gryder, B.E., et al., *PAX3-FOXO1 Establishes Myogenic Super Enhancers and Confers BET Bromodomain Vulnerability.* Cancer Discov, 2017.
180. Belyea, B., et al., *Embryonic signaling pathways and rhabdomyosarcoma: contributions to cancer development and opportunities for therapeutic targeting.* Sarcoma, 2012. **2012**.
181. Takebe, N., et al., *Targeting Notch, Hedgehog, and Wnt pathways in cancer stem cells: clinical update.* Nat Rev Clin Oncol, 2015. **12**(8): p. 445-64.
182. Rota, R., et al., *Notch signaling in pediatric soft tissue sarcomas.* BMC Med, 2012. **10**: p. 141.
183. Belyea, B., et al., *Embryonic signaling pathways and rhabdomyosarcoma: contributions to cancer development and opportunities for therapeutic targeting.* Sarcoma, 2012. **2012**: p. 406239.
184. Ignatius, M.S., et al., *The NOTCH1/SNAIL1/MEF2C Pathway Regulates Growth and Self-Renewal in Embryonal Rhabdomyosarcoma.* Cell Rep, 2017. **19**(11): p. 2304-2318.
185. von Maltzahn, J., et al., *Wnt signaling in myogenesis.* Trends Cell Biol, 2012. **22**(11): p. 602-9.
186. Clevers, H., *Wnt/β-catenin signaling in development and disease.* Cell, 2006. **127**(3): p. 469-480.
187. Anastas, J.N. and R.T. Moon, *WNT signalling pathways as therapeutic targets in cancer.* Nature reviews. Cancer, 2013. **13**(1): p. 11.
188. Kephart, J.J., et al., *Secreted Frizzled-Related Protein 3 (SFRP3) Is Required for Tumorigenesis of PAX3–FOXO1-Positive Alveolar Rhabdomyosarcoma.* Clinical Cancer Research, 2015. **21**(21): p. 4868-4880.
189. Chen, E.Y., et al., *Glycogen synthase kinase 3 inhibitors induce the canonical WNT/beta-catenin pathway to suppress growth and self-renewal in embryonal rhabdomyosarcoma.* Proc Natl Acad Sci U S A, 2014. **111**(14): p. 5349-54.
190. Drager, J., et al., *LEF1 reduces tumor progression and induces myodifferentiation in a subset of rhabdomyosarcoma.* Oncotarget, 2017. **8**(2): p. 3259-3273.
191. Brack, A.S., et al., *A temporal switch from notch to Wnt signaling in muscle stem cells is necessary for normal adult myogenesis.* Cell stem cell, 2008. **2**(1): p. 50-59.
192. Cohn, M.J. and C. Tickle, *Limbs: a model for pattern formation within the vertebrate body plan.* Trends Genet, 1996. **12**(7): p. 253-7.
193. Jessell, T.M., *Neuronal specification in the spinal cord: inductive signals and transcriptional codes.* Nat Rev Genet, 2000. **1**(1): p. 20-9.
194. Ehlen, H.W., L.A. Buelens, and A. Vortkamp, *Hedgehog signaling in skeletal development.* Birth Defects Res C Embryo Today, 2006. **78**(3): p. 267-79.

195. Maeda, Y., et al., *Indian Hedgehog produced by postnatal chondrocytes is essential for maintaining a growth plate and trabecular bone.* Proc Natl Acad Sci U S A, 2007. **104**(15): p. 6382-7.
196. Bitgood, M.J., L. Shen, and A.P. McMahon, *Sertoli cell signaling by Desert hedgehog regulates the male germline.* Curr Biol, 1996. **6**(3): p. 298-304.
197. Varjosalo, M. and J. Taipale, *Hedgehog: functions and mechanisms.* Genes Dev, 2008. **22**(18): p. 2454-72.
198. Ma, Y., et al., *Hedgehog-mediated patterning of the mammalian embryo requires transporter-like function of dispatched.* Cell, 2002. **111**(1): p. 63-75.
199. Torroja, C., N. Gorfinkiel, and I. Guerrero, *Patched controls the Hedgehog gradient by endocytosis in a dynamin-dependent manner, but this internalization does not play a major role in signal transduction.* Development, 2004. **131**(10): p. 2395-408.
200. Hui, C.C. and S. Angers, *Gli proteins in development and disease.* Annu Rev Cell Dev Biol, 2011. **27**: p. 513-37.
201. Ruiz i Altaba, A., P. Sanchez, and N. Dahmane, *Gli and hedgehog in cancer: tumours, embryos and stem cells.* Nat Rev Cancer, 2002. **2**(5): p. 361-72.
202. Robbins, D.J., D.L. Fei, and N.A. Riobo, *The Hedgehog signal transduction network.* Sci Signal, 2012. **5**(246): p. re6.
203. Stecca, B. and I.A.A. Ruiz, *Context-dependent regulation of the GLI code in cancer by HEDGEHOG and non-HEDGEHOG signals.* J Mol Cell Biol, 2010. **2**(2): p. 84-95.
204. Amakye, D., Z. Jagani, and M. Dorsch, *Unraveling the therapeutic potential of the Hedgehog pathway in cancer.* Nat Med, 2013. **19**(11): p. 1410-22.
205. Camp, D., et al., *Ihog and Boi elicit Hh signaling via Ptc but do not aid Ptc in sequestering the Hh ligand.* Development, 2014.
206. Mille, F., et al., *The shh receptor boc promotes progression of early medulloblastoma to advanced tumors.* Dev Cell, 2014. **31**(1): p. 34-47.
207. Allen, B.L., T. Tenzen, and A.P. McMahon, *The Hedgehog-binding proteins Gas1 and Cdo cooperate to positively regulate Shh signaling during mouse development.* Genes Dev, 2007. **21**(10): p. 1244-57.
208. Kwong, L., M.F. Bijlsma, and H. Roelink, *Shh-mediated degradation of Hhip allows cell autonomous and non-cell autonomous Shh signalling.* Nat Commun, 2014. **5**: p. 4849.
209. Briscoe, J. and P.P. Therond, *The mechanisms of Hedgehog signalling and its roles in development and disease.* Nat Rev Mol Cell Biol, 2013. **14**(7): p. 416-29.
210. Canettieri, G., et al., *Histone deacetylase and Cullin3-REN(KCTD11) ubiquitin ligase interplay regulates Hedgehog signalling through Gli acetylation.* Nat Cell Biol, 2010. **12**(2): p. 132-42.
211. Gorlin, R.J. and R.W. Goltz, *Multiple nevoid basal-cell epithelioma, jaw cysts and bifid rib. A syndrome.* N Engl J Med, 1960. **262**: p. 908-12.
212. Gorlin, R.J., *Nevoid basal cell carcinoma (Gorlin) syndrome: unanswered issues.* J Lab Clin Med, 1999. **134**(6): p. 551-2.
213. Farndon, P.A., et al., *Location of gene for Gorlin syndrome.* Lancet, 1992. **339**(8793): p. 581-2.

214. Reis, A., et al., *Localisation of gene for the naevoid basal-cell carcinoma syndrome.* Lancet, 1992. **339**(8793): p. 617.
215. Johnson, R.L., et al., *Human homolog of patched, a candidate gene for the basal cell nevus syndrome.* Science, 1996. **272**(5268): p. 1668-71.
216. Hahn, H., et al., *Mutations of the human homolog of Drosophila patched in the nevoid basal cell carcinoma syndrome.* Cell, 1996. **85**(6): p. 841-51.
217. Hahn, H., et al., *Rhabdomyosarcomas and radiation hypersensitivity in a mouse model of Gorlin syndrome.* Nat Med, 1998. **4**(5): p. 619-22.
218. Tostar, U., et al., *Deregulation of the hedgehog signalling pathway: a possible role for the PTCH and SUFU genes in human rhabdomyoma and rhabdomyosarcoma development.* J Pathol, 2006. **208**(1): p. 17-25.
219. Pressey, J.G., et al., *Hedgehog pathway activity in pediatric embryonal rhabdomyosarcoma and undifferentiated sarcoma: a report from the Children's Oncology Group.* Pediatr Blood Cancer, 2011. **57**(6): p. 930-8.
220. Paulson, V., et al., *High-resolution array CGH identifies common mechanisms that drive embryonal rhabdomyosarcoma pathogenesis.* Genes Chromosomes Cancer, 2011. **50**(6): p. 397-408.
221. Ragazzini, P., et al., *Amplification of CDK4, MDM2, SAS and GLI genes in leiomyosarcoma, alveolar and embryonal rhabdomyosarcoma.* Histol Histopathol, 2004. **19**(2): p. 401-11.
222. Oue, T., et al., *Increased expression of the hedgehog signaling pathway in pediatric solid malignancies.* J Pediatr Surg, 2010. **45**(2): p. 387-92.
223. Zibat, A., et al., *Activation of the hedgehog pathway confers a poor prognosis in embryonal and fusion gene-negative alveolar rhabdomyosarcoma.* Oncogene, 2010. **29**(48): p. 6323-30.
224. Sathesha S., M.G., Bovay A., Casanova E., Bode P., Belle R., Feuchtgruber S., Jaaks P., Dogan N., Koscielniak E., and Sch√§fer B.W., *Targeting hedgehog signaling reduces self-renewal in Embryonal Rhabdomyosarcoma.* paper in preparation.
225. Bridge, J.A., et al., *Novel genomic imbalances in embryonal rhabdomyosarcoma revealed by comparative genomic hybridization and fluorescence in situ hybridization: an intergroup rhabdomyosarcoma study.* Genes Chromosomes Cancer, 2000. **27**(4): p. 337-44.
226. Calzada-Wack, J., et al., *Analysis of the PTCH coding region in human rhabdomyosarcoma.* Hum Mutat, 2002. **20**(3): p. 233-4.
227. Nitzki, F., et al., *Uncommitted precursor cells might contribute to increased incidence of embryonal rhabdomyosarcoma in heterozygous Patched1-mutant mice.* Oncogene, 2011. **30**(43): p. 4428-36.
228. Hahn, H., et al., *Patched target Igf2 is indispensable for the formation of medulloblastoma and rhabdomyosarcoma.* J Biol Chem, 2000. **275**(37): p. 28341-4.
229. Mao, J., et al., *A novel somatic mouse model to survey tumorigenic potential applied to the Hedgehog pathway.* Cancer Res, 2006. **66**(20): p. 10171-8.
230. Lee, Y., et al., *Loss of suppressor-of-fused function promotes tumorigenesis.* Oncogene, 2007. **26**(44): p. 6442-7.

231. Svard, J., et al., *Tumor suppressor gene co-operativity in compound Patched1 and suppressor of fused heterozygous mutant mice.* Mol Carcinog, 2009. **48**(5): p. 408-19.
232. Rajurkar, M., et al., *Distinct cellular origin and genetic requirement of Hedgehog-Gli in postnatal rhabdomyosarcoma genesis.* Oncogene, 2013.
233. Hatley, M.E., et al., *A mouse model of rhabdomyosarcoma originating from the adipocyte lineage.* Cancer Cell, 2012. **22**(4): p. 536-46.
234. Rubin, B.P., et al., *Evidence for an unanticipated relationship between undifferentiated pleomorphic sarcoma and embryonal rhabdomyosarcoma.* Cancer Cell, 2011. **19**(2): p. 177-91.
235. Manzella, G. and B. W Schäfer, *Interfering with Hedgehog Pathway: New Avenues for Targeted Therapy in Rhabdomyosarcoma.* Current drug targets, 2016. **17**(11): p. 1228-1234.
236. Pui, C.-H., et al., *Treating childhood acute lymphoblastic leukemia without cranial irradiation.* New England Journal of Medicine, 2009. **360**(26): p. 2730-2741.
237. Adamson, P.C., et al., *Drug discovery in paediatric oncology: roadblocks to progress.* Nat Rev Clin Oncol, 2014. **11**(12): p. 732-9.
238. Giard, D.J., et al., *In Vitro Cultivation of Human Tumors: Establishment of Cell Lines Derived From a Series of Solid Tumors 2.* Journal of the National Cancer Institute, 1973. **51**(5): p. 1417-1423.
239. Collins, S.J., R.C. Gallo, and R.E. Gallagher, *Continuous growth and differentiation of human myeloid leukaemic cells in suspension culture.* Nature, 1977. **270**(5635): p. 347-9.
240. Lee, J., et al., *Tumor stem cells derived from glioblastomas cultured in bFGF and EGF more closely mirror the phenotype and genotype of primary tumors than do serum-cultured cell lines.* Cancer cell, 2006. **9**(5): p. 391-403.
241. Persson, C.U., et al., *Neuroblastoma patient-derived xenograft cells cultured in stem-cell promoting medium retain tumorigenic and metastatic capacities but differentiate in serum.* Sci Rep, 2017. **7**(1): p. 10274.
242. Daniel, V.C., et al., *A primary xenograft model of small-cell lung cancer reveals irreversible changes in gene expression imposed by culture in vitro.* Cancer Res, 2009. **69**(8): p. 3364-73.
243. Westwood, G., et al., *Basic fibroblast growth factor (bFGF)-induced cell death is mediated through a caspase-dependent and p53-independent cell death receptor pathway.* Oncogene, 2002. **21**(5): p. 809.
244. Williamson, A.J., et al., *Basic fibroblast growth factor-induced cell death is effected through sustained activation of p38MAPK and up-regulation of the death receptor p75NTR.* Journal of Biological Chemistry, 2004. **279**(46): p. 47912-47928.
245. Orlowski, R.Z. and D.J. Kuhn, *Proteasome inhibitors in cancer therapy: lessons from the first decade.* Clin Cancer Res, 2008. **14**(6): p. 1649-57.
246. Chen, D., et al., *Bortezomib as the first proteasome inhibitor anticancer drug: current status and future perspectives.* Current cancer drug targets, 2011. **11**(3): p. 239-253.

247. Tiffin, N., et al., *PAX7 expression in embryonal rhabdomyosarcoma suggests an origin in muscle satellite cells.* Br J Cancer, 2003. **89**(2): p. 327-32.
248. Ren, Y.X., et al., *Mouse mesenchymal stem cells expressing PAX-FKHR form alveolar rhabdomyosarcomas by cooperating with secondary mutations.* Cancer Res, 2008. **68**(16): p. 6587-97.
249. del Peso, L., et al., *Regulation of the forkhead transcription factor FKHR, but not the PAX3-FKHR fusion protein, by the serine/threonine kinase Akt.* Oncogene, 1999. **18**(51): p. 7328-7333.
250. Jothi, M., et al., *AKT and PAX3-FKHR cooperation enforces myogenic differentiation blockade in alveolar rhabdomyosarcoma cell.* Cell Cycle, 2012. **11**(5): p. 895-908.
251. Pommier, Y., et al., *Apoptosis defects and chemotherapy resistance: molecular interaction maps and networks.* Oncogene, 2004. **23**(16): p. 2934-49.
252. Adams, J.M. and S. Cory, *The Bcl-2 protein family: arbiters of cell survival.* Science, 1998. **281**(5381): p. 1322-6.
253. Tsujimoto, Y., et al., *Cloning of the chromosome breakpoint of neoplastic B cells with the t(14;18) chromosome translocation.* Science, 1984. **226**(4678): p. 1097-9.
254. Vaux, D.L., S. Cory, and J.M. Adams, *Bcl-2 gene promotes haemopoietic cell survival and cooperates with c-myc to immortalize pre-B cells.* Nature, 1988. **335**(6189): p. 440-2.
255. Walton, M., et al., *Constitutive expression of human Bcl-2 modulates nitrogen mustard and camptothecin induced apoptosis.* Cancer research, 1993. **53**(8): p. 1853-1861.
256. Kamesaki, S., et al., *bcl-2 protein inhibits etoposide-induced apoptosis through its effects on events subsequent to topoisomerase II-induced DNA strand breaks and their repair.* Cancer Research, 1993. **53**(18): p. 4251-4256.
257. Margue, C.M., et al., *Transcriptional modulation of the anti-apoptotic protein BCL-XL by the paired box transcription factors PAX3 and PAX3/FKHR.* Oncogene, 2000. **19**(25): p. 2921-9.
258. Heere,ÄêRess, E., et al., *Bcl,ÄêXL is a chemoresistance factor in human melanoma cells that can be inhibited by antisense therapy.* International journal of cancer, 2002. **99**(1): p. 29-34.
259. Shoemaker, A.R., et al., *A small-molecule inhibitor of Bcl-XL potentiates the activity of cytotoxic drugs in vitro and in vivo.* Cancer Res, 2006. **66**(17): p. 8731-9.
260. Lebedeva, I., et al., *Bcl-xL in prostate cancer cells: effects of overexpression and down-regulation on chemosensitivity.* Cancer Research, 2000. **60**(21): p. 6052-6060.
261. Schoenwaelder, S.M., et al., *Bcl-x L,Äìinhibitory BH3 mimetics can induce a transient thrombocytopathy that undermines the hemostatic function of platelets.* Blood, 2011. **118**(6): p. 1663-1674.
262. Rudin, C.M., et al., *Phase II study of single-agent navitoclax (ABT-263) and biomarker correlates in patients with relapsed small cell lung cancer.* Clin Cancer Res, 2012. **18**(11): p. 3163-9.

263. Van Delft, M.F., et al., *The BH3 mimetic ABT-737 targets selective Bcl-2 proteins and efficiently induces apoptosis via Bak/Bax if Mcl-1 is neutralized.* Cancer cell, 2006. **10**(5): p. 389-399.
264. Kotschy, A.s., et al., *The MCL1 inhibitor S63845 is tolerable and effective in diverse cancer models.* Nature, 2016. **538**(7626): p. 477-482.
265. Shi, J., et al., *Navitoclax (ABT-263) accelerates apoptosis during drug-induced mitotic arrest by antagonizing Bcl-xL.* Cancer Res, 2011. **71**(13): p. 4518-26.
266. Inuzuka, H., et al., *SCFFbw7 Regulates Cellular Apoptosis By Targeting Mcl-1 for Ubiquitination and Destruction.* Nature, 2011. **471**(7336): p. 104.
267. Harley, M.E., et al., *Phosphorylation of Mcl-1 by CDK1-cyclin B1 initiates its Cdc20-dependent destruction during mitotic arrest.* EMBO J, 2010. **29**(14): p. 2407-20.
268. Willis, S.N., et al., *Proapoptotic Bak is sequestered by Mcl-1 and Bcl-xL, but not Bcl-2, until displaced by BH3-only proteins.* Genes & development, 2005. **19**(11): p. 1294-1305.
269. Satheesha, S., et al., *Targeting hedgehog signaling reduces self-renewal in embryonal rhabdomyosarcoma.* Oncogene, 2016. **35**(16): p. 2020-30.
270. Banerjee, U. and M.K. Hadden, *Recent advances in the design of Hedgehog pathway inhibitors for the treatment of malignancies.* Expert Opin Drug Discov, 2014. **9**(7): p. 751-71.
271. Infante, P., et al., *Gli1/DNA interaction is a druggable target for Hedgehog-dependent tumors.* EMBO J, 2014.
272. Merchant, A.A. and W. Matsui, *Targeting Hedgehog--a cancer stem cell pathway.* Clin Cancer Res, 2010. **16**(12): p. 3130-40.
273. Tang, J.Y., et al., *Inhibiting the hedgehog pathway in patients with the basal-cell nevus syndrome.* N Engl J Med, 2012. **366**(23): p. 2180-8.
274. Sekulic, A., et al., *Efficacy and safety of vismodegib in advanced basal-cell carcinoma.* N Engl J Med, 2012. **366**(23): p. 2171-9.
275. Letai, A., P.A. Coulombe, and E. Fuchs, *Do the ends justify the mean? Proline mutations at the ends of the keratin coiled-coil rod segment are more disruptive than internal mutations.* J Cell Biol, 1992. **116**(5): p. 1181-95.
276. Letai, A., et al., *Disease severity correlates with position of keratin point mutations in patients with epidermolysis bullosa simplex.* Proc Natl Acad Sci U S A, 1993. **90**(8): p. 3197-201.
277. Cheng, J., et al., *The genetic basis of epidermolytic hyperkeratosis: a disorder of differentiation-specific epidermal keratin genes.* Cell, 1992. **70**(5): p. 811-9.
278. Tostar, U., et al., *Reduction of human embryonal rhabdomyosarcoma tumor growth by inhibition of the hedgehog signaling pathway.* Genes Cancer, 2010. **1**(9): p. 941-51.
279. Kawabata, N., et al., *Pharmacological inhibition of the Hedgehog pathway prevents human rhabdomyosarcoma cell growth.* Int J Oncol, 2011. **39**(4): p. 899-906.
280. Srivastava, R.K., et al., *GLI inhibitor GANT-61 diminishes embryonal and alveolar rhabdomyosarcoma growth by inhibiting Shh/AKT-mTOR axis.* Oncotarget, 2014.

281. Yamanaka, H., et al., *Hedgehog signal inhibitor forskolin suppresses cell proliferation and tumor growth of human rhabdomyosarcoma xenograft.* J Pediatr Surg, 2011. **46**(2): p. 320-5.
282. Eichenmuller, M., et al., *Betulinic acid induces apoptosis and inhibits hedgehog signalling in rhabdomyosarcoma.* Br J Cancer, 2010. **103**(1): p. 43-51.
283. Ecke, I., et al., *Cyclopamine treatment of full-blown Hh/Ptch-associated RMS partially inhibits Hh/Ptch signaling, but not tumor growth.* Mol Carcinog, 2008. **47**(5): p. 361-72.
284. Chen, J.K., et al., *Inhibition of Hedgehog signaling by direct binding of cyclopamine to Smoothened.* Genes Dev, 2002. **16**(21): p. 2743-8.
285. Srivastava, R.K., et al., *GLI inhibitor GANT-61 diminishes embryonal and alveolar rhabdomyosarcoma growth by inhibiting Shh/AKT-mTOR axis.* Oncotarget, 2014. **5**(23): p. 12151-65.
286. Buonamici, S., et al., *Interfering with resistance to smoothened antagonists by inhibition of the PI3K pathway in medulloblastoma.* Sci Transl Med, 2010. **2**(51): p. 51ra70.
287. Kimura, H., J.M. Ng, and T. Curran, *Transient inhibition of the Hedgehog pathway in young mice causes permanent defects in bone structure.* Cancer Cell, 2008. **13**(3): p. 249-60.
288. Park, H.L., et al., *Mouse Gli1 mutants are viable but have defects in SHH signaling in combination with a Gli2 mutation.* Development, 2000. **127**(8): p. 1593-605.

9. Acknowledgements

I would first of all like to thank Prof. Dr. **Beat Schäfer** for his guidance, support and trust in my work, for giving me responsibilities that helped me to grow up not only as scientist but also from a personal point of view. I will be always grateful to him, without his visions I would not have come that far.

I would also like to thank the members of my thesis committee Prof. Dr. **Lukas Sommer** and Prof. Dr. **Konrad Basler** for their helpful suggestions, opened discussions and brilliant ideas. I was very lucky for having met so clever persons.

I would like to deeply thank all the **Cancer Network** for organizing stimulating courses, scientific events and for giving me the opportunity of interacting with other PhD students and not only scientifically!! It was very beneficial for expanding my network in Zurich and I felt really privileged to be part of this nice community.

I cannot forget the "familiar" environment of August-Forel Strasse, a place where excitement and frustration were part of the daily life and only thank to the friendly and nice people that I could keep going and enjoy my time there. Thank you Dr. **Marco Wachtel** for sharing your unlimited scientific knowledge, for teaching me many aspects of the lab work, for your precious ideas, for your inspiring discussions, for always finding solutions where everything seemed lost and for your great "hands" into the project. I really learned a lot from you. Thank you **Sam** for introducing me to the lab and for guiding me at the beginning of my Phd. Thank you **Giuliano** my Roman connection. You helped me in everything since I came to Zurich for the first time, a real friend to hang out, laugh and drink with as well as a 'shoulder to cry on'. Thank you **Irina**, the worse "coffeemaker" ever, but a great friend to talk, complain and laugh with every day. Many thanks to all present and past colleagues, "**Mauro"**, **Peter**, **Elisa**, **Maria**, **Verena**, **Florian**, **Jurgen**, **Dimitra**, **Michele**, **Katharina**, **Joana**, **Johannes**, **Dominik**, **Michaela**, **Eva**, **Markus**, **Blaz, Riccardino** and others for the nice time spent in the lab.

I would like to express my gratitude to **my family** for their support throughout my whole life. A special thank goes also to my super **grandparents** who always felt proud of me and me of them.

Thank you to all my 'caxxettini friends', **Gigi**, **Simona**, **Marco Baggio**, **Marco "Hombre"**, **Francesca**, **Uliander**, **Gabi**, **Karun** for all the fun we had that made my stay in Zurich special and wonderful.

Finally, a special thank you to my **Giotini**, the love of my life that supported me everyday and made me a better person. Thank you for believing in me, for over-estimating me, for teaching me that science is not everything and for being the wonderful person you are.

10. Curriculum Vitae

Name: GABRIELE MANZELLA

Date of birth: August 26, 1988

Nationality: Italian

Postal Address: Hofwiesenstrasse, 236
CH-8057, Zurich

Mobile: +41 (0) 786 5238 14

Email: gabriele.manzella@kispi.uzh.ch
manzella.gabriele@gmail.com

Education and Qualifications

PhD Cancer Biology — June 2013-December 2017
University of Zurich, Switzerland

Thesis: 'Exploiting Precision Medicine in Rhabdomyosarcoma'
Supervisor: Prof. Dr. Beat W. Schaefer
Department of Oncology
University Children's Hospital Zurich
Zurich, Switzerland

MSc in Molecular and cellular Biology — November 2010-September 2012
University of Pisa, Italy
Finished master study with summa cum laude

Thesis: 'Role of PHD2 in cancer: B55alpha as new hub in the understanding of hypoxia driven-tumorigenesis"
Supervisor: Prof. Massimiliano Mazzone
Lab of Molecular Oncology and Angiogenesis
VIB Vesalius Research Center
University of Leuven (Belgium)

BSc in Biology — September 2007-October 2010
University of Salerno, Italy
Finished bachelor study with summa cum laude

High School Liceo Scientifico Pierpaolo Pasolini — September 2002-June 2007
Potenza, Italy

Publication list

1. Satheesha S.[1], **Manzella G.**[1], Bovay A., Casanova E.A., Bode P.K., Belle R., Feuchtgruber S., Jaaks P., Dogan N., Koscielniak E., Schäfer B.W.
   Targeting hedgehog signaling reduces self-renewal in embryonal rhabdomyosarcoma. Oncogene. 2016 Apr 21;35(16):2020.
   [1] Equal contribution

2. **Manzella G.**, Schäfer B.W.
   Interfering with Hedgehog Pathway: New Avenues for Targeted Therapy in Rhabdomyosarcoma. Current drug targets. 2016 Sep 1;17(11):1228-34.

Selected Poster presentations and awards

Forschungzentrum für das Kind (FZK)-Children's Research Center 6th Annual Retreat (October 2016; Zurich).
Unraveling mechanisms of chemoresistance in rhabdomyosarcoma.

American Association for Cancer Research Annual Conference (April 2016; New Orleans, USA).
Hedgehog pathway inhibition sensitizes embryonal rhabdomyosarcoma to standard chemotherapy.

Poster Prize. Cancer Network Zurich Student's Retreat (April 2015; Zurich).
Targeting hedgehog pathway and characterization of tumor initiating populations in embryonal rhabdomyosarcoma.

Selected Oral presentations and awards

Kolloquium in angewandter Krebsforschung (November 2017; Zurich).
Characterization of pre-clinical models of rhabdomyosarcoma to guide personalized treatments

Oral Presentation Prize. Forschungzentrum für das Kind (FZK)-Children's Research Center 7th Annual Retreat (October 2017; Zurich).
A personalized Pre-clinical Platform to Guide Treatment Decisions for Rhabdomyosarcoma Patients

Kolloquium in angewandter Krebsforschung (December 2016; Zurich).
Unraveling mechanisms of chemoresistance in embryonal rhabdomyosarcoma